UNIVERSITÀ
DEGLI STUDI
FIRENZE

SCUOLA DI DOTTORATO IN SCIENZE

Dottorato di Ricerca in Scienza per la Conservazione dei Beni Culturali

Ciclo XXVII

REMOVAL OF VARNISH AND OVERPAINT LAYERS FROM EASEL PAINTINGS USING PULSED Nd:YAG LASERS

AUTHOR: DANIELE CIOFINI

TUTOR: DOTT. SALVATORE SIANO
CO - TUTOR: PROF. PIERO BAGLIONI

Scuola di Dottorato in SCIENZE
Dottorato di Ricerca in
Scienza per Conservazione dei Beni Culturali
Ciclo XXVII

Coordinatore Prof. Piero Baglioni

REMOVAL OF VARNISH AND OVERPAINT LAYERS FROM EASEL PAINTINGS USING PULSED Nd:YAG LASERS

SSD FIS/07

Dottorando
Daniele Ciofini

Tutore
Dott. Salvatore Siano

Co-tutore
Prof. Piero Baglioni

Coordinatore
Prof. Piero Baglioni

2012-2014

CONTENTS

Chapter 2

Chapter 3

Chapter 4

Chapter 5

ABSTRACT

With the aim of finding less invasive and selective cleaning strategies for paintings restoration, this thesis provides novel insights and successful applications on the use of pulsed Nd:YAG lasers to safely remove aged varnish coatings and overpaint layers. The laser-material interaction under different irradiation conditions of several painting materials, such as terpenoid-based varnishes and oil paint layers, was extensively characterized using different analytical techniques. Laser ablation tests carried out on a large number of naturally and artificially aged varnish samples using the fifth (213 nm) and fourth (266 nm) harmonics of a Q-Switch (15 ns) Nd:YAG laser evidence the fundamental importance of following a wavelength-based approach for the selective removal of painting varnishes. The promising results achieved on samples irradiated at 213 nm envisage very good prospects for the transfer of this laser cleaning approach in the field.
Similarly, Long Q-Switching Nd:YAG (1064 nm) laser with a pulse duration of 120 ns was successfully tested for dealing the conservation problems of two female portraits dated around 1930 and 1910, respectively. The latter painting was found on the backside of a signed artwork by Giacomo Balla, one of the founding members of the Futurist Painters. These artworks were almost completely disguised by thick layers of oil overpaintings, which did not have any artistic relevance. Thorough characterization of the original pigments, binders, overpaintings and deterioration mechanisms allowed performing the complete restoration of the painting from Balla's studio, which returned an unknown Pre-Futurist artwork, and to plan that of the other female portrait by anonymous. At the same time, a systematic laboratory experimentation on prepared samples simulating the uncovering problems encountered in the real case has been carried out. This improved the knowledge of the laser induced-effects and ablation processes on different modern pigments and allowed to exploit such features for the selective removal of the undesired layers. The results reported disclose a significant application perspective for Nd:YAG laser ablation in conservation of modern easel paintings.

PREFACE

Gradual and selective removal of old varnishes and overpaints from easel paintings is one of the major conservation issues encountered by painting restorers, conservators and scientists. Ageing and degradation phenomena affect the chemical and physical properties of the material to be removed, thus making difficult any restoration attempt.

Thus, autoxidative degradation processes induce in varnish films changes as cracking, hazing, loss of gloss and yellowing. Findings indicated that owing to the light and oxygen most of the oxidation products, mainly high molecular weight compounds, are generated in the uppermost layer. Similarly, ageing and degradation mechanisms of oil paints involve pigment-binder interactions that generate cross-linked networks, low molecular weight compounds and insoluble carboxylate salts.

The traditional methods of dealing with these problems rely on the use of mechanical means such as scalpels or chemical stuffs. Thus, for instance, the removal of a well-oxidized mastic varnish from a thoroughly dried oil film using, for example spirits of wine has been carried out for centuries and still in use today. The alternative of using abrasion to break up the friable mastic film has also been a long-standing mainstay of cleaning paintings. The removal of tough old oil films, as well as overpaints and retouchings, foresees the use of mechanical methods of scraping or lifting with a scalpel, sometimes combining reagent, solvent, and scalpel methods iteratively and carefully. Despite this, they can be very difficult to remove because of their close similarity, in physical and chemical properties, to the underlying paint layers

In this picture, the need of fine-tuned cleaning methodologies becomes imperative for preserving the underlying original paint layer without affecting its structural integrity.

In this work, exploiting the potentialities offered by the latest laser cleaning methodologies, it has been tried to investigate and deepen the

knowledge of the laser-induced effects and the ablation processes in order to provide a controllable and selective method for restoring old and/or damaged paintings. On the basis of a detailed state-of-the-art regarding the laser cleaning techniques, wavelengths and pulse durations were finely selected paying attention to the chemical and physical properties of the material to be removed, as well as to the impact that the laser approach can exercise on aged and degraded painting material.

Taking advantage from the compactness and versatility offered by solid-state laser sources, two different approaches were exploited to address the removal of aged varnish coatings and overpaint layers. The fifth (213 nm) and fourth (266 nm) harmonics of a pulsed Q-Switch (15 ns) Nd:YAG laser were selected for dealing the varnish problem, whereas the Long Q-Switching (120 ns) Nd:YAG laser's fundamental wavelength (1064 nm) for the selective ablation of overpainting layers.

As regards the varnishes, the systems studied comprise two different categories: (i) “spirit” varnishes prepared dissolving dammar, mastic, colophony, sandarac and bleached shellac in opportune solvents and (ii) mastic, colophony, sandarac and Manila copal pre-heated at high temperatures with linseed oil.

Trasmission FTIR spectroscopy, colorimetric and gravimetric measurements were used for monitoring the light-induced effects under the exposure to accelerated light (above 290 nm) conditions. This procedure led to the understanding of the photo-induced effects (photoxidation, cross-linking, radical polymerization) on solvent and oil varnishes and at the same time, allowed obtaining highly polymerized systems suitable for laser irradiation tests and useful information for interpreting the lased-induced effects.

These artificially aged systems together with ones kept to natural ageing conditions were subjected to an extensive systematic investigation aimed at assessing the laser-induced modifications upon laser irradiation at 213 and 266 nm. A significant effort was primarily devoted to study the optical absorption properties of the varnish films by means of UV-Vis absorption spectroscopy, which allowed also to estimate the linear absorption coefficient and the temperature rise associated to the laser

irradiation. Chemical and physical changes were accurately characterized using Confocal μ-Raman and Laser Induced Fluorescence spectroscopies. These analytical techniques provided useful information about the laser induced effects suggesting the formation of more pronounced changes upon irradiation at 266 nm, whereas at 213 nm, being a highly absorbed wavelengths, they can be considered practically negligible or absent. In this way, the layer by layer removal is provided by a resolution in the sub-micron scale, thus allowing an high degree of control and selectivity during the lightening of a thin varnish layer. Findings indicated that irradiation at 213 nm with pulses of 15 ns of photosensitive paint layers (i.e.,vermillion, lead chromate, lead white and azurite) covered with shellac varnish did not result affected by laser radiation.

On the same way, controlled laser removal of overpaintings is a difficult challenge since undesired and original paint layers are both constituted by similar mixtures of organic and inorganic compounds, which make their discrimination very hard. For this reason, a laser approach based on short wavelengths, as the above mentioned for varnish layers, cannot be exploited for ablating thick overpainted layers. The submicrometric penetration of UV laser sources, in this case, does not permit to discriminate between different materials due to the high absorption of both organic and inorganic materials. Photomechanical effects accompanied by plasma formation can potentially induce injuries to the substrate, especially when repetitive irradiation is needed for removing thick overpaint layers. In contrast to what reported in literature, in this thesis a different approach based on the use of Long Q-Switched (LQS) Nd:YAG (1064 nm) laser with a pulse duration of 120 ns has been proposed for the first time for the selective removal of overpainting layers. This laser wavelength offers interesting interaction features, such as lower-pressure peak generation into the paint layer, as well as lower recoil stresses in fluid dynamic ablation regimes. These features were evaluated through a systematic laboratory experimentation on prepared samples simulating the stratigraphy of two female portraits dated around 1930 and 1910, respectively. The latter, which is attributable to Giacomo Balla's studio, after unsuccessful removal attempts using organic solvents,

was subjected to a first laser treatment. The uncovering results have been very satisfactory and then the laser ablation treatment has been extended to the whole overpainted surface thus allowing to recover an unknown Pre-Futurist artwork.
The restoration work has been associated with a thorough characterisation of the original pigments, binders, and overpaintings by means of microscopic inspections, portable Vis reflectance, and Raman spectroscopy measurements, along with FTIR spectroscopy equipped with attenuated total-reflection (ATR) and stratigraphic examinations (optical and ESEM-EDX) of small material samples. On the basis of these analytical results, laboratory simulations were carried out in order to measure laser ablation threshold, the optical absorption properties at 1064 nm, and pressure transient associated to the removal process. The selected pigments were lithopone, titanium white, zinc oxide, cadmium yellow, green copper carbonate, artificial ultramarine blue, cobalt blue, chromium oxide green and many others.

Finally, with aim of finding alternative laser cleaning methodologies for the removal of varnish and overpaint layers this thesis is structured as follows:

Chapter 1 starts with a brief description on the main types of varnish formulations which can be found on paintings. Afterwards, these materials will be treated from a compositional standpoint, with special remarks on the aging processes. A further section is dedicated to drying and ageing mechanisms of drying oils and oil paints. Lastly, follows a section focused on the common cleaning practices employed nowadays for dealing the aforementioned conservation issues.

Chapter 2 provides a thoroughly state-of-the-art on the different laser approaches proposed for the removal of varnish and overpaint layers from easel paintings. A general explanation of the photophysical mechanisms involved from UV to IR laser wavelengths with different pulse durations is reported.

Chapter 3 is aimed at the understanding of the photo-oxidative degradation pathways occurring during the accelerated light-ageing of painting varnishes. The photo-induced effects on tri (dammar and mastic), di (sandarac, colophony, copal) and sequiterpenoid (shellac) resins, prepared as spirit and linseed oil mixtures, are illustrated by means of results obtained using Trasmission FTIR spectroscopy, colorimetry and gravimetric measurements.

Chapter 4 is substantially focused on the systematic assessment of the laser induced modifications occurring in solvent and oil varnish coatings after laser removal treatment. The fifth (213 nm) and fourth (266 nm) harmonics of a pulsed QS (15 ns) Nd:YAG laser were selected for irradiating the prepared varnish samples. UV-Vis absorption spectroscopy, Confocal μ-Raman and Laser Induced Fluorescence spectroscopies have been used for the chemical and physical characterization of the samples and laser-induced modifications.

Chapter 5 shows the methodological approach exploited for the removal of overpaint layers. The uncovering results achieved on two female portraits dated around 1930 and 1910 using the Long Q-Switching Nd:YAG (1064 nm) laser with a pulse duration of 120 ns are shown. Microscopic inspections, portable Vis reflectance, Raman and ATR-FTIR spectroscopy, stratigraphic examinations, ESEM-EDX, pressure measurements, have been used to characterize material composition and laser ablation processes.

Chapter I

OPEN ISSUES ON CONSERVATION OF EASEL PAINTINGS: ASPECTS ON THE AGEING AND CLEANING OF VARNISHES AND OIL PAINTS

Gradual and selective removal of old varnishes and overpaints from easel paintings, which is the focus of the research in this thesis, is one of the major conservation issues encountered by painting restorers, conservators and scientists. Basically, varnish films undergo ageing processes that lead to yellowed products which can obscure colours, craze and become very brittle and insoluble over time. On the same way, ageing and degradation of oil paints involve pigment-binder interactions that generate cross-linked networks and insoluble metal salts. In some extent, these changes affect the chemical and physical properties of the material to be removed and hence the need of a fine-tuned cleaning methodology becomes imperative for preserving the underlying original layers.

Within this framework, this chapter starts with a brief description of the main types of varnish formulations, which can be found on paintings. Afterwards, these materials will be treated from a compositional standpoint, with special remarks on the aging processes. A further section is dedicated to drying and ageing mechanisms of drying oils and oil paints. Lastly, follows a section focused on the common cleaning practices used nowadays for dealing the aforementioned conservation issues.

1.1 Use of terpenoid resins as painting varnishes

Varnishes were usually applied on panel and canvas paintings as protective coatings and to enhance both the color saturation and the overall gloss (de la Rie 1987, Mills and White 1994, Elias et al. 2006). Egyptians were the first to use protective coatings, but it was not until the Middle Ages in Europe that paint as a protective coating came into widespread use. It has long been recognized that different types of varnish give different optical appearances to a painting. A varnish layer has the ability to produce a smooth surface when applied to a rough paint surface. This is dependent both from refractive index and molecular weight, but the latter parameter has been demonstrated to be rather dominant in how a varnish resin affects the appearance of an oil painting (Berns and de la Rie 2003). Recently, this has also been proved by multi-interface OCT (Optical coherence tomography) profilometry applied to the dynamic monitoring of varnish coatings on rough substrates (Lawman and Liang 2011).

Besides this, painters and restorers can use the resins as varnish, as additive to paints (e.g. glazes, lacquers), as pigment (copper resinates) and mordant (adhesive for e.g. gold leaf). A variety of recipes for preparing coloured varnishes, which can be applied as decorative or protective films on painting and wood artifacts, have been reported. For instance, these coloured varnishes were prepared using a number of pigments, colophony resin and drying oil. Furthermore, resins may have been introduced by previous restoration attempts, both on the *recto* of a painting, as retouching varnish and for regeneration purposes, and on the *verso,* as wax/resin lining paste for repairing and strengthening the support.

A schematic drawing of a cross section of a typical Old Master painting is shown in Fig. 1, illustrating where terpenoid resins may be present in the complex layer structure of a painting. Materials and preparation procedures have undergone a continuous evolution over time, according to the different artistic and/or restoration needs. As regards the varnishes applied as protective coatings, numerous recipes are reported on historical treatises and artist' accounts (De Mayerne 1901, Theophilus 1961, Cennini 1954, Merrifield 1849, Eastlake 1847).

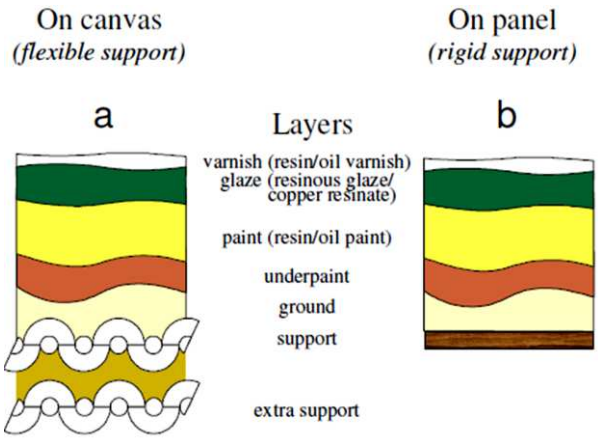

Fig. 1 - Cross section of a typical Old Master painting a) on canvas and b) on panel and the possible source of terpenoid resins which may be found in the different layers (van den Berg 2012).

From a chemical standpoint, they can be considered as heterogeneous systems of two types. A first type of formulations, which may be defined *oil-resin varnishes*, are constituted of resins, oils, thinners and dryers. The second ones are the so called "*spirit varnishes*", which are formed by a resin dissolved with thinners or solvents.

Resins mixed with a drying oil were the earliest type of varnish blend used in the Middle Ages whereas the so called "spirit varnishes" were introduced for commercial purposes only later in the sixteenth century. Nevertheless, oil-resin varnishes were still in use as late as the nineteenth century (Mills and White 1999, Sutherland 2001, 2003).

The most commonly used materials for the oil varnishes were poppy, nut and/or linseed oil mixed with copal, amber, sandarac and/or colophony resins. Although sources suggest that pine colophony-drying oil mixtures were used frequently as e.g. lacquers, due to its high tendency to darkening as varnishes. Manufacturing of oil varnishes for paintings involved vigorous boiling of the resin with the drying oil at high temperatures in the range of 300-350 °C (Carlyle 1991). Oil of turpentine was employed to dissolve the resin prior to the heat processing and/or to dilute the final viscous product. Driers, such as lime, lead, zinc, cobalt

and manganese, were occasionally added in low percentage for controlling the drying time (Mallègol et al. 2000).
Thus for instance, the “vernice liquida”, frequently mentioned by Cennini in his *Libro dell'Arte* (Cennini 1954), which appeared around 1390, was a solution of sandarac in linseed oil (de la Rie 1989). The “vernice comune”, constituted of colophony or oleoresin and linseed oil, was commonly used in Italy since the Middle Ages. About “vernice liquida” Eastlake, during its stay in Florence, concluded this was 'the ordinary term used by early writers, to designate the varnish for tempera pictures' and not simply an adjective describing the viscosity of the varnish (Reifsnyder 1996). Nevertheless, all these types of varnish formulations were primarily used as finishing coatings for paintings, but also for tin, iron and stone materials.
As regards the spirit varnishes, diterpenoid resins from *Pinaceae*, *Cupressaceae*, *Araucariaceae* and *Leguminosae* families and triterpenoid resins from *Burseraceae*, *Anacardiaceae* families and the *Dipterocarpaceae* sub-family were usually dissolved in spirits of wine and turpentine.
Concerning with the triterpenoid resins, the most important ones used as spirit varnishes are mastic (*Anacardiaceae* family) and dammar (*Dipterocarpaceae* family). Mastic has been widely used as a picture varnish throughout the centuries, starting from the IX century but only from the seventieth century was introduced in replacing coatings made of oil or mixtures of oils and resins. Carlyle, who studied traditional British varnish recipes of the nineteenth century, reported that mastic was often used also along this time period (Carlyle 1991). It was primarily used as spirit varnish and prepared by dissolution of the resin in turpentine or alcohol either with or without heat. Owing to a reported tendency to become more yellow with age than dammar, mastic became less popular and was replaced, to an extent, by the somewhat paler dammar, which had been introduced into the market in 1829 (de la Rie 1989). Dammar is also applied as a spirit varnish, using mainly turpentine or, in the twentieth century, white spirit or turpentine. Like mastic, dammar is a highly glossy varnish. In cases where the strong gloss of dammar varnish is not desirable, beeswax was often added (Mills and Werner 1955, Reifsnyder

1996, Doelen 1999). Furthermore, these triterpenoid resins have always been considered the most suitable as painting varnishes because they maintain for a long time the character of reversibility (solubility in suitable solvents).

The diterpenoid resins, as sandarac, colophony, amber, Venice turpentine and copals, were mainly employed as additional ingredients of varnishes. This is the case of sandarac, which has been added to the mastic varnish for enhancing the hardness of the coating film. Frequent application of diterpenoid resins as binding medium (i.e Roberson's medium) has been also reported (Gettens & Stout 1966).

Copals were often used by Flemish painters to prepare varnishes and oil paint media. Copal varnishes were appreciated because of their hardness and durability and because they were not susceptible to blooming. Their popularity increased in the second half of the 19th century when they were also used for varnishing woodwork and in general, all artifacts requiring a tough coating. Most of the earliest formulations for copal oil varnishes simply included copal, oil and turpentine. The oil, usually a drying oil, was incorporated into the resin during heating. In the 19th century, other recipes explaining how to prepare copal varnishes without oils and heating were formulated. The ingredients included copal, ether, alcohol, camphor or essential oils such as oil of spike, rosemary and lavender.

Shellac is a further type of resin which has long been popular for different applications as finishing coating. Its use in Europe began towards the end of the 16th century mainly as a varnish (mostly known as 'French polish') for wooden objects, musical instruments and gilding, as a protective for vinyl disks and mural paintings, as an insulating material for earlier radios and other electrical tools and as an adhesive in the restoration of pottery (Colombini et al. 2003). Its use in association with paintings is not widely documented, either as an artist's or a conservation material. One of the main reason is related to its orange-brown tint, a property attributable to coloured components (including the 'lac dye'), which are not entirely removed during the process of extracting the resin from the crude lac. In the early nineteenth century, several methods for decolourizing shellac resin were introduced, including chemical bleaching processes using

chlorine, which were developed in London by the colour manufacturer George Field and in Philadelphia by the chemist Robert Hare. The bleached shellac—or 'white lac'—was promoted as a picture varnish, and widely adopted by artists. Its use became the subject of considerable discussion in painting manuals and technical journals (Sutherland 2010).

1.2 Ageing processes of terpenoid resins

Resins employed as painting varnishes are composed of complex mixtures of terpenoids derived by isoprene. They are polymeric substances exuded mainly by plants or secreted by insects, known since antiquity and widely used, due to their film-forming properties, as finishing coatings in all types of artifacts. Before to describe the ageing processes underlying each type of varnish an informative note which clarifies the meaning of terpenoid[1] is given. At present, several groups of terpenoids, classified in terms of C_{10}-units are recognized (see Table 1).

Table 1 Classification of terpenoids compounds

Classification	No. of carbon atoms	No. of isoprene units
Hemiterpenoids	5	1
monoterpenoids	10	2
Sequiterpenoids	15	3
Diterpenoids	20	4
Sesterterpenoids	25	5
Triterpenoids	30	6
Tetraterpenoids	40	8
Polyterpenoids	>40	>8

[1] The term "Terpen" (English, "terpene") is attributed to Kekule who coined it to describe $C_{10}H_{18}$ hydrocarbons occurring in turpentine (German, "Turpentin") oil. This term has, over the years, acquired a generic significance and is used to designate isoprene-based secondary metabolites. The term terpenoid which has come into considerable usage since 1955, is now considered to be synonymous with terpene and is the preferred generic name for this class of natural products.

Within each class, members are often grouped together according to the number of carbocyclic rings – e.g, acyclic diterpenoids, monocyclic diterpenoids, etc (Rowe 1989). In conservation field, with special regards to that of easel paintings, the most relevant resins employed involve sesquiterpenoid (shellac), diterpenoid (colophony, Venice turpentine, sandarac, copal) and triterpenoid (mastic, dammar, elemi) (Mills and White 1999).

Various authors working in the field have studied the aging of terpenoid resins, with the goal of understanding and slowing their deterioration. Studies dealing with photochemical and thermal degradation of terpenoid varnishes have been performed by means of UV-Vis, IR and fluorescence spectrophotometry (de la Rie 1982, 1988), Fourier transform infrared (Van der Doelen 1999, Derrick et al. 2000) and micro-Raman spectroscopies (Vandenabeele et al. 2000, Nevin et al. 2009). Several chromatographic techniques coupled with mass spectrometry (Colombini et al. 2000, Scalarone et al. 2002, 2003) have also been extensively used in the characterization of ageing processes of terpenoid resins. Studies performed using graphite-assisted laser desorption/ionization mass spectrometry allowed sensitive detection of a very wide variety of oxidation products, especially in the early stage of aging. It was demonstrated that aging of a single triterpene compound results in literally hundreds of oxidation and aging products, and up to seven oxygen atoms can be incorporated into a single triterpenoid molecule (Zumbühl et al. 1998, Dietemann et al. 2000, 2003).

In the following sections some general details about the ageing processes underlying to each class of terpenoid compounds used as painting varnishes are reported. Particular attention will be dedicated to light-induced effects (photoxidation pathways), since these are believed to be the major intitiation and degradation pathways when the material has been exposed to short-wavelength light. Such frame can provide useful information about the composition of aged varnishes as well as general keys for interpreting the laser induced effects.

1.2.1 Triterpenoids

Triterpenoid resins are complex mixtures of a number of saturated molecules which have been exhaustively and comprehensively reviewed (De la Rie 1988b, Van der Doelen 1999, Dietemann 2003). At molecular level, triterpenoids are usually classified according to their carbon skeleton type (Fig. 2).

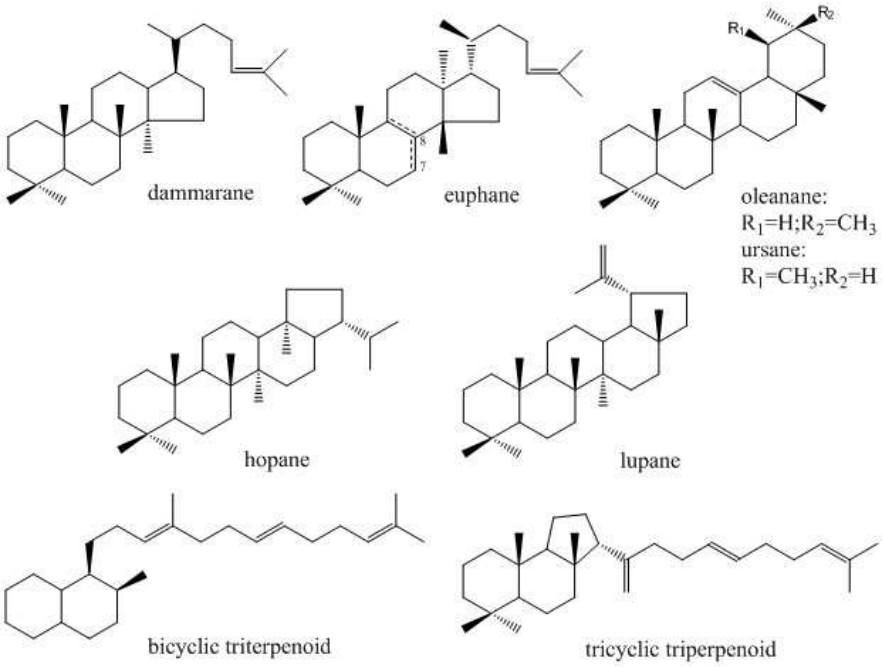

Fig. 2 Main skeleton types of triterpenoids occurring in dammar and mastic resin. Figure adapted from Van der Doelen 1999.

Dammar (*Dipterocarpaceae* family) consists largely of compounds of the tetracyclic dammarane skeleton series, but the pentacyclic oleanane, ursane and hopane derivatives are also present. In addition, dammar contains a small sesquiterpenoid (C15) fraction. Similar to dammar resin, triterpenoids present in mastic (*Anacardiaceae* family) resin are of the tetracyclic euphane and dammarane skeleton type and of the pentacyclic oleanane and lupane skeleton type. In addition, bicyclic and tricyclic

triterpenoids are also found to occur in mastic resin as well as polymer fraction identified as *cis*-1,4-poly-β-myrcene (Feller 1958, Brewis et al 1961, Mills and Werner 1955, Horie 1987, Van der Doelen 1999).
In principle, aging has been characterized as an oxidative process, initially leading to the addition of oxygen-containing functional groups to the original triterpenoid hydrocarbon backbones. The main recognized degradation pathway, which is of general valence for all the organic molecules, involve chain radical reactions summarized as follows (see Table 2): after the chain is initiated by formation of a radical (i), oxygen from the air is inserted (ii). The resulting peroxy radical (ROO·), which is relatively stable, abstracts a hydrogen atom from another molecule, leading to a hydroperoxide and a new radical that propagates the chain reaction (iii). Homolytic cleavage of hydroperoxides is induced via heat or light depending on the energy (iv), producing alkoxy radicals RO·, which are very reactive with alcohols, ethers and ketones.

Table 2 Representative autoxidative process through radical chain reactions

Initiation:	R-H	+	X·(initiator) → R· + X-H	(i)
Propagation:	R·	+	O_2 → ROO·	(ii)
	ROO·	+	RH → ROOH + R·	(iii)
Branching:			ROOH → RO· + OH	(iv)
Termination:	RO·	+	R'O· → ROOR'	(v)
	RO·	+	R'· → ROR'	(vi)
	R·	+	R'· → RR'	(vii)

However, the homolytic cleavage of peroxide bonds formed in the process leads to two new radicals (branching of the chain, step v), allowing autoxidation to proceed despite some degree of recombination (Dietemann et al. 2009). For instance, also drying oils are subjected to this type of decay.
Radical chain reactions are usually initiated by absorption of (UV)-light. The energy to initiate these reactions can also come from the thermal energy. In addition, air pollutants, such as ozone, are known to initiate autoxidation (de la Rie 1988a, 1988b, van der Doelen 1999).
It was demonstrated that the role played by light is not so critical in determining the oxidation kinetics of mastic and dammar resins. In fact, it

was showed that the ageing mechanism is mainly driven by auto-oxidation. The only difference between light and darkness conditions is the slower kinetics of self-formations of radicals in dark conditions (Dietmann et al. 2009). However, natural ageing leads to side chain oxidation of triterpenoids with the dammarane skeleton and oxidation in positions C-11, C-17 and C-28 of oleanane and ursane skeletons. Products as hydroxy, ether, carbonyl and carboxylic acid groups has been detected (Van der Doelen 1999). Similar oxidation products have been observed after accelerated ageing under fluorescent tube light and xenon-arc light excluding the UV wavelengths, methods which simulate museum lighting conditions. Nevertheless, these conditions generate a lower degree of cross-linking than that found on natural aged varnishes. In samples aged under xenon-arc light with UV light it was demonstrated that additional reactions and photo oxidized products, which no occurring during natural ageing, are formed. These reactions are probably initiated in triterpenoid resins at the ubiquitous aliphatic keto groups (Zumbühl et al. 1998) due to the absorption of light of 275-295-nm wavelength (Fig. 3).

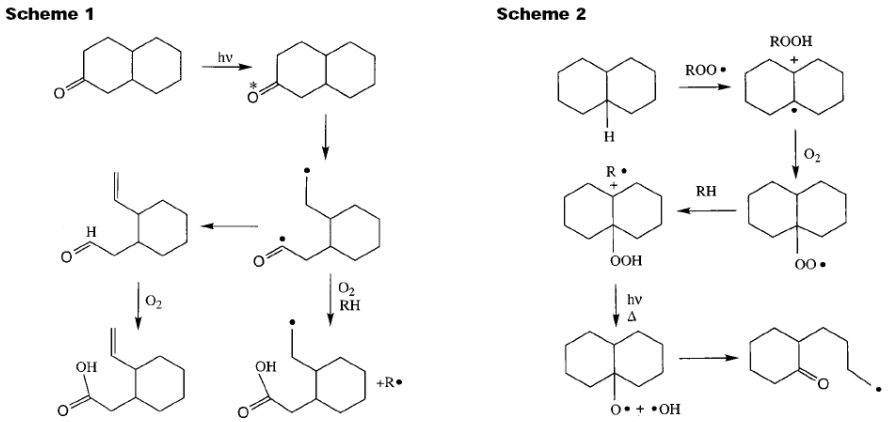

Fig. 3 Primary photo-induced processes occurring in presence of UV light (Sheme 1). Secondary propagating autoxidation reactions (sheme 2) (Zumbühl et al. 1998)

This light excites the n→π* transition of these groups followed by bond homolysis and ring opening (Norrish type I reaction); see reaction

Scheme 1. The resultant R-ring cleavage to a diradical (Norrish type I reaction) can be followed by oxygen insertion leading to carboxylates, aldehydes, peroxides, and hydroperoxides. In addition, intramolecular recombination termination reactions can lead to unsaturated species (Zumbühl et al. 1998).

Despite with or without UV light take place different radical reactions all these changes are only the beginning (primary reactions) of an autoxidation process leading to: (1) radical polymerization (cross-linking and condensation) in both the triterpenoid resins of the polymer fractions. The cadinene polimerise to polycadinene and the monoterpene (C10) molecule β-myrcene to cis-1,4-poly-β-myrcene (2) oxidative modifications in the side chain or in the functional groups on the tetra- or the pentacyclic ring triterpenoid structures (3) shortening of the side chain, and (4) eventual defunctionalization, bond-breaking, and disintegration of the triterpenoid carbon skeleton.

Upon degradation, natural triterpenoid varnishes lose their transparency and become yellow as a result of condensation reactions (secondary reactions). These are caused by dimerization of two ketones that due to autoxidation and the occurrence of dehydration reactions generate unsaturated quinones within the polymeric fraction of the aged triterpenoid varnishes. The generation of unsaturated quinones accounts for the strong absorption of the aged triterpenoid varnishes at 400 nm, which causes the *yellowing problem* (De la Rie 1988b, Van der Doelen 1999, Dietemann 2003, Theodorakopoulos et al. 2007). This is consistent with findings showing that yellowing is associated with the formation of insoluble high molecular weight fraction of triterpenoids (de la Rie 1989, Van der Doelen 1999). The increase of molecular weight raises the viscosity and the refractive indices of the aged triterpenoid varnishes, which in turn affects the appearance of colored substrates, as a consequence of the rise of light scattering in the varnish–substrate interface.

In experimental ageing tests, yellowing was mainly observed to develop in darkness and not under accelerating light exposure, in which autoxidation is much stronger (De la Rie 1988a, Feller 1995). This has been attributed to *bleaching* of the yellow chromophores under intense

light (De la Rie 1988a). It was also demonstrated that autooxidative reactions and yellowing are newly formed after exposure to free oxygen conditions and subsequent storage in the dark (Theodorakopoulos et al. 2007). As consequence, ageing with UV light generates a considerable degree of condensation similar to that found on naturally aged varnishes.

1.2.1.1 Oxidation gradient

To date there are several indications pointing to inhomogeneous degradation processes across the depth-profile of aged resins. As ageing progresses, the varnish polymerizes in a three dimensional manner and in parallel, oxidation, auto-oxidation and cross-linking processes, catalyzed by the absorption of light (De la Rie 1988, 1989), take place. Gas chromatography–mass spectroscopy (GC/MS) findings indicated that owing to the strong light intensity and the availability of oxygen at the surface of the varnish, most of the oxidation products are generated in the surface. For instance, the high molecular weight fraction mentioned above is thought to produce a thin yellow layer at the interface of the varnish over time. To confirm this hypothesis, it was shown that the optical densities of a wide range of light-aged dammar films increased with decreasing thickness.
As consequence, given the limited amounts of oxygen in the bulk, it appears that termination reactions of free radicals producing non oxidative cross-links are promoted in the sub-surface varnish layers.
It was also found that the gradient of oxidation across the film thickness is directly related to an equivalent gradient of solubility throughout the thickness of varnish layer (Theodorakopolus and Zafiropulos 2002, Theodorakopoulos et al. 2007, 2009, 2009). Solubility tests of laser ablated 19th century varnishes on paint substrates showed that polarity decreases as a function of depth.
Consequently, the deeper one goes into the varnish layer the more dilute solution (of the appropriate chemical agent) is required to remove the remaining layer. As a general rule the required concentration drops by a factor of two when going from surface to a depth of about 10 micron.

1.2.2 Diterpenoids

As previously mentioned, the diterpenic resins commonly used as artists' materials were colophony, Venice turpentine, copals and sandarac. They are constituted of acids with a skeleton formed by a bi- or tricyclic C20-hydrocarbon (four isoprene units). The major resin constituents have the COOH group at position 4 in the ring system or alcohols (CH_2OH), as depict in Fig. 4.

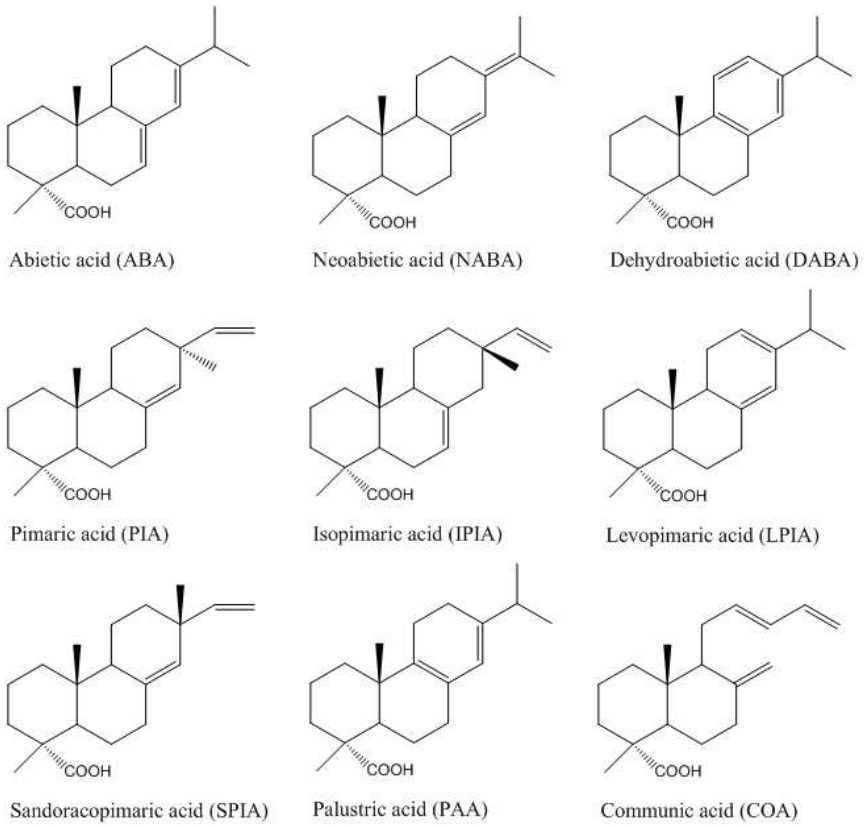

Fig. 4 Chemical structures of the main diterpenoid acids in conifer resins (Findeisen et al. 2007).

They can be classified in three main skeletal groups, namely the abietane (abietic, neoabietic, palustric, levopimaric acids) pimarane (pimaric, isopimaric and sandaracopimaric acids) and labdane (agathic, torusol,

communic acids) diterpenoids. As can be seen, abietane compounds differ only in the positions of the conjugated double bonds and they are interconvertible, each passing on heating to an equilibrium mixture of the four in which abietic acids predominates and laevopimaric acid is almost absent. This is why the composition of the colophony, the residue left after the distillation of oil of turpentine, differ from that of the fresh pine resin (Mills and White, 1977, Horie 1987). The pimarane compounds differ only slightly in basic structure from the abietane compounds but double bonds are not conjugated. Pimaric acid is identical to sandaracopimaric acid a part from having the opposite spatial arrangement (stereochemistry) of the vinyl group side-chain. Lastly, labdane compounds have only two rings, the remaining carbon atoms forming a longish side-chain and the carbon double bonds can be in various positions. Particularly significant is *trans*-communic acid in which the conjugated double bonds in the side-chain are very reactive and readily undergo polymerization (Carman et al. 1970).

The different diterpenoid resins used as painting varnishes are complex mixtures of the aforementioned resinous acids. Clearly, it is important to mention that the quantitative composition of each resins varies due to chemical processes during the production and the storage of the material.

Thus, in detail, fresh colophony resin consists almost entirely of abietane acids with highly reactive conjugated double bonds, 20–25% of more stable pimarane acids and 5–10% of acids that are much prone to oxidation (Scalarone et al. 2002). The ageing of *Pinaceae* diterpenoid resins, as colophony, on the molecular level is predominantly the result of the oxidation of conjugated diene element in abietane diterpenoid acids, properly known as dehydrogenation (Mills and White 1977). These acids are oxidised to form dehydroabietic acid (DABA), which in turn may be oxidised further by incorporation of oxygen (Fig. 5).

Pimarane type molecules, having no conjugated bonds, are more stable than abietanes to these oxidation reactions. The precise mechanisms involved in the oxidation process of abietane molecules is not completely understood, but may be similar to e.g. the oxidation of cholesterol, which is known in some detail. Oxidation processes resulting in the incorporation of oxygen are expected to occur by formation of a peroxide

functionality next to a double bond. Loss of water or reduction of this peroxide may form the oxo- or hydroxy compounds, respectively.

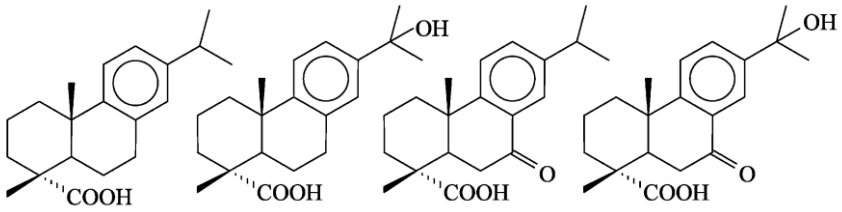

Fig. 5 Oxidised products of abietane acids in diterpenoid resins (From left to right: DABA, 15-hydroxy DABA, 7-oxo-DABA, 15-hydroxy-7-oxo-DABA) (Scalarone et al. 2002)

Moreover, highly oxidized DABA compounds, such as hydroxydehydroabietic acids (OH-DABA), 7-oxo-DABA, di-OH-DABA and 15-hydroxy-7-oxo-DABA, were proposed as useful marker compounds to assess oxidising environments in old paintings (Berg et al. 2000, Findeisen et al. 2007). A theoretical study which concerns the thermal degradation of abietane skeleton diterpenoids showed that dehydrogenation of abietic acid to dehydroabietic is only the early stage. This is followed by a decarboxylation to give dehydroabietin and by a full aromatization to retene (Marchand-Geneste and Carpy 2003).

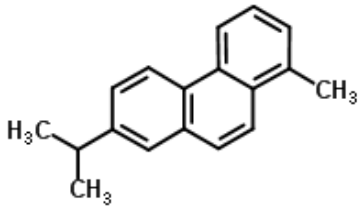

Fig. 6 Retene structure

This study leads to the conclusion that the most likely thermal degradation sequence to reach a polycyclic aromatic structure involves (i) a dehydrogenation of abietic acid to form dehydrobietic acid, (ii) a second dehydrogenation to reach 13- isopropyl-5a-podocarpa-6,8,11,13-tetraen-

16-oic acid, (iii) a demethylation yielding 7-isopropyl-1- methyl-1,2,3,4-tetrahydro-phenanthrene-1-carboxylic acid, (iv) a decarboxylation to obtain tetrahydroretene and (v) two more dehydrogenations to reach the aromatic product retene.

Nevertheless, this compound can be rarely found in a naturally aged varnish but it can be considered as an advanced degradation product of a conifer resin, which leads to its complete darkening.

Venice turpentine is composed by abietane and pimarane acids, together with smaller amounts of labdane alcohols. Two characteristic markers of Venice turpentine are larixol and larixyl acetate, which does not occur in any other resin. Previous studies have demonstrated that also Venice turpentine, like colophony, undergoes oxidation processes, as one could expect on the basis of its chemical composition (Scalarone et al. 2002).

Under different ageing conditions (natural and artificial external conditions with a xenon lamp, and artificial indoor conditions with fluorescent tubes) oxidation and polymerization of colophony and Venice turpentine leads to high molecular weight compounds. Artificial ageing with a Xenon lamp including UV radiation cause, apart from oxidation and polymerisation reactions, a further degradation of the chemical structure with formation of diterpenic fragments (Scalarone et al. 2002).

Contrarily to abietane-type resins, sandarac and several varieties of copals contain, apart from free labdane diterpenoids, a high amount of communic acid which are readily prone to polymerization. Double bond conjugation of the communic acid occurs outside the ring configuration of the molecule (C_{12}=C_{13} and C_{14}=C_{15}), while in the DABA in the C-ring, which makes the former more susceptible to breakdown and the latter more stable, respectively. In fact, it has been noticed that during intense light ageing the drying process leads to the occurrence of both cross-linking and scission though the mechanism reported in the figure 7.

According to this radical mechanisms in which β-scission and oxidative cleavage are in competition, the final ageing products are high-molecular weight, crosslinked and saturated molecules, consisting of bicyclic structures connected by a polymer chain (Fig. 7B).

This is possibly the reason why its monomer cannot be effectively detected in oil varnishes fabricated with copal resins, especially when the film is somewhat aged.

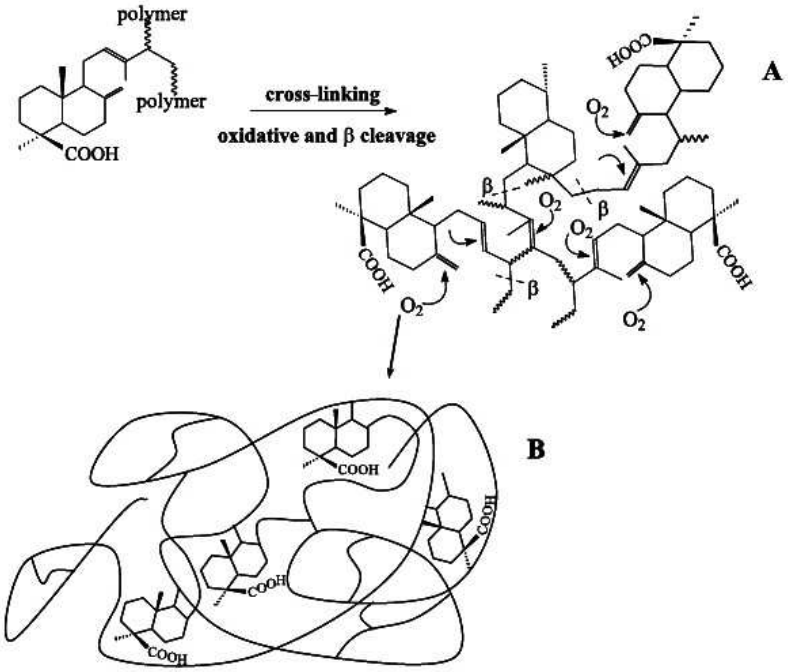

Fig. 7 Degradation scheme of the communic acid based polymers. (A) Carbon double bonds are active site for cross-linking and cleavage. Cleavage reactions occur with radical mechanisms: β-scission or oxidative scission. (B) Cross-linking proceeds further leading to a saturated network of bicyclic units connected by a polymer chain (Scalarone et al. 2003)

Finally, the main deterioration pathways regarding diterpenoid resins (colophony, Venice turpentine, sandarac and copal) employed in the formulation of picture varnishes have been reported. However, experimental investigation aimed at finding the presence of a scalar oxidation gradient across the thickness, as previously seen for triterpenoid resin, have not still been done.

1.2.3 Sesquitepenoids

Shellac is secreted by an insect (*Laccifer lacca Kerr*, also known as *Kerria lacca*), mainly found in India, that infects host trees. It is the only commercial resin of animal origin and has a considerable socioeconomic significance for India. The raw lac is scratched from branches and purified through crushing, sieving and water-washing procedures. Further processing occurs either by heating and filtering the resin through a cloth or wire mesh, or by solvent extraction, to produce the various grades of material known as shellac. The red lac dye, comprising a group of related compounds known as laccaic acids, is almost completely removed from the crude material in the initial washing stage. However, an additional, water insoluble colourant in the lac resin – erythrolaccin - remains after washing and filtering. It is this component that is responsible primarily for shellac's characteristic yellow-brown colour. A complete decolourization is achieved by treatment with chlorine-based bleaching agents to produce the material known as bleached or white shellac (Sutherland 2010).

Chemically, the lac (shellac) resin is not a single compound but consists of intimate mixture of several polar and non-polar components. The resin constituents depend on the nature of the host trees on which the insect grows. This variability may increase with the natural ageing of the resin giving rise to an enhanced degree of polymerisation, to changes in the hydroxy aliphatic and sesquiterpenoid acid content and causing the appearance of decomposition products (Colombini et al. 2003).

In some extent, raw stick lac is composed of 70-80% resin, which in turn can be divided into two parts: 25% soft (ether-soluble) resin, and 75% hard (ether-insoluble) resin. Both the resinous constituents, soft resin and hard resin, contain hydroxyl acid (primarily 9,10,16-trihydroxypalmitic or aleuritic acid) and their polar groups are present at the interface of the molecule. It is presumed that the ability of shellac to adhere strongly to smooth surfaces is the result of orientation of these polar groups (Mills and White 1999, Sharma et al. 1983).

Although the composition of Lac seems to vary according to host tree, according to many authors (Singh et al. 1969, Wadia et al. 1969, Upadhye et al. 1970, Sharma et al. 1983, Buch et al. 2009), two primary

acid groups have been identified in shellac; one being aleuritic (9,10,16-trihydroxypalmitic) and homologues of shellolic acids, which are aliphatic compounds related to fatty acids and make about the 70% of the resin composition (hard resin); and the other being jalaric acid, an alicyclic compound of the sesquiterpene series (soft resin) (Fig. 8).

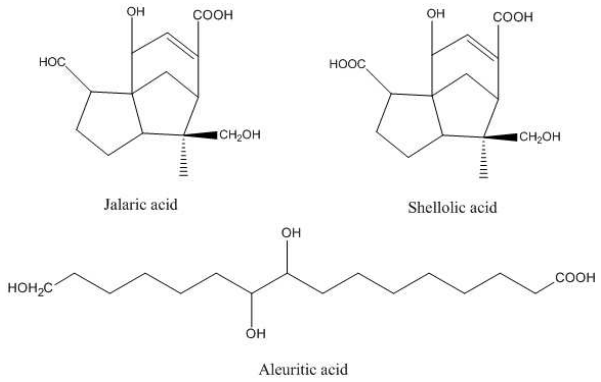

Fig. 8 Chemical structures of main shellac components (Buch et al. 2009)

The soft resin portion of shellac acts as a natural plasticizer, while the hard resin is a brittle substance, although the latter enhance the adhesion properties (Derry 2012). Besides the individual acids also several esters as well as lactide (cyclic diester) and ester linkages have been identified (Fig. 9).

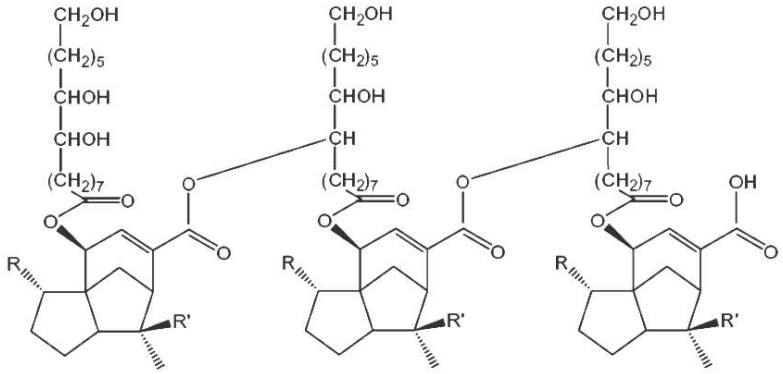

Fig. 9 The most plausible chemical structure of the pure lac resin (hard resin) polyester (Limmatvapirat et al. 2007)

Concerning shellac behaviour upon time, much less information have been found, especially those occurring in bleached shellac used as painting varnish. Since most of the acids contain more than one hydroxyl group and some more than one carboxyl group it is believed that aging is a result of self-esterification of the material.
This was proved in samples artificially aged using a mercury-vapour lamp (emission above 295 nm) (Coelho et al. 2012). Esterification is accompanied by a complete loss of solubility, a decrease in the acid value and an increase in the glass transition temperature (Limmatvapirat et al. 2007, Farag 2010). A schematic drawing of this ageing process is reported in Fig. 10.
It was further demonstrated that during thermal degradation no indication of inter-esterification or dehydration was evidenced. Contrarily, inter-etherification (dioxolan nation) and hydroperoxidation reactions were identified as the most likely (Sarkar et al. 2000).

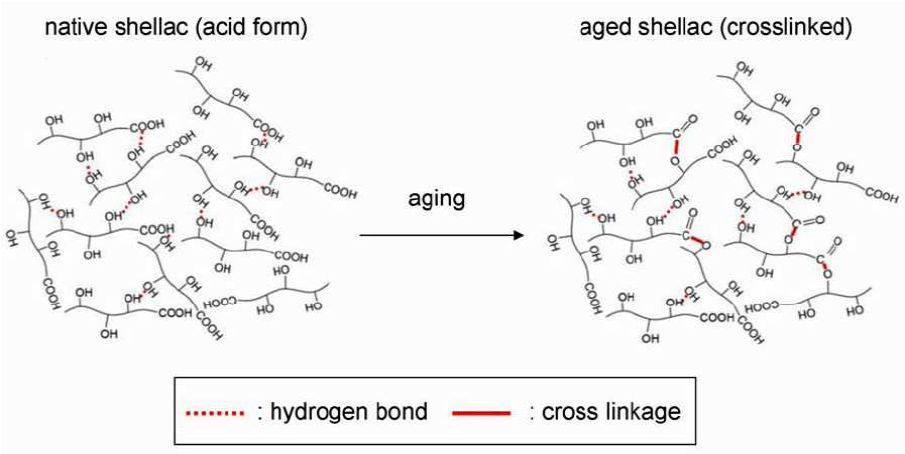

Fig. 10 Shematic representation of the esterification reaction of shellac resin during ageing (Limmatvapirat et al. 2007, Farag 2010).

1.2.4 Oil varnishes

1.2.4.1 Effects upon heat processing and ageing

Oil varnishes, being manufactured by heat-bodying at strong temperatures in the range of 300-350 °C, are high molecular weight, polymerised, condensed, polar and oxidised mixtures, even prior to exposure to deteriorative environments (Mills and White 1999, Carlyle 2001).
The evidently advanced oxidation state of oil varnish films, compared to that of the component drying oil prior to the varnish-making process, is significant in the presence of air during manufacturing, resulting in a very viscous material, whose volatile fraction evaporates from the boiling mixture. During boiling, the component drying oil degrades via three parallel actions (Van den Berg et al. 2002, 2004, Theodorakopoulos 2005): (a) hydrolysis in the glycerol ester bonds resulting in the formation of di- and monoacylglycerols, glycerol and free fatty acids. The concentration in free fatty acids influences both the acid value and the oxidation rate of the oil (b) *cis-trans* isomerisation of double bonds in fatty acids with non-conjugated double bonds in a *cis*-configuration (c) dimerisation by Diels-Alder type reactions, which eventually leads to polymerization. These are well known reactions between a conjugated diene and a compound with a single double bond resulting in cyclisation.
In addition, several products are formed via thermal breakdown of acyl chains on both sides of double bonds, generating free radicals (Van den Berg 2002). These react with hydrogen and generate alkanes, alkenes and short chain unsaturated fatty acids, which form low molecular weight triacylglycerols material. On the other hand free radicals may recombine and new species can be formed with increased molecular weights.
Driers, such as lime, lead, zinc, cobalt and manganese, which are occasionally employed during manufacturing to control the drying time of the oil varnish react with the volatile fraction of the mixture and enhance the viscosity of the final film (Mallégol et al. 2000).
Basically, upon heat processing and subsequent exposure under radiation the compounds with the higher degree of unsaturation oxidise faster, and hence decrease in concentration, than those with a lower degree of

unsaturation. Thus for instance, the ageing processes regarding a copal resin varnishes with linseed oil have been studied (Theodorakopoulos 2005). In this case, it was seen that the communic acid polymerises rapidly at two carbon-carbon double bond sites (C-8 and C-12), which along with cleavage reactions based on radical mechanisms (β-cleavage or oxidative scission) form a saturated network of bicyclic units connected by a polymer chain (Scalarone, et al. 2003). Such polymerization reaction decrease the concentration of communic acid, thus to impede effectively the detection in the oil-resin mixture. In any way, the effect of the addition of a copal resin in a oil varnish tend to increase the drying rate. In contrast, the abietane diterpenoids, which are typical molecules of colophony and Venice turpentine, are less reactive to speed up the polymerization process (Van den Berg, et al. 2002, Scalarone, et al. 2002). Upon heating, the abietane molecules isomerise giving a rich mixture of several isomers of abietic acid (Mills and White 1999).

1.3 Drying, ageing and deterioration mechanisms of drying oils

Linseed oil, poppy seed and walnut oils are the most widely used drying oils in paints formulation. Since the 15th century, especially linseed oil, has been extensively used in varnishes and oil-based paints (Lazzari and Chiantore 1999). From a chemical stand point, drying oils are natural triglycerides containing high percentage of polyunsaturated fatty acids that give to these oils the property of air-drying. These are esters formed between one molecule of glycerol and three molecules of various linear fatty acids (Fig. 11).

The most common fatty acids encountered in the composition of drying oils are saturated acids with 12, 14, 16 or 18 carbon atoms (lauric, myristic, palmitic and stearic acids, respectively) and C18 polyunsaturated acids with 1, 2 or 3 double bonds (oleic, linoleic and linolenic acids, respectively) (Lazzari and Chiantore 1999). The chemical structure of the major constituents are reported in Fig. 11 and its relative percentage for linseed, poppy seed and walnut oils respectively, is listed in Table 3. Depending on the source and provenance, the percentages can be slightly different, even for the same kind of oil.

Table 3 Typical fatty acid compositions of linseed, poppy seed and walnut oils after [Mills J. S., 1987; van den Berg, 2002]

Drying oil	**Fatty acids (% of total Fatty acids)**				
	Palmitic	*Stearic*	*Oleic*	*Linoleic*	*Linolenic*
Linseed oil	6-7	3-6	14-24	14-19	48-60
Poppy seed	9-11	2	11	72	5
Walnut	3-8	0.5-3	9-30	57-76	2-16

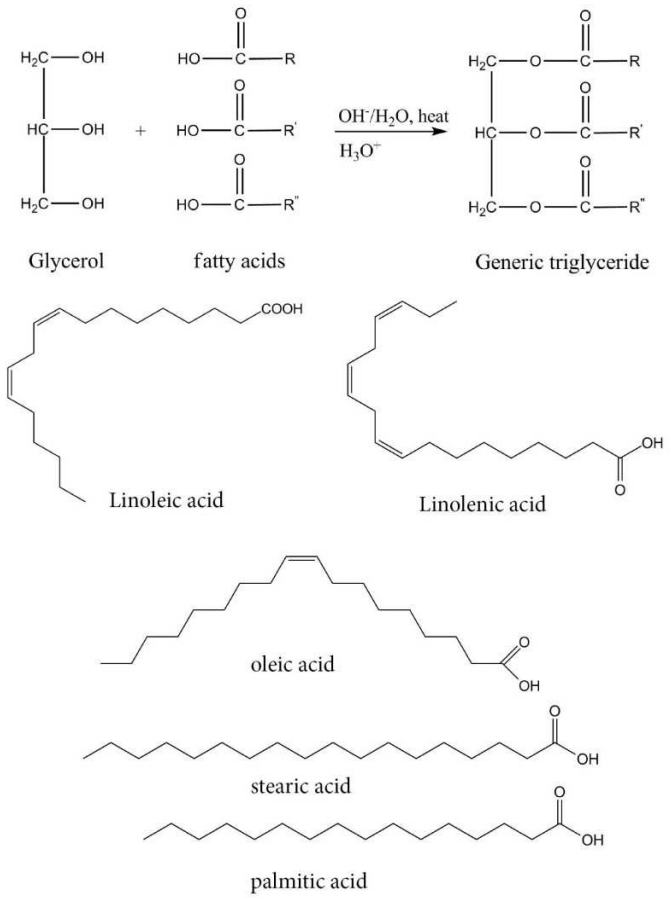

Fig. 11 Graphical representations of a generic triglyceride and the major constituents of drying oils

Besides the composition, the drying, ageing and deterioration processes of oils have been extensively studied and reviewed (Meilunas et al. 1990,

Mallégol et al. 1999, 2000a-b-c, 2001, Lazzari and Chiantore 1999, Boyatzis et al. 2002, Van den Berg et al. 2002, 2004, Dlugogorski et al. 2012).

The first important chemical reaction taking place during the initial drying process comes as a result of oxygen-mediated processes, generally referred to autoxidation (see Table 2). For first, it involves hydrogen abstraction on a methylene group between two double bonds in polyunsaturated fatty acid chain (Fig. 12).

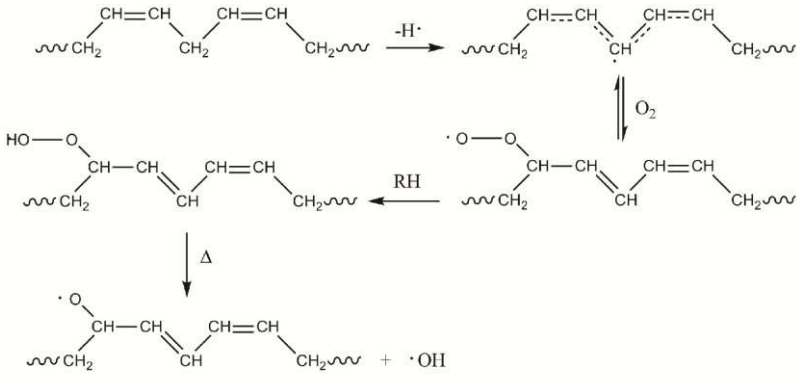

Scheme 1

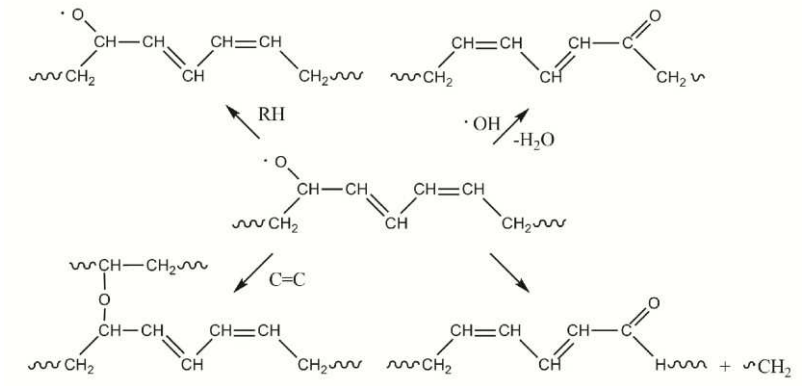

Scheme 2

Fig. 12 Simplified model of the early reactions taking place during the drying of oil.

According to literature, this leads to conjugated hydroperoxides (ROOH) in majority, as reported for linoleic acid in the Scheme 1 (de la Rie 1988,

Meilunas et al. 1990, Lazzari and Chiantore 1999, Van der Weerd et al. 2005). In general, the rate of autoxidation increases with increasing the rate of the initiation reactions. This is mainly done by factors that increase free radical concentrations, such as UV light or transition metals. Radical recombination produces cross-linking (alkyl, ether or peroxy bridges). Peroxy bridges can be thermally decomposed into alkoxy radicals. Alkoxy radicals arising from decomposition of hydroperoxides may give the reactions of Scheme 2, leading to the formation of oxygenated structures (secondary products), such as alcohols, aldehydes, ketones and different carbonyl groups or products of cross-linking, which tend to evaporate together with the water present in the oil matrix. These volatile compounds are easily detectable as they have a typical acrid smell.
The tertiary oxidation products derive from peroxide and hydroxyl radicals and from the secondary products. More low-molecular weight material is produced, which differently remains linked to glyceride molecules but do not take part into the cross-linking: the oxidative scission mainly leads to the formation of dicarboxylic acids, dihydroxy acids and hydroxylated monocarboxylic acids (sebacic, suberic, azelaic acids). The major product is azelaic acid, a nine-carbon dicarboxylic acid, which results from oxidative scission of a double bond at C9 in the unsaturated fatty acids (linolenic, linoleic, oleic).

1.3.1 The role of driers

As previously mentioned, to accelerate the polymerization reactions metallic salts, called metal soap or driers, were added in low amounts (0.01-0.5 %) to both oil varnishes and paints (Alphen et al. 1998).
Driers contain transition metals with several oxidation states are called primary driers and act during the oxidation. Co^{2+}, Mn^{2+}, and Fe^{2+} for example belong to this class. Basically, they act as catalyst of hydroperoxide decomposition in a redox reaction called Haber and Weiss mechanism (see the reaction below).

$$M^{n+} + ROOH \rightarrow M^{(n+1)} + RO^{\cdot} + OH^{-}$$
$$M^{(n+1)} + ROOH \rightarrow M^{n+} + ROO^{\cdot} + H^{+}$$

Activation energy required to decompose two moles of hydroperoxides is decreased from 90-170 to 40-50 KJ in the presence of metal catalyst. Metallic salts with only one oxidation state are called secondary and auxiliary driers. Pb^{2+}, Zr^{4+}, and Al^{3+} are secondary driers and active for polymerization (through-drier). Ca^{2+}, K^{+}, and Zn^{+} are auxiliary because they modify the activity of the primary driers.

It was seen that cobalt drier becomes inactive in decomposition of hydroperoxides after relatively short oxidation times (7 or 8 h) due to the carboxylic acid formed in the oil film. After this duration, carboxylic acids have already been formed in the dried oil film and they probably provoke a decrease in the activity of cobalt by complexing Co^{n+} in the form of fatty acid chain carboxylates with low or any mobility at the surface of the oil film (Mallègol et al. 2000).

Summarizing, from the previous descriptions of the different processes involved in autoxidation of lipid materials appears clear that the course and end-products of the reactions are very complex and depend on a variety of factors, including temperature, light, oxygen pressure, the balance of anti- and peroxidative compounds, and the presence and amount of catalysts like (transition) metals. To illustrate the basic processes, a hypothetical scheme displaying the autoxidation of a polyunsaturated lipid as function of time is reported in Fig. 13.

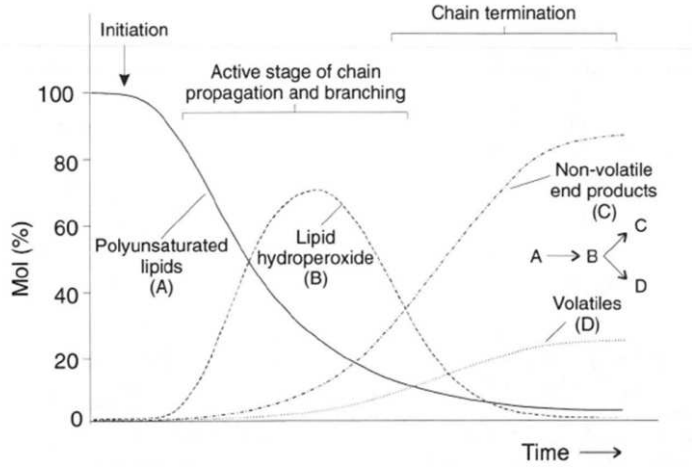

Fig. 13 Schematic time course of the autoxidation of a polyunsaturated lipid showing the various stages in the reaction (Van den Berg et al. 2002).

All these processes involve different reactions, someone will take place concurrently, while others will inhibit each other. This lead to complex kinetics and a large number of different low and high molecular weight oxidation products.

1.4 Oil Paints

In this section, the chemical and physical changes occurring during the initial stage of drying and subsequent ageing of oil paints are reported.
In addition to the processes already described in the previous section, new factors have to be taken in account in a oil paint system. The most important one is the addition of an inorganic pigment to the paint, which has been shown to have a major impact on the chemistry of the paint system. Traditional oil paints were made by grinding pigment in oil on a stone plate, in such a ratio that a workable paint was obtained. Other materials could be added, such as thinner or siccatives, to modify the flow characteristics and the drying properties. In modern paintings were also added fillers and other additives to improve specific properties of the paint, such as storage, working and drying properties (Osmond et al. 2012).
The type and amount of pigment added to a drying oil is an important factor, which influences both the properties of the paint and the overall stability over time. Physical and chemical interaction with the oil can be both depending on the type, the particle size, and the surface properties of the pigments.
The large variety in the nature of the pigments does not make it easy to give a general description of these interaction (Eastaugh et al. 2004). For instance, some pigments, including carbon blacks and the organic earth pigment as van Dyke brown, inhibit the drying process of oil. This is a consequence of minor components of these pigments having antioxidant properties, which interfere with the oxidative polymerisation of the oil. Zinc white, for example, inhibits the initial drying of oil paints and allows oxygen to enter the lower levels of the paint layer, thus eventually creating a paint layer that is drier throughout.
Other pigments, like lead white (basic lead carbonate; $2PbC0_3 \cdot Pb(OH)_2$), Naples yellow ($Pb_3(SbO_4)_2$), azurite (basic copper carbonate;

$2CuCO_3 \cdot Cu(OH)_2$), vermiglion (HgS), verdigris (copper acetate, $Cu(OCOCH_3)_2 \cdot 2Cu(OH)_2$), malachite ($CuCO_3 \cdot Cu(OH)_2$), umbers, red and yellow ochres (mainly $Fe_2O_3 \cdot H_2O$ or Fe_2O_3), the more recent as cobalt blue ($Co \cdot A1_2O_3$), have, in different extent, a catalytic effect on the oxidative degradation of the oil polymer (Rasti and Scott 1980, Meilunas et al. 1990, Van der Weerd 2002, et al. 2005).
All these effects will prevent the formation of an extensively cross-linked polymer, and will produce a paint film which may remain vulnerable indefinitely to solvent action. Clearly, additives to the oil medium, such as wax and natural resins, prevent the extensive polymerisation of the oil if present in large enough amounts. Additives such as these became common in painting techniques during the eighteenth and nineteenth centuries, and paintings from these periods often exhibit solubility problems (Sutherland 2001).

1.4.1 Curing and ageing mechanisms of oil paints

Initial chemical reactions involved in the curing process of the fresh oil paint after application are mainly a result of autoxidation, as previous reported for oil films. This very rapid process involves formation of hydroperoxide-substituted fatty acids, breakdown of the hydroperoxides, giving rise to highly reactive radicals and subsequent cross-linking. The breakdown process is accelerated (catalysed) by the presence of (transition) metals deriving from pigments or driers. The resulting cross-links are covalent ethers, peroxides and carbon-carbon bonds, which are spatially distributed in a 3D network (Van den Berg et al. 2002). Simultaneously, degradation reactions transform the triacylglycerol radicals into volatile low molecular weight (un)saturated aldehydes, ketones, alcohols, acids and hydrocarbons. Some of these products will evaporate and others will be trapped within the paint film for a longer period of time. Due to incorporation of oxygen into the paint film the weight increases and the film becomes more polar. At this point, the oil is finally dried and a very elastic skin, called linoxyn is formed. This is actually a rigid material, but, because of its content of non-drying constituents which act as plasticisers (such as liquid and/or semi-liquid

fractions of saturated triglycerides), the polymeric matrix acquires a particular flexibility. Along time, the action of light, oxygen and humidity proceed and the linoxyn skin becomes very fragile and brittle with the resulting cracks and further powdery consistency. This happens because of the rupture of the polymeric network mainly due to the effect of temperature and humidity. In such conditions, hydrolysis of the initial triglyceride ester bonds (de-esterification) occurs. This produces carboxylic acid groups as either free fatty acids (in the case of acid groups that have not reacted otherwise) or acid groups bound to the crosslinked oil matrix (in the case of acid groups that have engaged in polymerization reactions). These may react with pigments to form carboxylate salts, called metal soaps in the case of a fatty acid.

1.4.1.1 Formation of metal soaps

A mature oil paint can be described as an ionomeric network of metal carboxylates of mono- and dicarboxylic acids. The polyunsaturated moieties in the triglycerides of the fresh oil are activated to radicals that react with oxygen to form a cross-linked network. As the three dimensional network ages hydrolysis of the ester bonds occurs leading to free fatty acids groups, dicarboxylic fatty acids (diacids) and acid-rich network oligomers. These acid groups are immobilised and stabilised by coordination to metals, primarily lead and zinc, originating from pigment or drier, to form metal carboxylate bonds (Van der Weerd 2002, et al. 2005, Boon 2006).

The lead soaps appear to be a very common phenomena in 16th and 17th century painting (Keune 2005, Noble and Boon 2007; Townsend et al. 2007), while the zinc soaps have mainly been noted in 19th and 20th century paintings (Osmond et al. 2005, 2012, 2014; Poli et al. 2014, Van der Weerd et al. 2003). It is worth noting that the process mentioned above regards metal soaps which most likely have formed *in situ*, but they might have been added initially to formulations in some applications, especially starting from the 19th century.

From a chemical standpoint, metal soaps usually contain seven to 22 carbon atoms in the carboxylic chain (Fig. 14) (Robinet and Corbeil 2003).

It was seen that a problem with both zinc and lead soaps is that they can migrate and form soap aggregates. The soap inclusions can grow and protrude from the surface generating effluorescence, embritlement, stiffness of the oil paint (Keune 2005, Keune et al. 2011).

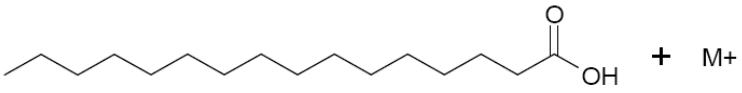

Fig. 14 Palmitic acid and a metal ion can form a metal soap

A scheme in which the lead white particles react with the fatty acids derived from de-esterifying cross linked oil is depicted in Fig. 15.

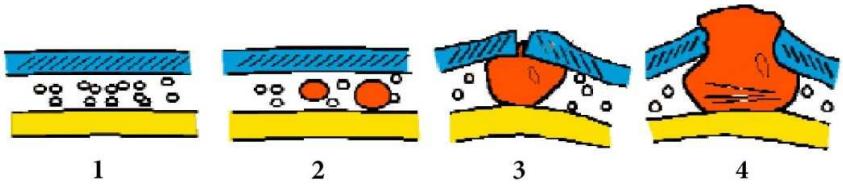

Fig. 15 Scheme of the formation of lead soap aggregates based on the mechanisms presented by Boon et al.: 1) intact paint, 2) early stage with small lead soap aggregates, 3) mature stage with aggregate expansion, 4) protusion with remineralisation. (Boon 2006, Boon et al. 2006; Keune 2005)

Usually, the main components of the inclusions found on paint layers have been shown to be the metal soaps of palmitic and stearic acids (both saturated monocarboxylic acids). Metal soaps of others fatty acids that are found in drying oils, such as dicarboxylic acids and unsaturated monocarboxylic acids, are known, but these species have not been found in inclusions or blooms (Higgitt et al. 2003); it appears, therefore, that only the palmitate and stearate migrate through the film. The absence of unsaturated fatty acids soaps (such as oleate and lineolate) in inclusions may be because they are more likely to undergo cross-linking reactions or decomposition. Furthermore, the dicarboxylic species are much more polar (having much shorter hydrocarbon chains and difunctionality) so their incorporation into the inclusion will not be favoured. The shorter hydrocarbon chain and difunctionality also means that the dicarboxylates

will not be readily compatible with the ordered lamellar structure that is likely to exist in regions containing long chain monocarboxylate soaps.
Similar aggregate masses of zinc stearate and palmitate have erupted through the surface of valuable modern paintings by artists including van Gogh and Mirò (Osmond et al. 2012) and accumulation of zinc soaps at the interface between paint layers has been implicated in adhesive failure and flaking. These physical changes can lead to serious drawbacks for the stability of the paint layers. Soap inclusions may also pose a problem during cleaning and/or revarnishing procedures. Thus, a better understanding of the formation, distribution, and phase separation of inclusions is a crucial issue for the conservation of paintings which show this phenomenon. Restorers and conservators must take care and choose properly how to treat such degraded and water sensitive paint surfaces.

1.5 Cleaning of easel paintings: conventional methods and current situation

In the previous sections, the most representative ageing and deterioration mechanisms of natural varnishes and oil paints has been reported.
The traditional methods of dealing with these problems rely on the use of mechanical means such as scalpels or chemical stuffs. Thus, for instance, the removal of a well-oxidized mastic varnish from a thoroughly dried oil film using, for example spirits of wine has been carried out for centuries. The alternative of using abrasion to break up the friable mastic film has also been a long-standing mainstay of cleaning paintings (Carlyle, 1990). The removal of tough old oil films, as overpaints and retouchings, foresees the use of mechanical methods of scraping or lifting with a scalpel, sometimes combining reagent, solvent, and scalpel methods iteratively and carefully to deplete the overpaint (Sutherland 2001, Mecklenburg et al. 2013). Despite this, they can be very difficult to remove because of their close similarity, in physical and chemical properties, to the underlying paint layers. The ability to selectively remove varnishes, overpaints and retouchings is of course meaningless, without first being able unequivocally to distinguish these additions from original layers (Ruhemann 1958). This is more of an issue for overpaint,

although local varnish residues can sometimes be confused with original glazes.
To date, application of these methods including pure organic solvents and mechanical action are still the main techniques used to remove selectively foreign and undesired components of an easel painting.
From a technical standpoint, the cleaning with solvents involves the softening of the material to be removed, thus requiring a mechanical action to eliminate the swollen, gummy material from the paint surface. This mechanical action is a very challenge procedure when insoluble high molecular weight compounds have to be removed. It is feasible that the cleaning process can take place leaving behind some high molecular weight residues. In this respect, the practice of thinning down a varnish layer may therefore selectively remove the soluble parts of an aged varnish, whereas the less soluble and probably higher molecular weight fractions remains concentrated on the painting (van der Doelen 1999).
A further limitations is related to the solvent penetration into the original paint layers (the average rate is of the order of some μm s^{-1}), especially via capillary action. This undesired process can lead to the well known swelling and leaching processes of varnishes and binders (such as surfactants) proper of the painted surface (Michalski 1990, Burnstock et al. 1992, Phenix 2002a-b). The degree of control, selectivity and discrimination between the original surface and the unwanted layer using these methods are very critical especially in applications where the paint layers are porous and characterized by weak adhesion, craquelure, losses, inhomogeneity, color lifting and structural fragility. These severe restrictions and the knowledge that the free use of organic solvents might be invasive for the paintings and health of restorers, have prompted the research from 80s and 90s, to seek alternative solutions, less invasive, from which have arisen the new classes of soaps, acqueous systems, solvent gels, emulsions and enzymes (Byrne 1991, Burnstock et al. 1992, Stavroudis et al. 2005).
The introduction of gels formulation enable various solvent combinations to be used dependent on the coating being removed and have the advantage of restricting diffusion and penetration through the paint structure. However, it is not always possible to ensure complete removal

of the gelling polymer after its application that must be removed by more conventional means (Stulik et al. 2004, Carretti et al. 2004).
To surpass these limits new methods based on high viscosity polymeric dispersions have been recently developed (Carretti et al. 2010). These rigid systems could be peeled from the surface by means of a simple mechanical action and without addition of a second liquid component. This would reduce the amount of the polymeric residues from the dispersion both on the painting surface and matrix to a greater extent than gels allowing very localized treatment. Recently, a versatile gel-like system for the treatment of art has been prepared from partially hydrolyzed poly(vinyl acetate), borax, and large fractions of ethanol, isopropyl alcohol, n-propyl alcohol, and acetone. Variables such as the concentrations of the two gelating components, the degree of hydrolysis and molecular weight of the polymer, and the type of liquid gelated were investigated to establish formulations of gels with physical and chemical properties that are best suited for specific applications. The gels were designed to have an elastic character that allows them to conform to the topography of complex surfaces and be removed with ease by being lifted from the surface. Results from fluorescence studies demonstrated that the solvent is constrained within the area of the gel, allowing for localized treatments. Polymer and boron residues were not detected after cleaning tests on fresh acrylic and dammar test paint-outs, and on two oil paintings with degraded surface coatings. The efficacy of the cleaning systems was determined visually. Studies of the materials removed during treatments showed that the gels appear to act by softening the coating surface while typically a pass with a solvent-dampened swab after gel treatment removes the softened coating. Studies of the materials removed from a varnished oil-painting suggest that the gels act by softening the varnish layer and facilitate its removal by a swab moistened with a mild solvent. (Carretti et al. 2013, Angelova et al. 2013).
Finally, cleaning results a complex and extremely important process for maintaining and/or recovering the aesthetics of the artwork and prolonging its lifetime without affecting its structural integrity. However, the removal of spirit varnishes, with special remarks to oil resin mixtures, highly polimerised overpaints and retouchings remain open conservation

issues for the chemical cleaning of paintings. One of the most concerning problems is the difficulty on the selective removal of the overpaints that are quite similar in composition to the original layers. Furthermore, it is not said that traditional restoration approaches offer a harmfulness treatment.

On the opposite, this fact has stimulated the scientific research to seek alternative and selective cleaning methodologies. Apart from the latest chemical treatments, over the last two decades, there has been a deepening on the experimental studies addressed to test and develop modern cleaning methodologies based on laser ablation techniques. This technique is a dry and non-contact method which may offer a viable solution since it permits a layer by layer removal at nanoscale. It can be used as standalone method or to complement other restoration approaches. Up-to-date, the selective removal of aged varnishes (spirit or oil varnishes) and oil-based overpaints from easel painting represent the main challenge of laser cleaning. Despite several works were reported since early eighties (Carlyle 1981, Wolbarsht et al. 1990, Hontzopoulos 1993), including systematic investigations on laser interaction effects induced on pigments, binders, and varnishes, as well as some case studies, the laser approach has to be fine-tuned and is still far away to be used conventionally.

Chapter II

LASER CLEANING OF EASEL PAINTINGS: A LITERATURE OVERVIEW

In this chapter the state-of-the-art of the laser ablation techniques focused on the removal of varnish and overpaint layers from easel paintings has been explored. Particular attention has been devoted to highlight the specific contribution of pulsed excimer and solid-state laser sources in conservation of easel paintings. A general explanation of the photo-physical mechanisms involved from UV to IR laser wavelengths using different pulse durations is reported.

2.0 Introduction

Easel paintings represent the main challenge of laser cleaning since undesired and original paint layers are both constituted by similar mixtures of organic and inorganic compounds, which make their discrimination layer-by-layer very hard. Since the early eighties, it was immediately shown an high cleaning potential toward specific conservation issues concerning easel paintings, such as the removal of various deposits (dirt, soot, candle wax etc.), but especially, for removing aged terpenoids varnishes and polymerized oil over-paints (Carlyle, 1981; Hontzopoulos, et al., 1993; Wolbarsht & de Cruz, 1990). The effectiveness of this cleaning method triggered numerous publications

over the past two decades, including systematic investigations on laser interaction effects induced on pigments, binders, and varnishes. Nowadays, many laser systems operating in different spectral regions and pulse durations, including UV excimers, Nd:YAG and Er:YAG lasers have been tested (see Table 1).

Table 1 - List of laser types tested on paint materials from various authors along with their main parameters.

Laser source	**Wavelength**	**Pulse duration**	**Pulse energy**	**Photon energy**	**References**
Pulsed Excimer laser					
ArF	193nm	10–20 ns	0.8 J	6.4 eV	Hontzopoulos, et al., 1993, Zergioti et al. 1997
KrF	248nm	20-50 ns	2 J	5 eV	Hontzopoulos, et al., 1993, Zergioti et al. 1997, Salimbeni et al. 1998, Georgiou et al. 1998, Scholten et al. 2000, Athanassiou et al., 2000, Castillejo et al. 2002, Teule et al. 2003, Theodorakopoulos 2003, 2007, Zafiropulos et al. 2000, 2002, 2003, Castillejo et al. 2003b, Abraham et al. 2005, Mc Glinnchey et al. 2005, Melessanaki et al. 2006, Fotakis et al. 2007, Selimis, et al. 2009; Vounisiou, et al. 2010, Bordalo et al. 2012,
KrF	248 nm	500 fs		5 eV	Zafiropulos et al. 2003, Pouli et al. 2008, Pouli et al. 2010, Oujja et al. 2013
XeCl	308nm	10-20 ns	3 J	4 eV	Carlyle, 1981, Hontzopoulos, et al., 1993, Zergioti et al. 1999, Hill et al. 1999, Mc Glinnchey et al. 2005
XeF	351nm	10–20 ns	0.65 J	3.5 eV	Abraham et al. 2005a, Abraham et al. 2005b
Pulsed Solid-State Laser					
Nd:YAG	213 nm	15 ns 150 ps	7.5 mJ	5.8 eV	Oujja et al. 2010, Oujja et al. 2011, Oujja et al. 2013
Nd:YAG	266 nm	5-10 ns	0.2 J	4.6 eV	Castillejo et al. 2003a, Chappé et al. 2003, Hildenhagen et al. 2003, 2005, Apostol et al. 2011,
Nd:YAG	355 nm	5-10 ns	0.75 J	3.5 eV	Castillejo et al. 2003a, Chappé et al. 2003, Sobott et al. 2003, Hildenhagen et al. 2003, 2005, Abraham et al. 2005a, Abraham et al. 2005b, Apostol et al. 2011,

Nd:YAG	532 nm	5-10 ns	1 J	2.3 eV	Gaetani et al. 2000, Castillejo et al. 2003a, Chappé et al. 2003, Sobott et al. 2003, Hildenhagen et al. 2003, 2005, Abraham et al. 2005a, Abraham et al. 2005b, Mc Glinnchey et al. 2005, Apostol et al. 2011,
Yb:YAG	515 nm	500 fs		2.4 eV	Rode et al. 2008,
Nd:YVO4	532 nm	12 ps		2.3 eV	Rode et al. 2008,
Nd:YAG	1064 nm	5-10 ns 120 ns	2 J	1.2 eV	Gaetani et al. 2000, Pouli et al. 2000, Sansonetti et al. 2000, Castillejo et al. 2003a, Pouli et al. 2000, Pouli et al. 2003, Chappé et al. 2003, Sobott et al. 2003, Hildenhagen et al. 2003, 2005, Abraham et al. 2005a, Abraham et al. 2005b, Schnell et al. 2005, Mc Glinnchey et al. 2005, Apostol et al. 2011, Siano et al. 2012
Nd:YAG	1064 nm	150 ps		1.2 eV	Oujja et al. 2010, Oujja et al. 2013
Er:YAG	2940 nm	100-400 μs	1 J	0.4 eV	Wolbarsht & de Cruz, 1990, deCruz et. al. 2000, Bracco et al 2003, Colombini et al. 2003, Andreotti et al. 2007, Camaiti et al. 2008, Marczak et al. 2008, De Cruz et al. 2014,
Er:YAG	2940 nm	60 μs		0.4 eV	Marczak et al. 2008
Er:YAG	2940 nm	125 ns		0.4 eV	Marczak et al. 2008
Ti:Sapphire	795 nm	120 fs	1 mJ	1.55eV	Zafiropulos et al. 2003, Gaspard et al., 2008, Oujja et al. 2011
Ti:Sapphire	398 nm	150 fs	0.3 mJ	3.1 eV	Oujja et al. 2011
Ti:Sapphire	265 nm	260 fs	40 μJ	4.7 eV	Oujja et al. 2011

Nevertheless, a deeper understanding of the physical processes and mechanisms involved into the interaction of laser light with matter at different wavelengths and pulse durations is still needed for the proper treatment of this type of painted artworks. In the next session an up-to-date presentation of laser cleaning applications focused on the removal of varnishes and overpaints using pulsed excimer and solid-state lasers is reported.

2.1 Pulsed excimer lasers

Excimer lasers emitting at 351 nm (XeF), 308 nm (XeCl), 248 nm (KrF), and 193 nm (ArF), have been widely employed in various disciplines, ranging from industry to medicine up to conservation science. Due to

their submicrometric optical penetration depth in many organic material, excimer lasers have demonstrated high potentialities for material processing, such as the etching of semiconductors and polymers (Dyer & Srinivasan, 1986; Bäuerle 2000, Lippert et al., 2003), for the precise excision of biological tissues (Niemz 2007) and finally, for the cleaning of paintings (Carlyle 1981, Zergioti et al. 1997, Salimbeni et al. 1998, Georgiou et al. 1998, Scholten et al. 2000, Castillejo at al. 2002, Teule et al. 2003, Theodorakopoulos 2003).

This approach, especially for the application on painting's varnishes, is driven by the high absorption and coupling of the UV laser radiation in the outer layers providing controlled ablation with high resolution. At the same time, for the safety of paint underneath, the approach requires that the thickness of the remaining protective coating is greater than the optical penetration depth.

On the basis of structural and analytical examinations, the most studied wavelength is the 248 nm of KrF but also ArF laser (193 nm) has been used for thinning aged varnish with excellent results (Hontzopoulos, et al., 1993, Zergioti et al. 1997). For the latter, the ablation efficiency has been found more high than 248 nm, in the submicrometer scale, which in combination with the low output energy (0.8 J/pulse), makes its use extremely time-consuming. In contrast, irradiation at 308 nm appears to result in significant thermal load to the remaining materials. This difference is in agreement with the lower absorption coefficient of the varnish at 308 nm (Georgiou et al. 1998, Hill et al. 1999). On the other hand, the 248 nm wavelength is shown to be well suited for achieving sufficient etching rates across the layers found in paintings due to the high pulse energy (2 J/pulse) and minimal light penetration (typically as low as 0.1 μm per pulse in depth). Also the thermal diffusion length is estimated to be of the same order of magnitude according to the typical laser pulse duration (20-50 ns) and the low thermal conductivity of the organic matrices involved (Hontzopoulos, et al., 1993, Zergioti et al. 1997, Salimbeni et al. 1998, Georgiou et al. 1998).

The mean ablation rates measured on different types of spirit and oil-based varnish layers, i.e dammar, mastic, copal oil varnish and shellac, span from 0.5 to 1 μm/pulse in a fluence range of about 0.2-0.6 J/cm^2.

Similar etching rates were found in different organic (alizarin) and inorganic (cinnabar, Naples yellow, burnt Sienna, smalt, zinc white) pigmented based-tempera paints models (Castillejo et al. 2002). Such high ablation efficiency can be explained by the intense absorption band of the varnishes at wavelengths below 250 nm. Thus for example, the absorption coefficient of the shellac, at 213 and 265 changes from 8600 cm^{-1} to 500 cm^{-1}, respectively. At 400 nm is negligible with an estimated value of around 120 cm^{-1} , which correspond to an optical penetration depth of about 80 μm (Oujja et al. 2011). Even more important, as reported in section (see Chapter 1 and 3), it is worth noting that during laser interaction with varnish there is an additional factor that must be considered. It was reported that upon aging, natural triterpenoid painting varnishes (i.e. dammar and mastic), which represent the most studied type of terpenoid resin in literature, develop depth-dependent gradients in their absorption owing to oxidation and condensation profiles. The decreasing amounts of cross-links and UV chromophores (unsaturated high molecular weight fraction) across the depth are expected to lead to changes in laser interaction. Thus, it was shown that at 320 nm the absorption coefficient of unaged and aged dammar and mastic films (thickness, 15 μm) shifts from 120-220 cm^{-1} to 1230-1160 cm^{-1}, respectively (Zafiropulos et al. 2000, 2002, Theodorakopoulos et al. 2007).

In any way, with proper optimization of the irradiation parameters, excimer laser cleaning can be a highly selective process with minimal damaging effects to the substrate especially when strongly absorbing materials are ablated using optimal laser fluences. Moreover, without using appropriate irradiation parameters, direct laser irradiation of paint can leads to charring and blackening of the incorporated pigments causing irreparable damage either in tempera that in oil based model systems (Castillejo et al. 2002, Bordalo et al. 2012).

A more detailed description of the processes involved with pulsed ultraviolet lasers has been reported below according to similar mechanisms in polymers ablation. Basically, the cleaning/material removal exploiting UV laser wavelengths include thermal, photomechanical and photochemical effects, which can act

simultaneously and in varying extent. By means of UV laser a photochemical process ($\lambda \leq$ 248 nm) takes place involving direct photolysis and homolytic bond breaking or photodissociation. On the other hand, in this region the photons energy (5-6.4 eV) are high enough to promote the electronic excitation (transition) and dissociation of the most common single and double bonds of organic molecules (Table 2).

Table 2 – Dissociation bond energies for the most common single and double bonds of organic molecules.

bonds	**Kcal/mol**	**KJ/mol**	**eV**	**wavenumber (cm^{-1})**	**wavelength (nm)**
C-C	84	351	3.6	29358	340
C=C	150	628	6.5	52488	190
C≡C	199	832	8.6	69558	144
C-H	98	409	4.2	34187	292
C-O	82	342	3.5	28623	349
C=O	175	734	7.6	61376	163
C-N	66	278	2.9	23235	430
N-H	83	349	3.6	29182	343
O-H	110	460	4.8	38450	260
O-O	35	146	1.5	12200	820
Si-O	110	460	4.8	38450	260

For instance, the weakest (single) bonds in organic molecules have a binding energy of 145 kJ/mol (e.g., O–O single bond), while strong (single) bonds such as C–H are of about 410 kJ/mol. The direct photolysis process leads to the formation of a large number of reactive radicals as intermediates, especially when the "optimum" laser fluence is not used. Upon optimum laser irradiation conditions, the relaxation of the excited compounds desorb in the gas phase and the laser light transmitted across the thickness of a polymer film can be completely minimized.

The extent of thermal effects are primarily determined by the thermal diffusivity of the material processed and from the laser pulse duration. In the nanosecond range (1-100 ns) heat and related thermal processes remain well confined within the irradiated volume. Thus for example, taking into account the range of thermal diffusivity (D_{th}) of the organic material, which span from 10^{-3} to 10^{-4} cm^2/sec, the corresponding thermal diffusion length for nanosecond laser pulses is of about 100-200 nm.

Irradiation with successive laser pulses (N≥100) at fluences below the ablation threshold introduces additional photo-thermal effects, known also as *incubation* effects, that result in vaporization and melting of the remaining film due to insufficient bond-breakage (Srinivasan et al. 1990). On the opposite, photomechanical effects may be dominant when resins, overpaintings or other polymerized materials are ablated with high fluences (>1 J/cm^2). They may cause shielding effects reducing ablation efficiency and inducing an intense photo-mechanical action accompanied by the generation and propagation of stress waves with amplitudes of several hundreds of bars into to the surrounding material. From this standpoint, studies on polymers showed that the shockwave velocity increases with decreasing irradiation wavelength (i.e max. for 193 nm). At the same time the higher photon energy and larger number of absorbing units (chromophores) result in a more pronounced fragmentation and therefore in a larger amount of small gaseous products. In any way, in the optimal range for the overpaints removal, which is about of 1-1.8 mJ/cm^2 upon laser irradiation at 248 nm, the generation of skockwaves and plasma formation can be significant (Zafiropulos et al. 2000). In the case of aged varnish with fluences generally well below 1 J/cm^2, the shock wave mechanism is espected to be of lesser importance (Georgiou et al. 1998, Fotakis et al. 2007, Theodorakopoulos 2009a, 2009b). This process can be simply extended to all the wavelengths and is related to the higher multiphoton absorption in presence of more absorbing units. Nevertheless, the consequences of the induced stress pulses will depend on the substrate's mechanical properties, presence and type of interfaces, binders and pigments. Thus for example, holografic interferometric techniques were used on model systems in order to assess the formation of cracks, detachments or other mechanical defects during the removal of overpaint layers with laser fluences in the range of 0.8-1.5 J/cm^2 (Georgiou et al. 1998, Fotakis et al. 2007). To avoid such collateral effects, an application study using the excimer laser together with a near-IR laser emitting at 1064 nm was carried out in order to remove a multi-layer acrylic overpaint from a 20th century modern painting from the Guggenheim Museum of New York. The painting was part of Ad Reinhardt's "Black Square" series (1966). It had travelled extensively

until the early 1980s, suffered various damages, and was completely over-painted with an acrylic emulsion and a transparent "sealant." Removal of these overpaint layers was not possible with standard conservation methods and therefore a collaboration between IESL-FORTH (Institute of Electronic Structure and Laser of the Foundation for Research and Technology-Hellas, Greece) and the Guggenheim Museum was set up to investigate the possibility of laser cleaning.

The cleaning results showed that the short-pulse IR laser was able to remove the residues of the acrylic overpaint from the oil paint below without inducing significant mechanical stresses or plasma formation. In this occasion, the IR laser was assessed being useful as a follow-up technique after excimer treatment (Mc Glinnchey et al. 2005, Stringari et al., 2007). To establish proper laser cleaning parameters that would give rise to controlled removal of the overpaint layers LIBS spectroscopy was used as a online monitoring tool to signal the end-point of cleaning (Melessanaki et al. 2006). Subsequently, Laser-Induced fluorescence (LIF) and other spectroscopic techniques, such as multiphoton excitation fluorescence (MPEF) and third-harmonic generation (THG) were employed to detect the chemical changes of photosensitive polymeric substrate upon the laser-assisted removal of the acrylic overpaint (Selimis, et al. 2009; Vounisiou, et al. 2010). It was concluded that a fluence of about 1.1 J/cm^2 can photo-chemically affect the doped substrate indicating the start for laser-induced effects. The suggested methodology is proven to reliably and accurately detect potential changes, and thus, it can be employed as a monitoring tool during a cleaning treatment.

Furthermore, as it will be shown in section 2.3, studies regarding the use of femtosecond excimer laser to overcome certain limitations involved with the nanosecond ablation of molecular overlayers from paintings have been reported (Pouli et al. 2008, Pouli et al. 2010, Gaspard et al. 2008, Oujjia et al. 2013). In the femtosecond regime chemical modifications are, qualitatively and quantitatively, highly defined, limited and nearly independent of the material properties, such as the absorptivity and the degree of polymerization/molecular weight. Thus, they can be highly potent in the treatment of molecular substrates, enabling new material

processing schemes that have not been possible with nanosecond laser technology, as for example, processing of ultrathin varnish layers.

2.2 Pulsed solid-state laser

Nd:YAG and Er:YAG lasers are the most commonly used pulsed solid state lasers for easel paintings applications. They represent, to date, a concrete solution for this restoration field due their compactness, flexibility and easy handling. A brief overview on their use in conservation of easel paintings is reported hereafter.

2.2.1 Nd:YAG lasers

Nd:YAG systems, especially the fundamental wavelength, are nowadays diffusively applied in many restoration works, such as historical facades, stone and metal reliefs, ancient archaeological and gilded bronze artifacts as well as wall paintings. This type of lasers typically emit in the near infrared region (NIR) at fundamental wavelength of 1064nm (ω) but can generate four additional harmonics wavelengths at 532nm (2ω), 355nm (3ω), 266nm (4ω) and 213nm (5ω). Generally, these systems can emit pulses with duration ranging from pico to milliseconds. Thus for example, Q-Switch Nd:YAG lasers (1064, 532, 355, 266 nm) emitting pulses of about 10 ns were mostly employed in laboratory tests aimed at assessing the laser-induced effects on pigments, binders, varnishes and their mixtures (Gaetani et al. 2000, Sansonetti et al. 2000, Pouli et al. 2003, Castillejo et al. 2003a, Chappé et al. 2003, Hildenhagen et al. 2003, 2005, Schnell et al. 2005, Oujja et al. 2010, Apostol et al. 2011, Siano et al. 2012). Lead white, zinc white, calcium carbonate, red lead, vermilion, Naples yellow, massicot, orpiment, red ochre, yellow ochre, raw and burnt sienna, malachite, verdigris, chromium oxide, cobalt blue, ultramarine and many others were investigated in powder form as well as in oil and protein based media. The studies carried out on such painted models have shown that in general highest discoloration thresholds occurred tipically at 1064 nm in contrast with highest sensitivity (lowest thresholds) at lower wavelengths (Chappé et al. 2003, Sobott et al 2003). On the other hand, different interaction mechanisms take place depending

on the irradiation wavelengths and pulse durations. In this spectral region, the photon energies (see table 1) is not high enough to breaking bonds of the constituting organic or inorganic material. For visible and near infrared wavelength the typical values of the optical penetration depth (δ) range from several nanometers of a metal, up to tens or hundreds of micrometers in pigmented paint layers. On the opposite, unpigmented varnish coatings can be practically considered transparent in this spectral region. At this wavelengths back and forward scattering is dominant and most of the absorbed energy is dissipated through the thermal channel. The main direct effect of the laser irradiation is a temperature rise within and in proximity of the irradiated volume. Hence, the material removal process is mainly driven by photothermal and photomechanical effects that may come significant at higher fluences due to the direct ionization or photodissociation of molecules. In the ns range, as like for pulsed excimer lasers, the laser treatment of paint surfaces with the fundamental and second harmonics (1064 and 532 nm, respectively) may induce various degrees of discoloration on paint layers. Generally, thermal degradation, phase changes or charring followed by darkening or bleaching of the painted surfaces (Castillejo et al. 2003, Pouli et al. 2003) are undesired phenomena that can take place. These effects are induced on pigments and transferred to the organic matrix, which absorbtion coefficient can be expected negligible in the NIR infrared wavelengths region. According to literature results, efficient ablation of the outermost varnish layers is achieved upon irradiation in the UV (266, 355 nm) without potentially disturbing the inner paint layers. Most recent advances have also pointed out that ns irradiation at 213 nm preserves the color of the tempera paint during the ablation of the outermost varnish layer. In addition the etching depth results sensibly better if compared with that achieved by KrF laser emitting at 248 nm (Oujja et al. 2011).

On the opposite, it was reported that for removing overpaints layers longer wavelengths are more suitable due to the higher degree of discrimination between different materials. Generally, the thickness of a varnish layer ranges from 5 up to 30 μm while that of an overpaint is usually of the order of 50-200 microns. For this reason, ablation with

laser wavelengths of 532 and 1064 nm results more efficient than UV shorter wavelengths (Hildenhagen 2003, Ciofini et al 2014).

2.2.2 Er:YAG lasers

A concrete alternative to UV lasers, in terms of exploiting low optical penetration, relies on the use of pulsed Free Running (FR) Er:YAG (2.94 μm) laser whose ablative action is based on the photons absorption through the resonance of vibrational energies of –OH bonds. On the other hand, in the mid-infrared region (MIR), which extension covers the frequency range from 4000 to 500 cm^{-1} (2.5-20 μm), falls the main vibrational transition modes of the organic molecules (see Table 3).

Table 3 – Stretching (ν) frequencies of IR absorption bands in varnishes and binding medium frequently used in paint layers.

bonds	**Kcal/mol**	**KJ/mol**	**eV**	**wavenumber (cm^{-1})**	**wavelength (nm)**
νO-H,ROOH, νN-H,	9-10	38-42	0.4-0.43	3200-3500	3125-2850
νC-H	8.1-8.4	34-35	0.35-0.36	2850-2950	3510-3390
νC=O, COOH	4.7-5	20-21	0.2-0.22	1650-1740	6060-5750

The photon energy at this IR wavelength is of about 0.4 eV not high enough for O-H bonds dissociation , which require an energy range from 3.4 to 4.5 eV. Furthermore, the irradiance of the laser is too small to allow a multiphoton effects, which might provide the necessary dissociation energy. In this way photons transfer their low energy to OH molecular bonds breaking bonds by the laser-induced vibrational excitation and causing swelling of polymers. Using Er:YAG laser, the main absorber as reported in table 3, is the OH in water (α=104 cm^{-1}) or in other solvent mixtures applied on the surface during the treatment. This wavelength is also absorbed by the carboxylic (ROOH) and amide groups (NH) often encountered in oil and proteinaceous binding media.
Similarly, experimentations using FR Er:YAG laser pointed out the occurrence of thermal side effects when directly irradiating the paint layer (Bracco et al 2003). Problems arise from the lack of thermal confinement due to the long pulse duration (200-400 μs), whose corresponding thermal

diffusion length is above one order of magnitude larger than the optical penetration depth in typical materials of interest. Recently, the temperature rise achieved upon laser irradiation with FR (120 μs) Er:YAG was measured using a thermocouple (De Cruz et al. 2014).
It was shown that the increase in surface temperature for the removal of old oil patina and varnishes is equal to $\Delta T=15$ °C when using isopropanol as wetting agent and a fluence of 0.2 J/cm^2 and 7.5 pulse/s. In this way, the original paint layer was not affected by the laser irradiation, even when the drying process was complete. Clearly, if the ablation is performed without solvents, the increase in surface temperature is higher, about $\Delta T=53$ °C, and though the ablation is effective, it is not considered suitable for the constituents of the underlying paint layer.
Despite the thermal effects are not confined, in the field of Cultural Heritage it has been widely employed. For instance, as a tool for the selective micro sampling of organic painting material (Colombini et al., 2003) and for cleaning applications on polychrome surfaces such as canvas and panel paintings (Wolbarsht et al. 1990, de Cruz et. al. 2000, Bracco et al. 2003, Andreotti et al., 2007). Preliminary treatments were carried out for the removal of mastic and dammar varnishes, linseed oil/sandarac varnishes, Paraloid B72 (acrylic resin), oil-based over-painting and protein based material on canvas and wooden panel paintings. Further investigations based on the OCT (Optical Coherent Tomography) analysis of Er:YAG ablation crater in varnish were carried out testing three pulse operation modes: QS (125 ns), SFR (60 μs) and FR (120 μs) (Marczak et al. 2008). However, systematic laboratory tests were initiated in order to investigate the laser-pigment interaction effects and the effectiveness of Er:YAG laser in the removal of aged varnishes and other protective coatings. At present, some pigments and some organic compounds used as varnishes or binder have been tested (Camaiti et al. 2008). However, chemical and chromatic behaviour of pigments and paint layers under laser irradiation is far to be completed. From the above discussion, it can be concluded that some of the approaches under investigations appear promising, especially those based on shorter laser pulses that can certainly lead to confine the thermal effects within the irradiated volume.

2.3 Ultra-short lasers

An additional perspective over nanosecond (ns) laser pulses is based on the use of ultra-short lasers emitting pulses of picoseconds (ps) and femtosecond (fs) pulse duration, which have been recently introduced in the field. They offer the possibility of processing of even transparent substrates optimizing the morphological aspects (melting, bubbling, crack formation, etc.) due to the minimization of photo-thermal, photo-mechanical and photochemical phenomena. More specifically, previous studies on tempera paints using Ti:Sapphire laser that emits pulses of hundreds of fs at 795, 398 and 265 nm have shown that a high degree of control may be achieved in comparison to using pulses of 25 ns at 248 nm. The modifications induced by 120 fs pulses at 795 nm were examined in unvarnished aged model temperas constituted by cinnabar and chrome yellow that are very photosensitive pigments. Irradiation at fluences below the ablation thresholds results in various degrees of discolouration and chemical changes as monitored by FT-Raman, micro-Raman and laser induced fluorescence spectroscopies. The chemical modifications are due to the photodegradation of proteins and lipids participating in the composition of the egg yolk-based binding medium. It is shown that the extent of chemical changes in the binder is affected by the presence of the pigment. Effects of fs irradiation in the colorimetric and spectral features of the pigment itself depend strongly on its composition, as shown by the different behaviour of cinnabar and chrome yellow. In all cases no build-up of extra bands of amorphous carbon (indicative of carbonization or charring) takes place, in contrast with previous observations upon irradiation with 248 nm, 25 ns pulses. The differences with these previous studies illustrate the participation of mechanisms of diverse origin in the ns and fs domains and the prevalence of multiphoton absorption processes in the latter (Gaspard et al. 2008). At the same time, processing by Ti:Sapphire irradiation (795 nm) with pulses of 100 fs has turned out to be ineffective for varnish removal (shellac) as well as the second harmonic at 398 nm (Oujja et al. 2011). However, irradiation at 248 nm and with 500 fs laser pulses results in an improved etched morphology as compared with results achieved with ns pulses of

the same wavelengths (Pouli et al. 2008). For the varnishes examined, material removal by Ti:Sapphire irradiation can be achieved only at fluences in excess of 2 J/cm^2. In addition, material removal is achieved after a significant number of pulses, evidently as a result of the accumulation of absorbing products (Pouli et al. 2008).

More recently laser irradiation of the unvarnished tempera samples was also carried out using two Nd:YAG laser systems emitting pulses of 150 ps at 1064 and 213 nm, respectively, and of 15 ns at 213 nm (Oujja et al. 2010). The ablation thresholds generally are higher at 1064 than at 213 nm, due to the increase of the effective absorption of both the binding medium and pigments upon irradiation in the UV region. The discoloration effects and chemical changes prior to ablation thresholds of pigments are most pronounced for longer wavelengths. These differences are attributed mostly to the absorption coefficients of the organic component, which are very high at shorter wavelengths (10^3-10^4 cm^{-1}) becoming negligible at longer wavelengths (i.e at 1064 nm) and less importantly from ns to ps laser pulses. Irradiation of varnish layers at 265 nm with 260 fs pulses (100 pulses) can induce a loss of glossy of the remaining varnish which acquires a whitish appeareance while at 213 nm with 15 ns pulses (single-shot) the film maintains its transparent appearance. In clear contrast with the induced modifications of color resulting from irradiation of the varnished systems with UV fs pulses, ns irradiation at 213 nm preserves the color of the tempera paint under the thinning of the outermost varnish layer. In addition the etching depths result sensibly better if compared with those achieved by KrF laser (Oujja et al. 2011).

The varnish removal under multiple pulse (N≥100) irradiation at 265 nm (260 fs) and single pulse irradiation at 213 nm (15ns) allows the selection of a fluence range in which partial elimination of the varnish layer would in principle safeguard the underlying paint. Measurements of removed layer thickness yield values of about 5 and 2 μm (out of a total 10 μm thickness) under the indicated fs (265 nm) and ns (213 nm) irradiation conditions.

Actually, it has been concluded that the use of long wavelengths (>250 nm) and pulse durations (ns) favors the thermal heating of the irradiated

area, thus inducing the strong mentioned side-effects. It was found that the induced modifications may be minimized when using laser pulses in the ns, ps, fs domains with wavelengths shorter than 250 nm. On the other hand, the parameters to ensure a safe laser cleaning of paintings relies on the efficient coupling of laser energy to the unwanted layer, a condition that can be fulfilled when the laser wavelengths fall within the high absorbance spectral region of the material to be removed (Oujja et al. 2011).

In addition, it was seen that in presence of a thin film of binder in the uppermost paint layer, the laser induced effects are attenuated if the applied laser wavelength is efficiently absorbed by the binder. Thank to the effective channeling of the photon energy to the binder, it is possible to protect the pigments against possible chemical alterations. Hence, the nature/composition of the paint (binder and pigments) will determine which effect of the two is dominant: change of the pigment chemical composition or degradation of the binder.

In spite of the obvious advantages of applying ultrafast, high-repetition-rate lasers to the conservation of artworks and heritage objects, there are still a few issues (top-hat beam, beam delivery, compact instrumentation etc.) to be addressed for the integration in the field of this powerful technology.

Chapter III

PHOTO-OXIDATIVE DEGRADATION OF SOLVENT AND OIL VARNISHES

The understanding of photo-induced effects (photoxidation, cross-linking, radical polymerization) of painting varnishes, under extreme accelerated lighting conditions, is crucial for optimizing new conservation practices based on laser ablation techniques. In this chapter, photo-induced ageing effects of tri (dammar and mastic), di (sandarac, colophony, copal) and sequiterpenoid (shellac) resins, prepared as spirit and oil mixtures, have been assessed. The oil mixtures were formulated heating resin and linseed oil at high temperature. Once casted on suitable supports, the varnish films were photo-aged by artificial sunlight (above 290 nm) for an overall period of 500h. Trasmission FTIR spectroscopy, colourimetric and gravimetric measurements were used for monitoring the photo-induced effects. After accelerated light ageing the samples were exposed to free oxygen laboratory conditions and subsequently, stored in the dark (inside a drawer) where autooxidative reactions and yellowing occur.

3.0 Introduction

Varnishes were usually applied on panel and canvas paintings as protective coatings and to enhance both the color saturation and the overall gloss (de la Rie 1987, Mills and White 1994, Elias et al. 2006). Resins mixed with a drying oil were the earliest type of varnish blend

used in the Middle Ages whereas the so called “spirit varnishes” were introduced for commercial purposes only later in the sixteenth century. Nevertheless, oil-resin varnishes were still in use as late as the nineteenth century (Mills and White 1999, Sutherland 2001, 2003).

Materials and preparation procedures have undergone a continuous evolution over time, according to the different artistic and/or restoration needs. As regards the painting varnishes, numerous recipes are reported on historical treatises and artist' accounts (De Mayerne 1901, Theophilus 1961, Cennini 1954, Merrifield 1849, Eastlake 1847). The most relevant resins employed involve complex mixtures of terpenoid compounds, which can be grouped according to their number of carbocyclic rings, as like sesquiterpenoids (compounds with 15 carbon atoms, i.e. shellac), diterpenoids (compounds with 20 carbon atoms, i.e. colophony, Venice turpentine, sandarac, copal) and triterpenoids (compounds with 30 carbon atoms, i.e. mastic, dammar, elemi) (Mills and White 1999). For preparing oil varnishes, such terpenoid resins were mixed with a drying oil, mainly poppy, nut and/or linseed oil, and heated at elevated temperatures (300-350 °C). Both spirit and oil varnishes undergo natural ageing processes that lead to yellowed products (unsaturated high molecular weight fraction) which can obscure colours, craze and become very brittle and insoluble over time. Many factors can influence these chemical and physical changes as the manufacturing treatments, the nature of the substitutents, material impurities, driers, the type of the interactions with other molecules and lastly, the conservation conditions (light, humidity, temperature, pollutants). Since natural aging is believed often to be initiated via photolytic reactions, this work is aimed at reproducing in some extent such natural processes on a large number of representative varnish samples following a systematic ageing procedure.

Considering that the quantum energies associated with light wavelengths of 300-400 nm are sufficient to break the chemical bonds in most polymers (Allen et al 1992), an artificial sunlight simulating outdoor exposure conditions (cut-off, 290 nm) has been chosen to accelerate cross-linking and polymerization reactions (Fotakis et al 2010).

3.1 Experimental

3.1.1 Formulation of solvent and oil varnishes

Solvent and oil-based varnishes were formulated on the basis of recipes reported on historical treatises and artist' accounts. All the materials selected (purchased from Zecchi, Florence) are listed in Table 1.

Table 1 List of solvent and oil-mixtures varnishes along with their composition and weight % ratios. Concentration of cobalt drier in linseed oil is lower than 0.05 %.

Resin	**Binder**	**Solvent**	**Wt % ratio**
Dammar	-	white spirit	30/70
Chios mastic	-	iso-propanol	30/70
Colophony	-	ethanol	30/70
Sandarac standard	-	ethanol	30/70
Light shellac (bleached)	-	ethanol	30/70
Chios Mastic	Linseed oil (Co)	Rectified turpentine oil	30:20:50
Colophony	Linseed oil (Co)	Rectified turpentine oil	30:20:50
Sandarac standard	Linseed oil (Co)	Rectified turpentine oil	30:20:50
Manila Copal	Linseed oil (Co)	Rectified turpentine oil	30:20:50

Solvent-based varnishes have been formulated with a 30% (by weight) of grinded natural resin, dissolved in the appropriate solvent and stirred for 1 h. When needed, an ultrasonic bath was used to speed up the dissolution process. Among the classes of resins under study, different solubility properties have been noticed. Thus, dammar resin was well soluble in chloroform even if some problems during its film formation were encountered, mainly due to the high volatility of the solvent ($T_{b.p.}$=61°C). Using the latter, the curing process was so fast to produce the rapid growth of bubbles along with the lifting and cracking of the varnish film especially if lying in thick layers. To prevent this, it was firstly chosen to dry the samples under vacuum conditions without achieving satisfactory results. The problem was resolved formulating a new varnish solution using white spirit (Tb.p.=150-200 °C), which produced a flat and high quality film.

The mastic resin both in ethanol and in iso-propanol formed a whitish insoluble residue similar to a waxy compound. It was therefore decided to use iso-propanol that allows obtaining a more clear solution than ethanol.

According to their composition, fresh sandarac, shellac and colophony resins revealed good solubility properties in ethanol, even if colophony dissolved in chloroform changed color from yellow-orange to brown. Manila copal exhibited remarkable differences of solubility with respect to the other diterpenoid resins. It was diluited up to 20% in chloroform obtaining a dense and waxy solution that was hardly spreadable as thin film. However, as reported in many ancient recipes, copal does not dissolve in the usual organic solvents but it may be preferably cooked heating the resin together with a drying oil up to the melting temperature (Dieterich 1920).
The linseed oil mixtures (see Table 1) were prepared according to traditional varnish recipes by heating the oil and the resin in separate pyrex containers using a sand bath (Gerhardt sand bath –type HS) (Fig. 1). The latter allows a gradual heating with a precision of 5 °C in the measuring range 25-400 °C temperature. Linseed oil containing a concentration of cobalt drier less than 0.05% was supplied by Zecchi (Florence). Cobalt drier reduce the induction time during the curing process (Mallegol et al 2000).

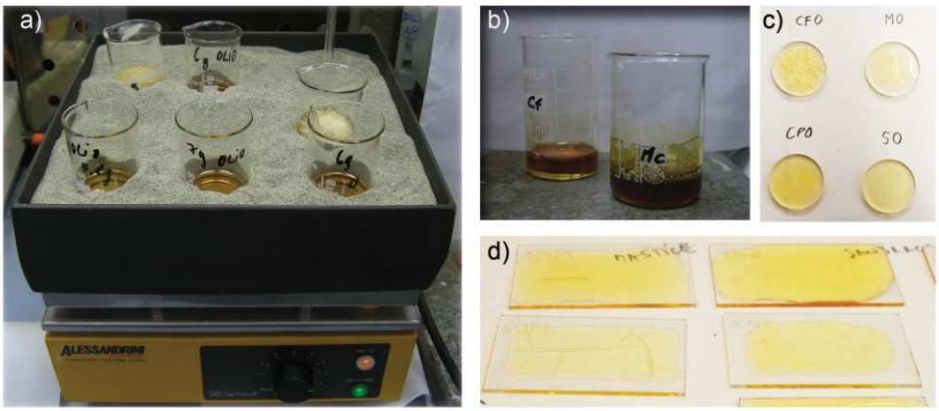

Fig. 1 - Formulating linseed oil mixtures in a sand bath a), a detail of the final product b). Linseed oil-resin varnishes films after casting on glass slides c) and on synthetic round quartz plates d).

Colophony and mastic resins were observed to start the melting at about 120 °C while sandarac and copal the softening at about 150 °C. At this

point, the oil heated simultaneously in the sand bath was mixed with the melted resin. The oil-colophony and oil-mastic mixtures were heated up to 220 °C while the oil-sandarac and oil-copal mixtures up to 285 °C and kept both to these temperature for about 15 minutes. After that, the mixtures were allowed to cool slowly in the sand bath until up to 60 °C when rectified turpentine oil was added in 1:1 wt % ratio with respect to the weight of the oil-resin mixture. Once cooled, the varnishes were filtered in order to isolate the insoluble residue (polymeric component) and introduced into dark bottles and closed hermetically with parafilm. The yield for the single varnishes differed: for mastic and colophony it was almost 100 %, while for the sandarac and copal less, around 50 %, due to of a gelatinous residue.

All the formulations were uniformly casted by means of graduated micropipettes on three different substrates; glass slides (2.6x4.5 cm), potassium bromide (KBr) and round quartz plates (∅=2.5 cm, 2.5 mm thick). Samples casted on glass plates were applied in different amounts of varnish solution, exactly 0.8, 0.4, 0.2 mg, in order to evaluated the morphological changes and the weight losses during accelerated photo-ageing. Each substrate has been cleaned in an ultrasonic bath, successively in acetone, ethanol and then dried.

For obtaining homogeneous films, the curing was primarily carried out on a leveled plane for one month under controlled laboratory conditions. To speed up the drying process, samples were then put in a ventilated oven at 25°C for 24 h without light and dried in *vacuo* until a constant weight was reached. This was taken as the starting time (t_0) for the gravimetric measurements.

Additionally, the varnish formulations shown in Fig. 2 and listed in Table 1 were applied also on primed linen canvas constituted of a commercial blend of calcium sulphate and calcium carbonate binded with rabbit skin glue. The pigment to binder ratio was about of 90/10 wt%. Such substrate was considered very suitable to evaluate the discolouration effects, as like yellowing or bleaching processes, during the over irradiation time. Each varnish solution was spread by brush in order to obtain a film thickness of 20-30 μm. A general picture of the varnished and unvarnished (reference) quadrants is shown in Fig. 2.

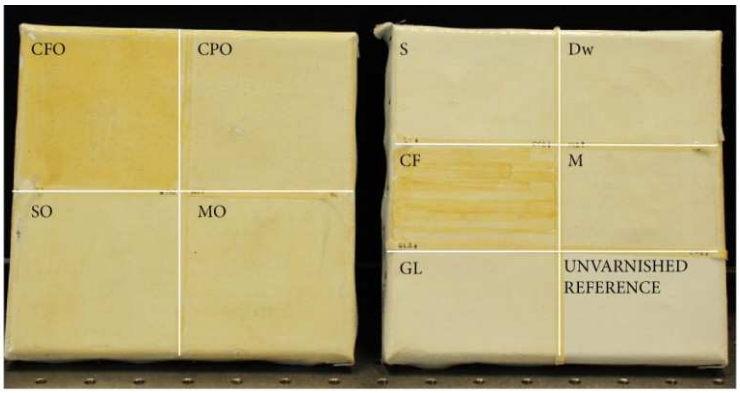

Fig. 2 Image of linseed oil mixtures (left) and solvent based varnishes (right) after applying on grounded canvas mounted on wooden stretcher. Each quadrant refers to a varnish formulation reported in Table 1 while the unvarnished one has been chosen as reference.

3.1.2 Accelerated ageing

In order to study the effects of the irradiation under accelerated lightning conditions and for increasing the rate of cross-linking, after a curing time of 1 month samples were artificially light-aged using a SOLARBOX (CO.FO.ME.GRA model 3000e) equipped with a continuous-wave (cw) air-cooled Xenon Lamp (Fig. 3).

Fig. 3 Xenon test chamber (CO.FO.ME.GRA model 3000e) and its spectral irradiance E in W/(m^2·nm) as function of the wavelength using indoor (blue line) and outdoor (red line) UV-filters.

Irradiation uniformity is guaranteed by a parabolic reflector chamber with the Xenon Lamp in the focus. The outdoor type UV-filter with a cut-off of 290 nm was used to imitate direct sunlight radiation and thus simulating and accelerating the oxidation and cross-linking processes as found on aged varnishes. Irradiance was kept at 50 mW/cm^2 and the temperature of the Black Standard Thermometer (B.S.T) at the surface of the samples did not overreach 50 °C, which is slightly above the glass transition (T_g) temperatures of these varnishes, but below the temperature necessary for purely thermal breakdown. The artificial ageing was carried out for an overall time of 500 hours.
The infrared and UV-Vis reflectance spectra were collected to monitor the ageing process exactly after 0, 20, 34, 52, 77, 102, 125, 150, 200, 252, 347 and 500 hours. Measurements corresponding to time zero refer to those collected after one month from the varnish formulation, when all samples were dry to the touch. At the end of the artificial ageing samples have been left under controlled laboratory conditions (T=20 °C and RH=45 %, E=80–100 lx) and then stored in the dark.

3.1.3 Gravimetric measurements

Weight losses of varnish coatings induced by polymerization and degradation reactions were determined gravimetrically using a microbalance with a readability of 0.01 mg.

3.1.4 Colorimetry

The specimens' surfaces were characterized by Konica Minolta CM-700d portable spectrophotometer equipped by Spectra Magic NX software. The CIE 1976 L*a*b* color parameters have been calculated considering 10 degrees CIE standards observer values, the illuminant D65 with specular component included (SCI) and excluded (SCE). The acquisition range is from 400 nm to 740 nm with a spectral resolution of 2 nm. Data were collected using a round target mask of 6 mm diameter.
For solvent-based varnishes the specimen was subdivided into 6 portions. Five portions were treated with varnishes (sandarac, colophony, shellac,

mastic, dammar); the last sector was left unvarnished as white reference (see Fig. 2). Each specimen portion was subdivided into 24 sectors (4 × 6, A-D × 1-6). Three measurements, each shifted horizontally by a 1 mm distance, were performed for a single sector, yielding total of 24 × 3 = 72 measurements for each specimen portion and 72 × 6 = 432 measurements. For linseed oil mixtures the specimen was subdivided into 4 portions, as shown on the left in Fig. 2. In this case, were performed 36x3=108 measurements achieving an overall number on four varnish type of 108x4=432.

3.1.5 Fourier Transform Infrared Spectroscopy

FTIR (Fourier Transform Infrared Spectroscopy) measurements were performed by means of Perkin Elmer - System 2000. The infrared spectra were collected in transmission mode on KBr discs from 4000 to 370 cm^{-1} with a resolution of 2 cm^{-1}. Spectra were acquired following three scans of 100 s and have been converted and plotted in absorbance units (Abs) following the Lambert Beer's law (Abs=-logT) (Derrick et al. 2000, Hesse et al. 2008). Spectra are presented without normalization, baseline corrections or smoothing filters. The photo-degradation kinetic of the prepared resin films were studied integrating the absorption bands, total-area, corresponding to the main stretching modes, such as the OH, CH and C=O regions. For each band has been chosen the same baseline points ranging between 3700-3100, 3100-2700 and 1900-1550 cm^{-1} for the OH, CH and C=O stretching bands, respectively.

3.2 Results

3.2.1 Gravimetric measurements

Fig. 4 shows the weight residue of the solvent based varnishes at different ageing times on glass plates containing 0.2 mg of casted varnish. For colophony in chloroform was decided to stop the ageing at 20 h since the rapid changes in the physical and chemical properties were considered in a larger extent with respect to the other varnish films.

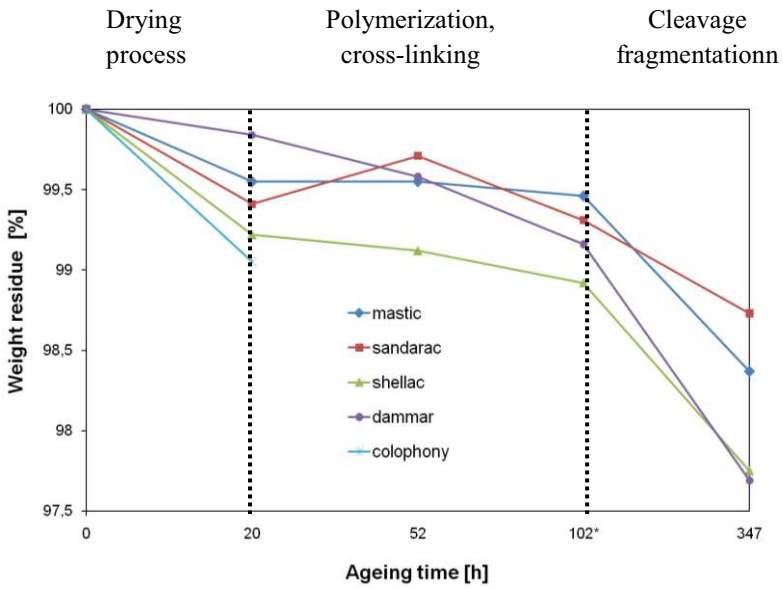

Fig. 4 - Weight residue of varnishes applied on glass as function of ageing time

It is worth noticing that all the samples, at the time zero, were dried in *vacuo* for 24 h thus drastically reducing any problem related to the presence of solvent retained in the bulk. In addition, the FTIR spectra at time zero did not show the presence of solvent residue and surely, during the early stages of ageing (after 20 h) the solvent was completely evaporated. In any way, one could be expected a weight rise due to oxygen uptake during the initial stage of the photo-oxidation, especially for the resins that are more prone to polymerization and cross-linking.

Thus for example hydration of di and triterpene double bonds and hydroxylation of triterpene keto group. On the contrary, the weight loss is quite negligible until 102 h (less than 1% by weight) of ageing after that decreases rapidly. At 347 hrs becomes more pronounced ranging from a minimum of 1.27% for sandarac to a maximum of 2.2-2.3% for shellac and dammar resins, respectively.

As observed by FTIR spectroscopy, during the photo-ageing the decreasing in the CH bands at 2955 and 2875 cm^1 were accompanied by a intensity increasing and broadening of the hydroxyl region (2700–3700 cm^1), carbonyl region (1400–1900 cm^1) and fingerprint region (600–1300 cm^1). These chemical modifications are caused by radical polymerization reactions of the varnish film leading to the strong loss of its starting mechanical properties. Thus, the resin film during light-induced ageing becomes more brittle and hard inducing also an evident cracking network, which is very pronounced in di and triterpenic resins and absent in the shellac resin.

The photo-induced polymerization process explains the slight decreasing of the polymer's molecular weight which is accompanied by the loss of volatile compounds, such as the evaporation of monoterpenes, low molecular weight terpenic degradation products and degradation products of the polymeric fraction. In addition, shortening of the side chain and bond breaking along with the degradation of the terpenoid carbon skeleton can take place during the exposure under high light fluxes.

As a consequence of this change the material becomes more brittle, with a reduction in its tensile, impact and elongation strength. Furthermore, discoloration and loss of surface smoothness are morphological changes accompanying photo-oxidation.

Such structural and morphological changes may resemble, in some extent, the physical properties of the varnish coatings found in old paintings.

3.2.2 Colorimetry

Fig. 5 displays the evolution of coordinates a^* and b* for mastic, dammar, sandarac and shellac as function of the ageing time. For comparison

purposes, the colour changes for colophony resin has been reported only in the text due to drastic yellowing just only after 20 h of photoxidation.

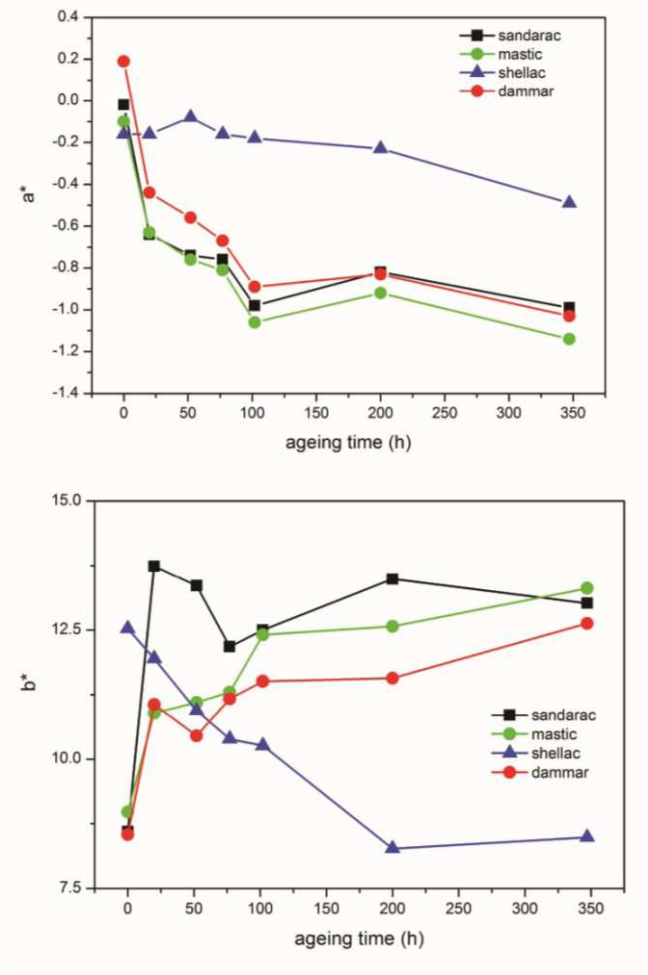

Fig. 5 a* and b* coordinates of solvent varnishes as function of the ageing time.

The fluctuations of a* factor span in a very narrow range from 0.2 to-1.2. Mastic, dammar and sandarac show a similar decay pattern suggesting a small shift toward the green direction. A very different behavior has been measured for shellac resin that shows a negligible decrease. This fact explains what observed in the b* coordinate whereas shellac exhibits an opposite trend with respect to others varnishes. In detail, the b* coordinate decrease for shellac suggests a bleaching effect, most probably

linked by its different composition. Mastic, dammar and sandarac undergo the same colour change moving toward a yellow component. It is worth noting that the trend for sandarac is slightly different in the first 50 h. This rapid yellowing suggests most probably a faster oxygen uptake than the other varnishes.

The evolution of the L parameter and the overall colour variations (ΔE) have been also reported (Fig. 6).

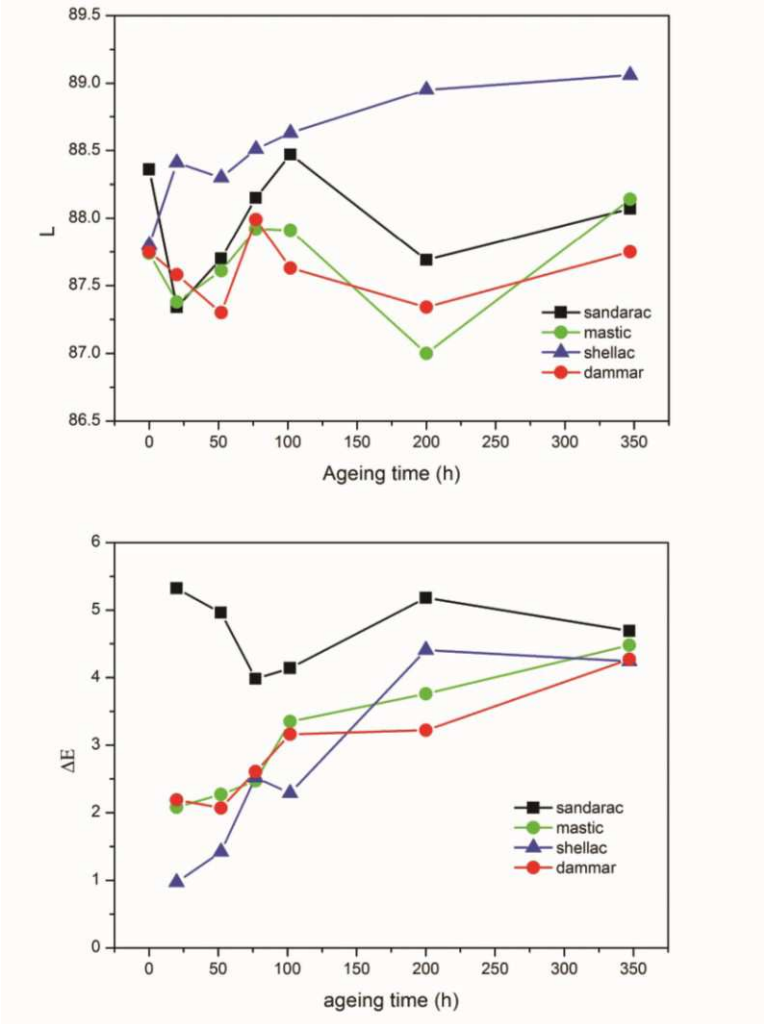

Fig. 6 L coordinate and total colour variation ΔE as function of the ageing time.

The behavior of L coordinate confirms as previously shown. Shellac resin tends to brighten up during the exposure to intense light while the other ones does not undergo noticeable changes in brightness. The total L variation is comprised between 87-88.
Concerning with colophony resin, it showed at t_0 time an a* value of -1.09 which raised up until 0.84 after 20 h of exposure. In the same time range, b* varied from 12.85 to 32.29, L from 88.6 to 81.65 and the ΔE was 18.66 just only after 20 h. These changes indicate a strong shift toward a deep brown-orange tones which could be well appreciate also to naked eye. This trend is in agreement with what reported in literature about pine resins. Among these, especially pine colophony, has the notoriously bad reputation of darkening and becoming brittle over time (Scalalarone et al. 2003, Theodorakopoulos 2005).

3.2.3 Fourier Trasform Infrared Spectroscopy

Photo-induced ageing of terpene compounds involves several modifications at molecular level, as shown by transmission FTIR spectroscopy along the whole spectral range. Specifically, the main interested parts are: the hydroxyl region (2700–3700 cm^{1}), C-H stretching region (2850-3000 cm^{-1}), carbonyl region (1500–1900 cm^{1}) and fingerprint region (600–1300 cm^{1}). A list of the frequency assignments of the absorbing bands which change with ageing is presented at the end of the section in Table 2.

3.2.3.1 Triterpenoid resins: mastic and dammar

Fig. 7 displays the FTIR spectra of the mastic (pre-dissolved in isopropanol) and dammar (pre-dissolved in chloroform) resin films, showing the temporal evolution induced by the ageing on the characteristic stretching bands. The dammar film dissolved in white spirit (results not shown) followed the same photo-degradation pathway but with a slower oxidation rate.
As shown, the wide O-H stretch vibrations increase in intensity and broadens during the overall irradiation time. Additionally, a noticeable

band shift from 3410 to 3440 cm^{-1} and 3417 to 3442 cm^{-1} respectively in mastic and dammar light-aged resins was observed. Furthermore, the growth of shoulder-peaks at about 3230 cm^{-1} and at 2600 cm^{-1}, in both the aged triterpenoids resins, could be related to the formation of carboxylic acids groups via condensation reactions (de la Rie 1988, Theodorakopoulos et al 2007, 2005). Carboxylic acid groups also have an absorption band in carbonyl stretching region.

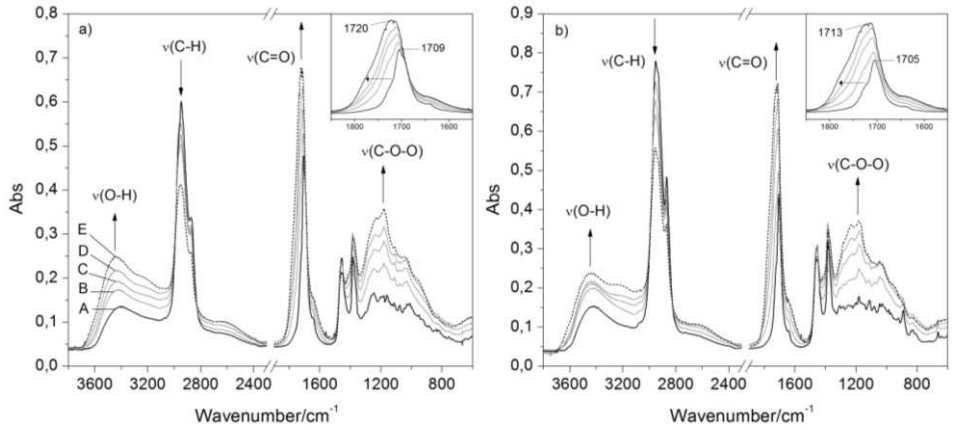

Fig. 7 Trasmission FTIR spectra of mastic a) and dammar b) films in the wavenumber ranges of 3800-2300 and 1900-600 cm^{-1} at different ageing times (A, t=0; B, t=20h; C, t=52h; D, t=102h; E, t=500h). The arrows show the changes of the main vibrational groups induced by the irradiation while in the inset, the shift and the broadening of the carbonyl band is highlighted.

The inset in Fig. 7 shows an intense increase and a notable broadening of the carbonyl C=O stretching bands, assigned to the carbonyl stretching vibration of aldehydes, ketones, and carboxylic acids. Carbonyl band results also shifted toward higher frequencies respectively of 11 and 8 cm^{-1} for mastic and dammar resins, which can be related to new intermolecular interactions, as the formation of hydrogen bonds.

The carbon double bond (C=C) stretching at 1640 cm^{-1} is only weakly affected by ageing, tough it is slightly broadened and enhanced in both the tritepenoid resins. Nevertheless, such modifications does not justify possible isomerization reactions of isolated double bonds into conjugated

systems. Other important modifications displayed in Fig. 7 are in the fingerprint region (600–1300 cm^{1}). The band at about 1230 and 1180 cm^{1} assigned to the stretch vibration of carboxylic and peroxide (COOH and COOOH) bonds are markedly characterized by an intensity increased, in particular way at 1180 cm^{1}. Additionally, in fresh (1-month-old) mastic resin the band at 1244 cm^{-1} shifts at 1234 cm^{-1} while in fresh dammar resin the same band at about 1240 cm^{-1} does not appear at the early stages of ageing but starts to increase markedly after 52hrs to be pronounced at the end at 1231 cm^{-1}.

Contrarily to this trend, a progressive decreasing in the C-H stretching absorbance of methyl and methylene groups indicating significant molecular changes to the hydrocarbon skeleton under light ageing was observed, which is in agreement with the above mentioned oxidation pathway. Furthermore, the absorption bands at 2948 and 2956 cm^{-1} in fresh mastic and dammar resins result also shifted both at 2953 cm^{-1}.

Structural information can be argued also from C–H bending vibrations. Particularly, the bands at 1455–1450 cm^{-1}, which include information on the C–H bending vibration of methyl and methylene groups, undergo to a slightly decrease in comparison to that of C–H bending of methyl groups at 1385–1380 cm^{-1}, which in effect implies a reduction of the CH bending vibration modes of methylene species. This observation is in line with a ring opening reaction, fragmentation and condensation of the original triterpenoid compounds.

Comparison with natural ageing

To verify similarities between naturally and artificially aged films, an example for dammar varnish is depicted in Fig. 8.

Even if it does not represent the aim of this chapter, it is worth noting that the artificial ageing simulates, in some extent, what observed during the natural ageing of a dammar varnish. For instance, after 1 year of natural ageing, the carbonyl region broadens toward lower wavelengths with the formation of a shoulder at about 1780 cm^{-1}. This band may be referred most probably to a lactonised side chain, which are the main components found on oxidized dammarane skeleton type molecules, as found to occur

also on aged paintings. The same trend follows in the fingerprint region, whereas the intensity increase of the CO groups can be highlighted.

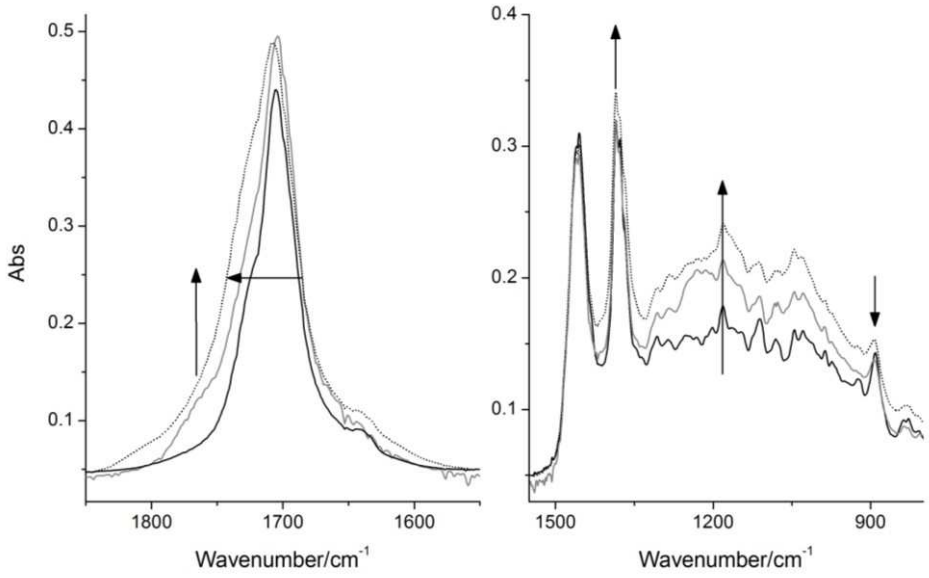

Fig. 8 Trasmission FTIR spectra of dammar varnish in the carbonyl region (left) and in the finger print region (right) as function of ageing time. The spectra reported refer to 1 month of natural curing (black line), 1 year of natural ageing (grey line) and 20h of artificial ageing (short dotted line).

As proposed in literature (Van der Doelen 1999), the formation of lactonised side chain in triterpenoid compounds may be represented as follows (Fig. 9). Such reaction can give an explanation for the broadening of the carbonyl peak.

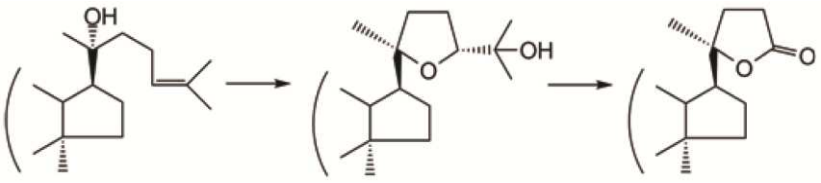

Fig. 9 Oxidation of the side chain in dammarane molecules (Van der Doelen 1999)

3.2.3.2 Diterpenoid resins: colophony and sandarac

Fig. 10 displays the compositional changes undergone by diterpenic resins, such as colophony and sandarac, during accelerated light ageing. Despite the two resin types belong to the *Pinaceae* family, they differ in the resinous acids content and hence in their photo-oxidation, polymerization and degradation pathways.
In artificially aged colophony resin the hydroxyl absorption is higher than in sandarac and shifts from 3383 to 3418 cm^{-1} without varying its intensity, while the broad weak double structured band at 2641 and 2536 cm^{-1} decreases markedly during the ageing time.

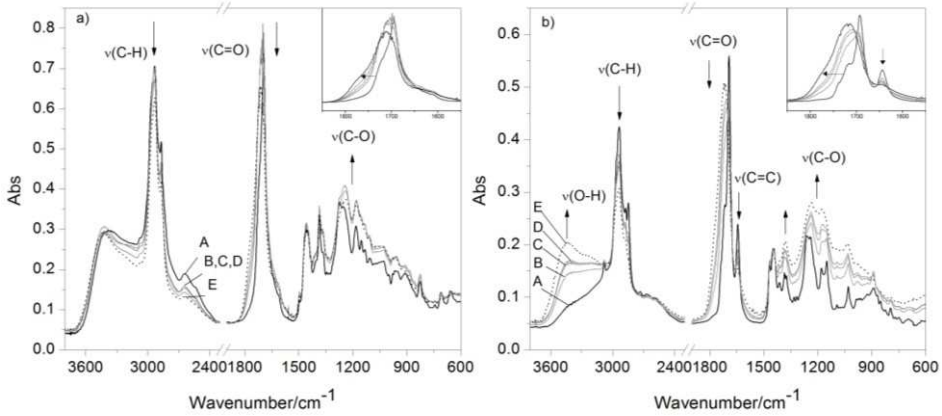

Fig. 10 Trasmission FTIR spectra of colophony a) and sandarac b) films (both pre-dissolved in ethanol) in the wavenumber ranges of 3800-2300 and 1900-600 cm^{-1} at different ageing times (A, t=0; B, t=20h; C, t=52h; D, t=102h; E, t=500h). The arrows show the changes of the main vibrational groups induced by the irradiation while in the inset, those ones of the carbonyl band are highlighted.

These bands can be related to the O-H stretch hydrogen bonded to carboxylic functional groups and are characteristic absorptions of abietadiene compounds, such as laevopimaric, abietic and neobiatic acids (Shearer 1989, Azémard et al. 2014). This feature does not compare in sandarac because it is mainly constituted of labdanes and pimaranes resin acids. Nevertheless, the OH absorption in fresh sandarac results quite negligible and increases strongly during ageing.

On the opposite, C-H stretching bands of methyl and methylene groups decrease slightly in both the diterpenic resins, even if colophony shows always a slower degradation kinetic. Thus, it was recorded a changes in the maximum intensity from 0.7 to 0.6 Abs units for colophony and from 0.4 to 0.3 for sandarac. The methylene bands at 2932 and 2870 cm^{-1} undergo a major change in sandarac while remain unvaried in colophony.
Notable important modifications can be appreciated in the carbonyl stretching region (see the inset in Fig. 10). First of all, the absorption maximum shifts of about 8-10 cm^{-1} for both the resins and tha band becomes broader in sandarac than in colophony. The shoulder band of the carboxylic acid group at about 1720 cm^{-1} disappears in fresh films (1-month-old) and a shoulder compares at about 1770 cm^{-1} after ageing indicating the formation of new molecular species, such as ketones, esters and lactones.
It is worth noting the change observed in the carbon-carbon double bonds region. For colophony the band at 1610 cm^{-1} gives a very low signal and the changes are mainly negligible. On the contrary, in sandarac the bands at 1640 and 888 cm^{-1}, that have been attributed respectively to the stretching of the carbon-carbon double bonds in the side chain and to the out-of-plain deformation of the exocyclic methylene groups result drastically reduced at the end of ageing (higher susceptibility to light). The latter two bands together with that attributed to CH ethylenic stretchings at 3080 cm^{-1} are representative of labdatriene molecules containing conjugated double bonds in the side chain, such as communic acid (Scalarone et al. 2002, 2003, Giuliano et al. 2007, Daher et al. 2010). The opening of carbon-carbon double bonds, together with the increase of the peaks at 1384 and 1449 cm^{-1}, due to the bending deformation of methyl groups and to the scissoring deformation of methylene groups, respectively, can be used to monitor the development of cross linking in sandarac resin.
The other minor amount of pimaranes molecules present in sandarac, such as agathic and sandaracopimaric acids, does not give a substantial contribution to cross-linking due to the lacking of conjugated double bonds. Reactive conjugated double bonds are present also in abietane molecules but were not evidenced the same cross-linking reactions

occurring in communic acid-based polymers. It's reported in literature that in many cases oxidation e.g. leads to a conversion of abietic and neoabietic acid into dehydroabietic acid, which is present in fresh material as 5-10%.
Further changes regard the increase in the region between 1300-1000 cm^{-1}. The most important one evidenced in sandarac, is a slight increase of the C-OH and C-O stretching bands at about 1250 and 1180 cm^{-1}, which change in the early stage (20 hrs) of ageing due to presence of new oxidized compounds (ketones, esters and lactones).

3.2.3.3 Shellac

Fig. 11 displays the sequence of the recorded FTIR spectra for unaged and artificially aged shellac resin films. All the spectra seem to change only in the peak intensity while the broadening is present in a lesser extent with respect to the other resin types.

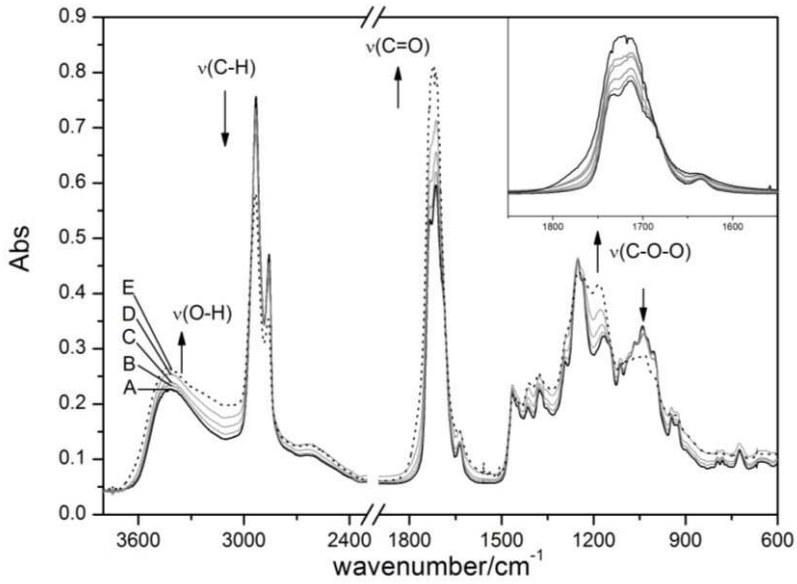

Fig. 11 Trasmission FTIR spectra of shellac varnish film (pre-dissolved in ethanol) in the wavenumber ranges of 3800-2300 and 1900-600 cm^{-1} at different ageing times (A, t=0; B, t=20h; C, t=50h; D, t=100h; E, t=500h). The arrows show the changes of the main vibrational groups induced by the irradiation while in the inset, those ones of the carbonyl stretching region are highlighted.

A slight increase in the OH stretching region due to the presence of hydroxyl and carboxylic groups has been observed. C-H stretching bands decrease together with the bending at 1464 cm^{-1}. At the same time, the bands at 1415 and 1377 cm^{-1} increase and shift slightly suggesting structural deformations in the region of skeletal vibrations.
This changes reflect what observed in the carbonyl stretching region. The band of the aldehyde groups at 1715 and the shoulders at about 1690 and 1735 cm^{-1} have been modified over the ageing time, as clearly shown in Fig. 11. This band increase leads to an overlapping of different signals, which makes difficult their discrimination. In any way, the overall intensity increases and shifts toward longer wavenumbers, thus indicating the formation of carboxylic and ester groups. The latter are surely formed, as demonstrated by the broadening of carbonyl band at 1780 cm^{-1} due to the possible formation of cyclic esters. The carbon-carbon double bonds signal deriving from shellolic and jalaric acids, is a little band at 1640 cm^{-1} which tends to be reduced during the ageing.
Other important features that further support the highlighted changes in the carbonyl region are in the 1300-900 cm^{-1} range. The C-O stretch/O-H deformation of primary or secondary alcohol at 1464 cm^{-1} does not undergo significant changes (Mills and White, 1999). The most relevant ones regard the continuous increase of the bending deformation of the ester bonds at 1171 cm^{-1} together with the reduction at 1035 cm^{-1}. These spectral features suggest clearly that the cross-linking process is driven by esterification. The starting point of such process may be related to the dissociation of aldehyde and carboxylic acid functions. A similar trend has been detected during thermal ageing by Farag (Farag 2010).

Table 2 – Infrared absorption peaks of solvent varnishes as naturally cured (1 month-old) and artificially aged (500 h) films. Bands which change in intensity after the ageing are indicated in italics while the abbreviation sh corresponds to shoulder peaks. Frequencies are given in wavenumber/cm^{-1}. Acronyms stay for: mastic (Ma), dammar (Da), colophony (Co), sandarac (Sa) and shellac (Sh).

Naturally dried films					**Artificially aged films**					**Approx Assignment**
Ma.	*Da.*	*Co*	*Sa*	*Sh*	*Ma*	*Da*	*Co*	*Sa*	*Sh*	
3410	3417	3383	3400sh	3417	*3440*	3442	*3418*	*3441*	*3423*	υ(O-H)
--	--	--	--	--	*3227sh*	*3213sh*	--	*3244sh*	--	υ(O-H)
3074	3071	3078	3080	--	--	--	*3076*	--	--	υ(C=CH) olefinic
--	--	2953sh	2962sh	--	--	--	*2956sh*	--	--	υ(CH_3)
2948	2956	2932	2934	2932	*2953*	*2953*	*2930*	*2940*	*2934*	υ(CH_3)
2877	2873	2870	2873	2858	*2874*	*2870*	*2869*	*2877sh*	*2860*	υ(CH_2)
--	--	--	2847	--	--	--	--	*2850sh*	--	--
2600	2600sh	2640	--	2642sh	*2600sh*	*2636sh*	*2640sh*	*2600sh*	*2641sh*	υ(O-H)
--	--	2540	--	--	--	--	--	--	--	υ(O-H)
--	--	--	--	--	*1776sh*	*1773sh*	*1780sh*	--	--	υ(C=O),cyclic esters
--	--	--	1735sh	--	--	--	--	*1735sh*	--	υ(C=O)
--	--	1720sh	1716sh	1732	--	*1721*	--	*1713*	*1720*	υ(C=O)
1709	1705	1695	1693	1713	*1720*	*1713*	*1713*	*1713*	*1713*	υ(C=O)
1649sh	1645	--	1644	1637	*1649sh*	*1651sh*	--	--	*1643*	υ(C=C)
--	--	1611sh	--	--	--	--	1611sh	--	--	υ(C=C) aromatic ring
--	--	1495	--	--	--	--	1495	--	--	--
--	1460	--	1469	1465	--	1461	--	--	1461	--
1450	1455	1460	1449	--	*1450*	1454	*1455*	1451	--	δ(CH_2), (CH_3)
--	--	--	--	1414	1415	--	--	--	*1415*	δ(O-H)
1385	1384	1385	1384	--	*1385*	*1385*	1383	*1383*	--	δ(CH_3)
--	1377	1366	1374	1375	--	--	*1365*	--	*1378*	δ(CH_3)
--	--	--	--	1293	--	--	--	--	*1293sh*	--
--	--	1273	1261	--	--	--	*1270sh*	--	--	--
1244	--	1250	1240	1252	*1234sh*	*1231*	1240	*1235*	1250	υ(C-C), δ(C-H), υ(C-O-O)
1180	1181	1180	1179	1167	*1180*	*1181*	*1178*	*1176*	*1180*	δ(C-H) , υ(C-O-O)
1158	--	1152	1150	1142sh	--	--	--	--	--	--
--	--	1131	--	--	--	--	*1131sh*	--	--	--
1113	1111	1106	--	1114	1108	--	*1106sh*	--	--	δ(C-H)
--	--	--	1031	--	--	--	--	*1034*	--	--
1076	1079	1084	--	--	--	--	--	--	--	δ(C-H), υ(C-O)
1029	1042	1047	--	1040	*1047*	*1048*	--	--	*1035*	δ(C-H) ,υ(C-O)
--	--	--	--	1000	--	--	--	--	*998sh*	---
947	--	--	--	945	*947sh*	--	--	--	*946*	δ(C-H)δ(O-H) "oop"
--	--	--	--	927	--	--	--	--	*930*	δ(C-H)δ(O-H) "oop"
--	--	896	--	899	--	--	--	--	--	--
--	--	879	--	--	--	--	--	--	--	--
--	--	824	--	--	--	--	825	--	--	--
--	757	--	--	796	--	--	--	--	*796*	--
--	--	--	--	780	--	--	--	--	*780*	--
--	--	710	--	723	--	--	--	--	*725*	--
--	--	657	--	--	--	--	--	--	--	--
--	890	880	890	--	--	--	--	--	--	δ(C-H)

3.2.3.4 Mastic oil varnish

The first step was to verify the chemical changes of the prepared oil-resin mixtures after the thermal treatment needed for their formulation. In this way, possible intermolecular interaction between the resin and oil and the influence of the heat processing on the end-products were evaluated. Once this has been done, for each type of oil-resin mixture the light-induced effects during drying process were evaluated, as previously shown for the solvent-based varnishes .

Mastic-oil mixture was heated in the 120-220 °C range, which comprises the onset for the softening and melting of triterpenoid resins. Spectral changes and bands assignment of the end-product together with those of fresh mastic and linseed oil samples are displayed in Fig. 12 and listed in Table 3, respectively.

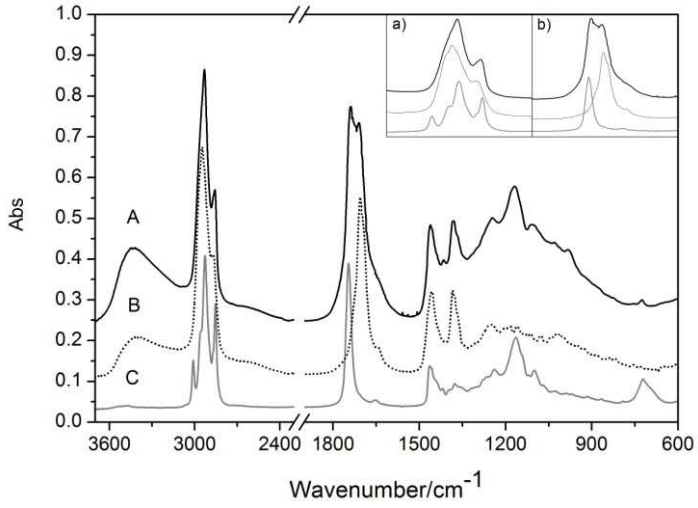

Fig. 12 Trasmission FTIR spectra of linseed oil-mastic varnish (A) after 1 month of natural curing in the wavenumber ranges of 3800-2300 and 1900-600 cm^{-1}. Fresh mastic (B) and linseed oil (C) spectra are also reported. In the inset the CH a) and C=O b) stretching regions are displayed and some changes highlighted.

The first important change after the varnish cooking regards the increase of hydroxyl groups (broad band centered at 3440 cm^{-1}), which comes both

from the added mastic resin and from the extensive oxidation occurring during heat aging (de la Rie 1988). The disappearance upon heating of the band at 3010 cm^{-1} and the decreasing of the out-of-plane deformation at 723 cm^{-1} are easily assigned to linseed oil. This implies that due to the heating process double bonds have changed position and/or configuration. Non-conjugated *cis* olefinic bonds along the aliphatic chain have been mostly transformed to non-conjugated *trans* double bonds, and in minor quantities to conjugated *trans* double bonds (a closer inspection of the FTIR spectra revealed new vibrations of trans-trans double bonds at 985 cm^{-1}). As reported in literature (Dlugogorski et al. 2012), oleic acid, as a monounsaturated acid, can be oxidised only at elevated temperatures, while polyunsaturated acids such as linolenic and linoleic acids undergo rapid oxidation even at room temperature. In addition, in presence of cobalt driers the cross-linking take place very quickly (200 min) and the kinetic is more faster than in pure linseed oil (240 h) (Mallégol et al. 2000, Van den Berg et al. 2004).

With regards to CH stretching bands, fresh linseed oil and mastic resin show respectively vibrations at 2927 and 2948 cm^{-1}. After the heat processing, these signals correspond to a unique broad band (see the inset in Fig. 12) with a maximum centered at 2931 cm^{-1} suggesting a frequency closer to linseed oil. This may probably come from the high content of methylene groups in the fatty acid chain.

A double structured band has been indeed detected in the carbonyl region due to the presence of both the components. In detail, the intense carbonyl band of the ester linkages at 1745 cm^{-1} of the linseed oil is likely shifted at 1738 cm^{-1} after thermal processing. On the opposite, the other one at 1709 cm^{-1} did not change and it can be attributed to the carbonyl band of aldehydes, ketones and carboxylic acids of mastic resin. This suggests that both the components after thermal treatment does not interact significantly to give new chemical compounds but conserve their own carbonyl absorption features. Nevertheless, a considerable broadening occurs, suggesting at longer wavelength the formation of unsaturated compounds. In particular, the weak C=C bands at 1654 cm^{-1} in fresh linseed oil and at 1640 cm^{-1} in mastic, which are sheltered by the broadening of the carbonyl peaks in the oil-resin mixture, probably

underwent some modifications during the heat processing, as observed also for the out-of-plane deformation at 722 cm^{-1} of linseed oil (Lazzari and Chiantore 1999, Mallégol et al. 1999). However, no notable increase in the vibration bands of conjugated carbon double bonds can be detected. Further interesting changes upon heat processing can be noticed from both the components in the region 1600-600 cm^{-1}. First of all, an overall intensity increase was observed, which suggests an oxygen uptake upon heating accompanied by the formation of hydroperoxides. As known, the first step of an oxidation process involves hydrogen abstraction on a methylene group between two double bonds in polyunsaturated fatty acids chain leading in the second step to peroxydes. With regards the CH bending bands, it can be seen that the mastic-oil mixture after cooking shows two bands at 1460 and 1380 cm^{-1}, which are typical identification markers of the presence of a triterpenoid resin and not at all of linseed oil. Concerning with these two bands, the latter shows only a band at 1464 cm^{-1}. As previously mentioned for the CH stretching mode, also the bending are closer to that of linseed oil. At the same time, C-O stretching band at 1166 cm^{-1} is clearly ascribable to linseed oil as wells the asymmetric C-O stretching at 1110 cm^{-1}. The changes related to the bands appearing at 980 and 722 cm^{-1} have already been discussed above.

Monitoring of the light-induced effects

In Fig. 13 FTIR spectra of linseed oil-mastic mixture exposed at different ageing times have been compared.
The assignments and the most relevant changes in band position have been reported in Table 3. Notable spectral differences can be seen upon intense light ageing of linseed oil-mastic varnish. In detail, an increased intensity in the hydroxyl region together with the appearance of a shoulder at ca. 2600 cm^{-1} due to hydroxyls bonded to carboxylic group have been detected. This behavior regards both the components, even if in presence of oil with cobalt driers hydroxyl formation is accelerated. As shown, the major changes appear in the early 20h of ageing.
Abs of CH groups is decreased of about 15% in the early 100 h and a further 20% was lost between 100 and 500 h, indicating a great and fast

hydrogen abstraction on methylene group both in fatty acids chain and polycyclic triterpenoid acids. This is in agreement with an oxidative chain cleavage reactions known to yield volatile oxidation products (Meilunas et al. 1990) and also with what observed in mastic resin.

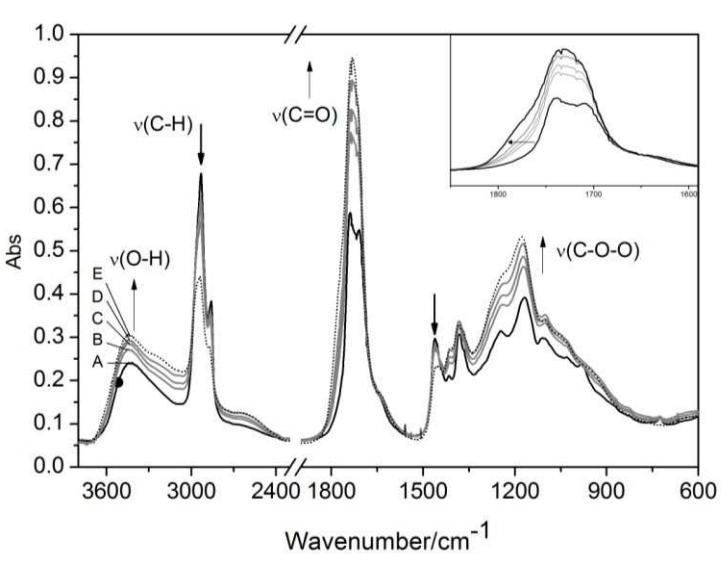

Fig. 13 Trasmission FTIR spectra of mastic-linseed oil mixture (cured) in the wavenumber ranges of 3800-2300 and 1900-600 cm^{-1} at different ageing times (A, after 1 month of natural curing; B, t=20h; C, t=50h; D, t=100h; E, t=500h). The arrows show the changes of the main vibrational groups induced by the irradiation

The intense decreasing of CH peak at 2932 is accompanied by a shift toward 2940 cm^{-1}, even if appears very interesting the change in the secondary peak, which decreases and changes from 2857 to 2876. The latter frequency is closer to mastic resin, as well as the drastic decreasing of the bending at 1460 cm^{-1}. As previously observed, this latter band has in fresh mastic an intensity similar to that at 1380 cm^{-1} and tends to become lower after exposure to intense radiation. In the oil is exactly the contrary because the intensity at 1460 is always higher than the vibration at 1380 cm^{-1} (Lazzari et al. 1999).

Table 3 – Tentative infrared absorption peaks after the heat processing (pre-heated) and artificial ageing (light aged) of linseed oil-mastic films. For comparison purposes fresh linseed oil and mastic films have been also reported. Bands which change in intensity after the light ageing treatment are indicated in *italics* while the abbreviation sh corresponds to shoulder peaks. Frequencies are given in wavenumber/cm^{-1}.

Linseed oil	Assignment[a]	Mastic	Assignment[a]	oil- mastic (pre-heated)	oil- mastic (light aged)
--	--	3410	υ(O-H)	3440	*3448*
3009	υ(C-H)=CH	--	--	--	--
2960 sh	υ_a(C-H)CH_3	2966sh	υ_a(C-H)CH_3	--	*2960sh*
2927	υ_a(C-H)CH_2	2948	υ(CH_3)	2931	*2940*
--	--	--	--	2870sh	--
2856	υ_s(C-H)CH_2	2877	υ(CH_2)	2858	*2876*
--	--	2600sh	υ(O-H)	2600sh	*2600sh*
--	--	--	--	--	*1780sh*
1745	υ(C=O) ester	1709	υ(C=O)	1741	*1731-36*
--	--	--	υ(C=O)	1709	*1714sh*
--	----	1640	υ(C=C)	1640sh	*1640*
1654	υ(C=C) of *cis* –CH=CH-	1455sh	υ(C=C)	1455sh	*1455*
1464	δ(CH_3), δ(CH_2)	1450	δ(CH_2), δ(CH_3)	1460	*1460*
1418	wag (CH_2)-CH_2-CO-O-	--	--	1415	*1415sh*
1378	wag (CH_2)	1385	δ(CH_3)	1380	*1380*
1238	υ_a(C-C-O) in ester	1244	υ(C-C),δ(C-H)	1247	*1240sh*
--	--	1180	δ(C-H), υ(C-O)	--	*1177*
1164	υ(C-O)	1158	--	1166	--
--	--	1113	δ(C-H)	1110	--
1100	υ_a(O-CH_2-C)	1076	δ(C-H), υ(C-O)	1100	*1100sh*
--	--	1029	δ(C-H), υ(C-O)	1030	--
--	--	--	C=C	985	--
723	γ-(CH_2)-+wag(C-H)=CH	--	--	725	--

[a] υ: stretching; δ:bending; wag: wagging; γ;rocking; $_a$:asymmetric; s: symmetric

Contrarily, additional ketone, ester and acid carbonyls appear to be formed during photo-oxidative polymerization. The double structured shape of carbonyl disappears and changes with a new one formed by a sum of several contributions, which can be hardly distinguished (see Fig. 13). Thus, these changes reflect the formation of ester linkages between the two components, as evidenced by an increase in characteristic absorbances at 1239, 1174 and 1100 cm^{-1}. The shoulder at 1715 cm^{-1} and the diagnostic C-O stretching vibration at 1418cm^{-1} of the oil, can suggest the formation of carboxylic acid products. A further important change is the broadening and the increased shoulder at 1780 cm^{-1}, which indicates the formation of secondary oxidation products, such as lactones and anhydrides both in oil and resin (Meilunas et al. 1990, Van der Doelen

1999, Mallègol et al.2000). The formation of anhydrides and lactones represents the final stages of cross-linking and occurs via dehydration reaction of carboxylic acids or esters with carboxylic acids and alcohols, respectively. Broadening of carbonyl band and the formation of lactones is very marked also in artificially aged mastic without oil. For comparison purposes, spectra of mastic and mastic-linseed oil mixture are shown in Fig. 14.

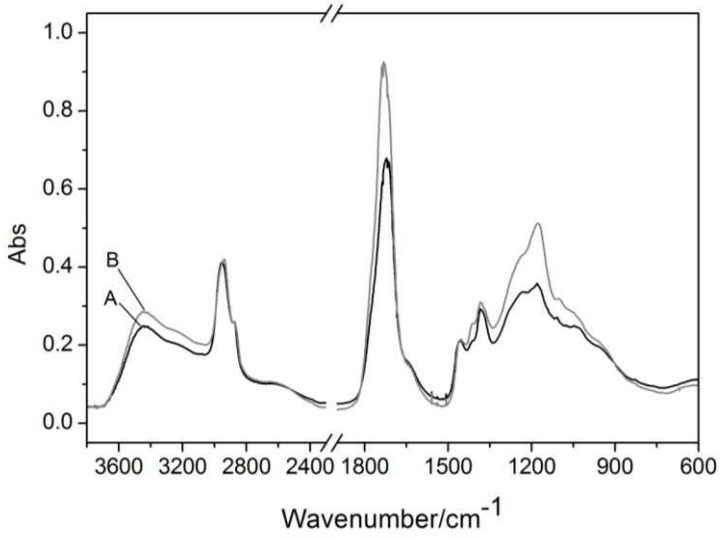

Fig. 14 Trasmission FTIR spectra of mastic (A) and linseed oil-mastic mixture (B) after 500h of accelerated lighting conditions.

Basically, the most relevant changes reside in the higher intensity of OH, C=O and CO stretching groups due to the high content of primary oxidation products deriving from polyunsaturated acids such as: allyl hydroperoxides, chemical moieties containing both allyl (−CH = CH–CH2–) and hydroperoxide (−OOH) groups as in –CH = CH–CH(OOH). Nevertheless, the intensity changes do not allow the identification of the oil component in the mixture, although the carbonyl band appears at higher wave number (1735 cm^{-1}) with respect to mastic (1720 cm^{-1}).
Other minor features that could be representatives for identifying the oil were transformed both during thermal treatment and photo-oxidation, thus adding new drawbacks in recognizing the oil. Despite this, IR spectrum of oil-resin mixture (B) is very similar to that of the pure mastic, suggesting

that mastic can be identified by the more intense band at 1380 cm^{-1} of methyl group, which is usually very weak or absent in aged oil binders (Azémard et al. 2014).

3.2.3.5 Colophony oil varnish

The infrared spectrum of linseed oil-colophony mixture after the heat processing (heated until up 220° for 1 h) is shown in Fig. 15 and the changes in band position are listed in Table 4.

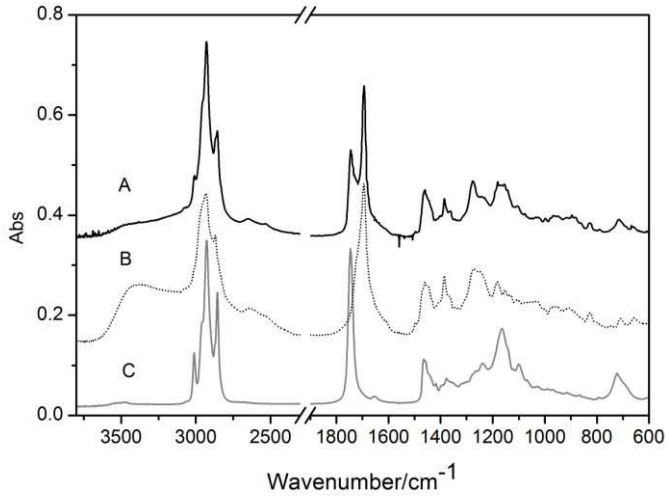

Fig. 15 Trasmission FTIR spectra of linseed oil-colophony varnish (A) after 1 week of natural curing (heated at 120 °C for 1 h) in the wavenumber ranges of 3800-2300 and 1900-600 cm^{-1}. For a qualitative comparison fresh colophony (B) and linseed oil (C) spectra are also reported.

It is worth to note that OH stretching band of carboxylic acids results less intense with respect to pure colophony, most probably is due to dehydrogenation of abietic acid taking place during the thermal treatment (Marchand-Geneste et al. 2003). Contrarily to linseed oil-mastic mixture, linseed oil-colophony varnish preserves many spectral features related to the presence of oil phase in the mixture.
The first one regards the CH stretching region which appears, as shape and bands position, very similar to that of linseed oil. (see Table 4).

Nevertheless, the characteristic stretching of the vinyl function in labdatriene molecules (at 3078 cm^{-1}) and the two bands at 2640 and 2535 cm^{-1} permit to recognize the colophony resin.
As for linseed oil-mastic mixture, the carbonyl region appears clearly double structured thank to the contribution of the oil and colophony at 1740 and 1694 cm^{-1}, respectively.
Shape and band positions suggest that any interaction between the two components took place due to the heating process. In addition, one can see that the intensity of CH groups in the mixture is higher than the unheated references (oil and resin), which is due to the superposition of frequencies close to each other. On the opposite, carbonyl peaks appear well resolved because are separated of about 50 cm^{-1}.
The weak C=C bonds give a very low signal, thus making difficult their discrimination or the assessment of possible changes upon thermal treatment. The bending of methyl and methylene groups do not show significant changes and also the overall intensity between 1300-900 cm^{-1}. This suggests that the peroxides formation did not take place during heating but most likely, a loss of volatile compounds can be noticed. Concerning with the identification of the type of oil varnish, at this degree of curing, all the spectral features of both the components are clearly detectable.

Monitoring of the light-induced effects

For first, some modifications before the exposure to accelerated lighting conditions have been noticed. In Fig. 16 the spectrum B regards the linseed oil-colophony mixture after 1 week of natural curing. The results indicate a rapid carboxylation reaction, leading to a material containing increased quantities of carbonyl and hydroxyl groups and decreased quantities of CH_2 and CH_3 groups (complete disappearance of *cis* unsaturation). This indicates that, light and oxygen together with driers catalyze the hydrogen abstraction of methylene groups. This leads to conjugated and non conjugated hydroperoxides, which via radical recombination produce cross-linking (alkyl, ether or peroxy bridges). The end-products are responsible for the observed enhanced yellowing of the film.

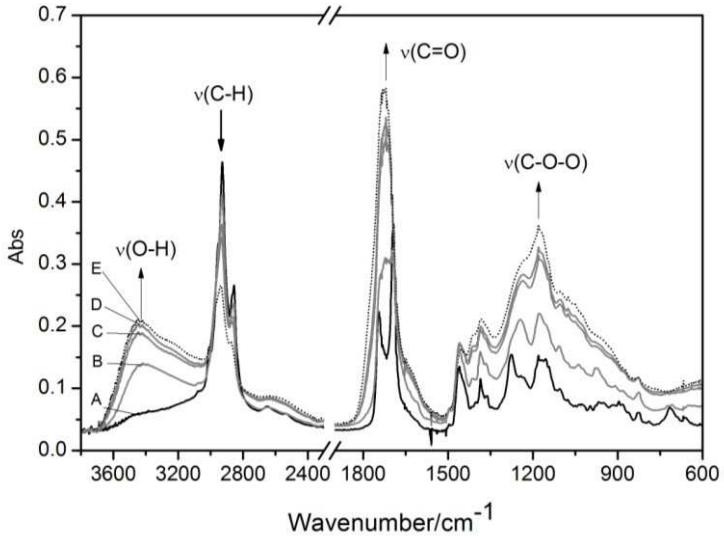

Fig. 16 Trasmission FTIR spectra of colophony-linseed oil mixture in the wavenumber ranges of 3800-2300 and 1900-600 cm^{-1} at different ageing times (A, after 1 week of natural curing) ; B, C, D and E after 25h, 50h, 100 h and 500 h of artificial ageing, respectively). The arrows show the changes of the main vibrational groups induced by the different lighting conditions.

This photoxidation pathway results to be drastically accelerated upon artificial irradiation conditions meaning that abietane-rich resins as colophony and Venice turpentine, contain highly reactive species. For instance, fresh colophony consists almost entirely of resinous acids differing in their oxidative behavior. Sixty percent are abietane acids with highly reactive conjugated double bonds, 20-25 % of more stable pimarane acids with no-conjugated double bonds and 5-10% of acids that are much prone to oxidation (dehydroabietic acid) (Scalarone et al. 2002). Despite this, such reactions were not assessed in colophony. The above results show that together with linseed oil (with Co salts) more carboxylic acids have been formed during the light-induced curing process.

As reported in literature (Mallégol et al. 2000), these acids groups can play a significant role in the activity of cobalt by complexing Co^{n+} in the form of fatty acid chain carboxylates with low or any mobility.

Table 4 Tentative infrared absorption peaks after the heat processing (pre-heated) and artificial ageing (light aged) of linseed oil-colophony film. For a qualitative comparison fresh linseed oil and colophony films have been also reported. Bands which change in intensity after the light ageing treatment are indicated in *italics* while the abbreviation sh corresponds to shoulder peaks. Frequencies are given in wavenumber/cm^{-1}.

Linseed oil	**Assignment[a]**	**Colop.**	**Assignment[a]**	**oil- coloph. (pre-heated)**	**oil- colophony (light aged)**
--	--	3383	υ(O-H)	3480sh	*3432*
--	--	--	--	--	*3240sh*
--	--	3078	υ(C=CH)	3078	3078
3009	υ(C-H)=CH	--	--	3009	--
2960 sh	υ_a(C-H)CH_3	2953sh	υ(CH_3)	2957sh	--
2927	υ_a(C-H)CH_2	2932	υ(CH_3)	2927	*2936*
2856	υ_s(C-H)CH_2	2870	υ(CH_2)	2857	*2872*
--	--	2640	υ(O-H)	2640	--
--	--	2540	υ(O-H)	2535	*2560sh*
1745	υ(C=O) ester	--	υ(C=O)	1745	*1740sh*
--	--	1720sh	υ(C=O)	--	*1730*
--	--	1695	υ(C=O)	1695	--
1654	υ(C=C) of *cis* – CH=CH-	--	--	--	--
--	--	1610sh	υ(C=C) *cis*	1610sh	*1620sh*
--	--	1495	aromatic ring	1495	--
1464	δ(CH_3), δ(CH_2)	1460	δ(CH_2), δ(CH_3)	1460	*1450*
1418	wag (CH_2)-CH_2-CO-O-	--	--	--	*1412sh*
1378	wag (CH_2)	1385	δ(CH_3)	1385	*1385*
--	--	1366	δ(CH_3)	--	--
--	--	1273	υ(C-C), δ(C-H)	1273	--
1238	υ_a(C-C-O) in ester	1250	υ(C-O)	1240	*1232sh*
--	--	1180	δ(C-H) ,υ(C-O)	1180	*1180*
1164	υ(C-O)	1152	--	1166	*1160sh*
--	--	1131	δ(C-H)	1110	*1142sh*
1100	υ_a(O-CH_2-C)	1106	δ(C-H), υ(C-O)	1100	*1100*
1100	υ_a(O-CH_2-C)	1084	δ(C-H), υ(C-O)	1100	*1075*
--	--	1047	δ(C-H) ,υ(C-O)	1030	--
--	--	--	--	985	--
--	--	824	--	824	*824*
723	γ-(CH_2)-+wag(C-H)=CH	--	--	725	--
--	--	707	--	717	--
--	--	658	--	660	--

[a] υ: stretching; δ:bending; wag: wagging; γ;rocking; $_a$:asymmetric; s: symmetric

This has led to the formation of a solid surface layer while in the bulk after 1 year was still viscous. Pour through-dry is one of the major drawback of drier use, because the subsequent curing will provoke tension at the interface, which could result in skinning tendency (apparition of wrinkles for example). Moreover, cobalt drier after this fast oxidation step becomes inactive and through-dry is then very slow. This behavior was observed on samples casted on glass and quartz substrates

but not in those spread by brush on grounded canvas. Equally, this behavior was not observed on KBr discs because the thickness was very low (about 10 μm).

3.2.3.6 Sandarac and Manila copal oil varnishes

Fig. 17 shows the sandarac-linseed oil mixture obtained after the heat processing. The results obtained on Manila copal were not reported because they did not show noticeable differences from those observed in the sandarac-oil varnish.

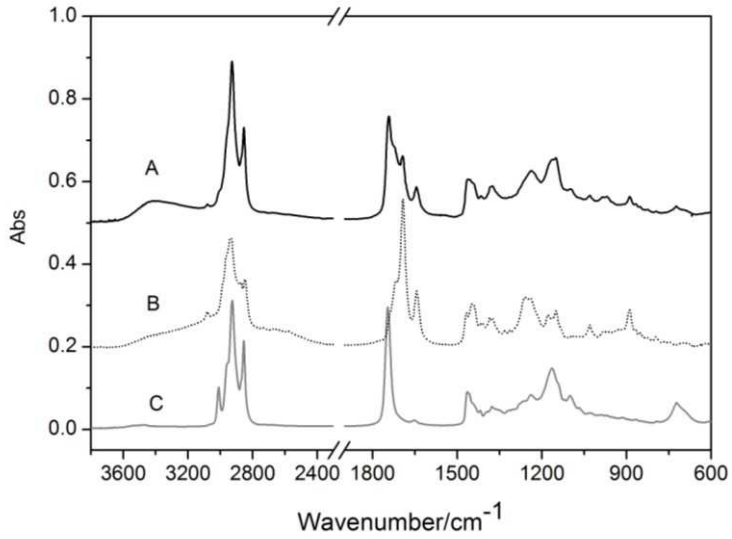

Fig. 17 Trasmission FTIR spectra of linseed oil-sandarac varnish (A) after 1 week of natural curing (heated at 285 °C for 1 h) in the wavenumber ranges of 3800-2300 and 1900-600 cm^{-1}. For a qualitative comparison fresh sandarac (B) and linseed oil (C) spectra are also reported.

Both the components did not interact significantly but rather result as a mixture of two separated compounds. All the spectral features can be appreciated, although the temperature was raised up to 285 °C. As already shown, the most relevant change regards the linseed oil phase, which undergoes a drastic decrease of *cis* unsaturation (band at 3009 cm^{-1}).

Concerning with the resin, the carbon-carbon double bonds are clearly detectable through the weak absorption of the olefinic group at 3080 and the most intense ones at 1643 cm^{-1}, which is related to molecules containing pimarane and labdane skeletons (see Fig. 17). These functional groups are converted into single bonds during the cross-linking and hence its presence suggests that polymerization reactions did not take place yet. The intensity of carbonyl absorption if compared with the band at 1643 cm^{-1} results drastically reduced. This arises from the thermal treatment which most likely, led to decarboxylation and fragmentation of polycommunic acid. On the other hand, the latter represents a highly cross-linked fraction conferring the typical hardness in such diterpenic resins (Carman et al. 1970, Scalarone et al. 2003).

Monitoring of the light induced effects

In Fig. 18 the infrared analysis performed on sandarac and Manila copal-linseed oil mixtures under accelerated light-ageing have been reported. The first important observation in the infrared spectra is that sandarac and copal mixed with linseed oil undergo similar polymerization and degradation processes. In fact, assignment and changes in band positions listed in Table 5 can be considered the same for both the diterpenoid resins.

In these resins, as previously shown for sandarac varnish, the polymerization reaction occurs with a radical mechanism starting from conjugated double bonds of labdatriene molecules such as communic acid, which readily polymerise when comes into contact with light and air. For this reason, after one month of natural curing both resins showed a notable oxygen content, which did not vary significantly during the artificial ageing. Linseed oil content gives also a significant contribution to oxidation through the developing of hydroperoxides.

Polymerization and cross linking can be seen and monitored through the significant reduction of the carbon-carbon double bond at about 1645 cm^{-1}, the disappearance of the out of plane deformation at 889 cm^{-1} and the drastic intensity decrease of the CH groups at 2930 and the scissoring deformation of methylene groups at 1454 cm^{-1}.

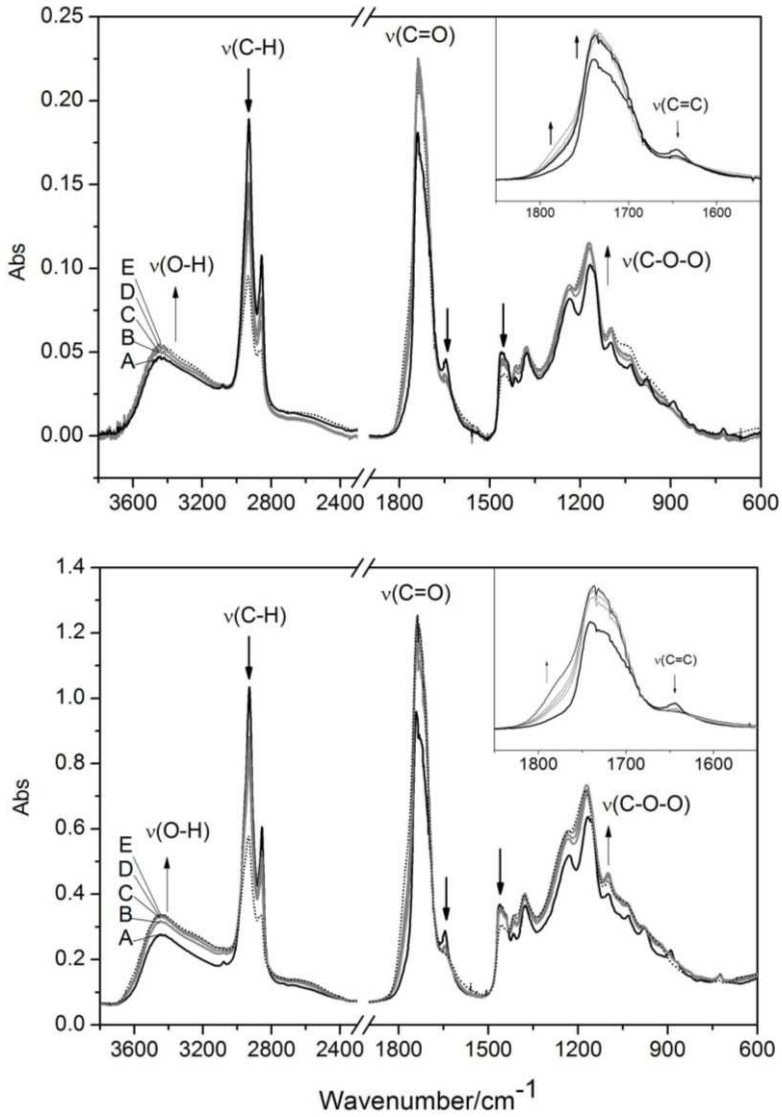

Fig. 18 Trasmission FTIR spectra of sandarac (top) and copal (bottom) linseed oil mixtures in the wavenumber ranges of 3800-2300 and 1900-600 cm^{-1} at different ageing times (A, after 1 month of natural curing) ; B, C, D and E after 25h, 50h, 100 h and 500 h of artificial ageing, respectively). The arrows show the changes of the main vibrational groups induced by the different lighting conditions.

Table 5 Tentative infrared absorption peaks of linseed oil-sandarac film after the heat processing (pre-heated) and artificial ageing (light aged). Linseed oil-Manila copal mixture shows the same spectral features. For a qualitative comparison fresh linseed oil and sandarac films have been also reported. Bands which change in intensity after both the treatments are indicated in *italics* while the abbreviation sh corresponds to shoulder peaks. Frequencies are given in wavenumber/cm^{-1}.

Linseed oil	**Assignment**[a]	**Sand.**	**Assignment**[a]	**oil-sandarac (pre-heated)**	**oil-sandarac (light aged)**
--	--	3400sh	υ(O-H)	3480sh	*3440*
--	--	--	--	--	--
--	--	3080	υ(C=CH) vynil	3078	--
3009	υ(C-H)=CH	--	--	3009sh	--
2960 sh	υ_a(C-H)CH_3	2962sh	υ(CH_3)	2960sh	--
2927	υ_a(C-H)CH_2	2934	υ(CH_3)	2929	*2933*
---	--	2873	υ(CH_2)	2870sh	--
2856	υ_s(C-H)CH_2	2847	υ(CH_2)	2855	*2860*
--	--	--	--	--	*1780*
1745	υ(C=O) ester	--	υ(C=O)	1742	1740
--	--	1716sh	υ(C=O)	1720sh	1720sh
--	--	1693	υ(C=O)	1694	--
1654	υ(C=C) of *cis* – CH=CH-	1643	υ(C=C) *cis*	1643	*1643sh*
--	--	1495	aromatic ring	1495	--
1464	δ(CH_3), δ(CH_2)	1469	δ(CH_2), δ(CH_3)	1464	*1454*
1443sh	δ(CH_3), δ(CH_2)	1449	δ(CH_2), δ(CH_3)	1442sh	--
1418	wag (CH_2)-CH_2-CO-O-	1412	--	1416	*1415*
1378	wag (CH_2)	1385	δ(CH_3)	1377	1377
--	--	1261	υ(C-C), δ(C-H)	--	--
1238	υ_a(C-C-O) in ester	1240	υ(C-O)	1238	*1232sh*
--	--	1179	δ(C-H) ,υ(C-O)	--	*1175*
1164	υ(C-O)	1150	--	1160sh-1150	--
1100	υ_a(O-CH_2-C)	1106	δ(C-H), υ(C-O)	1100	*1097*
1100	υ_a(O-CH_2-C)	1084	δ(C-H), υ(C-O)	1100	--
--	--	1030	δ(C-H) ,υ(C-O)	1030	*1030sh*
--	--	889	δ(CH_2) o-o-p	889	--
723	γ-(CH_2)-+wag(C-H)=CH	--	--	723	--

[a] υ: stretching; δ:bending; wag: wagging; γ;rocking; $_a$:asymmetric; s: symmetric

3.2.4 Kinetic study

The photooxidation kinetics of solvent and oil varnishes as function of ageing time are shown in Fig. 19.

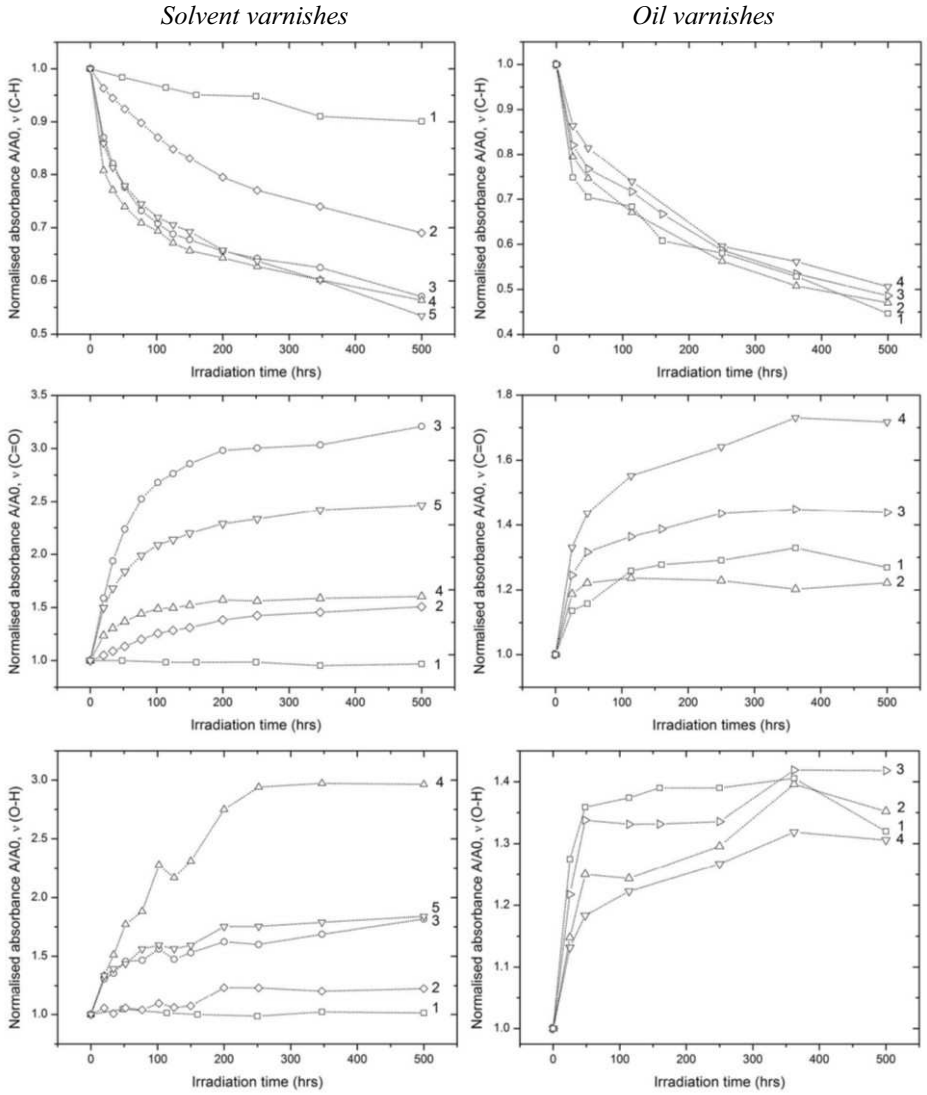

Fig. 19 Time evolution of C-H, C=O and O-H stretching bands for solvent (graphs on the left side: colophony **1**; shellac **2**; dammar **3**; sandarac **4**; mastic **5**) and oil- based varnishes (graphs on the right side: colophony **1**; sandarac **2**; copal **3**; mastic **4**) during the aging time (0→500h).

The absorbances collected at each ageing time have been normalized to the starting value (At_n/At_0), thus making data independent from the thickness of the varnish films. The time evolution of the main stretching modes (C-H, C=O and OH) shows that the photo-induced processes involved are similar for all the different natural resins either with or without oil. Decreasing of CH groups, increase in carbonyl and hydroxyl regions, even if a different slope depending from the type of varnish has been noticed. The interpretation of the different photoxidation kinetics observed have been discussed below on the basis of all the data acquired.

3.3 Discussion

3.3.1 Solvent varnishes

CH groups of dammar (3) sandarac (4) and mastic (5) undergo an exponential decay during aging, as shown in Fig. 19. The decrease of Abs ratios is of 25% within the first 50 h of ageing until reaching 50% after 500h. Shellac (2) and much less colophony (1), do not follow the same fast decay. These trends, even if they may appear negligible, suggest that kinetics of photooxidation reactions, which start with hydrogen abstraction from methyl and methylene functional groups depend from the molecular structure of the terpenoid compound. For first, triterpenoid resins follow the same decay pattern and strangely also sandarac, even if it belongs to diterpenoids. It appears very notable the drastic difference in comparison to colophony, which is always a ditepenoid resin.
As reported in literature (Zumbühl et al. 1998, Van der Doelen 1999, Dietemann 2003, Theodorakopoulos et al. 2007), oxidation of triterpenoids undergoes A-ring opening through Norrish I type reactions upon irradiation under intense light fluxes. The resultant A-ring cleavage to a diradical (Norrish type I reaction) can be followed by oxygen insertion leading to carboxylates, aldehydes, peroxides, hydroperoxides and lactones. The latter are the main components of oxidized dammarane skeleton type molecules, as found to occur on aged painting. All these reaction are in agreement with the increase and broadening observed in the C=O and OH groups, as well as in the 900-1300 cm^{-1} region due to

C-O stretching absorption. The initiation of photoxidation reactions is believed to occur in these resins at the ubiquitous aliphatic keto groups. Light of 275-295 nm wavelength excites the n-π * transition of these groups followed by bond homolysis and ring opening (Norrish type I reaction) (Zumbühl et al. 1998). However, hydratation of di and triterpene double bonds and hydroxylation of triterpene keto group cannot give a plausible explanation to the slight increase of the b* colourimetric coordinate, which indicates the beginning of a yellowing effect. This means that other degradation reactions take place simultaneously. Thus, intramolecular termination reactions lead to unsaturated ketones, such as quinones, to which yellowing of natural resins is ascribed (De la Rie 1988, Van der Doelen 1999, Dietemann 2003). It was demonstrated that these high molecular weight fractions are cross-linked in the outer varnish layer, precisely in the first 10 micron. Nevertheless, the increase in b* coordinate was not so intense to be appreciated to naked eye, indicating a very low amount of yellow chromophores. In fact, yellowing is mainly observed to develop in darkness and not under accelerating light exposure, in which bleaching occurs due to strong autoxidation (De la Rie 1988a, Feller 1995). However, from the FTIR data is not possible to detect the presence of such compounds.

Diterpenoid resins, as like sandarac (4) and colophony (1), do not follow the same photoxidation reactions kinetic. CH groups in sandarac decrease exponentially, as previously observed for triterpenoids resins, while in colophony the change is quite negligible. It is worth noting that the carbonyl absorption in both the diterpenoid resins decreases and broadens, which is exactly opposite to that of tritepenoid resins. This aspect is clearly distinguishable not from the kinetic study but observing the spectral intensities. It can be attributed to a major ability of diterpenoids to undergo polymerization in place of oxidation, with respect to triterpenoids. Besides this, hydroxilation is stronger in sandarac than colophony, which suggests that pimarane and labdane diterpenoids are more reactives to photoxidation. The same trend has been evidenced also in the C-O stretching region. Sandarac, being mainly constituted of pimarane compounds, is readily prone to polymerization due to the presence of a vynil group on the side chain. In fact, as shown by FTIR

data, sandarac polymerises rapidly at two carbon-carbon double bond sites (loss of unsaturations) which along with cleavage reactions based on radical mechanisms (β-or oxidative scission) form a saturated network of bicyclic units connected by a polymer chain (Scalarone, et al. 2003). Contrarily, abietane acids in colophony have conjugated double bonds inside the C-ring which result less susceptible to breakdown (Theodorakopoulos et al. 2007). For the latter, ageing lead to oxidized dehydroabietic acids, coloured chromophores which are characterized by a structure less photosensitive, due to the presence of an aromatic ring.

These compositional differences suggest that pimarane and labdane compounds are more susceptible than abietanes to photo-oxidation reactions, as evidenced also by quasi linear ageing kinetic of the colophony resin. Remarkable differences were detected also from a colourimetric standpoint. As previously mentioned for triterpenoids resins, the increase of b* coordinate for sandarac is below the detection limit of human eye whereas for colophony a strong darkening toward brown-orange tones could be well appreciated also to naked eye just only after 20h of ageing. The strong colour variation confirms the formation of dehydrobietic acid (Van den Berg et al. 2000, Findeisen et al. 2007, Scalarone et al. 2002).

Finally, the spectral features of bleached shellac upon photo-induced ageing suggest clearly that the cross-linking process is driven by self-esterification (Limmatvapirat et al. 2007, Farag 2010, Carretti et al. 2010). The starting point of such process can be related to the dissociation of aldehyde and carboxylic acid functions, as showed by the kinetic study. Surprisingly, the colourimetric measurments have shown that contrarily to the other terpenoid resins studied, bleached shellac undergoes further bleaching upon irradiation, which it was also appreciable to naked eye.

This effect can be related to a certain amount of chlorine residue, which through the absorption of the blue light component (around 400 nm) acts as a bleaching agent in the varnish. Most likely, a transfer of energy from chlorine to neighboring molecules starts a chain of chemical events which can be seen as post irradiation effect.

3.3.2 Oil varnishes

The FTIR spectra of oil varnishes showed noticeable differences after the heat processing at strong temperatures. The most relevant involves *cis-trans* isomerisation of double bonds in fatty acids (disappearance of *cis* bands at 3010 and 716 cm^{-1}, appearance of *trans* conjugated and *trans* nonconjugated bands at 985 cm^{-1}) and an increase of the OH and CO stretching regions. Clearly, the polyunsaturated acids such as linolenic and linoleic undergo rapid oxidation at elevated temperatures. After a curing period of one month in free oxygen conditions the infrared band related to the resin and oil were appreciable yet, but just only after 20 h of accelerated ageing it was more complicated to identify the type of oil varnish. The first important chemical reaction taking place during the initial drying of an oil varnish comes as a result of an intense oxygen-mediated process. The kinetic of CH groups shows also that such process does not depend from the type of terpenoid resin in the mixture. It is clearly governed by the oil via hydrogen abstraction on a methylene group between two double bonds in polyunsaturated fatty acid chain. Parallelly, the content of carbonyl and hydroxyl increase notably. This trend fits nicely with the formation of hydroperoxides (ROOH) which lead as secondary oxidation products to oxygenated structures, such as alcohols, aldehydes, ketones.

3.4 Conclusions

In this work , the photo-induced (above 290 nm) effects of different types of spirit and oil varnishes, as found on paintings, were monitored by using trasmission FTIR spectroscopy, colorimetric and gravimetric measurements. Overall, di (i.e. sandarac, colophony, copal) tri (i.e. mastic and dammar) and sesquiterpenoid (i.e. shellac) resins, either with or without the oil, follow similar photo-oxidative kinetics upon time. The light-induced effects start with an hydrogen abstraction process, which is more efficient when polyunsaturated fatty acids are present in the varnish. The action of oxygen-mediated processes catalyzed by intense radiation

and temperature lead to the formation of new acidic compounds, such as carboxylic acids groups ketones, esters and lactonised structures. Simultaneously, cross-linking, extensive polymerization and degradation phenomena occur, in different extent, depending from the type of unsaturations of the material. Thus for instance, the cross-linking reactions, being prominent in sandarac, copal and shellac resins due to the cleavage of carbon double bonds (loss of unsaturations), may be easily monitored by FTIR spectroscopy. Such reactions support also the slight weight loss observed, which is representative of the loss of volatile compounds, such as the evaporation of monoterpenes, low molecular weight terpenic degradation products and degradation products of the polymeric fraction. No significant yellowing appeareance was evidenced for dammar, mastic and sandarac. Colophony underwent a noticeable darkening just only after 20h of ageing, most likely due to the formation of coloured polycyclic aromatic structures ascribable to dehydroabietic acids. On the contrary, bleached shellac showed further bleaching during ageing most likely due to the residual chrlorine.

Finally, this study, aimed at preparing aged samples suitable for laser ablation tests (Chapter 4), gives useful information about the light-induced effects on painting varnishes and may represent the starting point for interpreting the laser induced effects upon laser irradiation.

Chapter IV

SPECTROSCOPIC ASSESSMENT OF THE UV LASER-INDUCED MODIFICATIONS IN SOLVENT AND OIL PAINTING VARNISHES

The chapter is substantially focussed on the systematic assessment of the laser induced modifications occurring in solvent and oil varnish coatings after laser removal treatment. For this aim, the fifth (213 nm) and fourth (266 nm) harmonics of a pulsed QS (15 ns) Nd:YAG laser were selected for irradiating different types of varnish samples. The coatings tested comprise two different categories: (i) "spirit" varnishes prepared by dissolving dammar, mastic, colophony, sandarac and bleached shellac in opportune solvents and (ii) mastic, colophony, sandarac and Manila copal pre-heated at high temperatures with linseed oil. These coatings were exposed to natural and artificial lighting conditions before to be irradiated at both the UV laser wavelengths. A significant effort was primarily devoted to seek the UV-Vis absorbing compounds of the varnish samples by means of UV-Vis absorption spectroscopy, which allowed to derive also their linear absorption coefficient at the laser wavelengths used. Subsequently, single-pulse laser ablation thresholds and processing of the films using three different scanning speeds were carried out. Chemical and physical modifications induced by laser irradiation were

systematically characterized using Confocal μ-Raman and Laser Induced Fluorescence spectroscopies.
Finally, in contrast with the induced modifications resulting from irradiation at 266 nm, the promising results achieved on a large number of samples irradiated at 213 nm emphasize, as demonstrated in previous studies conducted on shellac resin (Ouija et al. 2011), the importance of following a wavelength-based approach to safely remove different types of naturally and artificially aged varnishes.

4.0 Introduction

Nowadays, many laser systems operating in different spectral regions and pulse durations have been proposed for the cleaning of paintings. Nanosecond (20-50 ns) excimer lasers emitting at 351 nm (XeF), 308 nm (XeCl), 248 nm (KrF), and 193 nm (ArF) (Carlyle 1981, Zergioti et al. 1997, Salimbeni et al. 1998, Georgiou et al. 1998, Scholten et al. 2000, Castillejo at al. 2002, Teule et al. 2003, Theodorakopoulos 2003), Free Running (200-400 μs) Er:YAG (2.94 μm) laser (Wolbarsht et al. 1990, de Cruz et. al. 2000, Bracco et al. 2003, Andreotti et al., 2007, De Cruz et al. 2014), Q-Switch (5-15 ns) Nd:YAG lasers (1064, 532, 355, 266, 213 nm) (Gaetani et al. 2000, Sansonetti et al. 2000, Pouli et al. 2003, Castillejo et al. 2003a, Chappé et al. 2003, Hildenhagen et al. 2003, 2005, Schnell et al. 2005, Apostol et al. 2011, Oujja et al. 2011, Siano et al. 2012) were mostly employed in laboratory tests aimed at assessing the laser-induced effects on pigments, binders, varnishes and their mixtures.
With the aim to minimize photothermal, photomechanical and photochemical phenomena, ultra-short lasers emitting pulses of picoseconds (ps) and femtosecond (fs) pulse duration have been recently introduced in the field (Pouli et al. 2008, Pouli et al. 2010, Gaspard et al. 2008, Oujjia et al. 2013). Thus, Ti:Sapphire irradiation (795 nm) with pulses of 100 fs has turned out to be ineffective for varnish removal (i.e., shellac) as well as the second harmonic at 398 nm (Oujja et al. 2011).
Irradiation of varnish layers at 265 nm with 260 fs pulses (100 pulses) can induce a loss of glossy of the remaining varnish which acquires a whitish appearance. Processing by irradiation at 248 nm with 500 fs laser pulses

results indeed in an improved etched morphology as compared with results achieved with ns pulses of the same wavelengths (Pouli et al. 2008). In contrast, irradiation at 213 nm with pulses of 15 ns of tempera paint models (i.e.,vermillion, lead chromate, lead white and azurite) covered with shellac varnish allows the controlled pulse by pulse micrometric layer removal of the varnish and preserves the colorimetric and spectral properties of the underlying paints (Oujja et al. 2011).
Taking advantage from the latest findings, this work is aimed at assessing the UV laser-induced effects on naturally and artificially aged varnish systems by using the fifth (213 nm) and fourth (266 nm) harmonics of a pulsed QS (15 ns) Nd:YAG laser.

4.1 Experimental

4.1.1 Prepared laboratory samples

Solvent and oil based varnishes have been formulated using materials listed in Table 1 (Chapter 3). Solvent-based varnishes were prepared from a 30% solution of the natural resin in the appropriate solvent while oil based varnishes were prepared by heating oil and the resin in separate pyrex containers in a sand bath. The mixtures were allowed to cool slowly in the sand bath to 60 °C when rectified turpentine oil was added to oil-resin mixture. All the formulations were applied using graduated pipette on microscopy glass slides (2.6x4.5 cm), on synthetic round quartz glass plates (∅=2.5 cm, 2.5 mm thick) and on primed canvas. After curing, a set of samples were left to natural ageing simply keeping them under controlled laboratory conditions (T=20 ºC, R.H= 40-45%) behind glass-window and protected from dust and the direct sunlight radiation for an overall period of about two years. Another set of samples was artificially light-aged following a systematic procedure described in the previous chapter (Section 3.1.2). After accelerated light ageing the samples were exposed to free oxygen conditions for 1 months and subsequently, stored in the dark where autooxidative reactions (cross-linking and

polymerization) and yellowing occur (Dietemann 2003, Fotakis et al. 2010).

4.1.2 UV-Vis absorption spectroscopy

UV-Vis absorption spectra were acquired using a Shimadzu UV3600 recording double-beam spectrophotometer. Spectral window was settled in a wavelength range of 200-800 nm with a sampling interval of 1 nm and a scan speed of 200 nm min^{-1}. Samples had to be prepared on quartz plates as thin films to correctly measure the UV-Vis absorption features. For this reason, a small amount (order of mg) of each varnish film was weighted in a Sartorius Research balance with a readability of 0.01 mg. The weighted amount was grinded and then dissolved in equal concentration of about 0.086 % (0.00259 g/3cc) (weight to volume) for all samples choosing a suitable solvent or blend by Teas chart (see Table 1) (Horie 1987).
An ultrasonic bath was used to speed up the dissolution process. After that, a volume of about 3 ml was casted by graduated Gilson micropipette on round quartz plates (Ø=5 cm, 2 mm thick). Once films were dried and the solvent completely evaporated, the resulting thickness was measured using a Digital Comparator (Mahr Extramess) with a resolution of up to 0.2 µm. The measured values were between 1.5-2 µm for all casted films. Spectra acquired covered an absorbance range which is well-below the spectrophotometer saturation threshold of 3 absorbance units. All spectra reported are expressed as absorbance ($A=\log I_0/I$) and/or mean absorption coefficient (α_{mean}) as function of wavelength and no solvent subtraction was necessary to correct the absorption profiles.
1st order derivatives were calculated over the whole spectral window in order to find the correct position of the inflection point, which provides a useful information about the wavelength of maximum absorbance. After calculating derivative spectra, a slight (5 points) average-adjacent smoothing filter was performed for each samples in order to improve the signal-to-noise ratio.

Table 1 – Varnish samples, after natural and artificial ageing, and solvents used for preparation along with solubility characteristics.

sample description	**solvent**	**solubility**
Naturally aged		
dammar	dicloromethane	soluble
mastic	dicloromethane	soluble
mastic/linseed oil	dicloromethane	partially soluble
colophony	clorophorm	soluble
colophony/linseed oil	clorophorm	soluble
sandarac	isopropanol	soluble
sandarac/linseed oil	isopropanol/DCM	soluble
copal/linseed oil	clorophorm	partially soluble
shellac	ethanol	partially soluble
Artificially aged		
dammar	dicloromethane	soluble
mastic	dicloromethane	soluble
mastic/linseed oil	toluene/acetone (60/40)	partially soluble
colophony	clorophorm	soluble
colophony/linseed oil	clorophorm	soluble
sandarac	benzyl alcohol	insoluble
sandarac/linseed oil	isopropanol/DCM	partially soluble
copal/linseed oil	clorophorm	partially soluble
shellac	Methanol/DCM	insoluble

4.1.3 Confocal μ-Raman spectroscopy

Confocal μ-Raman analyses were performed on the varnish films applied on round quartz plates (see Chapter 3) both to study the material degradation processes following ageing and the laser-induced modifications. μ-Raman spectra were recorded with a Renishaw System spectrometer using a diode laser of 785 nm wavelength, as excitation source. The Raman signal was calibrated using the emission line at 520 nm of a standard silicium target. The grating was 1200 lines/mm, giving a spectral resolution of about 1 cm^{-1}. The laser was focused at the sample surface using an objective lens of 50x. All the spectra were acquired in

the 3500–200 cm^{-1} region. Series of 10 acquisitions at different depths were taken using a WIRE2 Depth series measurement with an axial resolution of 1 μm across the thickness varnish. These preliminary measurements were performed for checking some chemical changes through the thickness varnish, as the findings reported in literature about the scalar oxidation gradient (Theodorakopoulos et al 2007, 2009a, 2009b). All spectra acquired were processed as follows:

- *Smoothing*: spectra were smoothed using the 1st order Savitzky–Golay filter. The filtering method essentially performs a local polynomial regression to determine the smoothed value for each data point. This method is superior to adjacent averaging because it tends to preserve features of the data such as peak height and width, which are usually 'washed out' by adjacent averaging
- *Baseline correction*: when needed, the fluorescence background was corrected selecting manually the points for its subtraction.
- *Normalization*: to assess the laser induced modifications, the band at 1450 cm^{-1}, which did not vary significantly, was chosen for spectral intensity normalization after the subtraction of the same baseline for all spectra.

4.1.4 Laser Induced Fluorescence spectroscopy

In order to assess possible chemical modifications induced by laser irradiation on varnish films, Laser induced Fluorescence (LIF) spectroscopy was performed exciting at 266 nm. For this goal, the naturally and artificially aged varnish films applied on primed canvas were chosen as suitable samples for LIF measurements.
LIF spectra were measured using a 0.30 m spectrograph with a 300 lines mm^{-1} grating (TMc300 Bentham) coupled to an intensified charged coupled detector (2151 Andor Technologies). With the use of a grating with 300 lines/mm, a spectral range of 280 nm is covered at once. The temporal gate was operated at zero time delay with respect to the arrival of the pulse to the surface of the sample and with a width of 3 μs.

The sample was illuminated at an incidence angle of 45° with a pulse energy less than 0.1 mJ and a spot of about 3 mm^2 (F~3mJ/cm^2). A 320 nm cutoff filter was used to reject the second order laser of the excitation wavelengths in the Vis range. Each spectrum acquired was the average of 20 measurements acquired in two different points of each irradiated area (Oujja et al. 2011). The selected repetition rate was 1 Hz. All the recorded spectra were normalized to their maxima to be independent of the incident intensity and of the quantity of analyzed material.

4.1.5 Laser ablation thresholds

Laser irradiation tests were performed using a Q-switched Nd:YAG laser (Lotis II, LS-2147) operating at the 5th (213 nm) and 4th (266 nm) harmonics of the fundamental radiation with pulses of 15 ns at a repetition rate of 1 Hz. The average pulse-to-pulse energy fluctuations are of about 10% for the two Nd:YAG harmonics. The laser beam at both laser wavelengths was focused on the surface of the sample by means of a spherical planoconvex quartz lens with f= 80 mm at a fixed distance of 71 mm. For continuous control of the laser output, a high energy variable dielectric attenuator (Laser Optik) was used.

Ablation thresholds were determined for each system at the two wavelengths by measuring first the threshold onset energy at which smoke (desorbed material as gas phase) emission from the irradiated sample is observed, and second, the size of the irradiated area by applying the spot regression method (Liu 1982, Baudach et al. 1999, Oujja et al. 2010, 2011) using a sensitive photographic film.

For laser pulses with a Gaussian spatial beam profile, the maximum laser fluence, F, on the sample surface and the diameter, D, of the ablated area are related by $D^2=2\omega_0^2 \ln (F/F_{th})$, where ω_0 is the $1/e^2$ radius of the Gaussian beam distribution and F_{th} is the ablation threshold. The diameter of the ablated area was determined as observed on the photographic film by optical microscopy. From a plot of D^2 versus lnE, E being the pulse energy, F_{th} and ω_0 can be determined.

As an example, Fig. 1 shows the linear dependence of D^2 with lnE upon irradiation with a single pulse at 266 and 213 nm (15 ns) of photographic film.

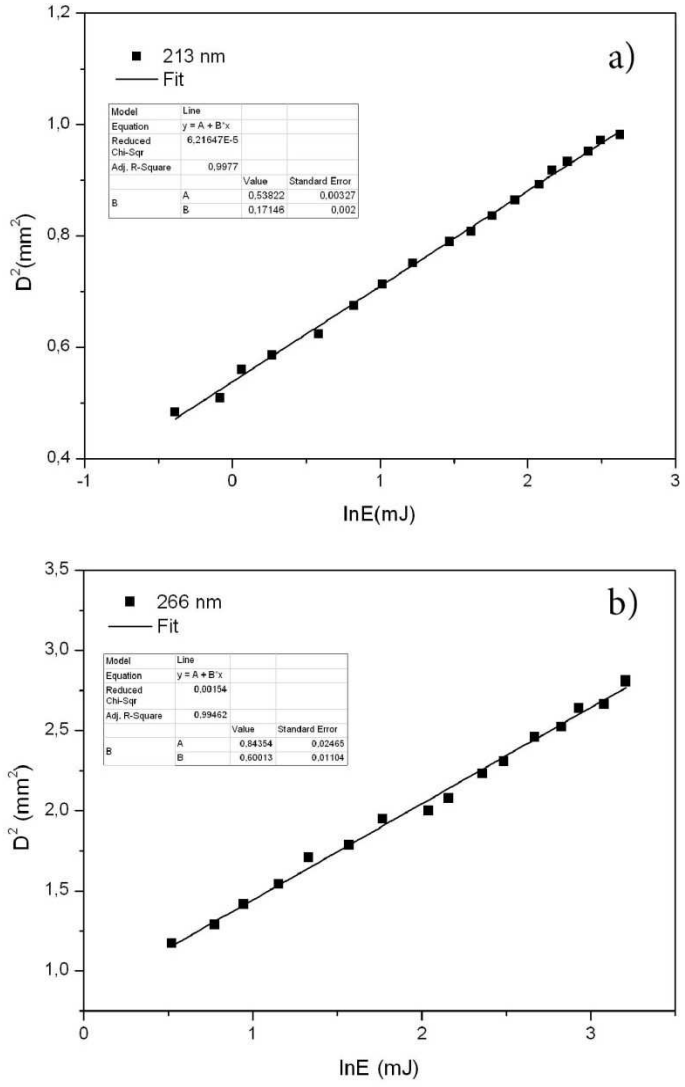

Fig. 1- Linear dependence of D^2 with lnE upon irradiation with a single pulse at a) 213 and b) 266 nm (pulses of 15 ns) on photographic film.

The value of ω_0 was calculated by a linear fit taking the slope as equal to $2\omega_0^2$. The calculated values of ω_0 are 0.3 and 0.55 mm at 213 and 266 nm respectively.

4.1.6 Laser processing

Laser processing was performed at the two irradiation wavelengths on grounded canvas samples, which was a suitable support for laser irradiation due to a lower degree of cracks of those films with respect to those on glass slides. Each varnish sample was processed at fluences two times higher ($2F_{th}$) than the corresponding single-pulse ablation threshold previously measured. The laser beam at both wavelengths was focused at the target surface using a cylindrical planoconvex quartz lens of f=150 mm which spot size was about 6.0x0.1 mm^2 at 213 nm and 5.5x0.1 mm^2 at 266 nm. Each area was processed at a repetition rate of 10 Hz following two different scanning procedures. The first one was performed turning manually a microstage over the entire scanned area, the second using a motorized stage setting 0.1, 0.2 and 1 mm/s as scan-speeds along x direction. The latter correspond respectively to 10, 5 and 1 laser pulses for each laser spot. By means of the following simple relation, n=1-l/2r, where n is the pulse overlap, l is the length between the center of two successive laser spots and r the spot radius (half width of the rectangular laser spot, r=0.05 mm), the pulse-overlap can be easily estimated. Considering the three scan speeds reported above the pulse overlap is equal to 90, 80 and 0 %, respectively. Chemical and physical modifications upon laser removal at 213 and 266 nm were evaluated on scanned areas at 0.1 mm/s.

4.2 UV-Vis light absorption features of aged varnishes

4.2.1 Results

4.2.1.1 Triterpenoid resins: dammar and mastic

Fig. 2 and 3 show the UV-Vis absorbance and mean optical density of the triterpenoid resin films with and without linseed oil.

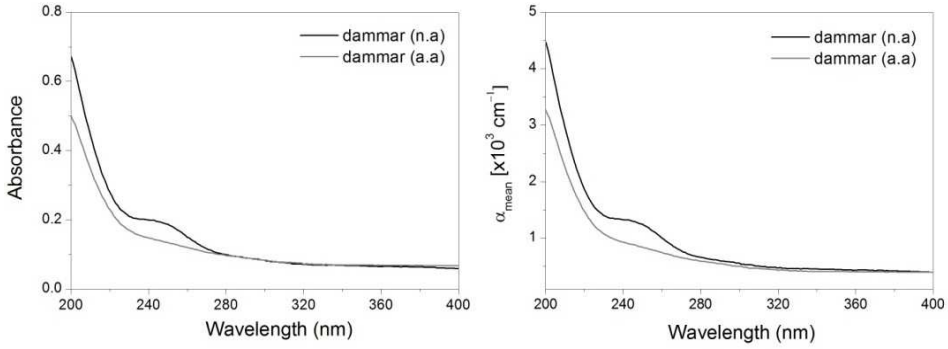

Fig. 2 – Absorbance and mean optical density of non-irradiated dammar varnish sample.

At a first qualitative comparison, spectra of naturally aged varnishes are characterized by broad shoulder-peaks in different positions with respect to artificially aged one that do not have this feature but rather show a lower degree of absorption in the region of 220-280 nm. These shoulder peaks are also different in shape. The dammar film shows a characteristic inflection point while mastic films are characterized by a non stationary inflection points.

For a more accurate calculation about the position of shoulder peaks, the 1st order derivative spectrum of dammar is shown in Fig. 4. The first intense negative peaks of both dammar samples (205 nm, $\alpha_{na\text{-}aa}$ ≈3850-2800 cm^{-1}) refer to the inflection points of the first absorption maxima, which fall out the spectrophotometer range, approximately at 190 nm. The second positive peak at 235-240 nm (α_{na} ≈1340 cm^{-1}) in the spectrum of dammar naturally aged is related to the shoulder shown in Fig. 3, whereas the sample artificially aged does not show this feature.

The peak at 235-240 nm may be considered an absorption maximum because it is a stationary point (f'=0).

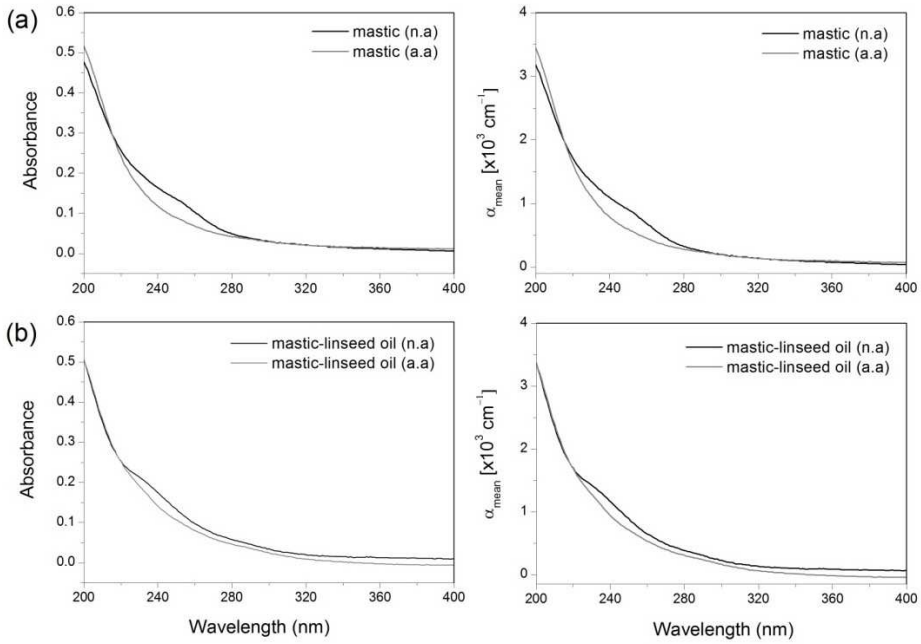

Fig. 3 – Comparison between absorbance and mean optical densities of non-irradiated mastic (a) and linseed oil-mastic films (b).

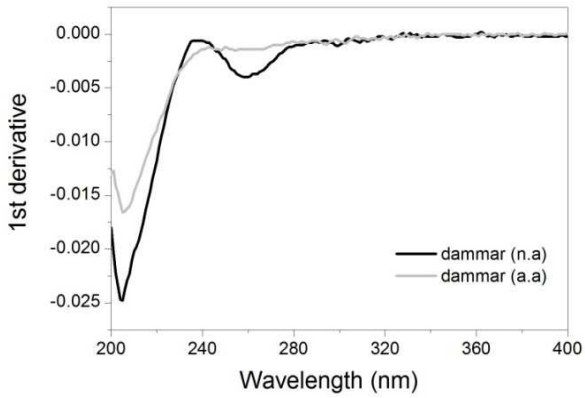

Fig. 4 1st order derivative UV-Vis absorption spectrum of quartz casted dammar films.

First derivative spectra of mastic films show different features with respect to those previously discussed in dammar (Fig. 5).
The negative peaks at about 205 nm ($\alpha_{na\text{-}aa}$≈3850-2800 cm^{-1}) present in dammar films are slightly shifted in mastic to about 206-210 nm ($\alpha_{na\text{-}aa}$≈2400-2500 cm^{-1}). This bathochromic shift between dammar and mastic resins indicates small compositional differences in the constituting triterpenoid compounds. Concerning with mastic films, two shoulder-peaks at 230 nm ($\alpha_{na\text{-}aa}$≈1400-1100 cm^{-1}) were observed in the 1st order derivative spectra. Naturally aged mastic films showed also a second positive band at about 245 nm (α_{na} ≈1000 cm^{-1}) which was undetected in the sample artificially aged (Fig. 5). These spectral features, which can be hardly appreciated in the absorption spectra shown in Fig. 3a, correspond to undulation points (f'≠0).

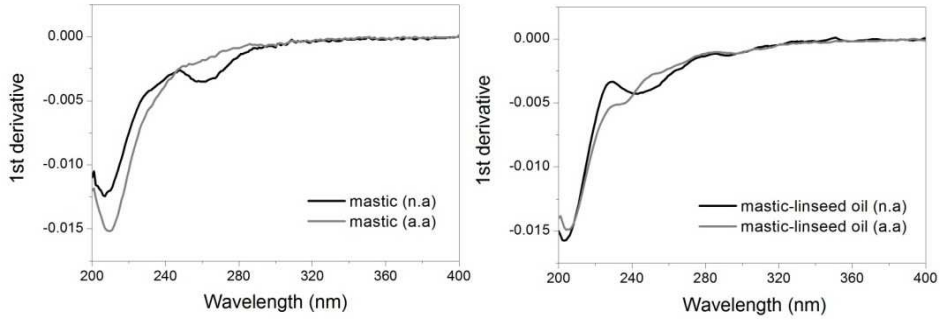

Fig. 5 1st order derivative spectrum of quartz casted mastic and linseed oil-mastic films

In presence of linseed oil the absorption pattern is slightly different with respect to pure mastic. The negative peaks are for both samples at about 203-204 nm ($\alpha_{na\text{-}aa}$≈3000-2950 cm^{-1}) and the optical density is almost the same. The shoulder-peak previously discussed in mastic at about 230 nm ($\alpha_{na\text{-}aa}$≈1400-1100 cm^{-1}) is now clearly visible as well-resolved band, in higher extent in naturally aged sample ($\alpha_{na\text{-}aa}$≈1450-1250 cm^{-1}) than in the light aged one ($\alpha_{na\text{-}aa}$≈1030-700 cm^{-1}).

4.2.1.2 Diterpenoid resins: colophony, sandarac and Manila copal

UV-Vis absorption spectra of diterpenoid varnishes, as the triterpenoid samples discussed in the previous section, showed different features mainly due to the different number and position of the carbon-carbon double bonds. Colophony (*Pinaceae* family) varnish films are characterized by a distinct absorption profile in comparison to sandarac and copal resins (Fig. 6). Thus, colophony shows a three structured shape spectrum due to the high content of abietane compounds, whereas sandarac and copal, being constituted mainly of pimarane and free labdane molecules, do not show these features. It is clear that such compositional differences reflect also in the overall shape of the UV-Vis absorption spectra.

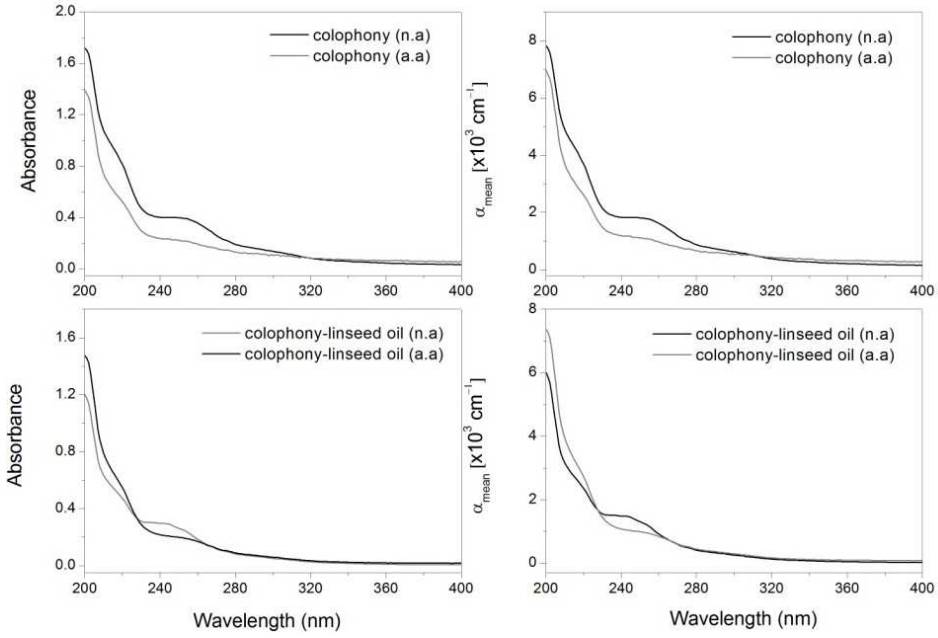

Fig. 6 UV-Vis absorbance and mean absorption coefficient of colophony varnish films with and without linseed oil.

For calculating more accurately the inflection points, the first order derivative spectra were reported also for diterpenoid varnishes, as depicted in Fig. 7.

In detail, colophony films without linseed oil are characterized by a rather sharp negative peak at about 203 nm ($\alpha_{na\text{-}aa}$≈6800-6000 cm^{-1}), a marked positive shoulder ($f'\neq0$) at 213-217 nm ($\alpha_{na\text{-}aa}$≈4500-2800 cm^{-1}), a low intensity absorption band ($f'=0$) at 240-245 nm ($\alpha_{na\text{-}aa}$≈1800-1100 cm^{-1}) and a very weak and wide band ($f'\neq0$) at about 270-280 nm (α_{na}≈700 cm^{-1}).

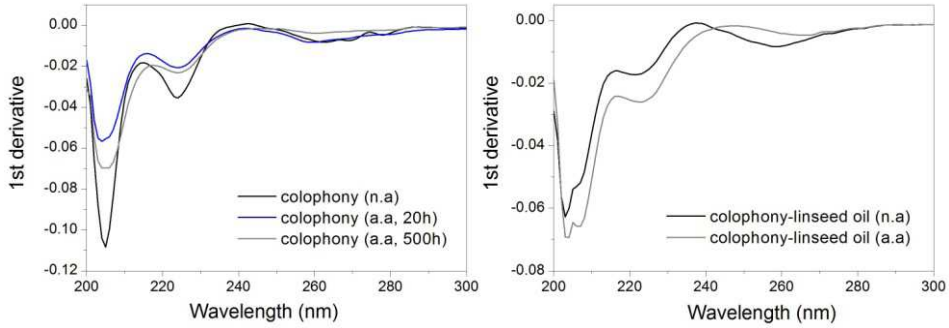

Fig. 7 First derivate spectra of quartz casted colophony films with and without linseed oil.

The latter is always detectable after 20h of artificial ageing and it completely disappears after 500h. It is also worth noting that artificial ageing induced a clear bathochromic shift in the 210-230 nm region, most likely due to the changes in conjugated carbon-carbon double bonds.
Regarding linseed oil mixtures, as for all the other samples, the presence of 30 wt% of linseed oil does not seem to differ significantly with the UV-Vis absorption profile of the resins film prepared. Despite this fact, first derivatives spectra resolved the overlapping bands showing some different spectral features in presence of linseed oil (Fig. 7).
The most important one is that the first intense negative peaks are now wider and splitted, as a "tooth", in two unresolved bands at 203 ($\alpha_{na\text{-}aa}$ ≈5340-6750 cm^{-1}) and 206 nm ($\alpha_{na\text{-}aa}$≈4065-5235 cm^{-1}). The latter shoulder in both samples may be related to the presence of linseed oil and it appears more resolved in the artificially aged sample.
Contrarily to what observed in pure resin films, the positive shoulder ($f'\neq0$) appears for both the samples at 216 nm. Different features were also noted in the 230-250 nm absorption region. In detail, the positive

bands (f'=0) are located at 235 (α_{na}≈1500 cm^{-1}) and 250 nm (α_{aa}≈1000 cm^{-1}) indicating a bathochromic shift from unaged to aged samples of 15 nm, respectively. This change can be attributed most probably to the loss or isomerization of double bonds during the photo-induced ageing.

As regards sandarac (*Tetraclinis articulata*) and Manila copal (*Agathis dammara*) varnish films the UV-Vis absorption spectra are shown in Fig. 8.

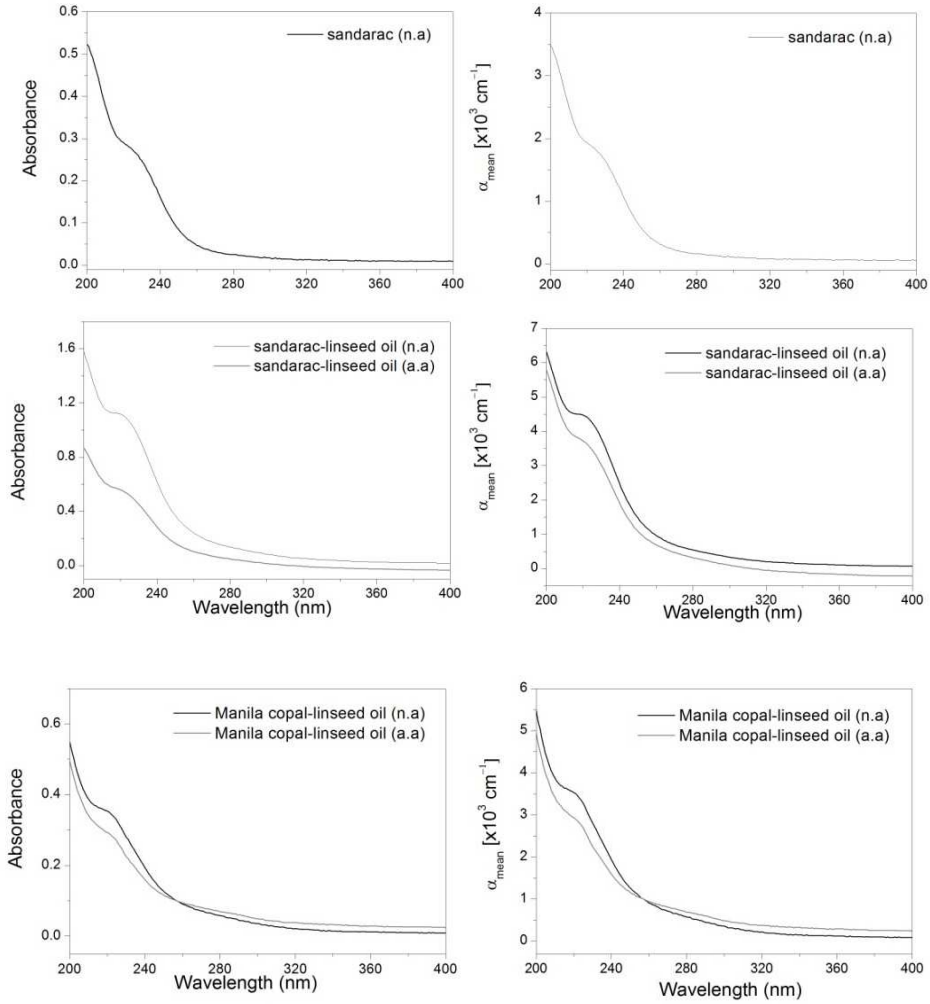

Fig. 8 UV-Vis absorbance and mean absorption coefficient of sandarac and Manila copal varnish films.

They have similar UV-Vis absorption features and can be well differentiate from colophony resin due to the apparently absence of abietane compounds, such as ABA and DABA, which is in agreement with their composition. Diterpenoids, such as sandarac and copal resins, consist mainly of free labdanes and of a highly cross-linked fraction of polycommunic acid. The composition of these diterpenoid resins makes them very hard, tough and almost insoluble in common organic solvents. In facts, sandarac artificially aged spectrum was not reported due to low amount of solvent-extractable compounds.

First derivative spectra of sandarac and Manila copal varnish films were reported in Fig. 9. As all the absorption spectra shown, they are characterized by a strong minimum at about 202-205 nm, even if for manila copal with linseed oil it falls out the spectrophotometer limit.

Sandarac naturally aged spectrum shows the first positive peak at about 220 nm ($\alpha_{na} \approx 1900$ cm^{-1}), although the extracted fraction was very low. On the opposite, sandarac and Manila copal linseed oil mixtures have the peak mentioned above respectively at ~217 nm ($\alpha_{na\text{-}aa} \approx 4500\text{-}3820$) and 218 nm ($\alpha_{na\text{-}aa} \approx 3650\text{-}3000$). Both the latter are slightly shifted toward lower wavelengths in comparison to the naturally aged sandarac sample.

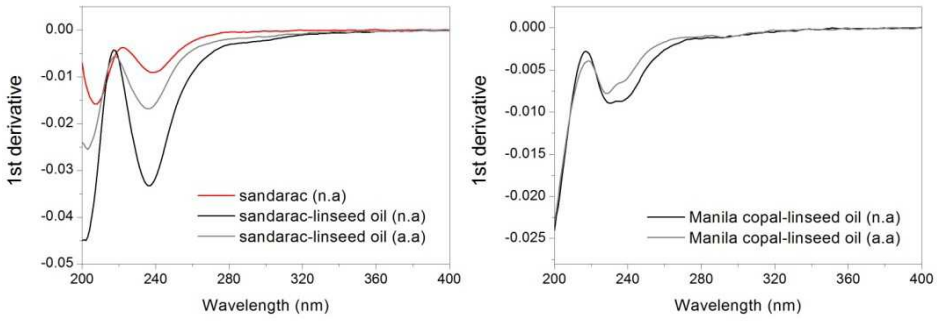

Fig. 9 1st derivative spectra of sandarac and Manila copal quartz casted varnish films.

4.2.1.3 Bleached shellac

UV-Vis absorption spectrum of naturally aged bleached shellac varnish film is shown in Fig. 10. The spectrum is characterized by a broad absorption peak with a maximum centered at about 230 nm ($\alpha_{na}\approx5150$ cm^{-1}). For this evident reason, no differentiation was applied. The artificially aged bleached shellac sample was not reported due to the complete loss of solubility in all the common organic solvents.

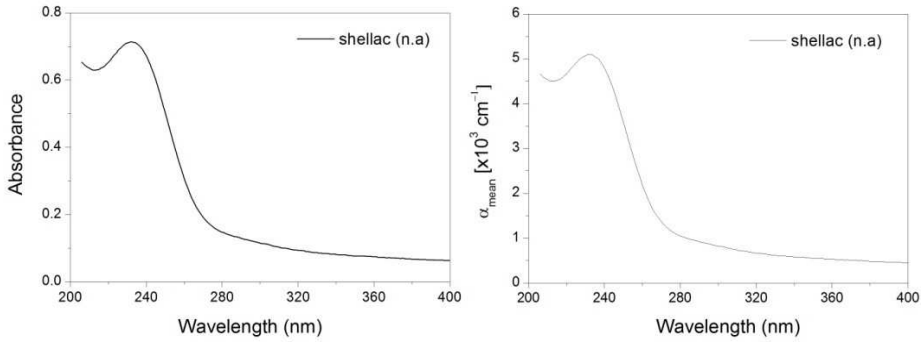

Fig. 10 UV-Vis absorbance and mean absorption coefficient of shellac varnish film.

4.2.2 Discussion

For all the terpenoid compounds analyzed, the absorption maximum lies in the far-ultraviolet (200–120 nm), which is accessible only by the use of vacuum spectrographs or spectrometers (Micheli and Applewhite 1961, Platt et al. 1953). Despite this fact, noticeable differences have been observed among different classes of naturally aged terpenoids films, such as tri (i.e. mastic and dammar), di (i.e. colophony, sandarac and Manila copal) and sesquiterpenoid (i.e shellac) resins. More difficulties were encountered for discriminating between different classes in artificially aged samples, especially those containing linseed oil. The results obtained are summarized in Table 2.

For first, all the UV absorption wavelengths reported can be related to $\pi\rightarrow\pi^*$ electronic transitions. Triterpenoid compounds consists mainly of

polycyclic saturated molecules with dammarane, oleanane, ursane skeletons, which absorb mainly in the 180-200 nm region.

Table 2 – UV absorption wavelengths of quartz casted varnish films in the stationary ($f'=0$) and non-stationary ($f'\neq0$) points of inflection, as calculated by the first derivative spectra. Wavelengths are given in nm and (sh) refers to non-stationary point of inflection.

sample	**naturally aged films**	**artificially aged films**
dammar	240	--
mastic	230 sh, 245sh	230 sh
mastic-linseed oil	230 sh	230 sh
colophony	213sh, 240-245, 270-280	217sh, 240 sh
colophony-linseed oil	216 sh, 235	216 sh, 250
sandarac	220 sh	n.m
sandarac-linseed oil	217sh	217sh
copal-oil	216 sh	218 sh
shellac	230	n.m

Within the investigated range, dammar and mastic naturally aged films showed a weak absorption at about 240 nm tailing until to 320 nm, which is most prominent in dammar. Mastic films reveal also a shoulder at 230 nm which was undetected in dammar. The rise at 240 nm may be referred to unsaturated ketones, which are characterized by the conjugation of a C=O bond with one C=C bond. In addition, triterpenoids contain, in some cases, aldehyde groups. These functional groups have also $n\rightarrow\pi^*$ transition at relatively high wavelengths (270–300 nm), which result in a weak absorption (Van der Doelen 1999, Van der Doelen et al. 2000, Brewis et al. 1961, Mills and Werner 1955, Schneider et al. 2009).
On the contrary, artificially aged triterpenoids films are characterized by the lacking of the band at about 240 nm, thus showing a smoothed profile. This is due to the cleavage of keto-group via Norrish type reactions, which leads to the formation of acids, such as carboxylic groups, aldehydes, peroxides, and hydroperoxides, as previously discussed in the Chapter 3. The $\pi\rightarrow\pi^*$ electronic transitions of these acids groups enhance the absorption close to 200 nm. Thus, for example, in absence of any additional chromophores, carboxylic acids absorb at 210 nm.

No products that account for the strong absorption of aged triterpenoid varnishes at 400 nm, which causes the yellowing problem, were observed (De la Rie 1988b, Van der Doelen 1999, Dietemann 2003, Theodorakopoulos et al. 2007).

Concerning with diterpenoid varnishes were detected some different bands that appear as marked shoulders for the three prepared samples. These shoulders give evidence of specific absorbing chromophores. Specifically for colophony the relatively intense shoulder at 240-245 nm indicates the presence of abietane compounds which are characterized by two conjugated double bonds in different position. In fact, it was shown by capillary electrophoresis that the different position of two conjugated C=C double bonds in ABA and NABA gives a clear UV absorption maximum at 240 and 250 nm, respectively (Brown et al. 1943, Luong et al. 1999, Findeisen et al. 2007). The weak absorption band at about 270-280 nm ($n \rightarrow \pi^*$ transition), which undergoes shifting after ageing, can be assigned to levopimaric acid (LEV) (Schuller et al. 1962, Luong et al. 1999, Nuopponen et al. 2004). The band at 213 nm in naturally aged colophony may come from different pimarane resinous acids which are present in colophony and absorb in that region. Pimarane compounds, such as PIA, IPIA and SPIA, have a relatively intense absorption at 200-210 nm due to presence of a vinyl group side-chain and the lack of conjugated carbon double bonds (Findeisen et al. 2007). In artificially aged sample the absorption at 213 nm results shifted at about 217 nm. This can be explained by the formation of DABA which has a strong absorption at 200 nm and a less intense shoulder at about 218-220 nm (Findeisen et al. 2007). This compound is formed in colophony over time through an oxidative process properly known as dehydrogenation (Mills and White 1977). Highly oxidized DABA compounds, such as hydroxydehydroabietic acids (OH-DABA), 7-oxoDABA, di-OH-DABA and 15-OH-7-oxoDABA, were also proposed as useful marker compounds to assess oxidising environments in old paintings (Berg et al. 2000, Findeisen et al. 2007).

Contrarily, diterpenoid fossil resins, such as sandarac and copal, consist mostly of free labdane compounds (two rings structure), such as communic acid (COA), agathic acid (R=COOH) and its monomethyl

ester (Mills and White 1977, Colombini Modugno 2009, Daher et al. 2010). These compounds have a weak absorption at 240 nm due to conjugated diene side chain (Carman et al 1970). It is also reported that oxidative degradation leads to the conversion of agathic acid (I) into a product related to abietic acid, which is known to have an absorption at 240 nm (Büchi & Pappas 1954). However, the low amount of solvent-extractable compounds did not allow to dissolve the cross-linked polymer fraction. The prepared samples showed characteristic absorption shoulders in the 216-220 nm region which may be attributed to pimarane compounds, such as PIA, IPIA and SPIA.

Finally, shellac varnish showed a clear absorption band centered at about 230 nm. As reported in literature (Upadhye et al. 1970, Sharma et al. 1983), the constituting terpene compounds of shellac have an αβ-olefinic carboxyl chromophore with a clear UV absorption in the 220-230 region with exception of aleuritic acid, which is essentially transparent in the near UV region. Thus, epishellolic acid has an λ_{max} at 226 nm, jalaric acid at 220 nm and shelloic at 218 nm (Wadia et al. 1963, 1969) suggesting a carboxylic function conjugated with an olefinic linkage.

A further general discussion is needed for artificially aged samples and linseed oil-resin mixtures being apparently weak UV absorbers. First of all, artificially aged samples showed an overall absorbance decrease along the whole spectral window, as result that the photoxidation reactions promote the conversion of carbon double bonds into single bonds. This change was observed also for the linseed oil-resin mixtures after the heat processing (see Chapter 3), which involves the disappearance of the conjugated double bonds in polyunsaturated fatty acids chain, primarily linolenic (Bradley & Richardson 1940, Van den Berg 2002).

Monounsaturated (oleic) and saturated acids (stearic, palmitic) do not contribute significantly to the general absorption in the near-ultraviolet region of the spectrum. All these observations allow to conclude that in the oil-resin films the oil component may not be easily discriminated. In addition, the partial solubility of the oil-resin mixtures gave a further drawback for discriminating the oil fraction by means of UV-Vis absorption spectroscopy.

4.3 Results and discussion

4.3.1 Laser ablation thresholds

Single-pulse ablation thresholds measured at 213 and 266 nm laser wavelengths for all the varnish samples are listed in Table 3. For comparison the linear absorption coefficient, as derived from UV-Vis spectroscopy, has been reported.

Table 3 – Comparison between single pulse laser fluence thresholds, (F_{th}, mJ/cm^2) and absorption coefficient (α, cm^{-1}) measured on naturally and artificially aged varnish films at 213 and 266 nm. The estimated error on F_{th} is less than 5 % while for α can vary from 15 to 30% for film that showed low solubility (see Table 1).

Laser wavelength	**213 nm**		**266 nm**		**ratios**	
Description	F_{th} (mJ/cm^2)	α (cm^{-1}) x 10^3	F_{th} (mJ/cm^2)	α (cm^{-1}) x 10^3	F_{th} 266/213	α 213/266
Naturally aged						
dammar	85±3	2.56	315±6	0.85	3.7	3
mastic	80±2	2.14	300±5	0.545	3.8	3.9
mastic-linseed oil	90±3	2.07	455±8	0.54	5	3.8
colophony	30±1	4.53	130±2	1.37	4.1	3.3
colophony-linseed oil	50±2	2.89	215±4	0.7	4.3	4.1
sandarac	65±2	2.33	360±6	0.3	5.5	7.8
sandarac-linseed oil	85±2	4.56	370±7	0.81	4.5	5.6
copal-linseed oil	60±2	3.7	370±7	0.78	6	4.7
shellac	85±2	4.63	530±9	1.27	6.4	3.6
Artificially aged						
dammar	60±2	1.97	275±5	0.68	4.5	2.9
mastic	70±2	2.2	275±5	0.38	3.9	5.8
mastic-linseed oil	80±2	2.23	475±9	0.52	5.7	4.8
colophony	30±1	3.435	120±2	1.075	4	3.2
colophony-linseed oil	45±1	3.515	255±4	0.7	5.7	5
sandarac	55±2	n.m*	320±6	n.m	5.8	n.m
sandarac-linseed oil	70±2	4.2	475±8	0.76	6.9	7.2
copal-linseed oil	80±2	3.08	370±7	0.72	4.6	3.7
shellac	85±2	n.m	520±9	n.m	6.3	n.m
*n.m refers to not measured value						

F_{th} ratio between the two wavelengths (266 nm/213 nm) spans from 3.4 up to 6.9 times indicating an evident higher absorption at 213 nm than 266 nm. Similarly, α_{mean} variation (213 nm/266 nm) ranges from 2.9 to 7.8 which is consistent with the previous F_{th} ratios. Furthermore, no remarkable differences were detected between the laser ablation thresholds and optical absorption of naturally and artificially aged samples.

4.3.2 Estimation of the temperature rise upon laser irradiation

The optical penetration depth ($\delta = 1/\alpha$) of the films can be easily derived from the value of the linear absorption coefficient (α) directly measured by UV-Vis spectrometer listed in Table 3. Clearly, the optical penetration depth estimated in this way will not be the same of that measured through a varnish layer upon laser treatment (non-linear condition) but it may be taken as a good approximation for the estimation of the temperature rise.
For nanosecond laser pulses, the effective optical penetration depth (δ) is much larger than the thermal diffusion length $z_{th}=2(D\cdot\tau)^{1/2}$ and hence laser heating occurs under thermally confined conditions. Thus for example, for organic material ($D \sim 10^{-3}$–10^{-4} cm^2/s [Fotakis et al. 2006)]) and laser pulse duration of 15 ns, z_{th} = 77.5–24.5 nm. The confinement condition ($z_{th}<<\delta$) allows calculating the depth distribution of the temperature rise as $\Delta T(z) = F_a\cdot e^{-z/\delta}/ \delta\rho C_p$, where ρ is the density and C_p the specific heat of the varnish layer. A rough estimation, based on volume-heating, could be carried out using the specific heat capacities C of the organic material that range from 1,1 J/g·K of an epoxy resin up to1,8 J/g·K of the natural rubber (Siano et al. 2012). Here, to give a more precise estimation of the temperature rise of terpenoid compounds upon UV laser irradiation, specific heat capacities Ci were calculated by using a computational analysis software (PerkinElmer-ChemOffice).
Considering the contribution of the main hydrocarbon skeleton types of each type of resin, the specific heat capacities estimated are listed in Table 4. Possible contributions arising from different substituent and oxidized groups were not taken into account in this simulation.

Table 4 Main skeleton types of terpenoid resins along with their computed chemical formula, monomer molecular weight and specific heat capacity. The skeleton types are depicted in Chapter 1.

Main compound	Skeleton types	Chemical formula	Monomer MW	C [J/mol·K]	C [J/g·K]
Triterpenoid	dammarane	$C_{30}H_{52}$	412.4	566.3	1.37
	euphane	$C_{28}H_{45}$	426.4	591.5	1.39
	oleanane/ursane	$C_{28}H_{44}$	412.4	545.8	1.32
	hopane	$C_{30}H_{52}$	412.4	553.5	1.34
	lupane	$C_{30}H_{50}$	410.4	542.5	1.32
	bicyclic triterpenoids	$C_{26}H_{44}$	356.4	499.9	1.4
	tricyclic triterpenoids	$C_{29}H_{48}$	396.4	545.2	1.4
Diterpenoid	abietane, ABA	$C_{20}H_{30}O_2$	302.2	374.2	1.24
	abietane, NABA	$C_{20}H_{30}O_2$	302.2	370.4	1.23
	abietane, DABA	$C_{20}H_{28}O_2$	300.2	366.1	1.22
	abietane PAA	$C_{20}H_{30}O_2$	300.2	373.9	1.25
	pimarane,PIA-IPIA-SPIA	$C_{20}H_{30}O_2$	300.2	368.8	1.22
	pimarane, IPIA	$C_{20}H_{30}O_2$	300.2	368.8	1.2
	pimarane, LPIA	$C_{20}H_{30}O_2$	300.2	374.2	1.24
	labdane COA	$C_{19}H_{28}O_2$	288.2	361.3	1.25
Sesquiterpenoid	Jalaric acid	$C_{15}H_{20}O_5$	280.1	322.4	1.15
	Shellolic acid	$C_{15}H_{20}O_6$	296.1	323.4	1.1
	Aleuritic acid	$C_{16}H_{32}O_5$	304.2	426.7	1.4

Table 5 Estimated temperature rise (z=0) for single-pulse fluence threshold of terpenoid varnishes upon laser irradiation at 213 and 266 nm.

Laser wavelength	**213 nm**		**266 nm**		**density**
sample	**ΔT (°C)**	**α (x 10^3 cm^{-1})**	**ΔT (°C)**	**α (x $10^3$$cm^{-1}$)**	**ρ (g/cm^3)**
Naturally aged					
dammar	149	2.56	181	0.85	1.04-1.13
mastic	116	2.14	111	0.545	1.07
colophony	100	4.53	132	1.37	1.07-1.1
sandarac	112	2.33	80	0.3	1.08-1.09
shellac	283	4.63	500	1.27	1.03-1.1
Artificially aged					
dammar	80	1.97	127	0.68	1.04-1.13
mastic	106	2.2	71	0.38	1.07
colophony	77	3.435	95	1.075	1.07-1.1
sandarac	--	n.m	--	n.m	1.08-1.09
shellac	--	n.m	--	n.m	1.03-1.1

Despite this approximation, the monomer molecular weight extrapolated from these calculations are only slightly lower, but of the same order of

magnitude, than those measured using different mass spectrometry techniques (Van der Doelen 1999, Van den Berg 2012).
For calculating the temperature rise for each class of resin, it was used an average value of the computed specific heat capacities. The latter correspond to 1.34, 1.23 and 1.22 J/g·K for triterpenoid (i.e. mastic and dammar), diterpenoid (i.e. colophony and sandarac) and sesuiterpenoid (i.e. shellac) resins, respectively.
The temperature rise attained at the surface (z=0) corresponding at the laser ablation fluence thresholds (see Table 3) have been reported in Table 5. The corresponding densities (Kg/cm^3) were taken from data reported in literature (Mills and White 1999).
Such average temperature rises in proximity of the varnish layer surface are indicative values and they can give useful information about the ablation mechanisms involved upon laser irradiation. Triterpenoid and diterpenoid resin films show, approximately, a similar temperature rise, with values close to the melting temperature range. As expected, shellac resin, being characterized by the highest fluence threshold and linear absorption coefficient, can reach very high temperatures upon laser removal treatment. Despite the predicted temperature rise may be apparently high, for short laser pulses, the thermal diffusion time $t_{th}=1/\alpha^2 \cdot D_{th}$ is equal to 0.1-2 ms at 213 nm and 10-100 ms at 266 nm. This means that thermal degradation rate is several orders of magnitude slower than the decomposition and material removal rate, which occurs on a very fast time scale (≈30-50 ns). This means that heat diffusion to the substrate is minimal upon laser removal treatment and any thermal side effect is confined within the ablated volume.

4.3.3 Laser processing and laser-induced morphological modifications

Laser processing was performed on all varnish samples using three different scanning speeds, as reported in section 4.1.6. An example showing the surface morphology of a naturally aged varnish sample irradiated at 213 and 266 nm is depicted in Fig. 11.

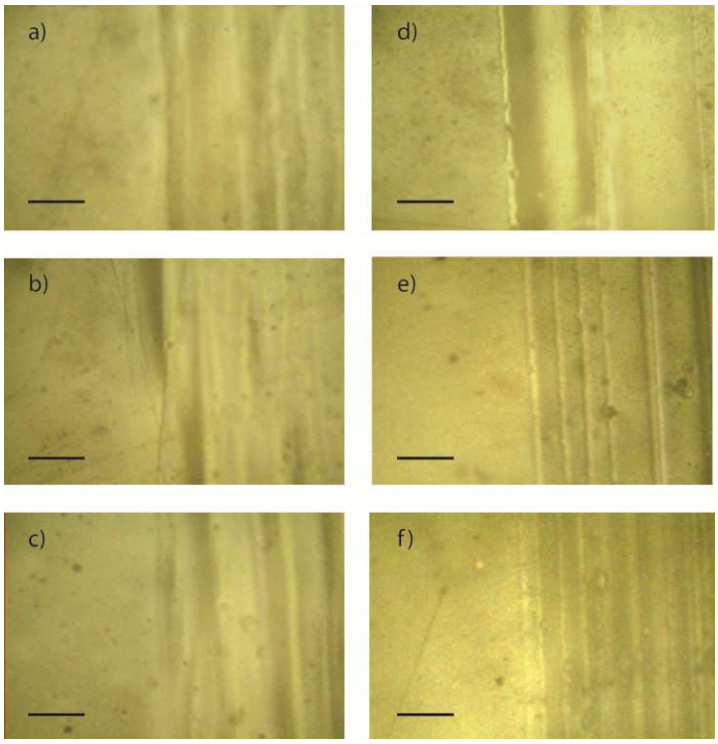

Fig. 11 Confocal micrographs of a naturally aged varnish sample resulting from laser processing at 213 nm (a-c) and 266 nm (d-f). Each laser treated area was performed at a fluence of 2 F_{th} (see Table 3) with a repetition rate of 10 Hz. The scanning parameters are: V=1 mm/s, 1 pulse each 0.1 mm, overlap 0% (a, d); V=0.2 mm/s, 5 pulses each 0.1 mm, overlap 80% (b, e); V=0.1 mm/s, 10 pulses each 0.1 mm, overlap 90% (c, f). The bar length is equal to 50 μm in all images.

Fig. 12 and Fig. 13 display the morphological effects induced on different naturally and artificially aged varnish samples after laser irradiation at fluences two times higher the ablation thresholds.

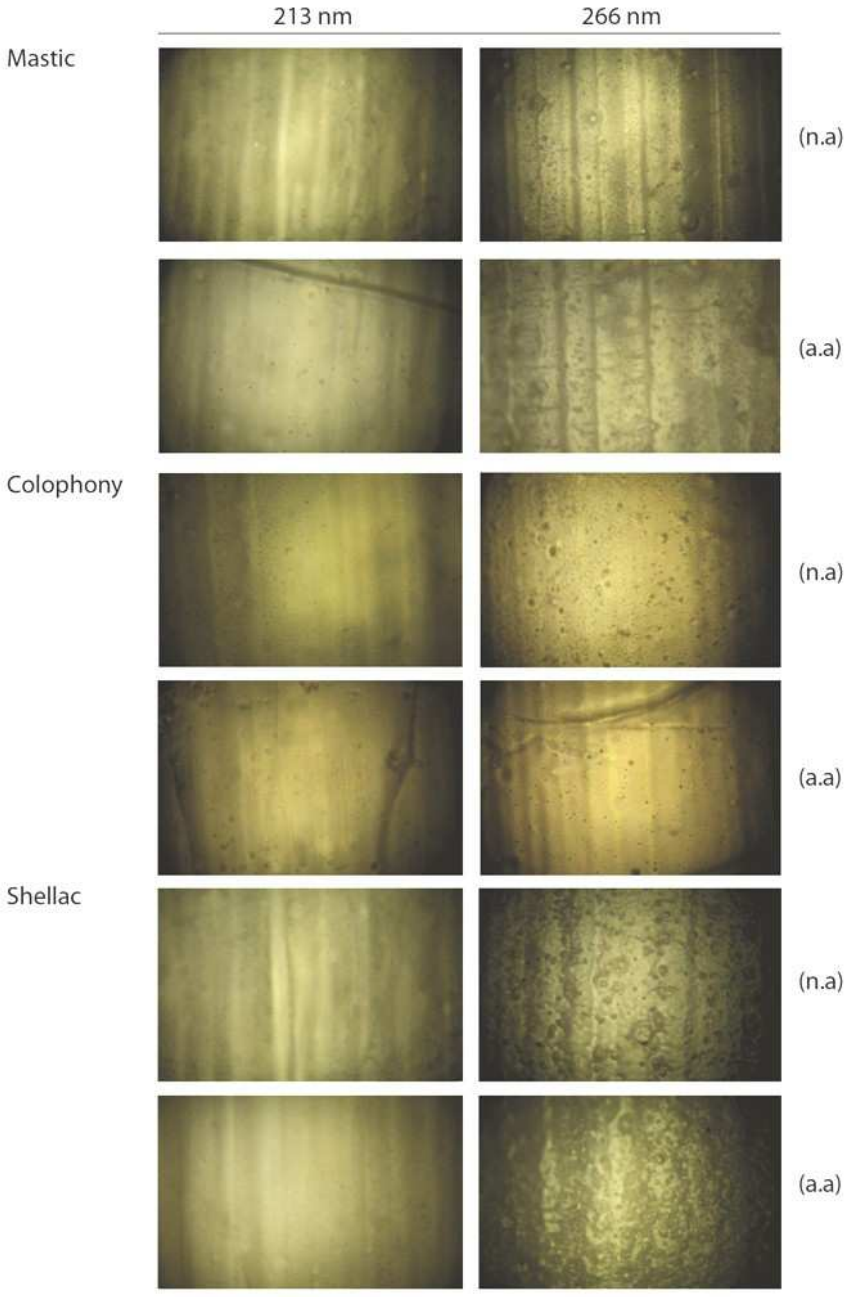

Fig. 12 Confocal micrographs (magnification 50x) of solvent based varnish films (i.e. mastic, colophony, shellac) irradiated with 10 laser pulses (V=0.1 mm/s) at fluence two times higher than F_{th} listed in Table 3. The size of each picture is 120x180 μm^2

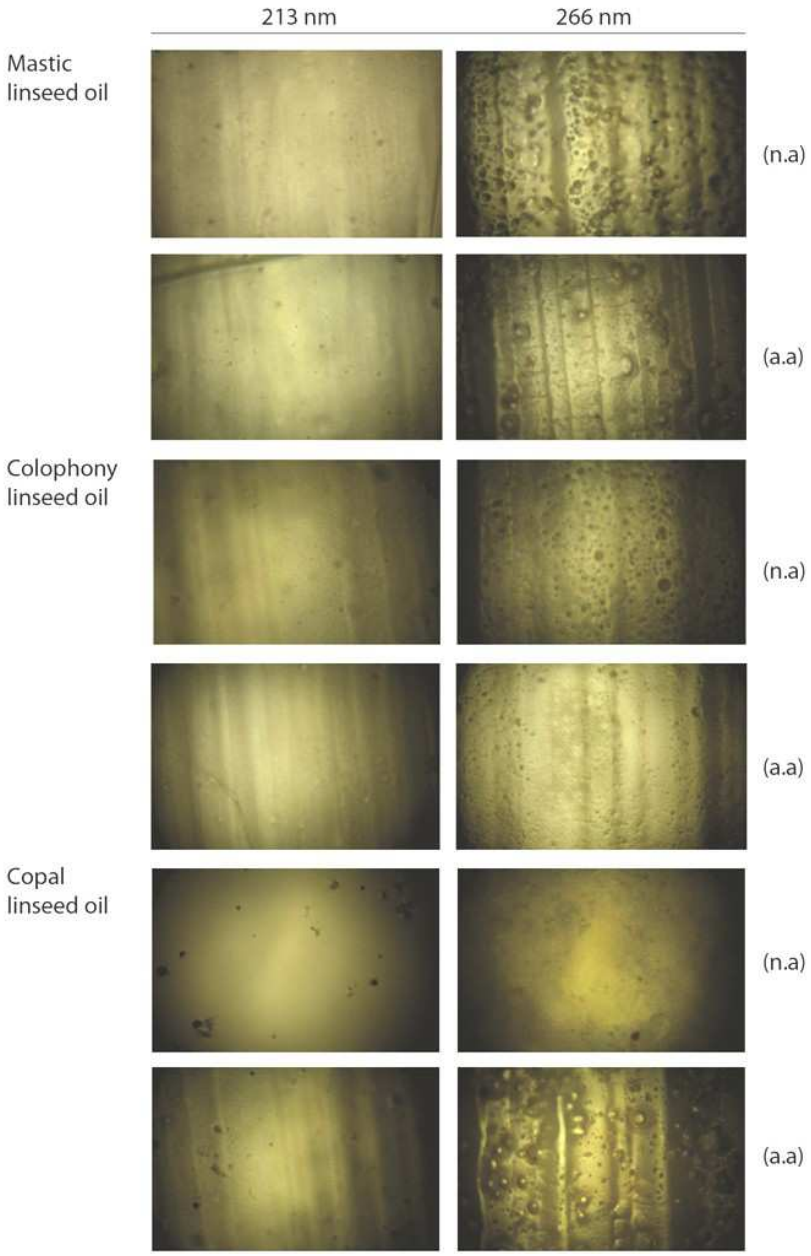

Fig. 13 Confocal micrographs (magnification 50x) of linseed oil prepared varnishes (i.e. mastic-oil, colophony-oil, Manila copal-oil) irradiated at 10 Hz (V=0.1 mm/s) with a fluence two times higher than F_{th} listed in Table 3. The size of each picture is 120x180 μm^2

Laser irradiated areas at fluence well above the single-pulse ablation threshold ($2F_{th}$) result in ablation and /or morphological modifications depending on the irradiation wavelengths, the type of varnish and degree of polymerization.

Irradiation at 213 nm induces ablation without noticeable morphological changes to the remaining varnish layer, which preserves its natural gloss. The layer by layer removal is provided by a high degree of resolution corresponding, on areas treated with 10 successive laser pulses with a fluence of $2F_{th}$, to about 4±0.5 μm.

Irradiation at 266 nm gives rise to the growth of microsized bubbles, as observed by means of confocal microscopy. Bubbles of about 5-15 μm were observed mostly in varnish films containing "hard resins", such as sandarac, copal and bleached shellac. In this case, the measured etch depth in the same irradiation conditions ($2F_{th}$) was of 14±0.5 μm. The remaining varnish layer, of the order of 5 μm, acquires a whitish appearance as result of increased surface light scattering.

In literature, several publications have been concerned with the physical changes upon UV laser irradiation of polymeric substrates (Dyer and Srinivasan, 1986, Srinivasan et al. 1986, Bäuerle 2000, Lippert et al., 2003, Bityurin 2005). It was widely demonstrated that nanosecond UV ablation of relatively transparent (weakly absorbing material at the irradiation wavelength) polymers reveals features of a first-order phase transition within the bulk material, bulk boiling, with bubbles creation. Formation of a foamy layer were also observed in films upon femtosecond laser irradiation at 265 nm of shellac varnish applied on tempera paints (Gaspard et al. 2008, Oujja et al. 2011).

As evidenced by Rebollar (Rebollar et al. 2006), the polymer molecular weight plays an additional role in the extent of the laser induced morphological modifications. For poorly absorbing polymers, swelling and bubbles formation at higher fluences, are more pronounced in polymers with high molecular weight. Similarly, as showed in this work by UV-Vis spectra and from the ablation threshold measurements, the laser wavelength of 266 nm is weakly absorbed by all the varnish systems studied, thus inducing the formation of bubbles. Ablation at 213 nm, which is a strongly absorbed wavelength, does not induce such drawbacks

(whitish appearance, bubbles) to the etched substrate leading to a clean surface morphology, as detected by confocal microscopy.

4.3.4 Confocal μ-Raman characterization of laser irradiated varnish samples

To assess the laser-induced modifications to the remaining varnish layer upon laser removal, a systematic Confocal μ-Raman characterization (exc. 785 nm) was carried out. All the μ-Raman spectra collected are reported in Appendix A at the end of the chapter. They correspond to areas treated with 10 laser pulses (scan-speed=0.1 mm/s, 10 pulses each 0.1 mm) at a fluence of 2 F_{th}.

4.3.4.1 Dammar and mastic

Confocal μ-Raman spectra of dammar and mastic varnish films before and after irradiation at 213 nm and 266 nm are shown respectively in Fig. 14 and Fig. 15 (Appendix A).
Raman spectra of films of dammar (n.a) and mastic (n.a) provide immediate indications of specific changes, which occur upon laser irradiation at 213 and 266 nm. The most relevant alteration following in naturally aged varnish samples involves the broadening and the intensity increase of bands at 1660, 1618 and 1590 cm^{-1}, which are related to the stretching mode of carbon double bonds (C=C). In addition, also the less intense carbonyl bands (small Raman cross section) at 1707 and 1705 cm^{-1} result slightly increased. The same trend is detected in the 3000-2600 wavenumber region, which contains bands assigned to the symmetric and asymmetric stretching of CH_2 and CH_3. Other minor changes, which appear more pronounced in mastic irradiated at both the laser wavelengths, are found in the 1490-1300 cm^{-1} region. They involve the appearance of new small bands at 1381, 1360, 1338, 1316 and 1303 cm^{-1}, which are assigned to the bending vibration of CH_2 and CH_3 groups (Brody et al. 2002, Yu et al. 2007, Nevin et al.2009).
Results from artificially light-aged dammar (a.a) and mastic (a.a) indicate an opposite alteration pathway in comparison to artificially aged ones and

it occurs in the same way for both the light-aged triterpenoid resins. It primarily involves the decrease of the weak carbonyl band, which result slightly shifted in aged dammar and mastic at 1712 and 1709 cm^{-1}, respectively. This change is accompanied also by a decreasing of CH groups, as shown in the insets of Fig. 14 and Fig. 15 (Appendix A). The above mentioned spectral modifications are induced only by irradiation at 266 nm, whereas no evidence of such alterations were observed upon irradiation at 213 nm.
As observed by confocal microscopy, the formation of bubbles at 266 nm, which involves the emission of gaseous products (CH_3OH, CH_4, $HCOOCH_3$, CO, and CO_2) during ablation, may be associated in highly oxidized compounds to the bond-breaking of the carbonyl functionalities and of methyl and methylene groups. Furthermore, in aged samples, carbon double bonds did not undergo any change upon laser irradiation because they reacted during the artificial ageing to form highly oxidized products (carboxylic acids functions, aldehydes and keto groups) in the outer varnish layer.

4.3.4.2 Colophony

μ-Raman spectra collected from naturally aged (n.a) colophony varnish after laser irradiation at 213 and 266 nm are plotted in Fig. 16 (Appendix A). Laser irradiated samples (n.a), although apparently do not show significant spectral changes, show a slight increase in intensity of the main stretching modes or loss of the weaker features. As previoulsy shown for dammar and mastic (n.a), the most dominant modifications are related to a slight increase between 1550 -1750 and 3000-2800 cm^{-1}.
The former region is quite complex and a detail description of the main stretching modes is needed before to describe the laser induced effects.
In the 1550-1750 cm^{-1} region, non irradiated colophony (n.a) is characterized by the presence of three representative signals ascribable to C=C stretch of abietane compounds, which are the main constituting resinous acids of colophony. The band at 1650 cm^{-1} is assigned to trans conjugated ν(C=C), the other one at 1611 cm^{-1} to the symmetric aromatic ring ν(C=C) and the less intense at 1565 cm^{-1} to the simple ν(C=C)

(Brody et al. 2002, Nuopponen et al. 2004). At 1660 cm^{-1} is also present the C=C stretch of terminal and cyclic groups of pimaric type resin acids. This means that the band at 1650 cm^{-1} is related to abietic acid while that at 1611 cm^{-1}, which is rather intense, to the presence of dehydroabietic acid. As known, the latter is formed upon oxidation in diterpenoid resins containing an abietane skeleton over time (see section 1.2.2, chapter 1).
In Fig. 16, μ-Raman spectra of laser irradiated colophony at both wavelengths show a slight increase of the band at 1650 cm^{-1}, although irradiation at 213 nm induces a more prominent increase, especially in the bands at 1611 cm^{-1}. A further band, at 1635 cm^{-1}, is formed upon irradiation at both wavelengths and it can assigned to ν(C=C) of dehydroabietic acid (Nuopponen et al. 2004). Pimaric type acids have also a band at 1635 cm^{-1} but its intensity is rather small in comparison to that at 1660 cm^{-1}. However, the appearance of a double structured band with peaks at 1565 and 1575 cm^{-1} in sample irradiated at 213 nm may suggest the presence of abietic acid or of a fused aromatic ring. A closer inspection reveals a decreasing of the bands at 1383 and 1234 cm^{-1} and an increase at 1055 cm^{-1} if compared with the close band at 1070 cm^{-1} (ν(COH)), thus confirming modifications to the aromatic ring of dehydroabietic acid and the correlated oxidized groups. These latter minor changes can be appreciated also in the sample irradiated at 266 nm.
Despite the high fluorescence background, μ-Raman spectra of artificially aged (a.a) colophony samples were acquired, as shown in Fig. 16 (Appendix A). For first, some different spectral features may be noticed in non irradiated colophony (a.a). The most important is the lesser intensity of the band at 1611 cm^{-1} referring to dehydroabietic aicd. The region between 1350-750 cm^{-1} is drastically affected by fluorescence background and hence less informative. Besides this, a marked change upon laser irradiation at 266 nm, especially in the increase and broadening of the 1550-1750 cm^{-1} region, may be well appreciated. Within this range, bands at 1650 and 1635 cm^{-1} are much more pronounced if compared to the relative intensity of the dehydroabietic acids band at 1611 cm^{-1}. Irradiation at 266 nm induces also a darkening effect, which was well appreciable to naked eye. These changes together with the reduction of the CH stretching groups, most likely due to the

hydrogen abstraction, may suggest that the remaining varnish layer was affected by laser irradiation at 266 nm.
Irradiation at 213 nm results indeed in a lesser degree of modifications, although a slight increase at 1650 cm^{-1} and the decreasing of CH groups have been detected, thus suggesting the same photo-induced changes observed at 266 nm.

4.3.4.3 Sandarac

μ-Raman spectra collected from naturally (n.a) artificially (a.a) aged sandarac varnishes after laser irradiation at 213 and 266 nm are shown in Fig. 17 (Appendix A). Laser irradiation at both wavelengths of sandarac (n.a) does not induce observable modifications. μ-Raman spectra of aged samples (a.a) are indeed affected upon irradiation at 266 nm while no evidence of laser damage is observed at 213 nm. Irradiation at 266 nm induces a slight decrease of the intense narrow band at 1646 cm^{-1}, which is assigned to C=C stretch of vinyl group of communic acid, and of the carbonyl stretching band at 1716 cm^{-1} (Nuopponen et al. 2004). Simultaneously, as previously observed in dammar, mastic and colophony, CH groups result decreased indicating a decomposition and fragmentation, in this case, of the polycommunic acids chains.

4.3.4.4 Bleached shellac

μ-Raman spectra collected from naturally (n.a) artificially (a.a) aged shellac varnishes after laser irradiation at 213 and 266 nm are shown in Fig. 18 (Appendix A). As observed for sandarac, bleached shellac is a very stable varnish upon laser UV irradiation. The most relevant changes regard the slight reduction of CH groups upon irradiation at 266 nm either in naturally and artificially aged samples. This changes is most probably related to the hydrogen abstraction in methyl and methylene groups, which is the first step for starting radicals chain reactions and oxidative processes. A further change induced at 266 nm in shellac (n.a) is the appearance of a small band at 1736 cm^{-1}, which in the non irradiated and irradiated (at 213 nm) samples appear with the same intensity only as a

weak shoulder. This band may be assigned to the C=O stretch of the ester linkages (Limmatvapirat et al. 2007, Farag 2010) thus indicating that irradiation at 266 nm increases the degree of polymerization. At same time, a very slight decrease in the bands at 1690 and 1709 cm^{-1} assigned to carboxylic acids groups and the increase between 950-800 cm^{-1} due to COC stretch strengthens the hypothesis that at 266 nm an esterification process occurs.
Aged bleached shellac samples (a.a) do not undergo the same photodegradation reactions because all the alcohol and carboxylic acids groups were converted in ester linkages. Appreciable changes may be observed in the decreasing of CH groups upon irradiation at 266 nm whereas they increase after irradiation at 213 nm.

4.3.4.5 Mastic-oil

μ-Raman spectra collected from naturally (n.a) and artificially (a.a) aged mastic-oil varnishes after laser irradiation at 213 and 266 nm are shown in Fig. 19 (Appendix A). For first, the shape of the bands in the spectra of oil varnishes result more smoothed due to the heat processing needed for their preparation. Irradiation at 266 nm of mastic-oil (n.a) varnish follows an opposite trend in comparison to films of pure dammar and mastic (n.a). The degradation kinetic resembles what observed in artificially aged varnish films containing triterpenoid resins. Practically, a decreasing of the carbonyl bands at 1706 and 1740 cm^{-1} assigned respectively to mastic and linseed oil has been observed. At same time, CH groups decrease indicating that irradiation at 266 nm generates gaseous products (CH_3OH, CH_4, $HCOOCH_3$, CO, and CO_2), as previously observed in mastic and dammar (a.a). Chemical modifications upon irradiation at 213 nm are negligible.
μ-Raman spectra of artificially aged (a.a) mastic-oil varnishes are affected by an high fluorescence background which impedes the accurate interpretation of the laser induced effects. However, a decrease at 1650 cm^{-1} and an increase between 3000-2800 cm^{-1} has been observed at both the irradiation wavelengths.

4.3.4.6 Colophony-oil

μ-Raman spectra of naturally (n.a) and artificially (a.a) aged colophony-oil varnishes following laser treatment at 231 nm and 266 nm are shown in Fig. 20 (Appendix A). A comparison with spectra acquired on pure colophony samples reveal noticeable changes due to the heat processing and the presence of linseed oil. Apart those between 1300-600 cm^{-1}, the most pronounced is observable at 1667 cm^{-1}, which probably arises from *cis-trans* conjugated double bonds resulting from abietane and unsaturated fatty acids molecules. Thus, this band in colophony-oil sample (n.a) undergoes a slight increase upon irradiation at 266 nm until reaching an intensity similar to the close band of dehydroabietic acid at 1611 cm^{-1}. This slight rise suggests the formation of unsaturations or isomerization of C=C following laser treatment. A similar reaction takes place in colophony-oil sample (a.a) after laser irradiation at 213 nm. It is worth noting that in artificially aged samples the band at 1667 cm^{-1} is more intense than the close one at 1611 cm^{-1} . This result indicates that during light ageing and after laser irradiation conjugated carbon double bonds are formed. Clearly, this reaction is more pronounced in abietane type resins and it results amplified if polyunsaturated fatty acids chains (linoleic, linolenic acids) are present in the mixture.

4.3.4.7 Sandarac-oil

μ-Raman spectra of naturally (n.a) and artificially (a.a) aged sandarac-oil varnishes following laser treatment at 231 nm and 266 nm are shown in Fig. 21 (Appendix A). As shown, irradiation at 213 does not induce significant modifications either to naturally aged (n.a) and artificially (a.a) aged sandarac-oil samples. Irradiation of sandarac-oil (n.a) at 266 nm generates the increase of the carbonyl functionalities belonging to resin and oil, which have a band at 1709 and a shoulder at 1738 cm^{-1} respectively. At same time, Raman scattering of CH groups result increased after laser treatment at 266 nm. Other minor changes involve the region between 1100-900 cm^{-1} where are found the stretching modes of C-C and COH bonds. These changes may be attributed to the formation

of oxidized products in the remaining varnish layer. Contrarily, in artificially aged sandarac-oil samples irradiation at 266 nm leads to decrease of the above described spectral features, indicating atom-hydrogen abstraction and emission of gaseous products.

4.3.4.8 Manila copal-oil

μ-Raman spectra of naturally (n.a) and artificially (a.a) aged Manila copal-oil varnishes following laser treatment at 231 nm and 266 nm are shown in Fig. 22 (Appendix A). Although Manila copal-oil varnish samples show a very stable behaviour upon laser irradiation at 266 nm some modifications may be highlighted. In particular, in naturally aged Manila copal-oil carbonyl bands at 1706 cm^{-1} do not change significantly, even if the band shape results affected in some extent. On the opposite, the intensity of CH groups increases at both the laser wavelengths and a new small band at 1364 cm^{-1} assigned to the bending of $\nu(CH_2)$ and $\nu(CH_3)$ appear only after irradiation at 266 nm. It is very difficult to understand the reason of the increase of CH groups in the bulk of the varnish layer, which is most probably related to an higher degree of oxidation in the uppermost layer. As previously shown by FTIR monitoring during artificial ageing (see section 3.2.3.6, Chapter 3), one of the most direct consequence is the exponential decreasing of the CH groups at the surface level followed by the increase of C=O, which differ slightly depending from the type of varnish. This suggests that in depth the amount of CH groups which reacted with oxygen is lower than in the outer layer thus justifying a most intense Raman scattering after laser ablation.
Contrarily, artificially aged copal-oil varnish samples show after laser irradiation at 266 nm a decrease either of CH and C=O bands indicating the emission of gaseous products. Ablation at 213 nm does not induce this alteration because this wavelength is highly absorbed by the varnish layer and hence chemical changes are completely negligible.

4.3.5 Laser Induced Fluorescence spectroscopy

Normalized fluorescence emission spectra of naturally and artificially aged varnish samples at laser excitation wavelength of 266 nm are shown in Fig. 24.

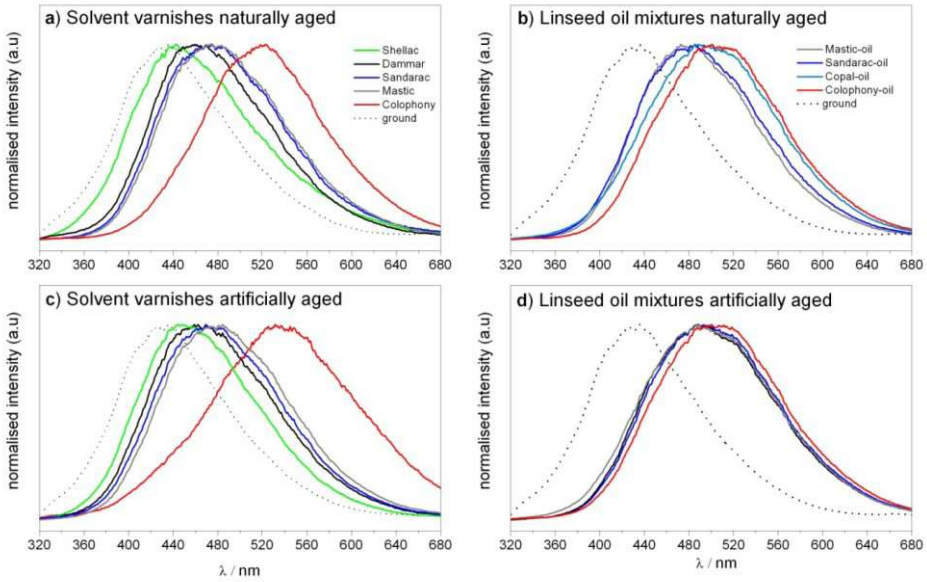

Fig. 24 – Normalised LIF spectra (exc. 266 nm) of the prepared varnish samples. Naturally aged solvent a) and oil b) varnishes; artificially aged solvent c) and oil d) varnishes. Dotted line show the fluorescence emission of the underlying layer (ground).

Fluorescence maxima of each prepared varnish are listed in Table 6. As observed, many factors can influence the position of the fluorescence maximum, such as composition, preparation methods and ageing conditions (Nevin et al., 2009, 2012). Naturally aged solvent varnish systems reveal fluorescence maxima at different emission wavelengths, which in most cases shift of 5-10 nm toward longer wavelengths in artificially aged samples. As expected, colophony resin fluoresces at longer wavelengths due to the higher number of unsaturations. Most of the constituting resinous acids (abietane compounds) contain two or three

conjugated carbon double bonds within the ring. After the light-ageing colophony undergoes further red shifting and broadening.
The fluorescence maxima of the naturally aged oil varnishes (cooked in oil) result quite similar, especially in artificially aged systems. This suggests that the thermal and light ageing treatments have degraded the terpenoid skeletons in the same manner.

Table 6 Fluorescence maximum (nm) of solvent and oil varnishes following natural (n.a) and artificial (a.a) ageing.

Varnish type	***n.a***	***a.a***
Solvent varnishes		
Mastic	473	484
Dammar	460	460
Colophony	520	530
Sandarac	474	485
Shellac	442	448
Oil varnishes		
Mastic	472	489
Colophony	500	500
Sandarac	485	487
Copal	489	487
support		
Ground	435	435

The general effect of aging is to create new fluorophores, which induce the shift of the emission spectrum (λ_{max}) usually toward larger wavelengths. In addition, a marked increase in the fluorescence intensity from naturally to artificially aged samples was observed
Results from LIF measurements after laser irradiation at 213 and 266 nm of all the prepared varnish samples are reported in Appendix B (Fig. 25-33) at the end of the chapter, where the changes in fluorescence intensity and band shifts upon laser irradiation may be better visualized.
Fluorescence maxima of the varnish samples after laser irradiation at 213 and 266 nm are summarized in the table below.

Table 7 Fluorescence maxima (in nm) of naturally and artificially aged varnish samples before and after laser processing at 213 and 266 nm. 1, 5 10 refers to the number of laser pulses placed on each laser scanned area.

Type of ageing	Naturally aged							Artificially aged						
varnish	non treat.	irradiated at 213 nm			irradiated at 266 nm			non treat.	irradiated at 213 nm			irradiated at 266 nm		
		1	5	10	1	5	10		1	5	10	1	5	10
Solvent prepared varnishes														
Mastic	473	485	485	475	485	485	485	485	485	485	472	485	487	485
Dammar	460	468	464	462	460	470	470	460	472	460	448	470	460	460
Colophony	520	518	522	519	522	523	472	530	523	528	520	531	523	486
Sandarac	474	470	470	470	470	474	473	485	485	485	472	475	460	470
Shellac	440	440	450	445	440	450	440	450	460	460	460	450	460	460
Linseed oil prepared varnishes														
Mastic	472	472	485	487	485	487	487	490	487	487	487	487	487	487
Colophony	500	500	497	493	487	500	497	500	497	518	497	497	497	522
Sandarac	485	485	487	485	470	485	471	487	487	498	498	485	487	485
Copal	489	489	511	492	500	511	514	487	493	488	487	486	487	500

4.3.5.1 Naturally aged varnishes

LIF spectra of naturally aged solvent varnishes irradiated at 213 nm (i.e dammar - Fig. 25, mastic - Fig. 26 and sandarac - Fig. 28) show as primary effect a decreasing of the fluorescence intensity. This change can be related to the different bulk composition (lower degree of yellowed and oxidized products) of these naturally aged varnishes. In fact, no shifts and/or broadening are detected indicating that new fluorophores have not been formed. Colophony (Fig. 27) due to its composition (higher content of conjugated carbon double bonds) is characterized by a singular fluorescence behaviour, which is opposite to the above described. Basically, fluorescence increases upon single pulse laser irradiation and decreases after 5 and 10 consecutive laser pulses. Besides this, an important band-broadening without noticeable shift is observed (see Table 7). The spectrum of naturally aged bleached shellac (Fig. 29) varnish results indeed slightly affected.

Contrarily to irradiation at 213 nm, LIF spectra of naturally aged solvent varnishes (i.e. dammar – Fig. 25, mastic – Fig. 26, bleached shellac – Fig. 29) irradiated at 266 nm show a notable increase of the fluorescence intensity which is, in most cases, accompanied by a bathochromic shift and broadening (Table 7). This means that new fluorophores are formed, as shown by the changes observed in μ-Raman spectra. Sandarac (Fig. 28)

show an increase of fluorescence but not undergoes shift and/or broadening while colophony (Fig. 27) results deeply affected upon irradiation at 266 nm. It shows a drastic fluorescence decreasing and a blue-shift of about 50 nm after 10 laser pulses, which is most probably related to a deeper ablation.
Irradiation at 213 nm of naturally aged oil varnishes (i.e. mastic-oil Fig. 30, colophony-oil – Fig. 31, sandarac-oil – Fig. 32, Manila copal-oil – Fig. 33) induces the increase of fluorescence intensity, a slight red-shift and broadening only in mastic and copal oil varnishes.
Irradiation at 266 nm of oil varnishes generates the same effects with the main difference that they are very more pronounced.

4.3.5.2 Artificially aged varnishes

LIF spectra of artificially aged solvent varnishes irradiated at 213 nm (i.e dammar - Fig. 25, mastic - Fig. 26 and sandarac - Fig. 28) show a decreasing of the maximum fluorescence intensity together with a shift toward lower wavelengths most probably due to the lowering of the varnish layer. Fluorescence of colophony (Fig. 27) does not results affected in intensity but a slight shift in same direction is observed. On the contrary, bleached shellac (Fig. 29) broadens but the intensity does not change significantly (see Table 7).
LIF spectra of aged solvent varnishes (i.e. dammar - Fig. 25, mastic - Fig. 26, colophony - Fig. 27), sandarac - Fig. 28) irradiated at 266 nm follows similar degradation pathways, even if the spectral changes are drastically magnified, especially for colophony varnish. Changes observed in shellac resembles what observed upon irradiation at 213 nm.
As regards aged oil varnishes, irradiation at 213 nm results in a increase in the fluorescence intensity for all the samples with exception of colophony, which unexpectedly does not undergo any change. Nevertheless, also for the other oil varnishes no important changes are observed indicating that oil varnishes are more stable upon laser irradiation at 213 nm.
Irradiation at 266 nm generates remarkable changes, as shifts and band broadening especially in oil colophony varnish, which shifts after 10 laser pulses toward longer wavelengths of about 25 nm.

4.4 Conclusions

In this work chemical and physical modifications induced by laser irradiation on different types of naturally and artificially aged varnish samples were systematically characterized using Confocal μ-Raman and Laser Induced Fluorescence spectroscopies. Irradiation at 213 nm induces ablation without noticeable morphological changes to the remaining varnish layer, which preserves its natural gloss. At this wavelength, the layer by layer removal is provided by a resolution in the sub-micron scale. On the contrary, irradiation at 266 nm induces the formation of microsized bubbles, as observed by means of confocal microscopy. On the other hand, the optical absorption at 266 nm is relatively low in all the varnish systems studied, thus involving during the ablation process the emission of gaseous products. As consequence of such modifications, carbonyl functionalities and methyl and methylene groups decrease, as observed by confocal μ-Raman spectroscopy. Further reactions, as formation of oxidized products and carbon double bonds, which induce the increase in intensity and the red-shift of the fluorescence signal, were observed.

Ablation at 213 nm, which is a strongly absorbed wavelength, involves direct photolysis and homolytic bond breaking. This photochemical process does not induce such drawbacks (whitish appearance, bubbles) to the etched substrate leading to a clean surface morphology, as detected by confocal microscopy. Similarly, chemical changes may be considered negligible in most of the varnish systems understudy.

Finally, this study represents the first investigation aimed at assessing the chemical and physical laser-induced modifications on a wide variety of painting varnishes using the fifth (213 nm) and fourth (266 nm) harmonics of the QS Nd:YAG laser.

In contrast with the induced modifications resulting from irradiation at 266 nm, the promising results achieved on samples irradiated at 213 nm emphasize, as demonstrated in previous studies conducted on shellac resin (Ouija et al. 2011), the importance of following a wavelength-based approach to safely remove different types of naturally and artificially aged painting varnishes.

Appendix A - Confocal μ-Raman spectra of laser irradiated varnish samples

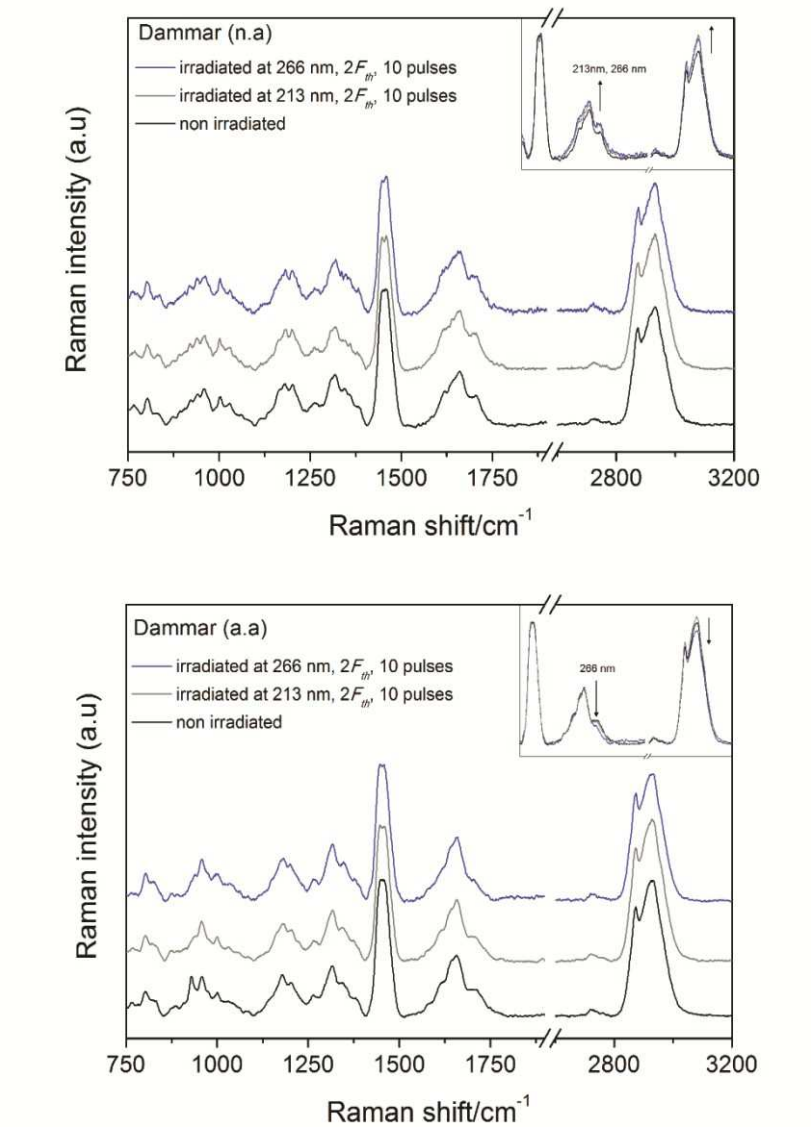

Fig. 14 A stack-plot of confocal μ-Raman spectra of naturally (n.a) and artificially (a.a) aged dammar varnish films upon laser irradiation at 213 and 266 nm. The most relevant laser-induced chemical changes are shown in the inset graph.

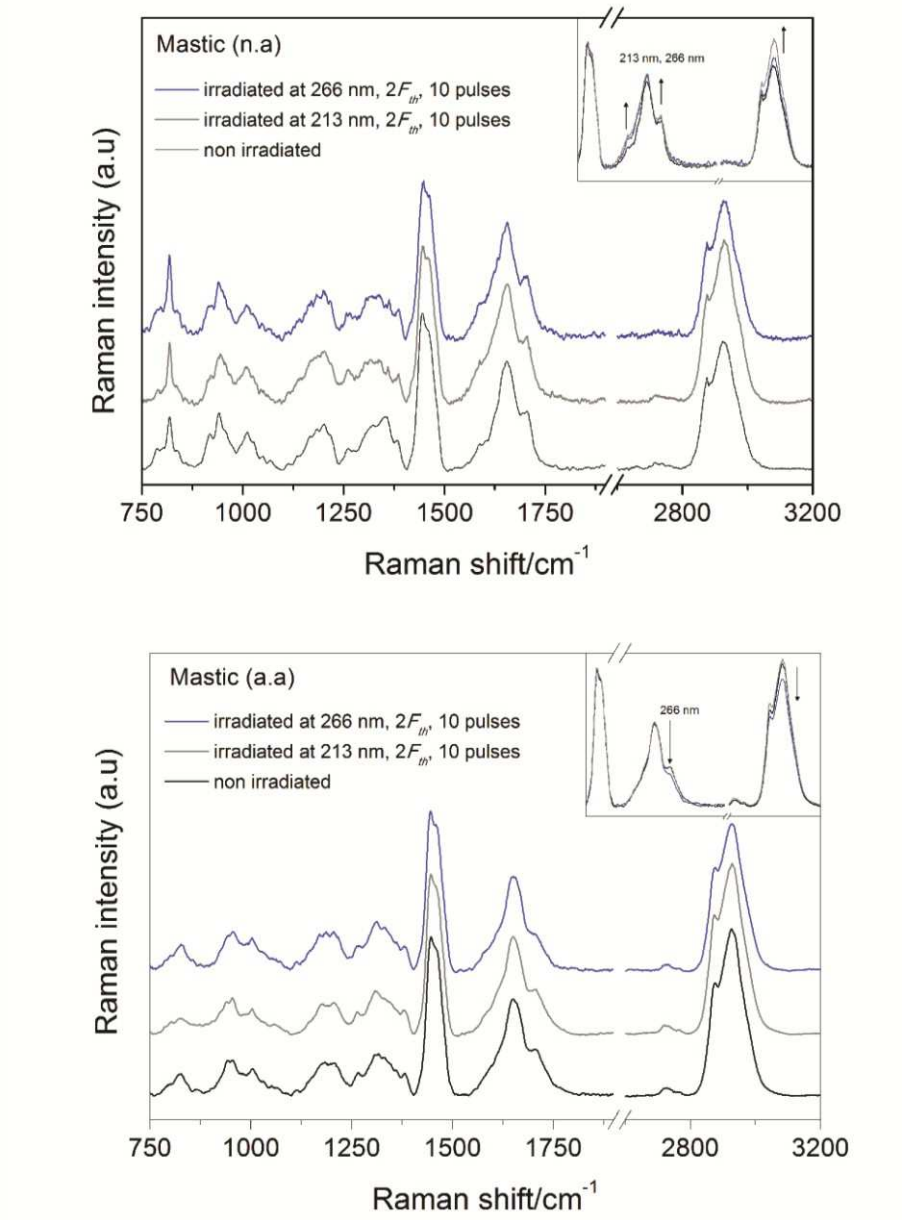

Fig. 15 Stack-plots of confocal μ-Raman spectra of naturally (n.a) and artificially (a.a) aged mastic varnish films irradiated at 213 and 266 nm. Laser induced chemical changes are shown in the inset graph.

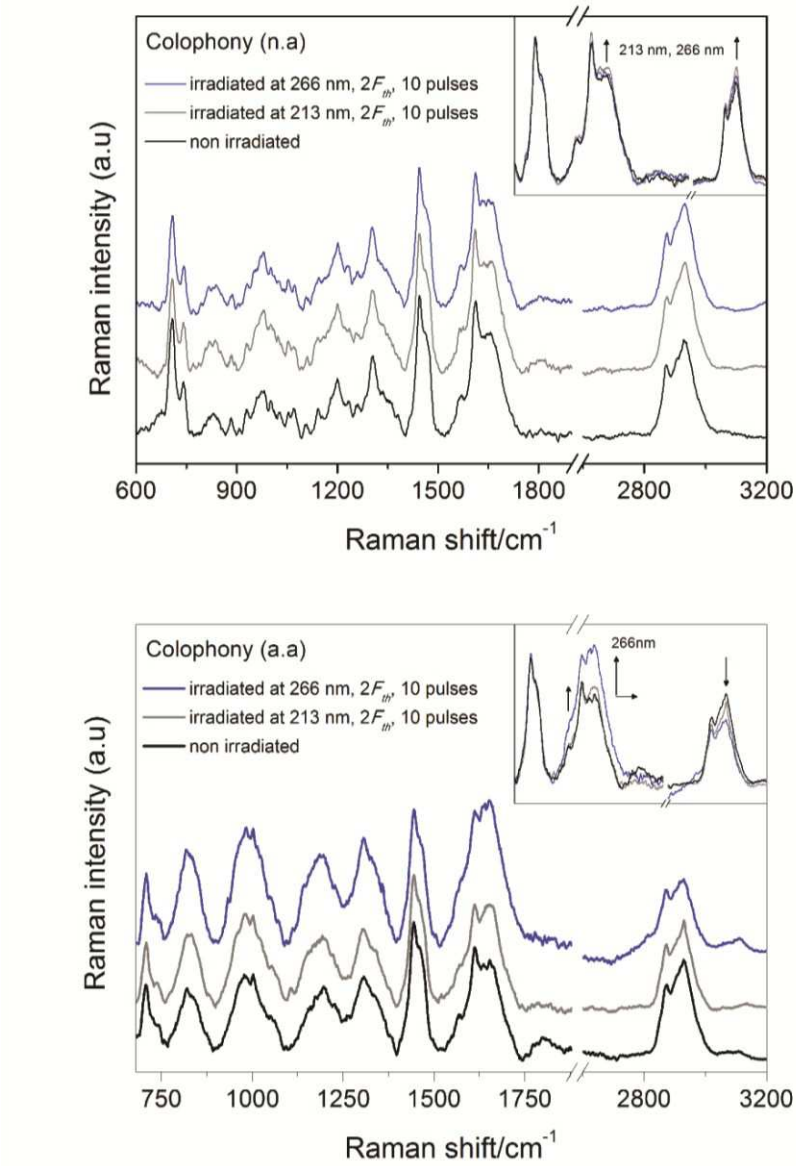

Fig. 16 Confocal μ-Raman spectra of naturally (n.a) and artificially (a.a) aged colophony varnish films irradiated at 213 and 266 nm. The most relevant laser induced chemical changes are shown in the inset graph.

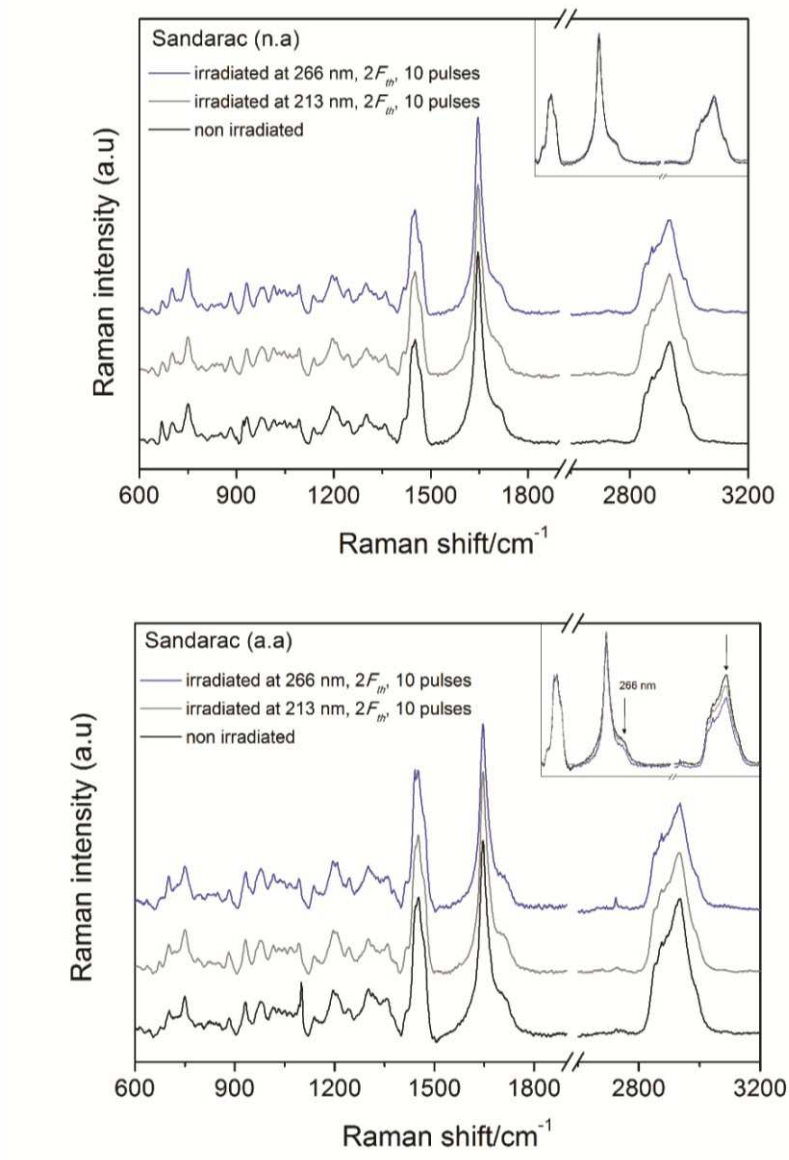

Fig. 17 Confocal μ-Raman spectra of naturally (n.a) and artificially (a.a) aged sandarac varnish films irradiated at 213 and 266 nm. The most relevant laser induced chemical changes are shown in the inset graph.

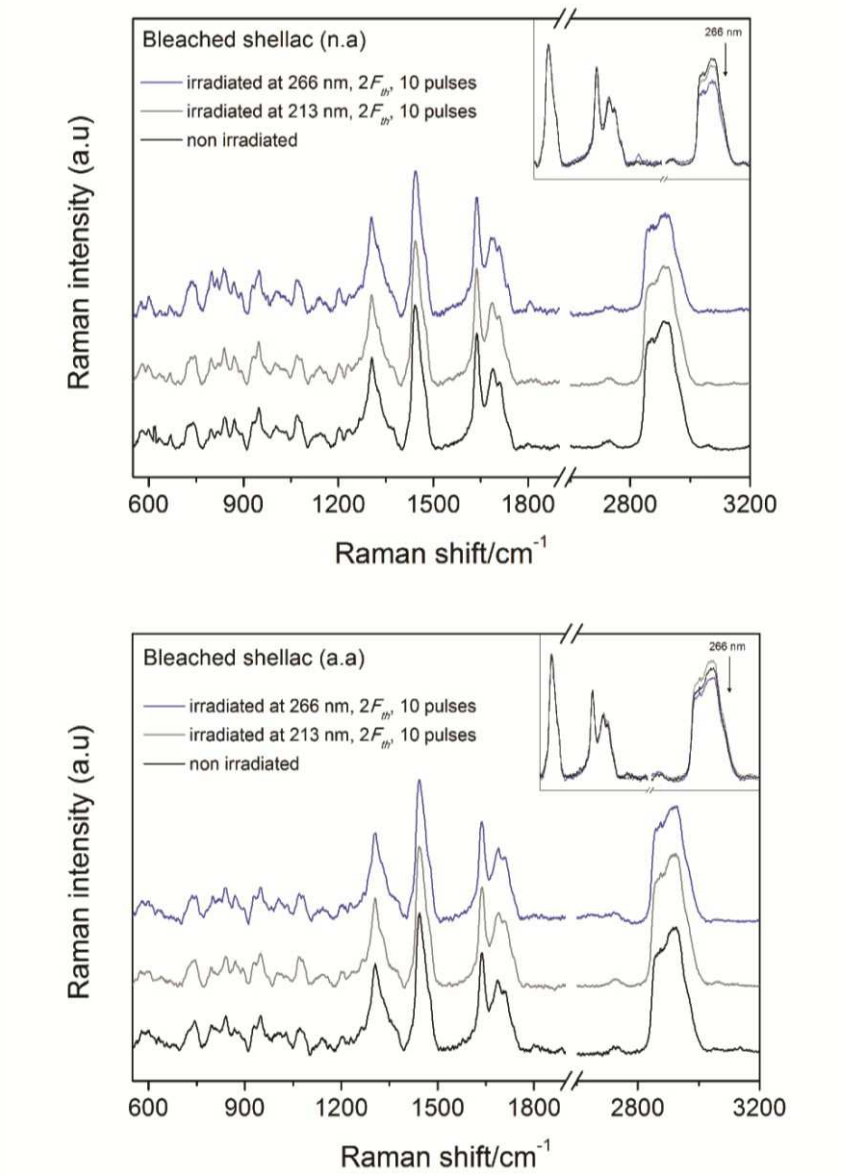

Fig. 18 Confocal μ-Raman spectra of naturally (n.a) and artificially (a.a) aged shellac varnish films irradiated at 213 and 266 nm. The most relevant laser induced chemical changes are shown in the inset graph.

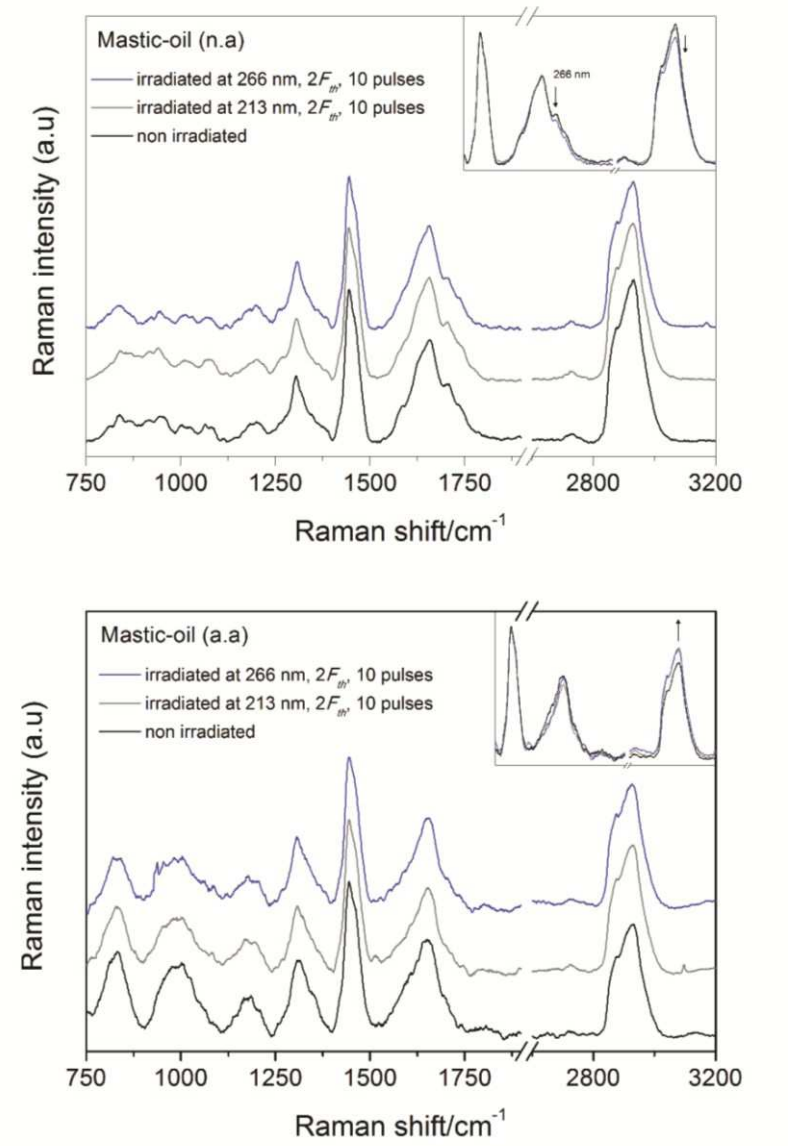

Fig. 19 Confocal μ-Raman spectra of naturally (n.a) and artificially (a.a) aged mastic-oil varnish films irradiated at 213 and 266 nm. The most relevant laser induced chemical changes are shown in the inset graph.

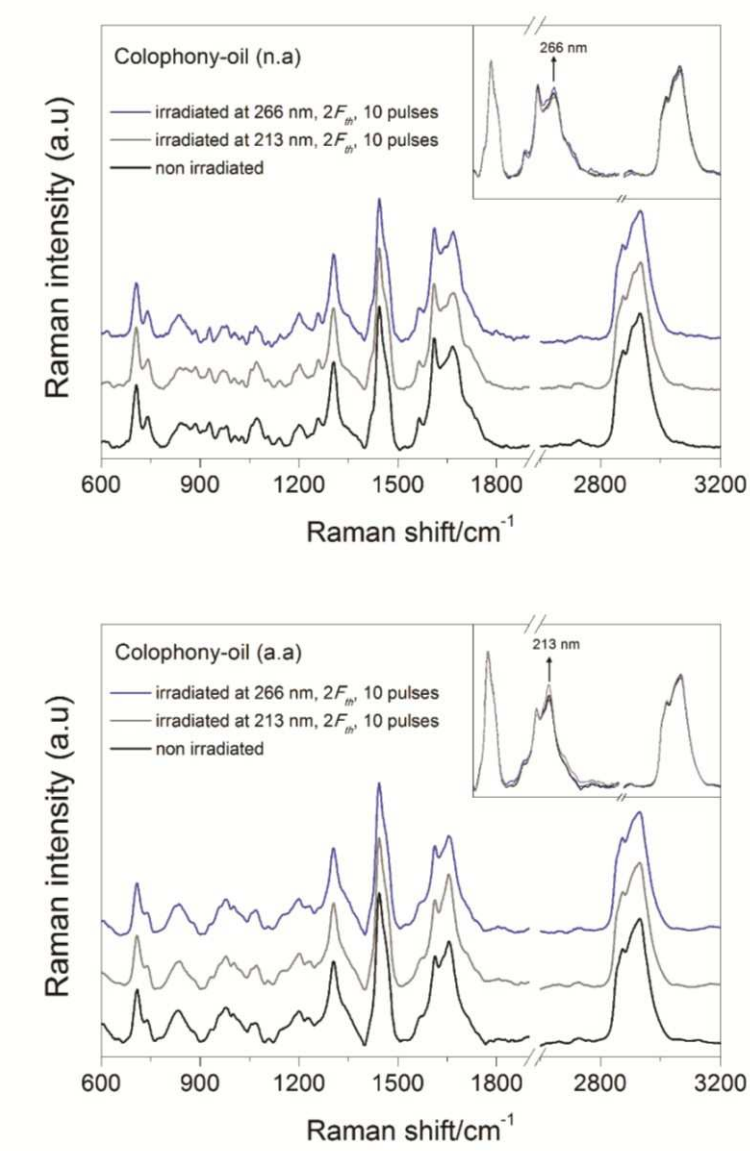

Fig. 20 Confocal μ-Raman spectra of naturally (n.a) and artificially (a.a) aged colophony-oil varnish films irradiated at 213 and 266 nm. The most relevant laser induced chemical changes are shown in the inset graph.

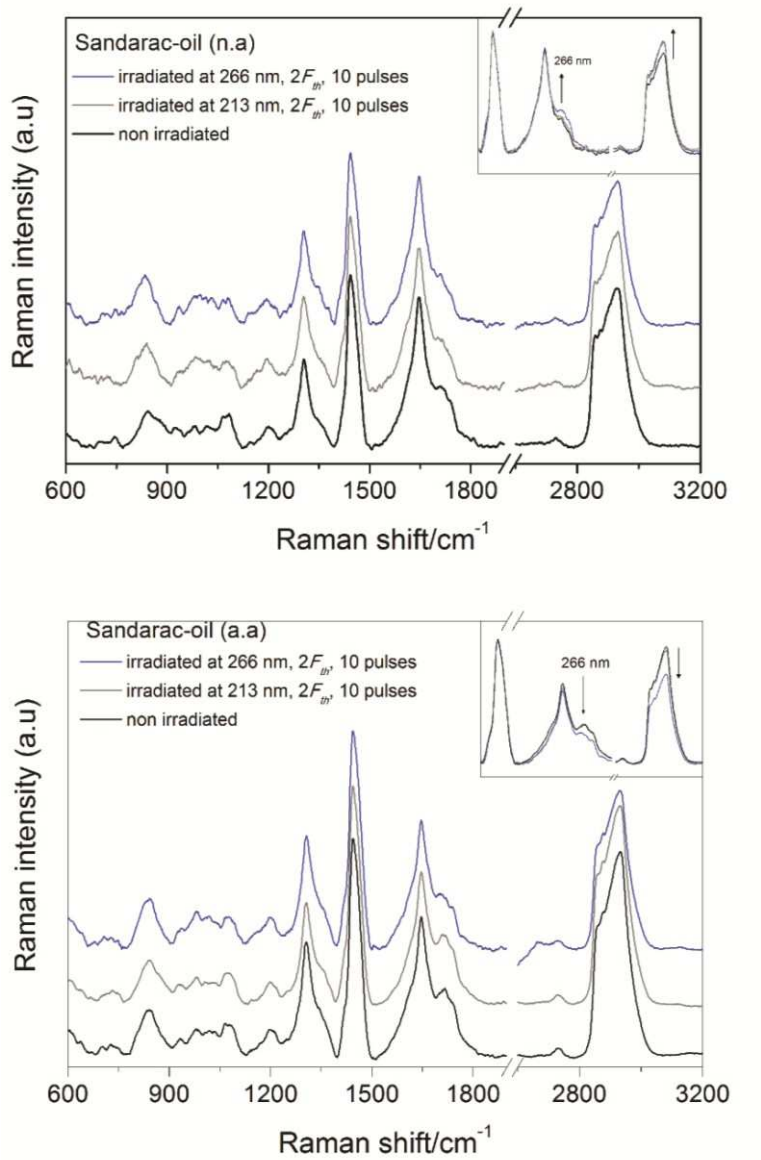

Fig. 21 Confocal μ-Raman spectra of naturally (n.a) and artificially (a.a) aged sandarac-oil varnish films irradiated at 213 and 266 nm. The most relevant laser induced chemical changes are shown in the inset graph.

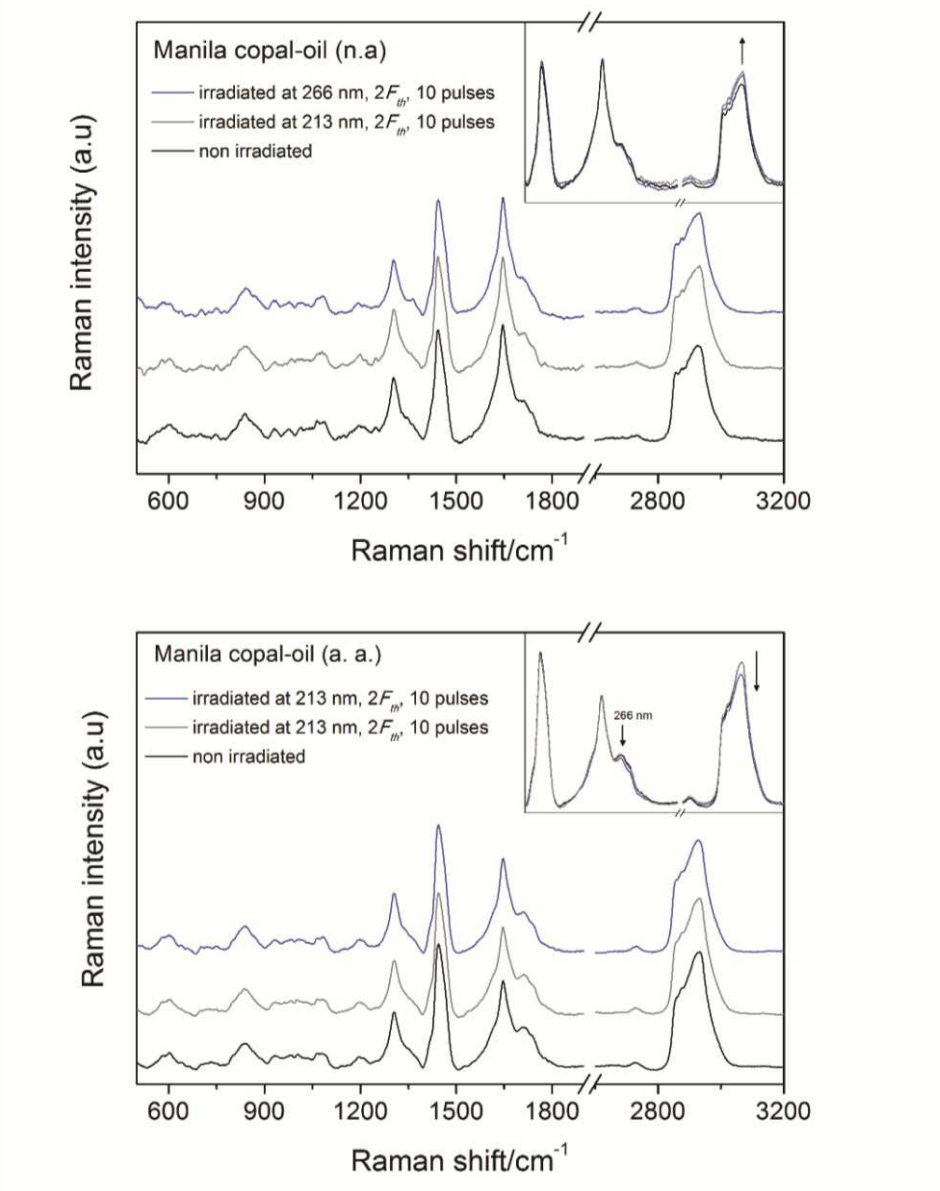

Fig. 22 Confocal μ-Raman spectra of naturally (n.a) and artificially (a.a) aged Manila copal-oil varnish films irradiated at 213 and 266 nm. The most relevant laser induced chemical changes are shown in the inset graph.

Appendix B – Laser Induced Fluorescence spectroscopy of laser irradiated varnish samples

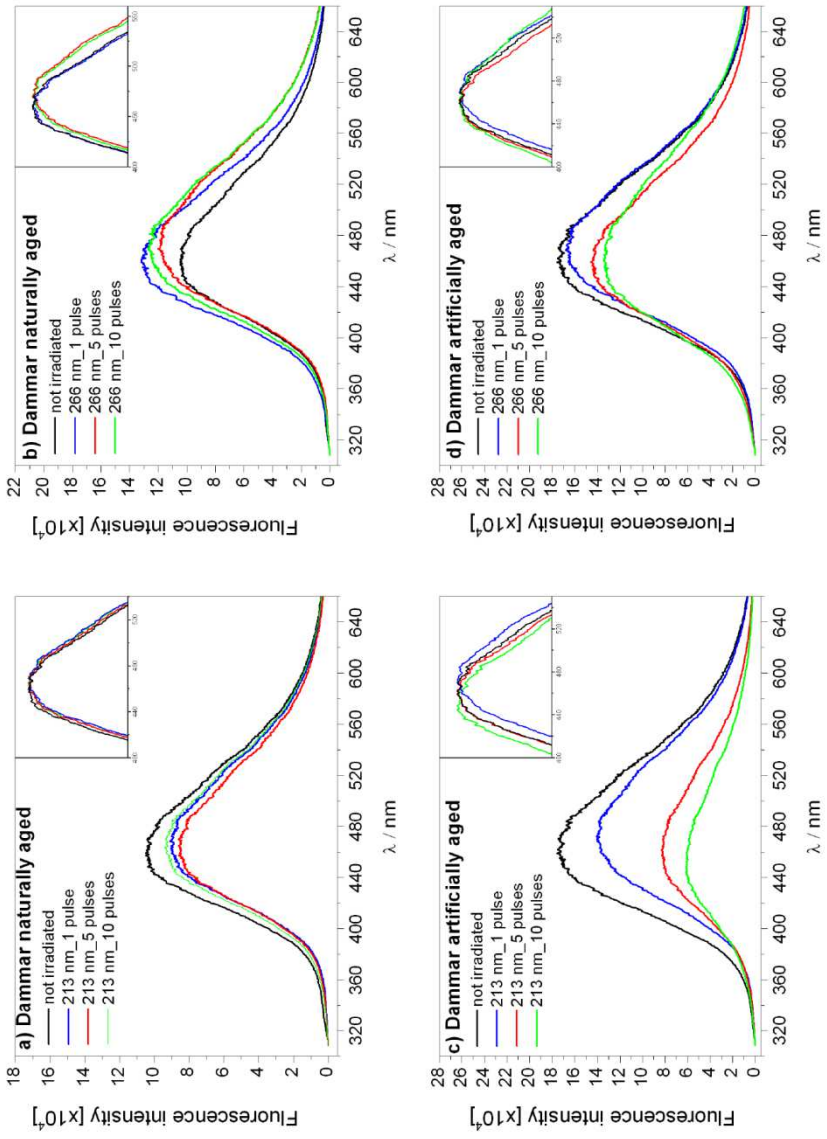

Fig. 25 LIF spectra of naturally and artificially aged dammar varnish samples irradiated at 213 (a-c) and 266 nm (b-d). Normalized spectra are shown in the inset.

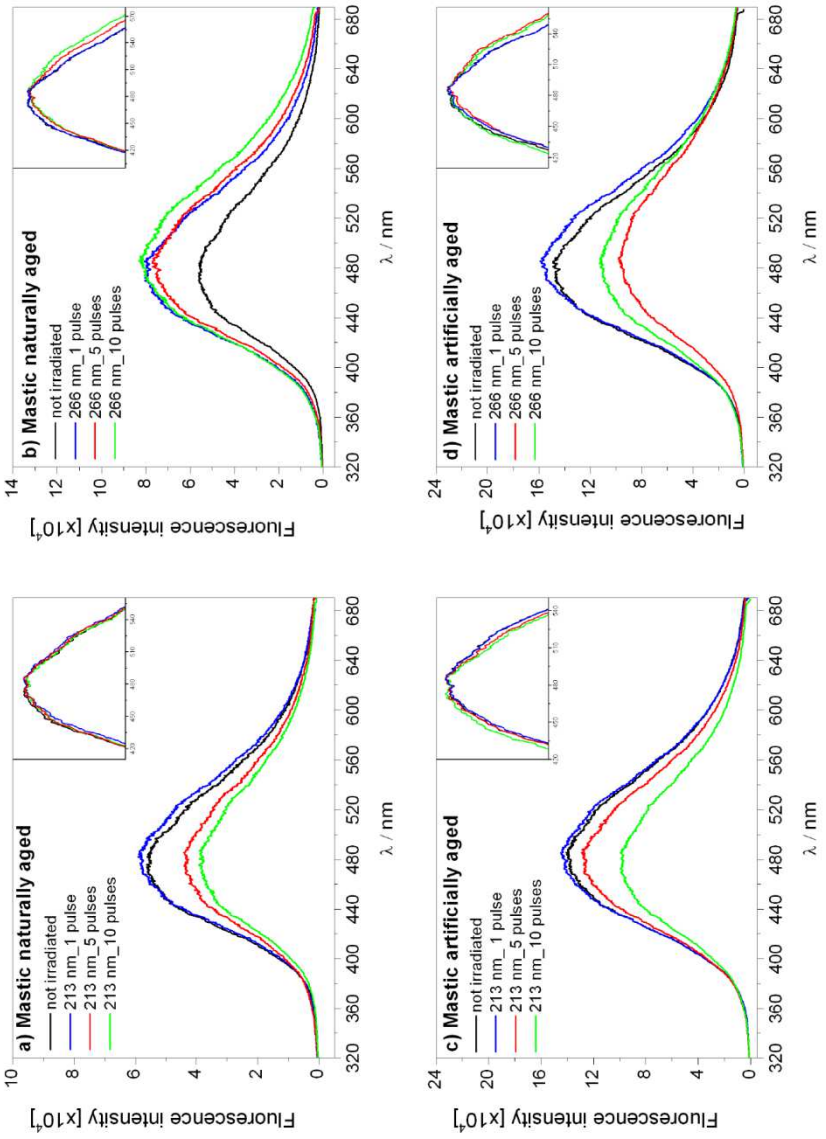

Fig. 26 LIF spectra of naturally and artificially aged mastic varnish samples irradiated at 213 (a-c) and 266 nm (b-d). Normalized spectra are shown in the inset.

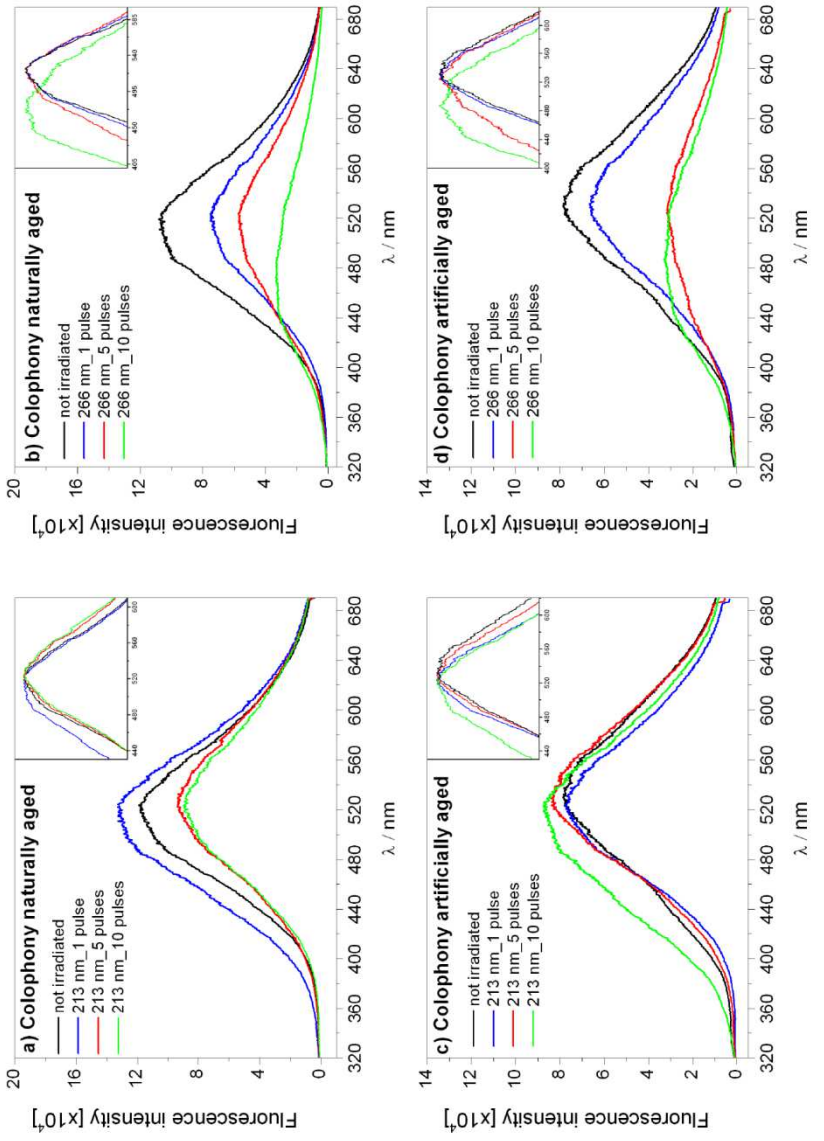

Fig. 27 LIF spectra of naturally and artificially aged colophony varnish samples irradiated at 213 (a-c) and 266 nm (b-d). Normalized spectra are shown in the inset.

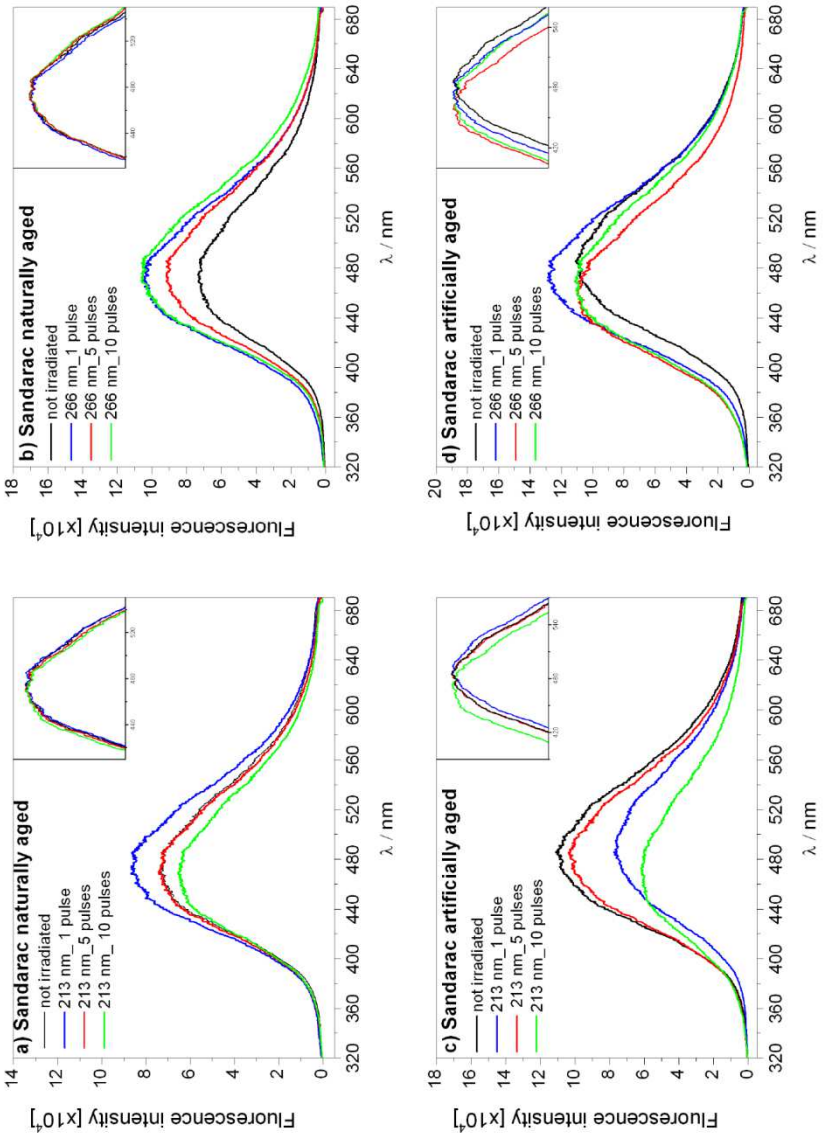

Fig. 28 LIF spectra of naturally and artificially aged sandarac varnish samples irradiated at 213 (a-c) and 266 nm (b-d). Normalized spectra are shown in the inset.

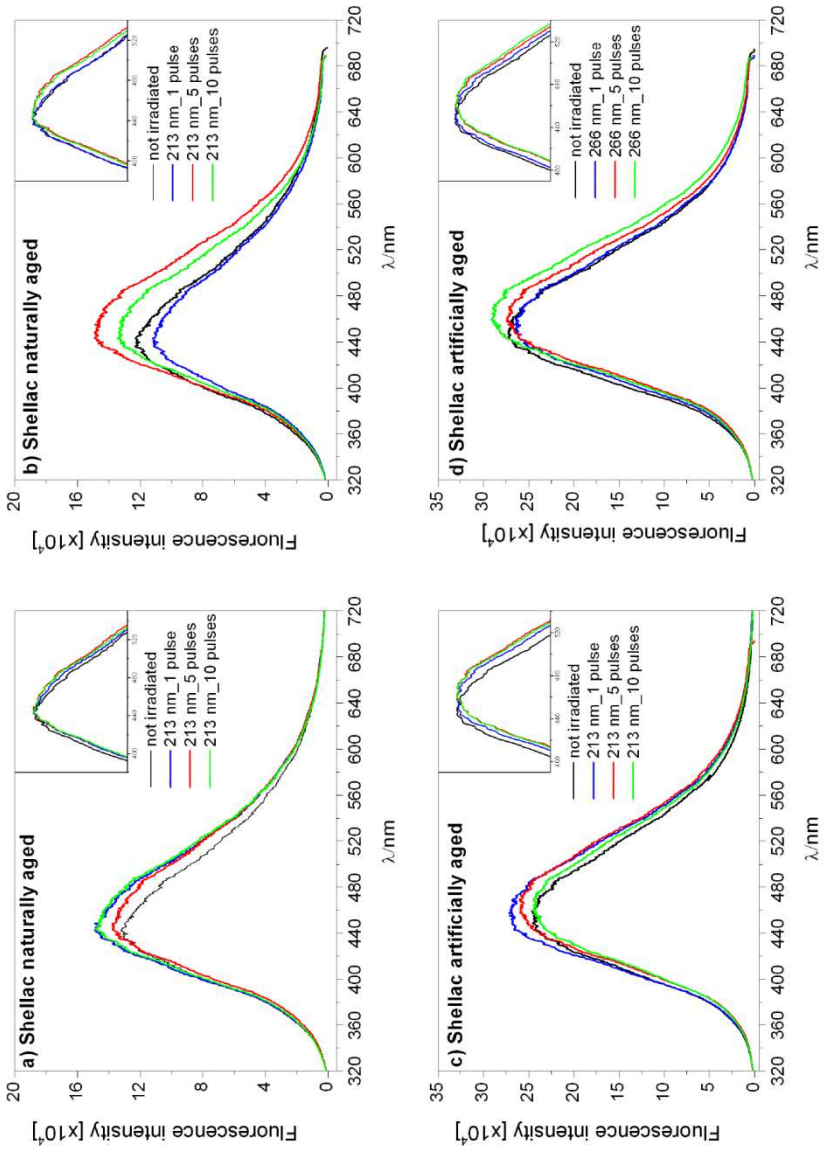

Fig. 29 LIF spectra of naturally and artificially aged shellac varnish samples irradiated at 213 (a-c) and 266 nm (b-d). Normalized spectra are shown in the inset.

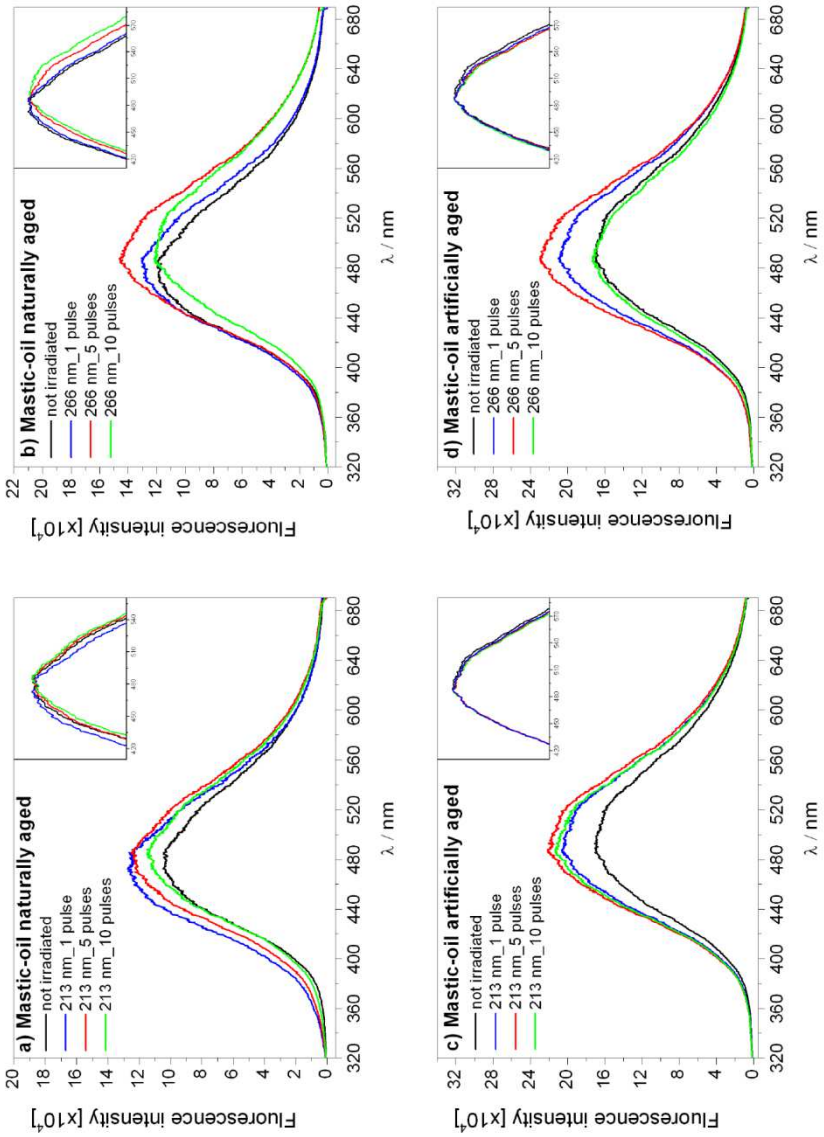

Fig. 30 LIF spectra of naturally and artificially aged mastic-oil varnish samples irradiated at 213 (a-c) and 266 nm (b-d). Normalized spectra are shown in the inset.

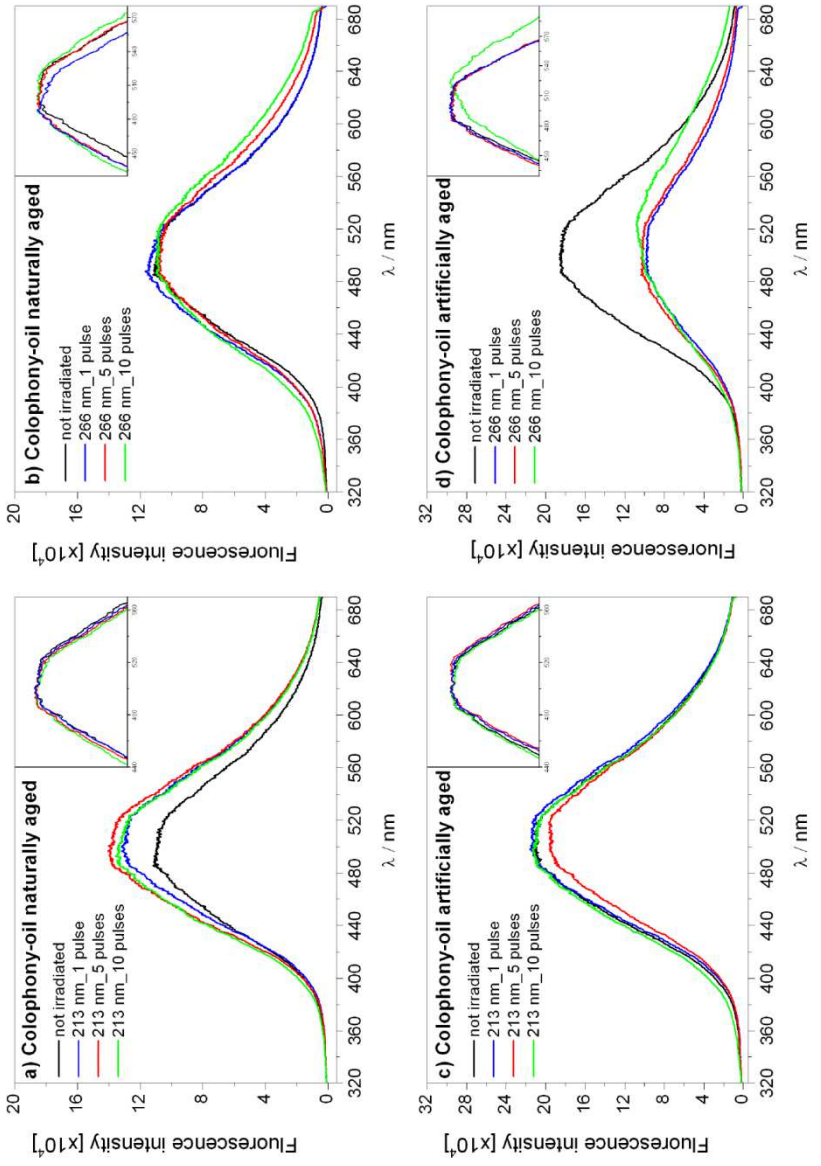

Fig. 31 LIF spectra of naturally and artificially aged colophony-oil varnish samples irradiated at 213 (a-c) and 266 nm (b-d). Normalized spectra are shown in the inset.

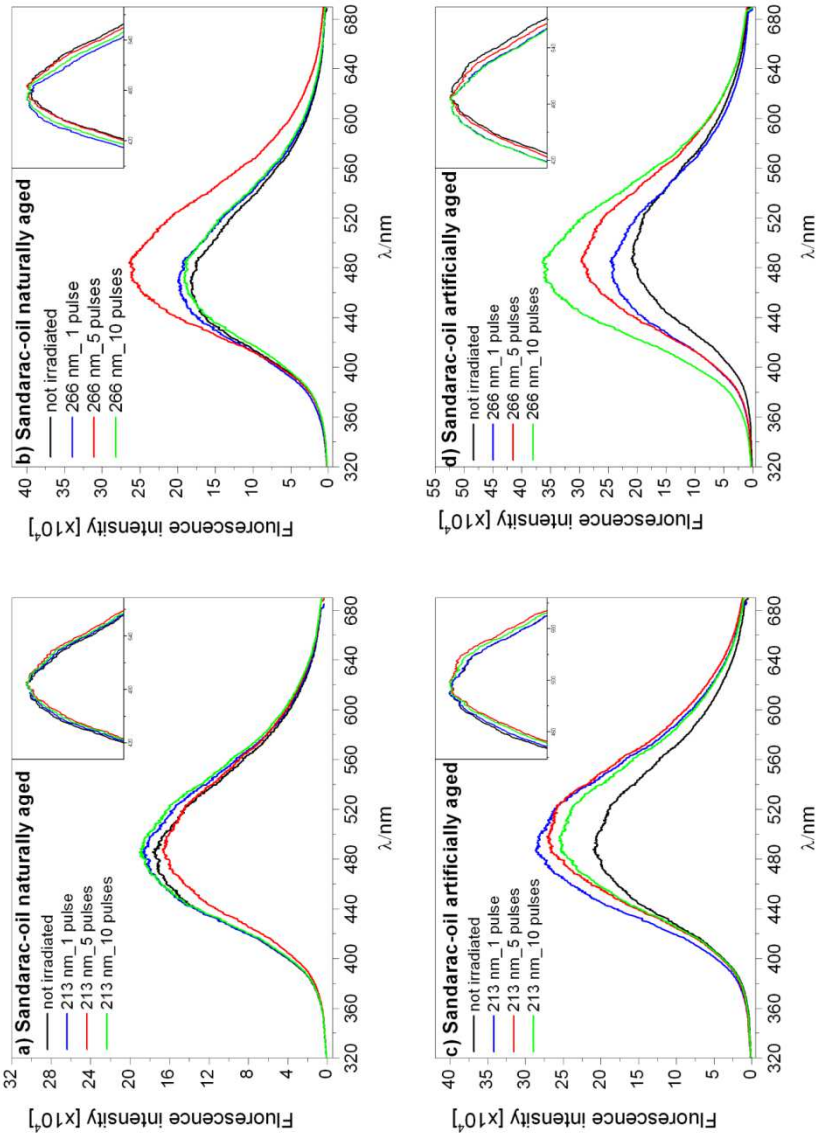

Fig. 32 LIF spectra of naturally and artificially aged sandarac-oil varnish samples irradiated at 213 (a-c) and 266 nm (b-d). Normalized spectra are shown in the inset.

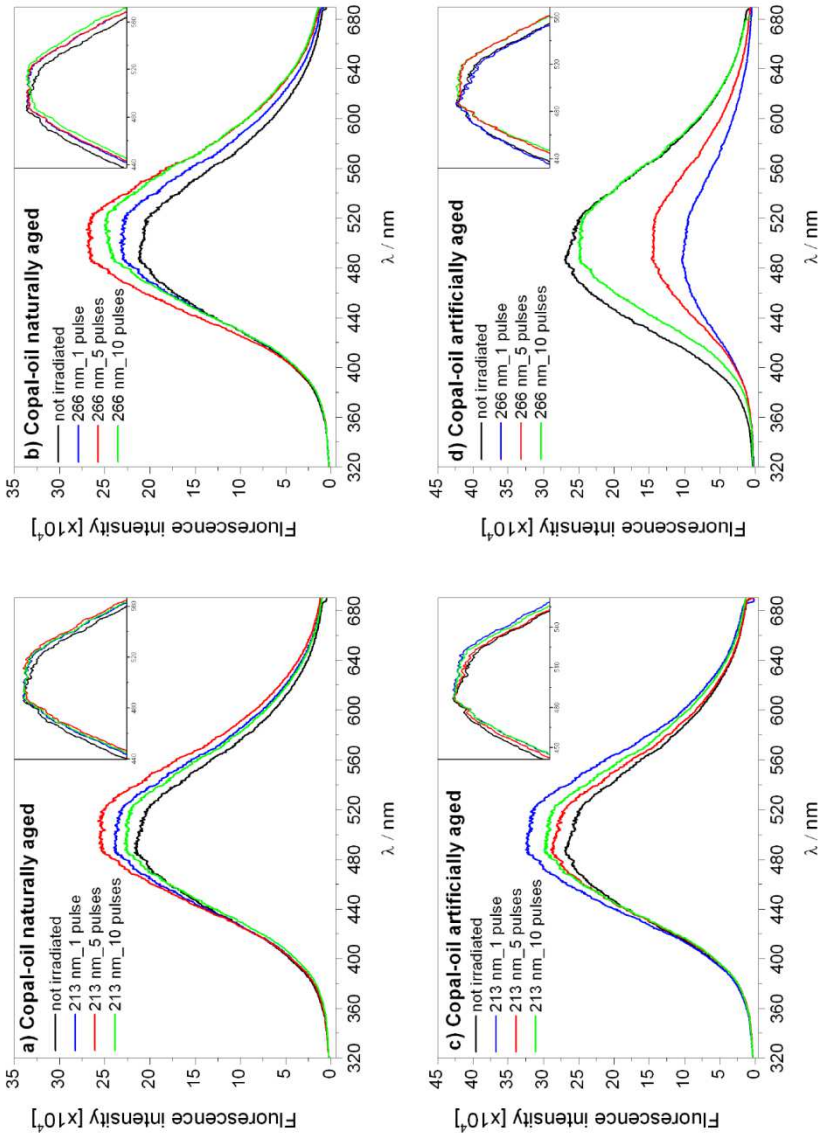

Fig. 33 LIF spectra of naturally and artificially aged copal-oil varnish samples irradiated at 213 (a-c) and 266 nm (b-d). Normalized spectra are shown in the inset.

Chapter - V

ANALYTICAL CHARACTERISATION AND LASER ABLATION TREATMENTS OF MODERN EASEL PAINTINGS

5.0 General introduction

The artificial pigments and binders introduced along the last two centuries extended the expressive possibilities of the modern painters and allowed them to execute complex artworks and masterpieces. Nowadays, such a technical and artistic evolution poses difficult characterisation and conservation problems. The materials mixing and superposition, as well as the deterioration phenomena usually encountered in modern easel paintings are less predictable than in previous artistic productions and then need significant diagnostic insights and very controllable treatments.
In the present work the conservation problems of two female portraits dated 1930 (Case study 1) and around 1910 (Case study 2), respectively, were investigated (Fig. 1). These artworks were almost completely disguised by thick layers of overpaintings, which did not have any artistic relevance. In particular, the latter painting was found on the backside of a signed artwork by Giacomo Balla, one of the founding members of the Futurist Painters, and was covered by broad brush strokes. The other

artwork was of unknown origin and disguised by overpaintings depicting an abstract vegetable theme, which was executed some decades after the underlying portrait.

Fig. 1 (a) Overpainted female portrait by anonymous (about 50 x 120 cm^2) with previous invasive uncovering attempt in the lower half of the artwork; (b) pre-Futurist painting by Giacomo Balla and (c) overpainted subject found at the backside, which was investigated and laser uncovered in the present work.

Thorough characterisation of the original pigments, binders, and overpaintings were achieved, as it will be shown in the following sections, using Raman and FTIR spectroscopy, along with stratigraphic examinations by means of optical and ESEM-EDX microscopy. All the paint layers were oil binder and included several modern pigments, such as phthalocyanine green, Ba, Zn and (Ca)-based pigments, white anatase

and lithopone, red quinacridone and synthetic azo, and other, which were commonly used during the last century. The characterisation of the original and undesired paint layers allowed identifying the pigments mixing and pointing out peculiar deterioration mechanisms.
LQS Nd:YAG (1064 nm) laser uncovering was successfully tested for both the mentioned easel paintings. This allowed performing the complete restoration of that from Ball's studio, which returned an unknown Pre-Futurist artwork, and to plan that of the portrait by anonymous. At the same time, a systematic laboratory experimentation on prepared samples has been carried out. These samples simulated the present uncovering problems encountered in the real cases, in order to investigate the laser interaction phenomenology for the different paint layers and then achieve general information on the potential of the laser approach to the removal of undesired layers. The results reported contribute to the knowledge of the deterioration mechanisms of the paint layers and disclose a significant application perspective for Nd:YAG laser ablation in conservation of modern easel paintings

5.1 Case study 1 – A female portrait by anonymous

The removal of overpaintings from valuable easel paintings represents a very difficult challenge, which is traditionally approached using solvents and moderate mechanical actions. Here, we explore for the first time the potential of Long Q-Switching Nd:YAG (1064 nm) laser with a pulse duration of 120 ns for selective ablation of overpainting layers. Mock-ups were prepared in order to approach in a systematic way a concrete uncovering problem concerning a modern painting on canvas. The former were prepared according to the stratigraphy and material compositions of the latter, as measured using optical and ESEM-EDX microscopy along with infrared and portable Raman spectroscopy. The parameterization achieved on the mock-ups allowed interpreting and maximizing the selectivity of the laser conservation treatment carried out on the real case.

5.1.1 Introduction

Controlled laser removal of overpaintings is a difficult challenge since undesired and original paint layers are both constituted by similar mixtures of organic and inorganic compounds, which make their discrimination very hard. During the last two decades a number of works were aimed at assessing the laser-induced effects on pigments, binding media and their mixtures, whereas only few were focused on the issue of the overpaint removal (Zergioti et al. 1997, Teule et al. 2003, Mc Glinnchey et al. 2005, Stringari et al. 2007, Fotakis et al. 2007, Selimis et al. 2009, Vounisiou et al. 2010, Apostol et al. 2011, de Cruz et al. 2012). KrF* excimer laser (248 nm) has been mostly used, taking advantage from its submicrometric optical penetration in polymeric materials. Similarly, also the thermal diffusion length is estimated to be of the same order of magnitude according to the typical laser pulse duration (20–50 ns) and the low thermal conductivity of the organic matrices involved.
The operative fluence range reported for overpainting removal was about of 1–1.5 J/cm^2 (Fotakis et al. 2007). In this range, photomechanical effects and plasma formation can potentially induce injuries to the substrate especially when repetitive irradiation is needed for removing thick overpaint layers. Recently, Selimis et al. (Selimis et al. 2009, Vounisiou et al. 2010) have developed a novel method for the in-depth assessment of modifications during the excimer laser treatment.
Laser-induced fluorescence (LIF) and other spectroscopic techniques, such as multiphoton excitation fluorescence and third-harmonic generation, were employed in order to detect the chemical changes of photosensitive polymeric substrate upon the laser removal of the acrylic overpaint. It was concluded that a fluence of about 1.1 J/cm^2 can photochemically affect the doped substrate thus evidencing the early phase of laser-induced side effects.
A similar conceptual approach based on very short optical penetration depth, supports the experimentation of the free running Er:YAG (2.94 μm) laser whose wavelength is highly absorbed by OH bonds (de Cruz et al. 2000, Bracco et al. 2003, de Cruz et al. 2014). However, the lack of thermal confinement due to the long pulse duration (200–400 μs) can

induce thermal side effects well beyond the optical penetration, which is usually prevented by wetting the surface under treatment.
Some preliminary tests using Q-Switched (QS) Nd:YAG (1064 nm) laser, as standalone treatment or in combination with excimer laser, were also carried out (Mc Glinnchey et al. 2005, Stringari et al. 2007). In some details, a feasibility study was performed in order to remove a multi-layer acrylic overpaint from a twentieth century painting. In this case, a QS Nd:YAG laser irradiation was found useful as finishing treatment after excimer ablation in order to remove the residues of the latter.
Within this framework, we aimed the present study at exploring the potential of Long Q-Switched (LQS) Nd:YAG (1064 nm) laser with a pulse duration of 120 ns. As shown in previous works, such a temporal regime exhibits interesting interaction features such as a lower-pressure peak generation into the paint layer (Siano et al. 2012, Ciofini et. 2013), as well as lower recoil stresses in fluid dynamic ablation regimes (see the scaling law in Siano et al. 1999). At the same time, LQS pulses are also associated with a broader photoacoustic linear range, which is characterized by the typical double phase pressure transient (Siano et al. 2012). Here, we investigated whether these characteristics can provide any practical advantage for addressing the delicate problem of overpainting removal from easel paintings. To this goal, a systematic phenomenological investigation on suitable mock-ups was carried out. These preliminary tests allowed us to plan and perform localized laser treatments of an original modern painting. The successful results achieved disclose new application perspectives of laser ablation in conservation.

5.1.2 Materials and methods

Mock-ups shown in Fig. 2 and listed in Table 1 were prepared according to the overpainting conservation problem of a modern painting by anonymous (see Sect. 3), which was preliminarily characterized using optical and ESEM-EDX microscopy along with FTIR and portable Raman (excitation wavelength 785 nm) spectroscopy. All the materials used were pictorial products commercialized by Zecchi (Florence) with exception of the Green Lake 290 (chlorinated phthalocyanine PG7) and

Red-Magenta 256 (quinacridone PR122) that were Maimeri linseed oil paint tubes.
Excluding the latter, the others paint layers were prepared by mixing raw pigments in boiled linseed oil with a high pigment to binder ratio (P wt%/B wt%), up to the limit for brush application. For inorganic synthetic pigments the P/B ratio was around 65/35 while for lead based pigments and for carbon black was 85/15 and 50/50, respectively. Subsequently, they were applied on canvas primed with gypsum and rabbit skin glue and directly on micro-glass slides. Once dried, they were naturally aged under controlled laboratory conditions (T = 20 °C and RH= 45 %, E = 80–100 lx) for an overall period of about 2 years.

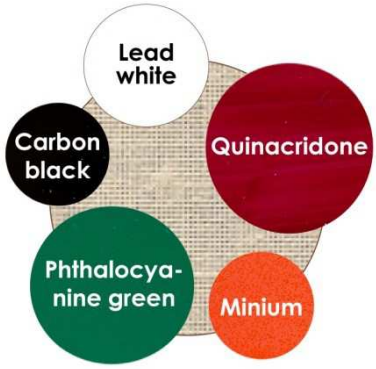

Fig. 2 Linseed oil prepared mock-ups for laboratory simulations.

Laser irradiation tests were carried out using a LQS Nd:YAG (1064 nm) laser emitting pulses of 120 ns and 150 mJ/pulse. These were executed on both the mock-ups and the easel painting under investigation according to the same irradiation procedure. The fluence and the number of laser pulses were gradually increased between 0.1 and 3 J/cm^2 and 1–100 shots per spot, respectively, up until damage effects were detected. Laser irradiation was performed in dry condition with a fixed spot diameter and pulse repetition frequency of 3 mm and 1 Hz, respectively, while the pulse energy and fluence were controlled by means of neutral filters. The optical parameters of the model samples realized were derived through reflectance and transmittance measurement on suitable paint

films applied on glass slide using an integrating sphere, according to a well-established method reported elsewhere (Siano et al. 2012). Diffuse reflectance (R) and transmittance (T) were averaged over 20 measurements.

The film thickness was measured using optical microscopy and contact profilometry (Hommelwerke T2000 Surface Profile Gage profilometer, 5 μm tip radius). The absorption and scattering coefficients (μ_a and μ_s, respectively) and then the effective optical penetration depth δ were derived through the Kubelka–Munk theory, which provides the Kubelka-Munk scattering and absorption coefficients *K* and *S* through the inversion of reflectance and transmittance formulas (Klier 1972, Cheong et al. 1990). In the case of isotropic scattering, as for the present paint layers, *K* and *S* are related with the scattering and absorption coefficients μ_s and μ_a through the following expressions:

$$\mu_a = \eta K, \quad \mu_s = \chi S,$$

$$\eta = \frac{(\phi - 1)(1 - a)}{\xi(\phi + 1)}, \qquad \chi = \frac{-a(\phi - 1/\phi)}{2\xi}$$

$$\frac{\phi^2 - 1}{2\phi} = \frac{1 + R^2 - T^2}{2R}$$

$$\phi = \frac{\xi + ln(1 - \xi)}{\xi - ln(1 + \xi)}, \qquad a = \frac{\mu_a}{\mu_a + \mu_s}$$

In this way the absorption and scattering coefficients, μ_a and μ_s, and hence the effective optical penetration depth δ were derived for all the pigments investigated.

VIS and UV fluorescence microscopies were employed in order to detect the laser damage threshold (LDT), intended as the minimum fluence inducing discoloration and/or ablation effects. Three combinations of the pass-band filters V2A (Exc: 380-420 nm, Bar:450 nm), B2A (Exc: 450-490 nm – Bar: 520 nm), and G2A (Exc: 510-560 nm – Bar: 590 nm) provided by Nikon, were used in the fluorescence setups.

5.1.3 Results and discussion

5.1.3.1 Systematic laser ablation studies on mock-ups

The irradiation methodology used for measuring the LDT of mock-ups put clearly in evidence that the fluences thresholds (F_{th}) significantly decrease with the number of pulses, which indicates the occurrence of cumulative effects depending on the total radiant exposure (Fig. 1).

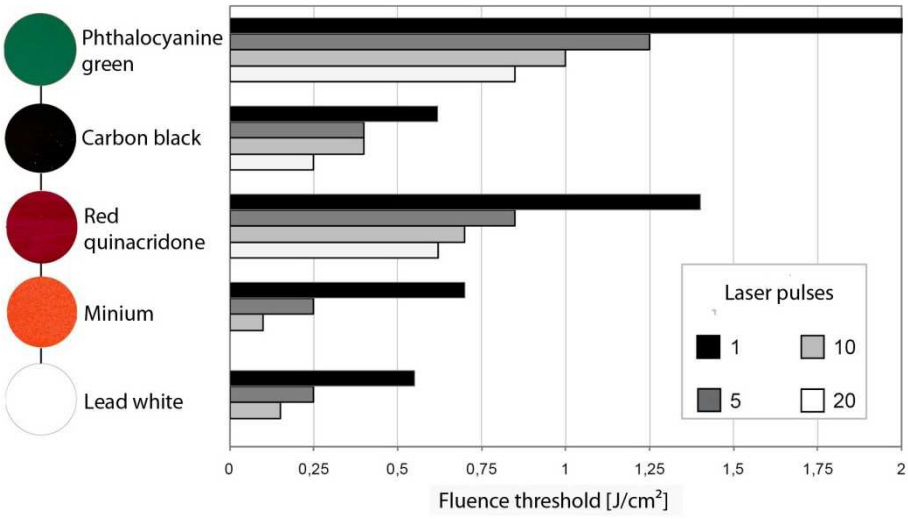

Fig. 3 Behavior of the LDT vs. laser pulses (logarithmic scale) of modern and traditional pigments in linseed oil binding medium

This phenomenon appears very pronounced for photosensitive lead-based pigments. Laser-induced morphological changes such as, cracking or ablation of the paint layer were observed through microscopic examination for chlorinated phthalocyanine green, lithopone and carbon black pigments. On the opposite, lead white and red lead pigments and red quinacridone showed darkening of the pigment particles easily detectable since the early stage as localized fluorescence quenching (Fig. 4).

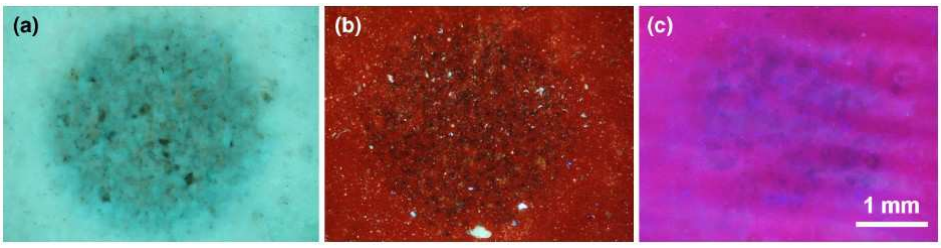

Fig. 4 UV fluorescence images (Ex 380–420 nm, DM 430 nm, BA 450 nm) of laser irradiated areas of: (a) lead white (5 pulses at 250 J/cm^2), (b) red lead (5 pulses at 250 mJ/cm^2), and (c) quinacridone (5 pulses at 850 mJ/cm^2)

Besides the precise determination of damage thresholds reported above (Fig. 3), before moving from tests on prepared samples to practical trials on the easel painting to be restored, we also estimated the optical penetration depth and associated laser heating of the paint layer. To this goal, reflectance, transmittance, and scattering measurements were carried out on the paint layers listed in Table 1.

Table 1 Optical parameters at 1064 nm: diffuse reflectance R (RSE: relative standard error) and transmittance T (z: sample thickness) measured along with the absorption coefficient (μ_a), scattering coefficient (μ_s), and effective optical penetration depth δ, as derived using the Kubelka–Munk theory.

Pigment/ paint layer	**Main compound**	**R_d (%)**	**RSE (%)**	**T_d (%)**	**RSE (%)**	**z (μm)**	**μ_a (μm^{-1})**	**μ_s (μm^{-1})**	**δ_{eff} (μm)**
Phthalocyanine	$C_{32}H_{0\text{-}2}N_8Cl_{14}Cu$	35	1	22	3	123±3	0.0028	0.014	83.4
Quinacridone	$C_{22}H_{16}N_2O_2$	9	1	72	3	93±12	0.0014	0.0023	250.6
Carbon black	amorphous carbon	7	1	n.d[a]	4	120±1	0.048	0.023	9.9
Lead white	$2PbCO_3{\cdot}Pb(OH)_2$	61	2	8	4	128±7	0.0019	0.044	61.2
Minium	Pb_3O_4	76	2	7	3	127±6	0.00092	0.071	70.9

[a]non detected

Apart from carbon black, which determines a strongly absorbing regime, all the remaining pigments presented μ_s values around one order of magnitude larger than μ_a which allowed estimating the effective optical penetration depth as: $\delta = \{3\mu_a [\mu_s (1\text{-}g) + \mu_a\}^{-1/2}$, where g is the anisotropy factor. As pointed out in a previous work through the measurement of the

scattering phase function (Siano et al. 2012), g≈0 (isotropic scattering). The effective optical penetration depth listed in Table 1 is much larger than the thermal diffusion length $z_{th} = 2(D \cdot \tau)^{1/2}$ and hence laser heating occurs under thermally confined conditions.
Thus for example, for minum (red lead, Pb_3O_4) ($D \approx 1.7 \times 10^{-2}$ cm^2/s [http://webbook.nist.gov/chemistry/]), z_{th} = 0.9 μm, while for organic substances ($D \approx 10^{-3}$–10^{-4} cm^2/s [Fotakis et al. 2006]), z_{th} = 70–220 nm. The confinement condition allows calculating the depth distribution of the temperature rise as $\Delta T(z) = Fa \cdot e^{-z/\delta} / \delta \rho C$, where ρ is the density and C the specific heat of the paint layer. Thus, the irradiation of Pb_3O_4 (C = 0.22 J/g K, ρ = 8.3 g/cm^3) at an absorbed fluence $F_a = F_0$ (1-R) = 100 mJ/cm^2 produces a maximum temperature rise (z = 0) of about 8 °C. This means that for a single pulse at F_{th} = 0.7 J/cm^2 (F_a = 0.17 J/cm^2) $\Delta T(z) \approx 13$ °C while for an incident fluence of 0.2 J/cm^2 it is about 3–4 °C. Such average temperature rises in proximity of the paint layer surface are not sufficient to justify the observed damages and then suggest the alteration mechanism is driven by inhomogeneous absorption (Danileiko et al. 1972), which is also supported by the alteration phenomenology displayed in Fig. 4b. In the cumulative effect also the low thermal diffusivity of the organic matrix plays an important role, making its relaxation time ($t_{th} = \delta^2/4D$) relatively long.

5.1.3.2 Analytical chracterisation

Raman spectroscopy and ESEM-EDX showed that chlorinated copper phthalocyanine green and Ba, Zn (Ca)-based pigments commonly used in early twentieth century, are the main components of the overpainting (Fig.5a, site A). Traces of Cr and Pb were also detected, which suggest the presence of chrome yellow (Fig. 5a, page A1).
FTIR analysis revealed a lipid-based binder, which is likely linseed oil (Fig. 5c, site C). Traditional inorganic pigments (lead white, red lead and carbon black) and modern organic dyes (red synthetic azo pigment) applied in linseed oil were identified in the paint layers (Fig. 5b). The canvas was primed with gypsum or chalk and glue.

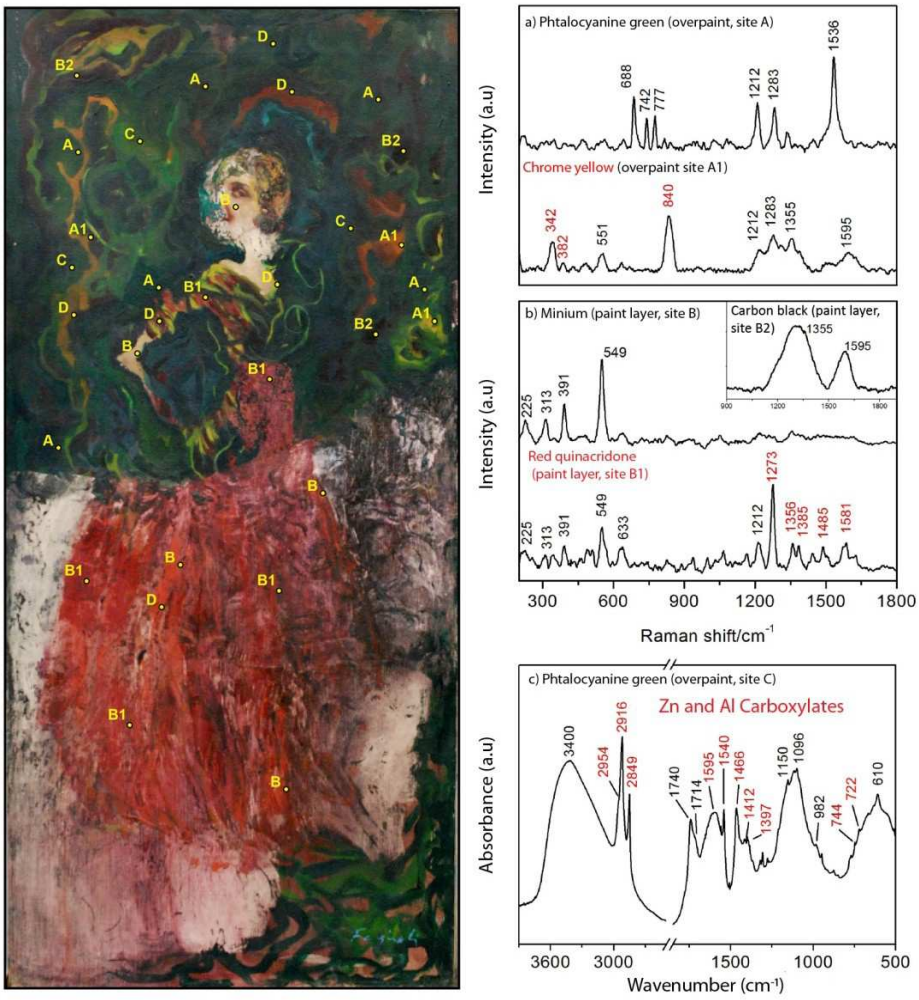

Fig. 5 Analytical characterisation of the female portrait by anonymous. Raman spectra (exc. 785 nm) of overpaints (a) and paint layers (b). Trasmission FITR spectroscopy of the phtalocyanine-based overpaint (c).

5.1.3.3 Laser removal tests on modern painting

The case under investigation is an oil on canvas painting (Fig. 6) extensively overpainted without any conservation intent using green, yellow and brown hue paint.

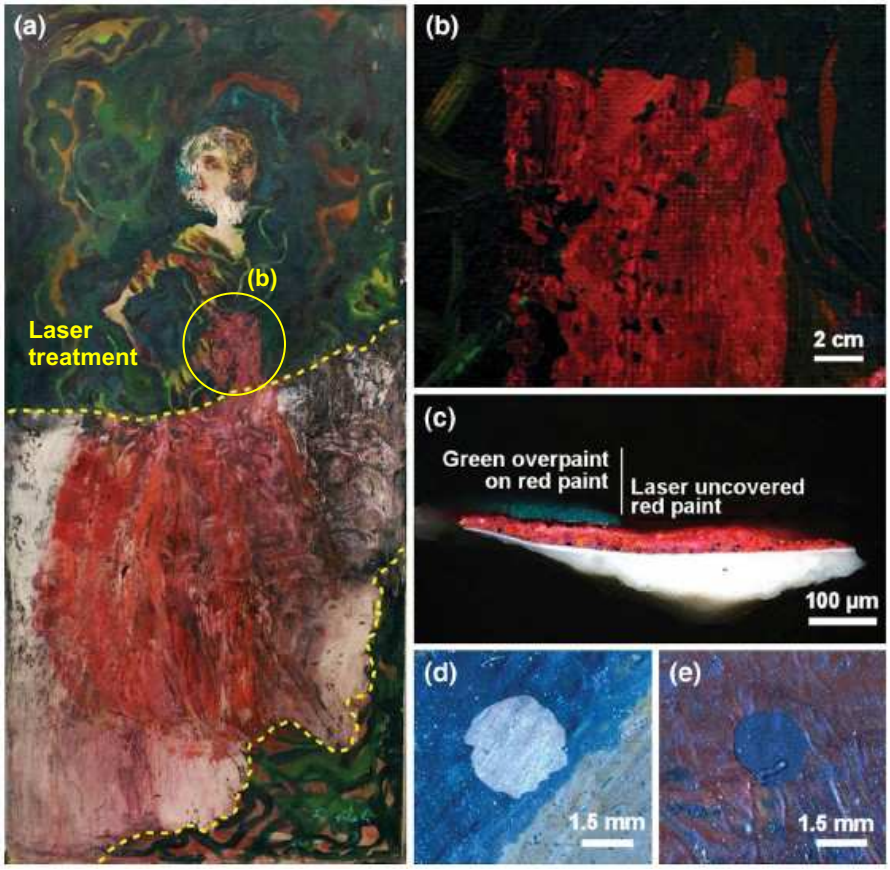

Fig. 6 - (a) Overpainted female portrait by anonymous (about 50 x 120 cm^2) with previous invasive uncovering attempt (between dashed lines). (b) Laser removal of dark green hue chlorinated phthalocyanine oil-based overpaint from a mixture of a red lead and red synthetic azo oil-based paint layer. (c) Cross-section showing a laser uncovering transition, as achieved by a single-pulse laser irradiation at F = 0.85 J/cm^2. (d) Spot of lead white paint uncovered by a single laser pulse. (e) Spot of carbon black paint uncovered by a single laser pulse. All the pigments mentioned were identified using Raman spectroscopy.

As dramatically demonstrated by a previous undocumented restoration attempt, which produced serious damaged to lower half of the artwork (see the area between dashed lines in Fig. 6a), traditional methods based on solvents do not allow removing the overpaint. Successful uncovering results (Fig. 6b–e) were achieved on the present painting using laser

fluences well below 1 J/cm^2 although the process appeared to be not sufficiently self-terminated and then very critical.
The damage fluence thresholds achieved for the mock-ups simulating the original paint layers, F_{th} (*mock-up*), were compared with the removal threshold of the real case, F_{th} (*overpaint*) in order to assess the nature of the discrimination observed.
This comparison summarized in Table 2, suggests that the F_{th} (*overpaint*) values mainly depend on the composition and optical properties of both the overpaint and of the paint layer underneath, as well as on the number of pulses released to the target (i.e., on the total radiant exposure).

Table 2 - Laser removal thresholds of the real case vs. LDT of the mock-ups for one and ten laser pulses.

F_{th} (J/cm^2)	$F_{th,\ overpaint}$		$F_{th,\ mock\text{-}up}$		$\frac{F_{th,\ overpaint}}{F_{th,\ mock\text{-}up}}$	
Laser pulses	1	10	1	10	1	10
Overpaint/mock-up						
green/quinacridone	0.85	0.6	1.4	0.7	0.6	0.86
green/red lead	0.85	0.6	0.7	0.2	1.2	3
green/lead white	0.85	0.6	0.55	0.2	1.5	3
green/carbon black	0.6	0.35	0.6	0.4	1	0.88
yellow/carbon black	0.6	0.45	0.6	0.4	1	1.12
Brown/carbon black	0.35	0.25	0.6	0.4	0.58	0.62

In the case of superimposed absorbing layers (i.e., brown/ carbon black), F_{th} (*overpaint*) was relatively low while for weakly absorbing materials (i.e., green/red quinacridone and lead-based pigments) was significantly higher. The removal mechanism in any case does not involve an intermediate discoloration or, even less, plasma formation but starts with the spallation of flakes whose number and total sizes increases with the laser fluence up until complete single-pulse removal (Fig. 7), in agreement with a similar phenomenology observed during the tests performed on mock-ups.
When F_{th} (*overpaint*)/F_{th} (*mock-up*) ≥ 1 the exposure of the paint layer underneath can be very dangerous. In the case of single-pulse removal, the ratio F_{th} (*overpaint*)/F_{th} (*mock-up*) changed from 3 up to 1.2–1.5 for uncovering lead-based pigments, which make them the worst situation for

laser treatments, although the damage thresholds of the original paint layers are usually slightly higher with respect to the mock-ups. Thus for example, the LDT measured on the present painting for lead white layer were, respectively, 0.25 J/cm^2 after ten pulses and about 0.8 J/cm^2 for single pulse, against 0.2 and 0.7, respectively, of the model samples. This slight fluence rise could be due to the presence of a thin deposit layer on the painting surface pointed out during the stratigraphic examinations.

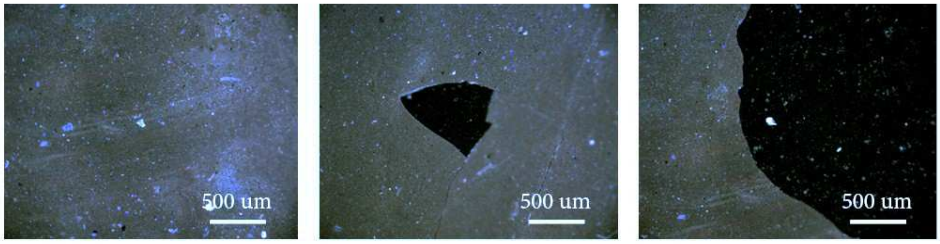

Fig. 7 - UV fluorescence images of brown overpainting on carbon black paint layer. From left to right: F = 0.15 J/cm^2, 100 pulses, F = 0.25 J/cm^2, 10 pulses, F = 0.35 J/cm^2, single pulse

Despite the lack of optical discrimination in most cases, successful removal tests were achieved by single shot thanks to the shielding effect of the overpaint layer, which protects the sensitive pigment underneath. Thus for example, as derived from the optical characterization, when F_{th} (*overpaint*) = 0.85 J/cm^2 for single shot, only 0.1–0.2 J/cm^2 of the incident fluence reaches the original paint layer, which is well below its single-pulse damage threshold. Such an estimation holds if assuming the thickness of lithopone and phthalocyanine samples really simulate the composition and thickness of the overpaint found in the case study.
Fluorescence microscopy inspections and Raman spectroscopy analyses were carried on the original painted surface uncovered, which did not evidence any detectable alteration, thus demonstrating the significant selectivity of the LQS Nd:YAG laser ablation.

5.1.4 Conclusions

In this work, the use of LQS Nd:YAG (1064 nm) laser for the removal of overpaints has been reported for the first time. Laser damage thresholds on model samples significantly decrease with the number of pulses applied on the irradiated area and more drastically when the pigments are photosensitive due to cumulative effects, which could make the ablation process not selective and then impracticable. Despite this trend, the laser removal tests performed on the modern painting investigated using single shot laser irradiation showed high selectivity in the removal of the overpainted layer, even when the latter covered photosensitive lead-based pigments. This can be explained by considering the fluence attenuation due to the optical absorption and scattering of the overpaint layer, which prevented the overexposure and alteration of lead white and red lead. Thus, despite the single-pulse spallation process here proposed was quite critical, it can be considered practicable according to the usual caution that any conservation treatments of easel painting requires.

5.2 Case study 2- A female portrait found on the backside of a Giacomo Balla's work

In this work laser ablation has been applied for removing overpainting layers from an easel painting, which was found on the backside of a signed artwork by Giacomo Balla, one of the founding members of the Futurist Painters. After unsuccessful attempts to remove selectively the overpaint layers using organic solvents, LQS Nd:YAG laser (1064 nm, 120 ns) ablation has been successfully tested thus allowing planning and performing the overall laser uncovering of the disguised artwork. This has been associated with a thorough characterisation of the original pigments, binders, and overpaintings using Raman, and FTIR spectroscopy, along with stratigraphic examinations through optical and ESEM-EDX analyses. At the same time, a systematic laboratory experimentation on prepared samples simulating the uncovering problems encountered in the real case, has been carried out in order to interpret the specific laser removal processes exploited and to achieve suitable keys of generalisation of the present methodological approach to the removal of overpaintings.

5.2.1 Introduction

To date, significant efforts have been dedicated to investigate the potential of laser ablation in conservation-restoration of easel paintings. The first documented attempts to approach such a complex problem date back to the early 1980s (Carlyle, 1981), while the scientific publications on the topic began during the early nineties (Hontzopoulos et al., 1993, Salimbeni et al., 1998). Previous thorough studies and successful application of excimer laser (193 and 248 nm) for finely ablate polymers and corneal tissue (Srinivasan et al., 1986) formerly suggested to focus on the experimentation of this type of laser sources. Their submicron ablation rates represented a peculiar feature, which could be exploited for removing deposits and altered varnishes from easel paintings. The effectiveness of such a laser selection has been demonstrated in some cases of interest (Teule et al., 2003) and possible improvements

associated with the use of ultrashort pulses have been recently reported (Pouli et al., 2010). At same time, application tests also pointed out the need to control the ablation process because of the lack of intrinsic discrimination due to the high absorption of all the organic materials in the UV spectral region. Besides this limitation, the costs and maintenance issues of the excimer lasers have impeded the practical exploitation of their potential. In principle, the Nd:YAG laser's fourth harmonic (266 nm) could represent an alternative to excimer lasers, but the pulse energy of the latter is higher and their beam quality better suited for ablation than those of the former in common commercial sources.

Free Running (FR) Er:YAG laser (2.94 μm) has also been systematically experimented on paintings and applied in some practical case studies (Bracco et al., 2003). Similarly to excimer lasers, this solid state source was formerly tested for biotissue ablation (Cubeddu et al., 1996), thank to the high absorption of the OH groups at 2.94 μm. The potential of FR Er:YAG laser in the conservation of easel paintings is strictly related with this feature, which allows the photothermal alteration and disaggregation of the material layer under irradiation. As for excimer lasers, its action is not self-terminated. Furthermore, the long pulse duration of the FR temporal regime (200-400 μs) also involves some thermal issues, thus affecting the practical exploitation of the short optical penetration (~ 1 μm).

Finally, preliminary laboratory tests aimed at assessing the stability of several pigments under laser irradiation have been carried out using QS Nd:YAG (1064, 532, 355, 266 nm) lasers (Sansonetti and Realini, 2000; Pouli et al., 2003; Hildenhagen et al., 2005, Siano et al., 2012), as well as ultrashort laser systems (Pouli et al., 2008, Gaspard et al., 2008, Oujja et al. 2011), which can potentially allow minimising undesired side effects produced by QS Nd:YAG sources. Despite the above mentioned works provided some encouraging results, the laser treatments of easel painting are still far from the common conservation practice.

To date, Nd:YAG laser's fundamental wavelength (1064 nm) is mostly used in conservation institutions and restoration enterprises for stone, metal, and wall painting conservation-restoration treatments. The introduction of the Short Free Running (SFR) and Long Q-Switching

(LQS) temporal regimes, providing pulse duration in the range of several tens of nanoseconds and microseconds (see Siano et al., 2012 and references therein), respectively, have significantly extended the application domain to this solid state laser source. The present availability of both these temporal regimes in the same laser system (Siano et al. 2013) will likely further promote the use of Nd:YAG(1064 nm).
The effectiveness of LQS Nd:YAG (1064 nm) laser has been formerly demonstrated for cleaning treatments of encrusted amalgam gilding (Siano and Salimbeni, 2001), then various successful applications to wall painting have been reported along the last decade for removing limewashes, aged Paraloid, and calcareous growths . Ablation tests have also been carried out in order to evaluate the potential of pulse durations around 100 ns for removing dark varnishes (S. Siano et al., 2012). Despite the optical penetration at 1064 nm of the paint layers encountered in easel paintings is relatively large and variable, according to the type of pigment and the pigment/binder content ratio, in a specific case such a laser approach was preliminarily tested for removing overpaints by suitably selecting the irradiation conditions (Ciofini, *et al*. 2014).
Here, LQS Nd:YAG(1064 nm) laser ablation has been applied for the first time for removing overpaint layers from a modern easel painting dated around 1910, which is attributable to Giacomo Balla's studio. After unsuccessful removal attempts using organic solvents, laser ablation has been tested. The uncovering results have been very satisfactory and then the laser ablation treatment has been extended to the whole overpainted surface thus allowing to recover an unknown Pre-Futurist artwork.
The restoration work has been associated with a thorough characterisation of the original pigments, binders, and overpaintings. Furthermore, following this successful application, we carried out laboratory simulations in order to interpret the underlying basic mechanisms and extract laser process features of general valence.

5.2.2 Materials and methods

A scene with a female subject was indistinctly visible on the backside of the canvas of a signed Pre-Futurist painting by Giacomo Balla from private collection. It was disguised by a dense distribution of broad and

superimposed rectilinear brush strokes of different colour hues. Apparently, such rough overpaintings did not have any artistic intent but rather they suggested the backside-painting surface of Balla's artwork was likely used in order to clean the brushes while executing other paintings (Fig. 8).

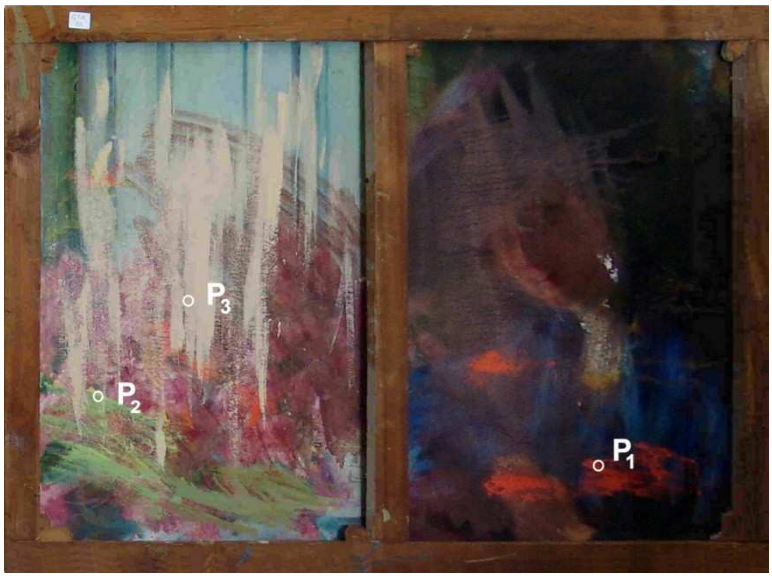

Fig. 8 – Overpainted painting on the backside of a Giacomo Balla's work. P_{1-3} refers to the sampling areas .

The owner and the restorer decided to try to uncover the disguised painting using suitable solvent blends provided by Teas solubility chart. The preliminary tests pointed out the possibility to solubilise the undesired layers but the effect was uncontrollably extended to the original paint underneath thus making impracticable its discrimination. This led to explore alternative approaches.

The successful applications carried out on wall paintings along the last decade and the encouraging results achieved in a preliminary study focused on the removal of dark varnishes from paint layers by means of LQS Nd:YAG (1064 nm) laser (Siano et al., 2012), suggested to investigate the potential of this tool in order to approach the present recovery problem. Laser ablation tests were associated with a thorough

material characterisation, which was carried out by means of microscopic inspections, portable Vis reflectance, and Raman spectroscopy measurements, along with with FTIR spectroscopy equipped with attenuated total-reflection (ATR) and stratigraphic examinations (optical and ESEM-EDX) of small material samples. The Raman spectrometer was a compact device using an excitation wavelength of 785 nm and a thermooptically cooled detector (2048 pixels). Its spectral range and resolution were 260–3200 cm^{-1} and 6 cm^{-1}, respectively. The mentioned techniques were used for both for preliminary characterisation and post-treatment assessments.

Three material samples (P_{1-3}) were taken from the painting under investigation. They were embedded in polyester resin and dry polished with 4000 grit abrasive. Visible and fluorescence microscopy using Nikon Fluorescence Filter Blocks V2A (Exc.: 380-420 nm. Bar.: 450 nm), B2A (Exc.: 450-490 nm. Bar: 520 nm), and G2A (Exc.: 510-560 nm. Bar.: 590 nm) were carried out in order to collect combined colour, fluorescence, and morphology information.

As mentioned above, we also carried out a systematic laboratory experimentation on prepared samples simulating the uncovering problems encountered in the real case. Linseed oil paint mock-ups were prepared on primed canvas and glass slides using a pigment/binder ratio of 65 wt%/35 wt%. The selected pigments were lithopone (Liw), titanium white (Tiw), zinc oxide (Znw), cadmium yellow/orange (Cdy), green copper carbonate (Cug), artificial ultramarine blue (Ub), cobalt blue (Cob), chromium oxide green (Crg).

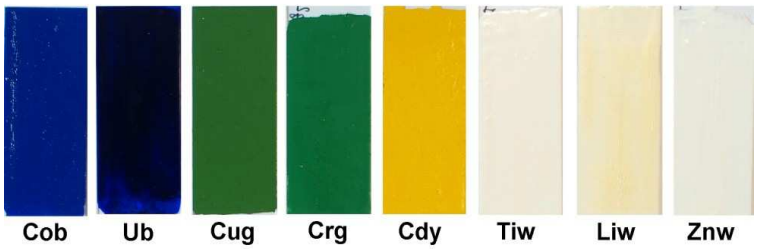

Fig. 9 – Prepared linseed oil paint samples for laboratory simulations.

These were subjected to natural ageing in controlled laboratory conditions (T=20 °C and RH=40-45%, E=100 lx) for an overall period of about 2 years, then their optical properties at 1064 nm and laser damage thresholds (LDTs) were experimentally derived. The former were estimated by means of the Kubelka-Munk theory, which allows deriving the absorption coefficient, scattering coefficient, and then the effective optical penetration depth δ from the measurement of the diffuse reflectance (R) and transmittance, as reported previously for the case study 1. The latter were estimated by gradually increasing the fluence and the number of pulses on the same test area up until material alterations were detected through Vis and/or fluorescence microscopy. A constant spot diameter of 3 mm was used throughout the trials while the fluence variation was achieved using neutral density filters. This method led to evaluate the onset threshold at each irradiation fluence as function of shot number (Arenberg 2009, Arenberg et al. 2010).
Finally, photoacoustic measurements using 9 μm thick metalized PVDF (polyvinylidene difluoride) sensors were carried out in order to better describe the basic mechanisms driving the photomechanical ablation processes in the different stratigraphic conditions. The set-up used for optical and pressure transient measurements was similar to those reported in a previous work (Siano *et al.*, 2012). A schematic drawing is depicted in Fig. 10.

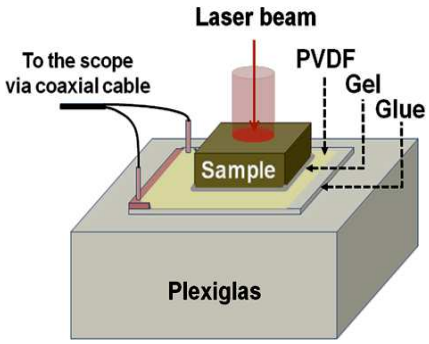

Fig. 10 - Setup for measuring pressure transient generated by laser irradiation.

Briefly, the irradiated sample was the upper component of a sequence of strata including a thin gel layer to ensure the mechanical continuity

between the sample itself and the underlying PVDF foil, which is in turn glued to a thick Plexiglas base taking care to avoid the formation of air bubbles. The two metalized sides of the PVDF foil were connected through a short coaxial cable to the high impedance input of the oscilloscope. In this configuration the voltage *V (t)* is proportional to the pressure *p(t)* with sensitivity in the order of 1 mV/bar, depending on the area of the pressure front.

5.2.3 Results and discussion

5.2.3.1 Material characterisation

The cross-section examination, FTIR and Raman spectroscopy of the material samples taken from the painting understudy allowed achieving a clear stratigraphic compositional picture of the superimposed paint layers Fig. 11.

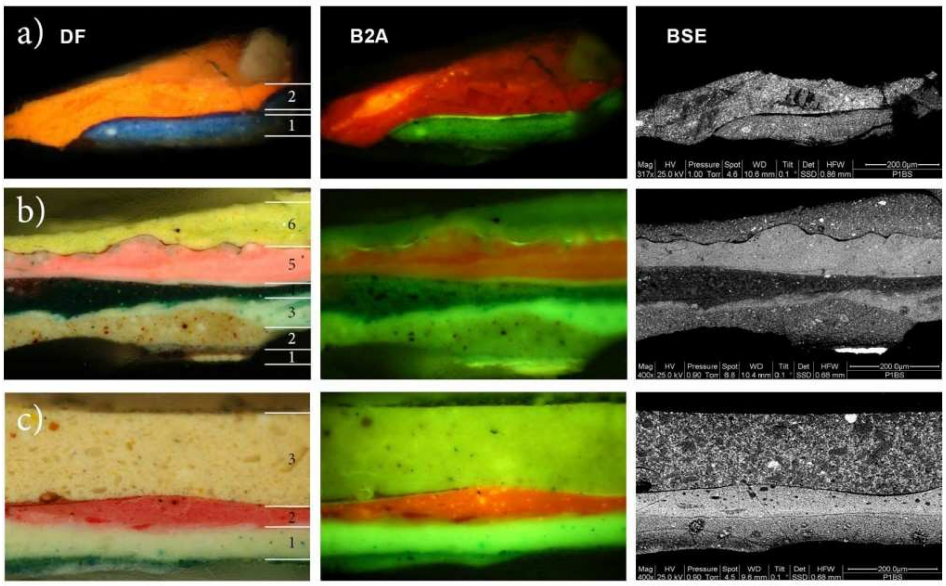

Fig. 11 Paint cross-section P_1(a), P_2 (b) and P_3 (c). From left to right: dark field microscopy (DF), UV-VIS fluorescence at an emission wavelength of 520 nm (λ_{exc} = 450-490 nm) (B2A filter) and BSE (back scattered electrons) images. The layers are numbered from bottom to top.

The composition features were further investigated by performing a number of Raman measurements directly on the painting during the laser uncovering treatments. This allowed a rigorous definition of the conservation-restoration problem and the documentation of the laser treatment.

Sample P_1

As shown in Fig. 11a the sample P_1 (cross section, a) included a relatively thick (about 100 μm) orange layer, which was overpainted on a paint layer (about 50 μm) composed by blue microparticles in a whitish matrix. This inner layer presented a dark hue in proximity of its outer surface (within about 10 μm) and a pale green hue at the inner level (within about 20 μm). Furthermore, the blue paint also included whitish agglomerates of roundish shape and variable size (5-15 μm) with a pronounced fluorescence when excited at 450 nm, which recall in mind the typical features of the metal soaps (i.e. compounds of metal salts with fatty acids from vegetable oils).
The two main layers of the sample P_1(a) were separated by a thin film of transparent varnish (about 5 μm), as highlighted by means of fluorescence and ESEM imaging (see B2A in Fig. 11a). The presence of this finishing layer, evidenced the overpaints were applied on a finished artwork and hence they did not belong to the original artistic program by the author.
ESEM-EDX analysis revealed a predominance of S, Ba, and Zn and a minor content of Cd in the overpaint (layer 2), while Zn, Al, and Si were the main elements in the underlying blue paint (layer 1), which also included minor amounts of Cd and Co (Table 3).
Raman spectroscopy of the former detected cadmium yellow, CdS, and traces of anatase, TiO_2 (Fig. 12), while the mentioned high EDX peaks of S, Zn, and Ba were compatible with the simultaneous presence of lithopone, ZnS + $BaSO_4$ (Burgio et al. 2001, Eastaugh *et al.*, 2004).

Table 3 Stratigraphic ESEM-EDX analyses of the material samples: letter and number refer to the stratigraphies of Fig. 11.

Section	Layer	Elements
a)	2	Al, Si, P, S, Cd, Ca, Ba and/or Ti, Zn
	1	Na, Al, Si, S, Cd, Co, Zn
b)	6	Mg, Al, Si, S, Cd, Cr, Ba and/or Ti, Cu, Zn, Pb
	5	Zn
	4	Al, Si, S, Cd, Cr, Co, Zn, Pb
	3	S, Cd, Cr,Cu, Zn
	2	Fe, Zn
	1	Zn, Pb
c)	3	Si, S, Ca, Ba, Fe, Zn
	2	Zn
	1	Al, Si, S, Ba, Cd, Cr, Cu, Zn, As

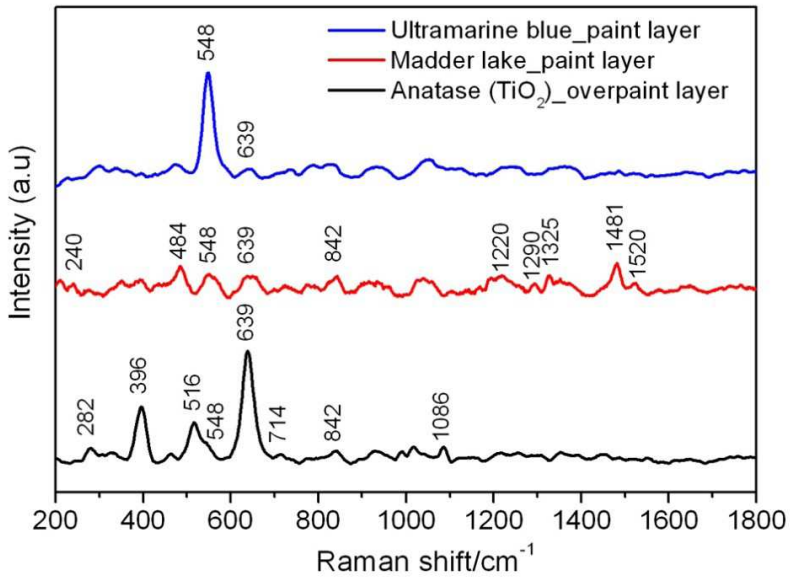

Fig. 12 Representative Raman spectra (exc. 785 nm) of paint and overpaint layers (see the text).

Moreover, the orange hue of the overpaint also suggested the possible addition of a red lake. Raman peak at 545 cm^{-1} showed that the underlying paint (layer 1 in Fig. 11a) was artificial ultramarine blue (Fig.

12). The corresponding EDX detection of cobalt indicated it was likely a cobalt based ultramarine blue.

The FTIR-ATR spectra showed that both the pictorial and overpaint layers were made using an oily binder (likely linseed oil) and evidenced the chemical changes induced by pigment-binder interaction (Fig. 13).

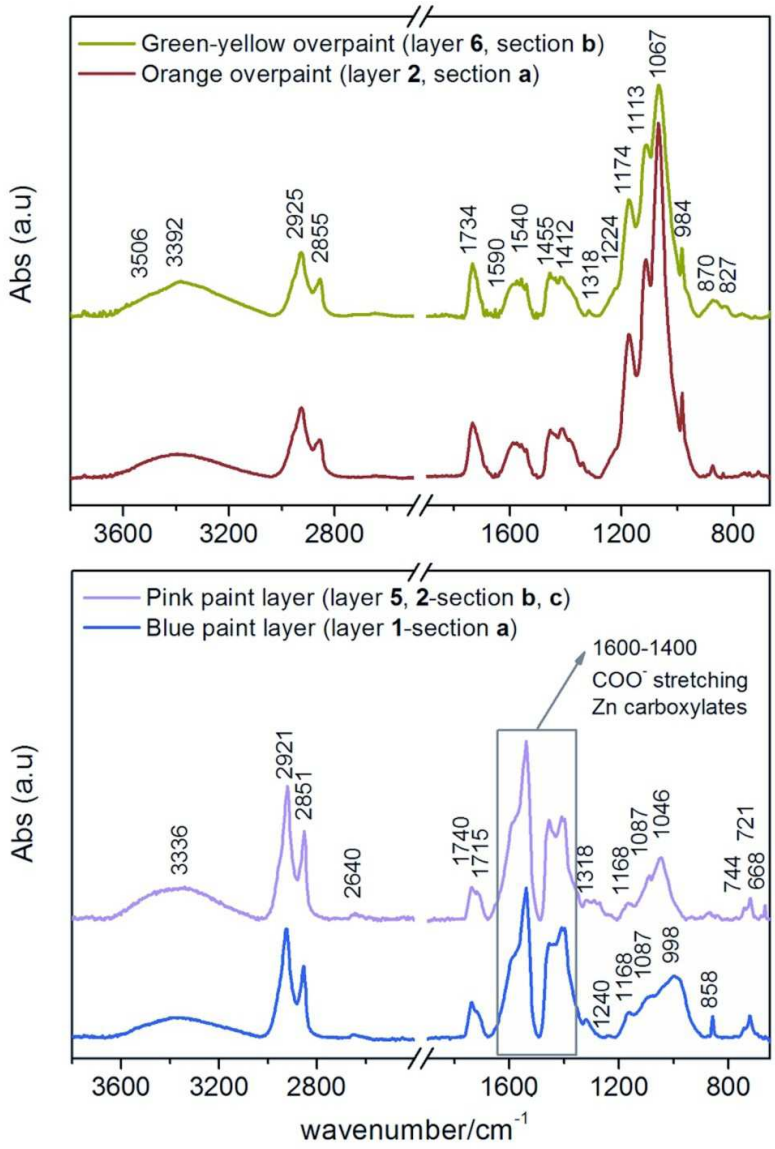

Fig. 13 Two representative ATR-FTIR spectra showing different composition and degradation mechanisms between overpaint (top) and paint layers (bottom).

Similar features were noticed in the spectra of the blue and pink paint layers. The CH vibrational band at 2921 cm^{-1} and 2851 cm^{-1} were more intense than the narrow carbonyl peak indicating that the amount of intact ester bonds was relatively low. This fact, along with the free fatty acids shoulder band at 1715 cm^{-1} and the broad OH stretching band at 3336 cm^{-1} suggest the formation of carboxylic acid products, properly dicarboxylic fatty acids (diacids) and acid-rich network oligomers (Meilunas *et al.*, 1990, Van der Weerd *et al*., 2005).
In fact, both spectra presented intense asymmetric and symmetric COO- stretching bands in the spectral range of 1600-1400 cm^{-1} (Fig. 13). In detail, the position of the vibration peak at 1540, 1398 and 1465 cm^{-1} are related to the presence of zinc stearate/palmitate, while shoulders at about 1589 e 1469 cm^{-1} to Zn lactate and Al stearate. These bands are representative for asymmetric metal carboxylates vibration, probably a mixture of carboxylates with different molecular weight. The C-H bending vibration at 1408 and 1455 cm^{-1} may instead be attributed to symmetric zinc carboxylate vibration (Newman 1979, Osmond et al., 2012, Poli et al., 2014). It is worth noting that the intensity and the band shapes of the oil medium and metal soaps in the overpaints suggest a lower degree of saponification in comparison with that found in the original paint layers indicating the use of different material and ageing processes.

Sample P_2

The cross-section of the sample P_2 was the most complex (Fig. 11b). This included the following layers (see also Table 3);

1) A whitish ground layer (20 μm) with a pronounced fluorescence and a high lead and zinc contents, which were reasonably ascribable to the preparation of the canvas. Above the latter, a thin layer probably made using a glue binder (5-10 μm) was also applied as supported by the intense fluorescence and BSE image.
2) Zinc white and iron red mixture composed with a very variable thickness.

3) Light green layer including S, Cd, Cr, Zn and Pb.
4) Dark green layer composed of Al, Si, S, Cd, Cr, Co, Zn and Pb traces, most probably a chrome based green.
5) A zinc-based pink paint layer including traces of calcium and a red alizarin-based dye, as shown by Raman spectroscopy (Fig.12).
6) Chrome yellow and a Cu-based pigment along with Ca, Ba, Zn and Ti are the main compounds of the pale yellow-green overpaint.

Sample P_3

The ESEM-EDX analysis of the whitish overpaint (layer 3) in the sample P_3 (Fig. 11c, Table 3) detected Al, Si, S, Ca, Ba, Fe and Zn while titanium dioxide (anatase form) was revealed by Raman spectroscopy (Fig. 12). Zinc oxide in layer 2 was the main of red particles than P_2, whose organic nature was confirmed also by BSE observation. This support the possible use of madder lake for painting the flower theme indistinctly visible in Fig. 8. A closer inspection of the layer 2 by means of ESEM-EDX analysis, revealed the presence of roundish agglomerated of Zn and a small dispersed fraction of Al, most likely due to the Zn and Al palmitate/stearate, as observed by ATR-FTIR.

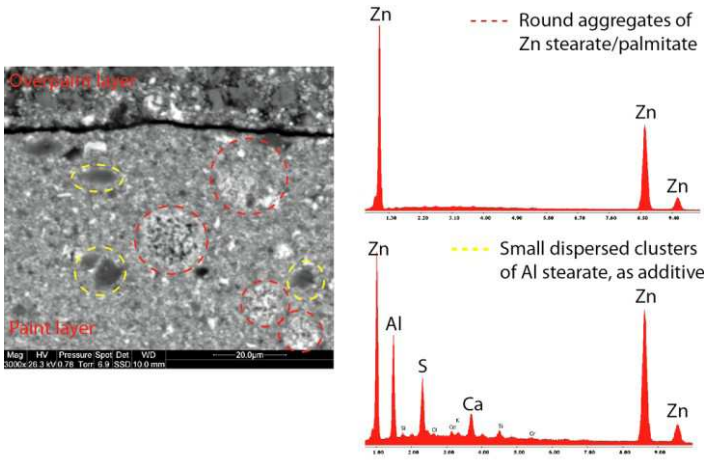

Fig. 14 BSE image (magnification 3000x) illustrating the presence of zinc and aluminum clusters in the pink paint layer (layer 2, sample P_3).

Similarly to P_1, the zinc based light green layer (layer 1) included relatively large translucent zinc agglomerates exhibiting the typical properties of the metal soaps. The ATR-FTIR spectra of P_2 and of P_3 confirmed the presence of the latter and the use of an oily binder.
Finally, Table 4 summarizes the results of the pigment identification of the overpaint and original paint layers, based on the described analyses, as well as on a number of Raman measurements carried out *in situ*.

Table 4 - Pigments identified in the overpaint and original paint layers of the present artwork (Fig. 8). All the paint layers were applied in oil based binder.

Pigment assignment	**Main compound**
Overpaint layers	
Lithopone (Liw)	$ZnS+BaSO_4$
Titanium white (Tiw)	TiO_2
Cadmium yellow/orange (Cdy/o)	CdS
Green copper carbonate (Cug)	$Cu_2CO_3(OH)_2$
Chrome yellow (traces)	PbCrO4
Zinc yellow (Zny)	$ZnCrO_4$
Paint layers	
Artificial ultramarine blue (Ub)	$Na_{6-8}Al_6Si_6O_24S_{2-4}$
Zinc oxide (Znw)	ZnO
Madder lake (alizarin)	$C_{14}H_8O_4(OH)_2$
Chromium oxide green (Crg)	Cr_2O_3

5.2.3.2 Laser ablation tests on real painting

As mentioned above, LQS Nd:YAG(1064 nm) laser with a pulse duration of 120 ns (FWHM) was used in the present work. Ablation tests were carried out in various zones presenting different stratigraphic situations in order to assess the potential of the technique and possibly define the operative fluences. In all the cases, the fluence was gradually increased up until the observation of a satisfactory removal of the overpaint. The final operative fluence was set just slightly above such a threshold. The results

of this optimisation is summarised in Table 3 listing the effective operative fluences for removing the different overpaints, which ranged between 0.5-0.7 J/cm^2, along with some observations.

Table 5 - Measured removal thresholds of the various overpaints from the paint layers of the present artwork.

Overpaint layer/ (main pigment)	**F_{th} (J/cm^2)**	**Observations**
Orange on blue (like the layers 1-2 superposition in Fig. 11a)	0.7	Safe uncovering of the blue area of the dress. The LTD of the blue paint was about 1.2 J/cm^2.
Yellow-green (like the layer 6 in Fig. 11b) on green	0.5	Safe uncovering of the chrome green paint layer. The LTD of the latter was about 0.9 J/cm^2
Yellow-green on pink (like layers 5-6 superposition in Fig. 11b)	0.5	Several pulses were needed for the removal from the pink pictorial layer of the flowers zone. The LTD of the paint layer was about 0.7 J/cm^2.
White on pink (like layers 2-3 superposition in Fig. 11c)	0.5	The most harmful situation (many pulses needed low discrimination), which was observed in the flowers zone. The LTD of the paint layer was about 0.7 J/cm^2.

The ablation phenomenologies, as observed to the naked eye, included single pulse spallation in zones presenting thin whitish overpaint layers along with gradual ablation and weakening in other areas with thicker stratifications. As arguable from Fig. 15, the results of the laser ablation tests were very satisfactory. A practicable degree of self-termination was observed during the trials. No any micromorphological, chromatic or chemical alteration of the original paints was pointed out by microscopy, optical, and Raman assessments carried out in the laser uncovered sites.

Fig. 15 - LQS Nd:YAG(1064 nm) laser removal tests of whitish lithopone-based overpaint (left) covering the areas of the flowers (Fig. 8) and of an orange layer (right) from the dress of the figure (Fig. 8) using 0.5 J/cm^2 and 0.6 J/cm^2, respectively.

Two representative cross-sections of material samples taken at the edges of test areas with orange (mostly CdS with ZnS+$BaSO_4$) and whitish (mostly ZnS+$BaSO_4$ likely mixed with Cu-based pigment) overpaints on ultramarine blue and pink (ZnO and likely madder lake), respectively are displayed in Fig. 16.

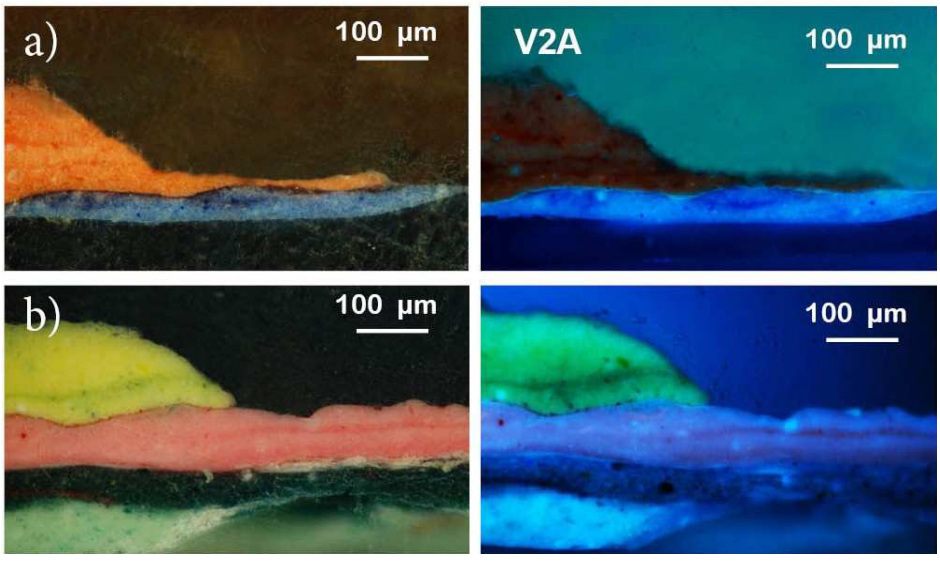

Fig. 16 Laser transition between untreated (left) and laser treated (right) areas. The two samples correspond to the surface situations displayed in Fig. 15 (a) and Fig. 15 (b), respectively.

These stratigraphies and the cleaning spots of Fig. 15 suggest the occurrence of different ablation regimes. Apparently, lithopone (Fig. 15), especially when applied as a thin layer, underwent to a massive spallation (note the flacking) without a significant thermal alteration, whereas the orange overpaint was finely ablated, as usually occurs for highly absorbing materials. However, these naked eye observations can only be considered the starting point of the physical diagnostics of the ablation processes, which is described hereafter.

5.2.3.2 Insights on the laser interaction process

A set of mock-ups were prepared using single pigments selected among those identified through the material characterisation of the present painting: zinc white (Znw), lithopone white (Liw), titanium white (Tiw), cadmium yellow (Cdy), chromium green (Crg), ultramarine blue (Ub), cobalt blue (Cob), copper green (Cug) (Fig. 9). As described above, effective optical penetration depth (δ) and LDTs were measured according to the described protocol (5.2.2). The optical properties of the prepared oil paints are plotted in Table 6.

Table 6 Optical parameters at 1064 nm: diffuse reflectance R and transmittance T (z: sample thickness) measured along with the absorption coefficient (μ_a), scattering coefficient (μ_s), and effective optical penetration depth δ, as derived using the Kubelka–Munk theory.

sample	main compound	R_d (%)	T_d (%)	z (μm)	μ_a (μm^{-1})	μ_s (μm^{-1})	δ (μm)
Crg	Cr_2O_3	21	n.d[a]	90 ± 6	0.027	0.05	12.4
Cug	$Cu_2(CO_3)(OH)_2$	11	20	109±5	0.0037	0.009	91
Ub	$Na_{6\text{-}8}Al_6Si_6O_{24}S_{2\text{-}4}$	30	25	100±3	0.0036	0.014	71.2
Cob	$CoAl_2O_4$	27	9	42±6	0.018	0.052	16.0
Znw	ZnO	70	13	83 ± 7	0.0013	0.066	61.8
Cdy	CdS	85	5.6	110± 5	0.00053	0.12	70
Tiw	TiO_2	93	6	80±6	0.000064	0.245	145.1
Liw	$ZnS+BaSO_4$	73	14	77±3	0.001	0.074	66.6

[a]not detected

The optical characterization of the mock-ups showed that the optical penetration depths at 1064 nm are lower or around the thicknesses of the

overpaints and hence between two-three order of magnitude larger than the thermal diffusion length.
The LDTs, measured accurately for each oil paint layer, were strongly dependent on the type of pigment and number of laser pulses (N). A decrease between 20-50% was observed when increasing N from 1 to 5 (Table 7).

Table 7 - LDTs of the mock-ups. (a) and (d) refer to ablation and fluorescence decrease, respectively.

Sample	Main compound	LDT	
		1 pulse	5 pulses
Overpaint			
Lithopone	$ZnS+BaSO_4$	1.4 (a)	0.84 (a)
Titanium White (anatase)	TiO_2	0.6 (a-d)	0.45 (d)
Cadmium yellow	CdS	0.3 (a-d)	0.17 (d)
Green copper carbonate	$Cu_2CO_3(OH)_2$	1.3 (a-d)	1 (a-d)
Paint			
Artificial ultramarine blue	$Na_{6-8}Al_6Si_6O_24S_{2-4}$	1.4 (a)	1 (a)
Cobalt blue	$CoAl_2O_4$	1.4 (a)	1.1 (a)
Zinc oxide	ZnO	0.5 (a-d)	0.35 (d)
Madder lake (alizarin)	$C_{14}H_8O_4(OH)_2$	n.m	n.m
Chromium oxide green	Cr_2O_3	2 (a-d)	1.4 (a-d)

It was also measured the trend of this decay for higher N ($0<N<100$), which was well fitted using the following fitting function, $LTD(N)=aN^b$, whith $-0.3<b<-0.16$, as shown in Fig. 17.
The early alteration phenomena observed between 1-5 laser pulses for the group of pigments with low LTDs (Znw, Tiw, Cdy) were essentially detected as a local fluorescence decrease of the irradiated area (discolouration precursor), whereas the group with higher LDTs (Crg, Ub, Cob, Liw) mostly exhibited surface texturing and ablation effects.
The comparison between the thresholds of the mock-ups with the removal thresholds in the real case understudy, evidenced the single-pulse removal fluences of the real Tiw and Cdy overpaints (0.5-0.7 J/cm^2) were close to the LDTs of the corresponding mock-ups, although the ablation thresholds of the latter were rather higher (likely above 1 J/cm^2).

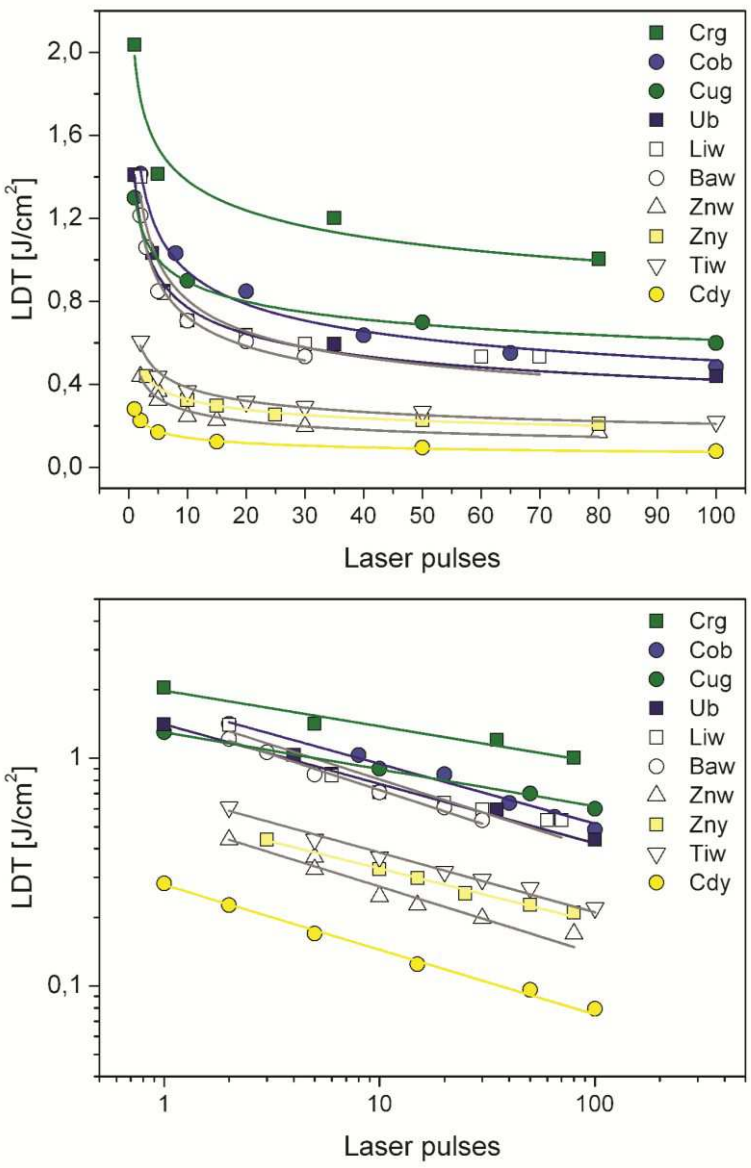

Fig. 17 – Decay of LDTs as function of the number released to the target. Fitting with allometric function (top) and related log-log plot (bottom).

The ablation thresholds of Liw and Cug overpaints were instead significantly lower (about 0.5 J/cm^2) than the LDTs of the corresponding prepared samples (0.8-1.4 J/cm^2). Both these behaviours suggest that the

successful laser uncovering shown in Fig. 15 at relatively low operative fluences (Table 5) was likely favoured by the ageing of the present overpaint layers, by the influence of the underlying original paint, and the weakened adhesion. Despite the mock-ups were aged for two years, this was likely insufficient in order to simulate the actual polymerisation of the oily binder, as well as the long-term alterations of the real overpaint and paint layers. In particular, the formation of Zn-metal soaps (Fig. 13 and Fig. 14) increases the stiffness and weakens the adhesion. In practical cases, such as the present one, these ageing phenomena can favour the photomechanical spallation of the overpaint at relatively low fluences. The role of the spallation channels in the present laser treatment problem was thoroughly investigated through the measurement of the pressure transients propagated through different paint stratigraphies using PVDF piezoelectric sensors.

Pressure profiles were detected for a very absorbing pigment, such a Crg (R=21%, δ=12.4 μm), a very diffusive pigment, such as Liw (R=73%, δ =67 μm), and their superposition. Furthermore, the photoacoustic generation was also investigated on a small fragment taken from the dress of the present female subject (orange overpaint on ultramarine blue paint). The behaviours of the pressure profiles generated in Crg at fluences between 0.2-1.2 J/cm^2 are reported in Fig. 18 along with the LQS laser pulse.

As shown, the pressure waves generally propagated through the paint layers as a sequence of a compressional (positive peak) and stretching (negative peak produced by the reflection at the paint-air interface) phases whose duration was determined by the laser pulse duration (120 ns). In some details, for both Crg and Liw the profiles were almost symmetrically double-phase up to 0.4 J/cm^2, which corresponds to the upper limit of the linear photoacoustic interaction regime. At higher fluences, both the compressional and stretching phases experienced an increasing broadening and delay of the maxima and minima, which are attributable to the occurrence of phase explosion and swelling, respectively. Above 0.4 J/cm^2, the amplitude of the negative phase decreased with respect to the positive one but some tens of bars were still detected. This indicates its relevant contribution to the swelling and

ablation process that were likely driven by a superposition of phase change and stretching.

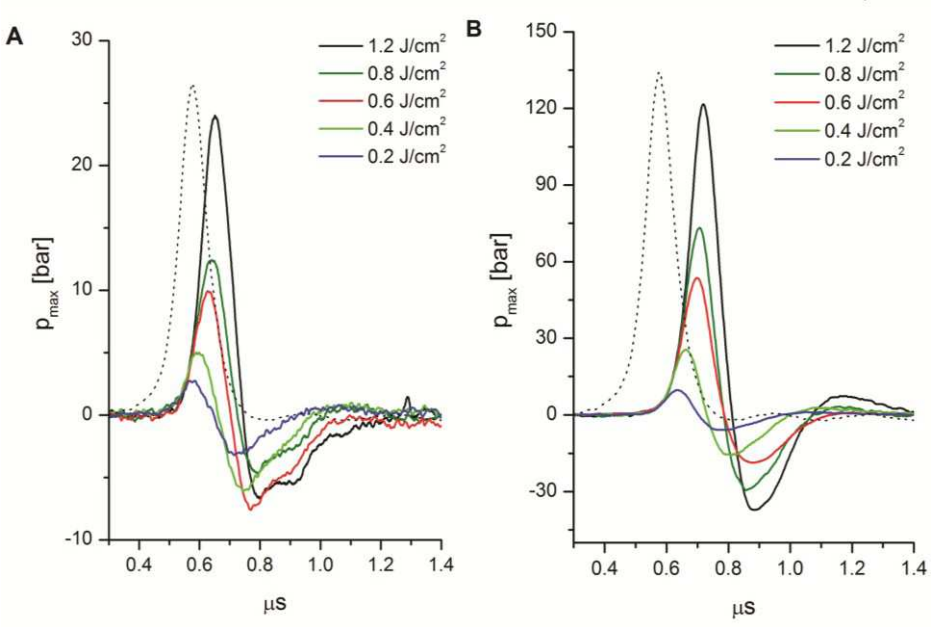

Fig. 18 - Pressure transients generated by laser irradiation of lithopone white (A) and chromium green (B) paints at different fluences. The laser pulse temporal profile is also shown in arbitrary units (dotted line).

The maximum and minimum pressures produced in the Crg layer (Fig. 7B) were significantly higher (of a factor 4-5) than the corresponding ones of Liw (Fig. 7A) because of the higher optical absorption of the former. The ablation depths and rates of the Crg were very low (between 2-8 μm/pulse within the present fluence range) and easily measurable, while those of Liw were measurable only at high fluence (above 2 J/cm^2) while at the present fluences irregular surface swelling and texturing were observed. In general, a similar behaviour as that of the Crg holds for very absorbing overpaint layers.

The single-pigment measurements were preliminary to the simulation of the irradiation of Liw (one of the main pigments found in the overpaints) superimposed to Crg (one of the main pigments of the present artwork), in

order to evaluate the possible influence of the latter on the ablation process.
Figure 8 displays the profiles measured beneath a mock-up of Crg overpainted with Liw. These clearly show that the main photoacoustic generation were driven by the inner layer (Crg).

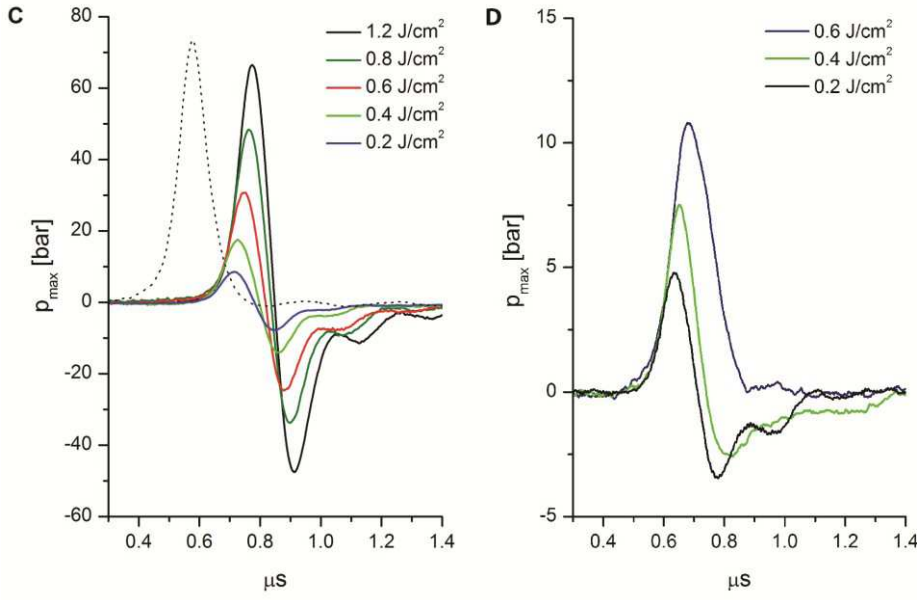

Fig. 19 - Pressure transients generated by laser irradiation of superimposed layers of lithopone white on chromium green (C). Photoacoustic generation of a small sample from the blue dress corresponding to the orange overpaint on ultramarine blue paint (D)

The pressure peaks were significantly higher than those associated with the irradiation of Liw (Fig. 18A) and the two phases (compression and stretching) were more symmetrical with respect to the single-pigment configuration. This is likely due to the confined generation of the compression in proximity of the Crg surface (rigid boundary condition) and to the significant internal reflection at the Liw-air interface. In this simulation no spallation of the Liw was observed because the elasticity of the overpaint was still rather high. In real conditions of aged overpaint, stretching peaks such as those of Fig. 18 can certainly drive the massive spallation of a thin lithopone-based overpaint. However, this is the

initiation process leading to a secondary laser spallation. Pressure measurements carried out on the real sample (Fig. 19) represent an opposite condition in comparison to that previously shown on superimposed layers of lithopone white and chromium green. The pressure peaks were significantly lower due to the higher absorption of the aged orange overpaint. The decrease of the negative peak at 0.4 J/cm^2 can be considered the onset of ablation, which occurs massively at 0.6 J/cm^2, in agreement with the measured removal threshold reported in Table 5.

5.2.4 Conclusions

An unknown painting, which was mostly overpainted, was discovered on the backside of a Pre-Futurist artwork by Giacomo Balla. The material characterisation proved the overpaints did not belong to the original artwork, thus removal trials were carried out. The LQS (120 ns) Nd:YAG (1064 nm) laser ablation was tested after an unsuccessful attempt to remove the overpaints using organic solvents. The observed selectivity and the uncovering results of the laser treatment were decidedly satisfactory. This brought to the decision to extend the laser ablation treatment to the whole artwork and to perform laboratory insights aimed at the interpretation of the ablation processes exploited.
Fig. 20 shows the painting after the laser removal of the undesired overpaintings, which allowed to completely recover its readability.
A signature and a date is now visible at the bottom-left side: “A Nathan 1910”. The artwork can hence reasonably be attributed to Annie Nathan that around 1910 was the most promising pupil of Giacomo Balla. Important information on the ablation processes were derived from laboratory simulations, which allow some generalisations of the present first extensive practical validation of the Nd:YAG laser in the conservation-restoration of easel paintings. The results of the laboratory tests showed that the ablation processes were driven by a superposition of phase change, such as glass transition, melting of wax impurities, vaporisation of solvent residues, and photoacoustic generation. The former altered the material within the irradiated volume while the latter

provided the mechanical action for its removal. The present study shows that such an important role of the photomechanical contribution is expected to be even more important in cases of aged overpaints encountered in real cases, where advanced polymerisation, presence of metal soaps, and craquelures can facilitate the laser detachment.

Fig. 20 The painting of Fig. 1C after the LQS Nd:YAG(1064) laser uncovering treatment.

In conclusion, the present work proves that for oily-binder overpaintings, the natural ageing over one century can significantly favour removal treatments using LQS Nd:YAG(1064 nm) laser. This discloses a new application perspective for this laser source, which will be further explored in forthcoming works.

Chapter VI

CONCLUSIONS AND FUTURE PERSPECTIVES

This thesis provides novel insights on the use of pulsed solid-state Nd:YAG lasers for removing varnish and overpaints layers from easel paintings. On the basis of a detailed state-of-the-art on the laser cleaning of easel paintings, the fifth (213 nm) and fourth (266 nm) harmonics of a pulsed QS (15 ns) Nd:YAG laser were selected for dealing the varnish problem, whereas the LQS (120 ns) Nd:YAG laser's fundamental wavelength (1064 nm) for the selective ablation of overpainting layers. To address such complex issues the laser-material interactions with several painting varnishes (i.e. solvent and oil varnishes) and paint layers (pigments in linseed oil) were systematically investigated. Concluding remarks achieved on the two different topics were reported hereafter.

6.1 Solvent and oil varnishes

Results obtained on laser irradiated varnish samples comprise two different categories: (i) “spirit” varnishes prepared dissolving dammar, mastic, colophony, sandarac and bleached shellac in opportune solvents and (ii) mastic, colophony, sandarac and Manila copal pre-heated at high temperatures with linseed oil. These coatings were exposed to natural and artificial lighting conditions before to be irradiated at both the UV laser wavelengths. Exposure under accelerated and intense light (above 290 nm) conditions led to the understanding of the photo-induced effects (photoxidation, cross-linking, radical polymerization) on solvent and oil varnishes and at the same time, allowed obtaining highly polymerized systems suitable for laser irradiation tests and useful information for interpreting the lased-induced effects.

Trasmission FTIR spectroscopy, colorimetric and gravimetric measurements were used for monitoring the light-induced effects occurring during artificial ageing. The chemical changes occurring in tri (i.e. mastic and dammar), di (i.e. sandarac, colophony, copal) and sesquiterpenoid (i.e. shellac) resins, either with or without the oil, follow similar photo-oxidative kinetics under accelerated lightning conditions.
The time evolution of the main stretching modes (C-H, C=O and OH) monitored by FTIR evidences a decreasing of CH groups and an increase in the carbonyl and hydroxyl regions, even if a different slope depending from the type of varnish has been noticed.
The light-induced effects start with an hydrogen abstraction process, which is more efficient when polyunsaturated fatty acids are present in the varnish. The action of oxygen-mediated processes catalyzed by intense radiation and temperature lead to the formation of new acidic compounds, such as carboxylic acids groups ketones, esters and lactonised structures. Simultaneously, cross-linking, extensive polymerization and degradation phenomena (cracking) occur, in different extent, depending from the type and amount of unsaturated bonds of the material.
These artificially aged systems together with ones kept to natural ageing conditions were subjected to an extensive systematic investigation aimed at assessing the laser induced effects upon irradiation at 213 and 266 nm. Chemical and physical modifications were accurately characterized using Confocal μ-Raman and Laser Induced Fluorescence spectroscopies. A significant effort was also devoted to study the optical absorption properties of the varnish films by means of UV-Vis absorption spectroscopy, which allowed also to estimate the temperature rise associated to laser irradiation.
Results from laser irradiated areas at fluence well above the single-pulse ablation threshold ($2F_{th}$) showed ablation and /or morphological modifications depending on the irradiation wavelengths, the type of varnish and degree of polymerization.
Irradiation at 213 nm induces ablation without noticeable morphological changes to the remaining varnish layer, which preserves its natural gloss. At this wavelength, the layer by layer removal is provided by a resolution

in the sub-micron scale. On the contrary, irradiation at 266 nm induces the formation of microsized bubbles, as observed by means of confocal microscopy. On the other hand, the laser wavelength of 266 nm is weakly absorbed by all the varnish systems studied, thus involving during the ablation process the emission of gaseous products. As consequence of such modifications, carbonyl functionalities and methyl and methylene groups decrease, as observed by confocal μ-Raman spectroscopy. Further reactions, as formation of oxidized products and carbon double bonds, which induce the increase in intensity and the red-shift of the fluorescence signal, were observed.

Ablation at 213 nm, which is a strongly absorbed wavelength, involves direct photolysis and homolytic bond breaking. This photochemical process does not induce such drawbacks (whitish appearance, bubbles) to the etched substrate leading to a clean surface morphology, as detected by confocal microscopy. Similarly, chemical changes may be considered negligible in most of the varnish systems understudy.

Finally, this study represents the first investigation aimed at assessing the chemical and physical laser-induced modifications on a wide variety of painting varnishes using the fifth (213 nm) and fourth (266 nm) harmonics of Pulsed Solid-State (Nd:YAG) lasers.

In contrast with the induced modifications resulting from irradiation at 266 nm, the promising results achieved on samples irradiated at 213 nm emphasize, as demonstrated in previous studies conducted on shellac resin (Ouija et al. 2011), the importance of following a wavelength-based approach to safely remove different types of naturally and artificially aged painting varnishes.

6.2 Overpaints layers

Controlled laser removal of overpaintings is a difficult challenge since undesired and original paint layers are both constituted by similar mixtures of organic and inorganic compounds, which make their discrimination very hard. For this reason, a laser approach based on short wavelengths, as the above mentioned for varnish layers, cannot be exploited for ablating thick overpainted layers. The submicrometric penetration of UV laser sources, in this case, does not permit to

discriminate between different materials, due to the high absorption of both the organic and inorganic compounds. Photomechanical effects accompanied by plasma formation can potentially induce injuries to the substrate, especially when repetitive irradiation is needed for removing thick overpaint layers. In this thesis, a different approach based on the use of Long Q-Switched (LQS) Nd:YAG (1064 nm) laser with a pulse duration of 120 ns has been proposed to overcome discrimination problems affecting shorter wavelengths. Taking advantage from interesting interaction features of the LQS regime, such as lower-pressure peak generation into the paint layer, as well as lower recoil stresses in fluid dynamic ablation regimes, it was investigated whether these characteristics can provide any practical advantage for addressing the delicate problem of overpainting removal from easel paintings.

This innovative approach was tested for the first time for dealing the conservation problems concerning two female portraits dated around 1930 and 1910, respectively. These artworks were almost completely disguised by thick layers of overpaintings, which did not have any artistic relevance. In particular, the latter painting was found on the backside of a signed artwork by Giacomo Balla, one of the founding members of the Futurist Painters, and was covered by broad brush strokes. The other artwork was of unknown origin and disguised by overpaintings depicting an abstract vegetable theme, which was executed some decades after the underlying portrait. Thorough characterization of the original pigments, binders, and overpaintings were achieved using Raman and FTIR spectroscopy, along with stratigraphic examinations by means of optical and ESEM-EDX microscopy. All the paint layers were oil binder and included several modern pigments, such as phthalocyanine green, Ba, Zn and (Ca)-based pigments, white anatase and lithopone, red quinacridone and synthetic azo, and other, which were commonly used during the last century. The characterization of the original and undesired paint layers allowed identifying the pigments mixing and pointing out peculiar deterioration mechanisms, such as formation of Zn and Al carboxylates and different degrees of saponification between paint and overpaint layers.

LQS Nd:YAG (1064 nm) laser uncovering was successfully tested for both the mentioned easel paintings. This allowed performing the complete restoration of that from Ball's studio, which returned an unknown Pre-Futurist artwork, and to plan that of the portrait by anonymous. At the same time, a systematic laboratory experimentation on prepared samples has been carried out. These samples simulated the present uncovering problems encountered in the real cases, in order to investigate the laser interaction phenomenology for the different paint layers and then achieve general information on the potential of the laser approach to the removal of undesired layers.

The results of the laboratory tests showed that the ablation processes were driven by a superposition of phase change, such as glass transition, melting of wax impurities, vaporisation of solvent residues, and photoacoustic generation. The former altered the material within the irradiated volume while the latter provided the mechanical action for its removal. The present study shows that such an important role of the photomechanical contribution is expected to be even more important in cases of aged overpaints encountered in real cases, where advanced polymerisation, presence of metal soaps, and craquelures can facilitate the laser detachment.

In conclusion, results achieved prove that for oily-binder overpaintings, the natural ageing over one century can significantly favour removal treatments using LQS Nd:YAG(1064 nm) laser. In addition, they disclose a significant application perspective for Nd:YAG laser ablation in conservation of modern easel paintings

7. BIBLIOGRAPHY

Abraham, M., Madden, O., Learner, T., & Havlik, C. (2005). Evaluation of the Effects of Laser Irradiation on Modern Organic Pigments. In *Lasers in the Conservation of Artworks* (pp. 263-275). Springer Berlin Heidelberg.

Allen, N. S., & Edge, M. (1992). Fundamentals of polymer degradation and stabilization. Springer.

Alphen, M. V., Puelles, M. M., Alvarez, R. J., Borinsky, M., Pinto, M., Vorobey, A., ... & Patton, T. C. (1998). Paint film components. In *National Environmental Health Forum*.

Andreotti, A., Bracco, P., Colombini, M. P., Lanterna, G., Nakahara, K., & Penaglia, F. (2007). Novel applications of the Er: YAG laser cleaning of old paintings. In *Lasers in the Conservation of Artworks* (pp. 239-247). Springer Berlin Heidelberg.

Angelova, L. V., Berrie, B. H., de Ghetaldi, K., Kerr, A., & Weiss, R. G. (2013). Partially hydrolyzed poly (vinyl acetate)-borax-based gel-like materials for conservation of art: Characterization and applications. *Studies in Conservation*.

Apostol, I., Damian, V., Garoi, F., Iordache, I., Bojan, M., Apostol, D., ... & Darida, I. (2011). Controlled removal of overpainting and painting layers under the action of UV laser radiation. *Optics and Spectroscopy*, *111*(2), 287-292.

Arenberg, J. W. (2009, October). Life testing for laser optics: a first look. In*Laser Damage Symposium XLI: Annual Symposium on Optical Materials for High Power Lasers* (pp. 75041I-75041I). International Society for Optics and Photonics.

Arenberg, J., Riede, W., Ciapponi, A., Allenspacher, P., & Herringer, J. (2010, October). An empirical investigation of the laser survivability curve. In *Laser Damage Symposium XLII: Annual Symposium on Optical Materials for High Power Lasers* (pp. 78421B-78421B). International Society for Optics and Photonics.

Athanassiou, A., Hill, A. E., Fourrier, T., Burgio, L., & Clark, R. J. (2000). The effects of UV laser light radiation on artists' pigments. *Journal of Cultural Heritage*, *1*, S209-S213.

Azémard, C., Vieillescazes, C., & Ménager, M. (2014). Effect of photodegradation on the identification of natural varnishes by FT-IR spectroscopy. *Microchemical Journal*, *112*, 137-149.

Baldwin, D., Loeblich, V., & Lawrence, R. (1958). Acidic Composition of Oleoresins and Rosins. *Industrial & Engineering Chemistry Chemical and Engineering Data Series*, *3*(2), 342-346.

Baudach, S., Bonse, J., & Kautek, W. (1999). Ablation experiments on polyimide with femtosecond laser pulses. *Applied Physics A*, *69*(1), S395-S398.

Bäuerle, D. (2000). *Laser processing and chemistry* (Vol. 3). Berlin: Springer.

Berg, K. J. V. D., Boon, J. J., Pastorova, I., & Spetter, L. F. (2000). Mass spectrometric methodology for the analysis of highly oxidized diterpenoid acids in Old Master paintings. *Journal of Mass Spectrometry*, *35*(4), 512-533

Berns, R. S., & de la Rie, E. R. (2003). The effect of the refractive index of a varnish on the appearance of oil paintings. *Studies in conservation*, *48*(4), 251-262.

Binder, R. G., Goldblatt, L. A., & Applewhite, T. H. (1965). Measurements on isolated double-bond systems. Ultraviolet absorption spectra of fatty acid esters. The Journal of Organic Chemistry, 30(7), 2371-2376.

Boon, J. J. (2006). Processes inside paintings that affect the picture: chemical changes at, near and underneath the paint surface. *Reporting Highlights of the De Mayerne Programme (JJ Boon and E. Ferreira eds), this volume*, 21-32.

Boon, J. J., Hoogland, F., & Keune, K. (2006). Chemical processes in aged oil paints affecting metal soap migration and aggregation. In *Annual Meeting in Providence, Rhode Island, June* (pp. 16-19).

Bordalo, R., Morais, P. J., Young, C. R., Santos, L. F., & Almeida, R. M. (2011). CHARACTERISATION OF LASER-INDUCED PHYSICAL ALTERATIONS OF PIGMENTED OIL LAYERS.

Boyatzis, S., Ioakimoglou, E., & Argitis, P. (2002). UV exposure and temperature effects on curing mechanisms in thin linseed oil films: spectroscopic and chromatographic studies. *Journal of applied polymer science*, *84*(5), 936-949.

Bracco, P., Lanterna, G., Matteini, M., Nakahara, K., Sartiani, O., de Cruz, A., ... & Colombini, M. P. (2003). Er: YAG laser: an innovative tool for controlled cleaning of old paintings: testing and evaluation. *Journal of Cultural Heritage*, *4*, 202-208.

Bradley, T. F., & Richardson, D. (1940). DRYING OILS AND RESINS Ultraviolet Absorption Study of Esters of the Acids of Drying Oils. Industrial & Engineering Chemistry, 32(7), 963-969.

Brewis, S., & Halsall, T. G. (1961) The chemistry of triterpenes and related compounds. Part XXXVIII. The acidic constituents of dammar resin. J. Chem. Soc., 646-650.

Brody, R. H., Edwards, H. G., & Pollard, A. M. (2001). A study of amber and copal samples using FT-Raman spectroscopy. *Spectrochimica Acta Part A: Molecular and Biomolecular Spectroscopy*, *57*(6), 1325-1338.

Brody, R. H., Edwards, H. G., & Pollard, A. M. (2002). Fourier transform-Raman spectroscopic study of natural resins of archaeological interest. Biopolymers, 67(2), 129-141.

Brown, R. F., Bachman, G. B., & Miller, S. J. (1943). The Irradiation of Abietic Acid with Ultraviolet Rays1, 2. *Journal of the American Chemical Society*, *65*(4), 623-626.

Buch, K., Penning, M., Wächtersbach, E., Maskos, M., & Langguth, P. (2009). Investigation of various shellac grades: additional analysis for identity. Drug development and industrial pharmacy, 35(6), 694-703.

Büchi, G., & Pappas, J. J. (1954). Terpenes. I. Structure and Synthesis of the C17H20 Hydrocarbon Obtained by Dehydrogenation of Agathic Acid. Journal of the American Chemical Society, 76(11), 2963-2966.

Burgio, L., & Clark, R. J. (2001). Library of FT-Raman spectra of pigments, minerals, pigment media and varnishes, and supplement to existing library of Raman spectra of pigments with visible excitation. *Spectrochimica Acta Part A: Molecular and Biomolecular Spectroscopy*, *57*(7), 1491-1521.

Burnstock, A., & Learner, T. (1992). Changes in the surface characteristics of artificially aged mastic varnishes after cleaning using alkaline reagents. *Studies in conservation*, *37*(3), 165-184.

Byrne A. (1991), Wolbers cleaning methods: introduction, Australian Institute for the Conservation of Cultural Materials (AICCM) Bulletin Vol. 17 N 3 and 4.

Bityurin, N. (2005). 8 Studies on laser ablation of polymers. *Annual Reports Section" C"(Physical Chemistry)*, *101*, 216-247.

Camaiti, M., Matteini, M., Sansonetti, A., Striová, J., Castellucci, E., Andreotti, A., & Colombini, M. P. (2008, August). The interaction of laser radiation at 2.94 μm with azurite and malachite pigments. In *Lasers in the Conservation of Artworks: Proceedings of the International Conference Lacona VII, Madrid, Spain, 17-21 September 2007* (p. 253). CRC Press.

Carlyle, L. (1990). "British Nineteenth Century Oil Painting Instruction Books: A Survey of Their Recommendations for Vehicles, Varnishes and Methods of Paint Application." In *Cleaning, Retouching and Coatings: Preprints of the IIC Brussels Congress*, ed. J. S. Mills and P. Smith, pp. 76–80. London: International Institute for Conservation.

Carlyle, L., (1991). A critical analysis of Artists' handbooks, manuals and treatises on oil painting published in Britain between 1800-1900: with reference to selected eighteenth-century sources, doctoral thesis, Courtauld Institute of Art, University of London

Carlyle, L. (1981). Laser interactions with paintings: results and proposals for further study. *Unpublished Report, The Canadian Conservation Institute, Ottawa, Canada*.

Carman, R. M., Cowley, D. E., & Marty, R. A. (1970). Diterpenoids. XXV. Dundathic acid and polycommunic acid. *Australian Journal of Chemistry*, *23*(8), 1655-1665.

Carretti, E., Dei, L., Macherelli, A., & Weiss, R. G. (2004). Rheoreversible polymeric organogels: the art of science for art conservation. *Langmuir*, *20*(20), 8414-8418.

Carretti, E., Natali, I., Matarrese, C., Bracco, P., Weiss, R. G., Baglioni, P., ... & Dei, L. (2010). A new family of high viscosity polymeric dispersions for cleaning easel paintings. *Journal of Cultural Heritage*, *11*(4), 373-380.

Carretti, E., & Giorgi, R. (2013). Cleaning IV: Applications and Case Studies.*Nanoscience for the Conservation of Works of Art*, *5*(28), 280.

Castillejo, M., Martín, M., Oujja, M., Rebollar, E., Domingo, C., García-Ramos, J. V., & Sánchez-Cortés, S. (2003). Effect of wavelength on the laser cleaning of polychromes on wood. *Journal of Cultural Heritage*, *4*(3), 243-249.

Castillejo, M., Martín, M., Oujja, M., Santamaría, J., Silva, D., Torres, R., ... & Silva, A. (2003). Evaluation of the chemical and physical changes induced by KrF laser irradiation of tempera paints. *Journal of Cultural Heritage*, *4*, 257-263.

Castillejo, M., Martín, M., Oujja, M., Silva, D., Torres, R., Manousaki, A., ... & Gouveia, H. (2002). Analytical study of the chemical and physical changes induced by KrF laser cleaning of tempera paints. *Analytical chemistry*, *74*(18), 4662-4671.

Cennini, C. (1954). *The craftsman's handbook* (Vol. 2). Courier Dover Publications

Chappé, M., Hildenhagen, J., Dickmann, K., & Bredol, M. (2003). Laser irradiation of medieval pigments at IR, VIS and UV wavelengths. *Journal of Cultural Heritage*, *4*, 264-270.

Cheong, W. F., Prahl, S. A., & Welch, A. J. (1990). A review of the optical properties of biological tissues. *IEEE journal of quantum electronics*, *26*(12), 2166-2185.

Ciofini, D., Osticioli, I., Pavia, A., & Siano, S. (2014). Removal of overpaintings from easel paintings using LQS Nd: YAG laser. *Applied Physics A*, 117, pp. 341-346.

Ciofini D., Scala A., Siano S. (2013a). Valutazione sistematico-fenomenologica delle potenzialità applicative di laser Nd:YAG (1064 nm) a diversa durata di impulso nella pulitura di dipinti su tela e tavola, in atti del Convegno Aplar 4 - Applicazioni laser nel restauro, pp. 193-204, Il Prato, Saonara (PD), ISBN 978-88-6336-202-2.

Ciofini D., Nakahara K., Hilling A.M., Frosinini C., Bellucci R., Siano S. (2013b). Assottigliamento di vernici nel restauro di dipinti su tela e tavola: confronto fenomenologico tra diversi sistemi laser, in atti del Convegno Aplar 4 - Applicazioni laser nel restauro, pp. 205-218, Il Prato, Saonara (PD), ISBN 978-88-6336-202-2.

Coelho, C., Nanabala, R., Ménager, M., Commereuc, S., & Verney, V. (2012). Molecular changes during natural biopolymer ageing–The case of shellac.*Polymer Degradation and Stability*, *97*(6), 936-940.

Colombini, M. P., Andreotti, A., Lanterna, G., & Rizzi, M. (2003). A novel approach for high selective micro-sampling of organic painting materials by Er: YAG laser ablation. *Journal of Cultural Heritage*, *4*, 355-361.

Colombini, M. P., Modugno, F., Giannarelli, S., Fuoco, R., & Matteini, M. (2000). GC-MS characterization of paint varnishes. *Microchemical Journal*,*67*(1), 385-396.

Colombini, M. P., Bonaduce, I., & Gautier, G. (2003). Molecular pattern recognition of fresh and aged shellac. *Chromatographia*, *58*(5-6), 357-364.

Colombini, M. P., & Modugno, F. (Eds.). (2009). Organic mass spectrometry in art and archaeology (p. 493). Chichester: Wiley.

Cubeddu, R., Brancato, R., Sozzi, C., Taroni, P., Trabucchi, G. Valentini, G., Verdi, M. (1996). Study of Photoablation of Rabbit Corneas by Er:YAG Laser, *Lasers in Surgery and Medicine,* 19, pp. 32-39.

Daher, C., Paris, C., Le Hô, A. S., Bellot-Gurlet, L., & Échard, J. P. (2010). A joint use of Raman and infrared spectroscopies for the identification of natural organic media used in ancient varnishes. *Journal of Raman Spectroscopy*,*41*(11), 1494-1499.

Danileiko, Y. K., Manenkov, A. A., Nechitailo, V. S., Prokhorov, A. M., & KHAIMOV-MAL'KOVll, V. Y. (1972). THE ROLE OF ABSORBING IMPURITIES IN LASER-INDUCED DAMAGE OF TRANSPARENT DIELECTRICS. *Zh. Eksp. Teor. Fiz*, *63*, 1030-1035.

De Cruz, A., Andreotti, A., Ceccarini, A., & Colombini, M. P. (2014) Laser cleaning of works of art: evaluation of the thermal stress induced by Er: YAG laser. Applied Physics B, 1-9.

de la Rie, E. R. (1982). Fluorescence of paint and varnish layers (Part III).*Studies in Conservation*, *27*(3), 102-108.

de la Rie, E. R. (1987). The influence of varnishes on the appearance of paintings. *Studies in conservation*, *32*(1), 1-13.

de la Rie, E. R. (1988a). Photochemical and thermal degradation of films of dammar resin. *Studies in conservation*, *33*(2), 53-70.

de la Rie, E. R., (1988b). *Stable Varnishes for Old Master Paintings*, PhD Thesis, University of Amsterdam.

de la Rie, E. R., (1989). Old master paintings: a study of the varnish problem. *Analytical chemistry*, *61*(21), 1228A-1240A.

De Mayerne, T. T. (1901). Pictoria, Sculptoria, Tinctoria, et quae subalternarum artium. *Manuscript)(British Museum London, Ms. Sloane 2052)*, 1620-1642.

Derrick, M. R., Stulik, D., & Landry, J. M. (2000). Infrared spectroscopy in conservation science. Getty Publications.

Derry, J. (2012). Investigating Shellac: Documenting the Process, Defining the Product.: A study on the processing methods of Shellac, and the analysis of selected physical and chemical characteristics.

Dietemann, P., Edelmann, M. J., Meisterhans, C., Pfeiffer, C., Zumbuhl, S., Knochenmuss, R., & Zenobi, R. (2000). Artificial photoaging of triterpenes studied by graphite-assisted laser desorption/ionization mass spectrometry.*Helvetica chimica acta*, *83*(8), 1766-1777.

Dietemann, P. (2003). *Towards More Stable Natural Resin Varnishes for Paintings: The Aging of Triterpenoid Resins and Varnishes*. Swiss Federal Institute of Technology (ETH).

Dietemann, P., Higgitt, C., Kälin, M., Edelmann, M. J., Knochenmuss, R., & Zenobi, R. (2009). Aging and yellowing of triterpenoid resin varnishes–influence of aging conditions and resin composition. *Journal of Cultural Heritage*, *10*(1), 30-40.

Dieterich, K., & Stocks, H. B. (1920). Analysis of resins, balsams and gum resins.

Dyer, P. E., & Srinivasan, R. (1986). Nanosecond photoacoustic studies on ultraviolet laser ablation of organic polymers. *Applied physics letters*, *48*(6), 445-447.

Dlugogorski, B. Z., Kennedy, E. M., & Mackie, J. C. (2012). Low temperature oxidation of linseed oil: a review. *Fire science reviews*, *1*(1), 1-36.

Eastlake, C. L. (1847). *Materials for a history of oil painting*.

Edwards, H. G. M., Farwell, D. W., & Daffner, L. (1996). Fourier-transform Raman spectroscopic study of natural waxes and resins. I. Spectrochimica Acta Part A: Molecular and Biomolecular Spectroscopy, 52(12), 1639-1648.

Elias, M., René de La Rie, E., Delaney, J. K., Charron, E., & Morales, K. M. (2006). Modification of the surface state of rough substrates by two different varnishes and influence on the reflected light. Optics communications, 266(2), 586-591.

Erhardt, D., Tumosa, C. S., & Mecklenburg, M. F. (2005). Long-term chemical and physical processes in oil paint films. *Studies in conservation*, *50*(2), 143-150.

Erhardt, D., & Tsang, J. S. (1990). The extractable components of oil paint films. In *Cleaning, retouching and coatings: technology and practice for easel paintings and polychrome sculpture: preprints of the contributions to the Brussels Congress, 3-7 September 1990* (pp. 93-97). International Institute for Conservation of Historic and Artistic Works.

Eastaugh, N., V. Walsh, T. Chaplin, and R. Siddal. (2004) Pigment compendium, a dictionary of historical pigments. Oxford: Elsevier Butterworth-Heinemannn

Farag, Y. (2010). Characterization of different shellac types and development of shellac coated dosage forms. Dissertation Department of Chemistry, Pharmacy, University of Hamburg.

Feller, R. L., & Bailie, C. W. (1972). Solubility of Aged Coatings Based on dammar, Mastic, and Resin AW-2. *Journal of the American Institute for Conservation*, *12*(2), 72-81.

Feller, R. L. (1958). Dammar and Mastic Varnishes-Hardness, Brittleness, and Change in Weight upon Drying. *Studies in conservation*, *3*(4), 162-174.

Feller, R. L., & Curran, M. (1975). Changes in solubility and removability of varnish resins with age. *Journal of the American Institute for Conservation*,*15*(2), 17-48.

Feller, R. L. (1995). *Accelerated aging: photochemical and thermal aspects*. Getty Publications.

Findeisen, A., Kolivoska, V., Kaml, I., Baatz, W., & Kenndler, E. (2007). Analysis of diterpenoic compounds in natural resins applied as binders in museum objects by capillary electrophoresis. *Journal of Chromatography A*,*1157*(1), 454-461.

Fotakis, C., Anglos, D., Zafiropulos, V., Georgiou, S., & Tornari, V. (2010). *Lasers in the preservation of cultural heritage: Principles and applications*. CRC Press.

Gaetani, C., & Santamaria, U. (2000). The laser cleaning of wall paintings.*Journal of Cultural Heritage*, *1*, S199-S207.

Galatis, P., Boyatzis, S., & Theodorakopoulos, C. (2012). Removal of a synthetic soiling mixture on mastic, shellac & Laropal® K80 coatings using two hydrogels. *e-Preservation Science*, *9*, 72-83.

Gaspard, S., Oujja, M., Moreno, P., Méndez, C., García, A., Domingo, C., & Castillejo, M. (2008). Interaction of femtosecond laser pulses with tempera paints. *Applied Surface Science*, *255*(5), 2675-2681.

Gordon Sobott, R. J., Heinze, T., Neumeister, K., & Hildenhagen, J. (2003). Laser interaction with polychromy: laboratory investigations and on-site observations. *Journal of Cultural Heritage*, *4*, 276-286.

Guiliano, M., Asia, L., Onoratini, G., & Mille, G. (2007). Applications of diamond crystal ATR FTIR spectroscopy to the characterization of ambers. *Spectrochimica Acta Part A: Molecular and Biomolecular Spectroscopy*, *67*(5), 1407-1411.

Marchand-Geneste, N., & Carpy, A. (2003). Theoretical study of the thermal degradation pathways of abietane skeleton diterpenoids: aromatization to retene. *Journal of Molecular Structure: THEOCHEM*, *635*(1), 55-82

Gettens, R. J., & Stout, G. L. (1966). *Painting materials: a short encyclopaedia*. Courier Dover Publications.

Glinnchey G. Mc, Stringari C., Pratt E., Abraham M., Melessanaki K., Zafiropulos V., Anglos D., Pouli P. & Fotakis C. (2005), Evaluating the Effectiveness of Lasers for the Removal of Overpaint from a 20th C Minimalist Painting. In LACONA V Proc., Springer, Heidelberg, pp.209-215.

Hesse, M., Meier, H., & Zeeh, B. (2008). Spectroscopic methods in organic chemistry (pp. 15-17). Stuttgart: Thieme.

Higgitt, A., Spring, M., & Saunders, D. (2003). Pigment-medium interactions in oil paint films containing red lead or lead-tin yellow. *The National Gallery Technical Bulletin*, *24*(1), 75-95.

Hildenhagen, J., Chappé, M., & Dickmann, K. (2005). Reaction of Historical Colours and their Components Irradiated at Different Nd: YAG Laser Wavelengths (ω, 2ω, 3ω, 4ω). In *Lasers in the Conservation of Artworks V* (pp. 297-301). Springer Berlin Heidelberg.

Hildenhagen, J., & Dickmann, K. (2003). Nd: YAG laser with wavelengths from IR to UV (ω, 2ω, 3ω, 4ω) and corresponding applications in conservation of various artworks. *Journal of Cultural Heritage*, *4*, 174-178.

Hill, A. E., Fourrier, T., Anderson, J., Athanassiou, A., & Whitehead, C. (1999). Measurement of the light absorption length of 308nm pulsed laser light in artificially aged varnishes. In *Triennial meeting (12th), Lyon, 29 August-3 September 1999: preprints. Vol. 1* (pp. 299-303). James & James.

Hontzopoulos, E. I., Fotakis, C., & Doulgeridis, M. (1993). Excimer laser in art restoration. In: *Ninth International Symposium on Gas Flow and Chemical Lasers*. Bellingham: SPIE - International Society for Optics and Photonics, pp. 748-751.

Horie, C. V. (1987). Materials for conservation: organic consolidants, adhesives, and coatings. Butterworth-Heinemann series in conservation and museology, Oxford, Boston.

Keune, K. (2005). *Binding medium, pigments and metal soaps characterised and localised in paint cross-sections*.

Keune, K., van Loon, A., & Boon, J. J. (2011). SEM backscattered-electron images of paint cross sections as information source for the presence of the lead white pigment and lead-related degradation and migration phenomena in oil paintings. *Microscopy and Microanalysis*, *17*(05), 696-701.

Klier, K. (1972). Absorption and scattering in plane parallel turbid media. *JOSA*,*62*(7), 882-885.

Lazzari, M., & Chiantore, O. (1999). Drying and oxidative degradation of linseed oil. *Polymer degradation and stability*, *65*(2), 303-313.

Lawman, S., & Liang, H. (2011). High precision dynamic multi-interface profilometry with optical coherence tomography. *Applied optics*, *50*(32), 6039-6048.

Limmatvapirat, S., Limmatvapirat, C., Puttipipatkhachorn, S., Nuntanid, J., & Luangtana-anan, M. (2007). Enhanced enteric properties and stability of shellac films through composite salts formation. *European Journal of Pharmaceutics and Biopharmaceutics*, *67*(3), 690-698.

Lippert, T., & Dickinson, J. T. (2003). Chemical and spectroscopic aspects of polymer ablation: special features and novel directions. *Chemical Reviews*,*103*(2), 453-486.

Liu, J. M. (1982). Simple technique for measurements of pulsed Gaussian-beam spot sizes. *Optics Letters*, *7*(5), 196-198.

Luong, J. H., Rigby, T., Male, K. B., & Bouvrette, P. (1999). Separation of resin acids using cyclodextrin-modified capillary electrophoresis. Electrophoresis, 20(7), 1546-1554.

Luong, J. H., Rigby, T., Male, K. B., & Bouvrette, P. (1999). Derivatization of resin acids with a fluorescent label for cyclodextrin-modified electrophoretic separation. Journal of Chromatography A, 849(1), 255-266.

Madden, O., Abraham, M., Scheerer, S., & Werden, L. (2005). The effects of laser radiation on adhesives, consolidants, and varnishes. In *Lasers in the Conservation of Artworks* (pp. 247-254). Springer Berlin Heidelberg.

Mallégol, J., Gardette, J. L., & Lemaire, J. (1999). Long-term behavior of oil-based varnishes and paints I. Spectroscopic analysis of curing drying oils. *Journal of the American Oil Chemists' Society*, *76*(8), 967-976.

Mallégol, J., Gardette, J. L., & Lemaire, J. (2000a). Long-term behavior of oil-based varnishes and paints. Photo-and thermooxidation of cured linseed oil.*Journal of the American Oil Chemists' Society*, *77*(3), 257-263.

Mallégol, J., Lemaire, J., & Gardette, J. L. (2000b). Drier influence on the curing of linseed oil. *Progress in organic coatings*, *39*(2), 107-113.

Mallégol, J., Gardette, J. L., & Lemaire, J. (2000c). Long-term behavior of oil-based varnishes and paints. Fate of hydroperoxides in drying oils. *Journal of the american oil chemists' society*, *77*(3), 249-255.

Mallégol, J., Lemaire, J., & Gardette, J. L. (2001). Yellowing of oil-based paints. *Studies in conservation*, 121-131.

Marchand-Geneste, N., & Carpy, A. (2003). Theoretical study of the thermal degradation pathways of abietane skeleton diterpenoids: aromatization to retene. *Journal of Molecular Structure: THEOCHEM*, *635*(1), 55-82.

Marczak, J., Koss, A., Targowski, P., Góra, M., Strzelec, M., Sarzyński, A., ... & Rycyk, A. (2008). Characterization of laser cleaning of artworks. *Sensors*,*8*(10), 6507-6548.

McGlinchey, C., Stringari, C., Pratt, E., Abraham, M., Melessanaki, K., Zafiropulos, V., ... & Fotakis, C. (2005). Evaluating the effectiveness of lasers

for the removal of overpaint from a 20th C minimalist painting. In *Lasers in the Conservation of Artworks* (pp. 209-215). Springer Berlin Heidelberg.

Mecklenburg, M. F., Charola, A. E., & Koestler, R. J. (Eds.). (2013). *New Insights into the Cleaning of Paintings*. Smithsonian Institution Scholarly Press.

Meilunas, R. J., Bentsen, J. G., & Steinberg, A. (1990). Analysis of aged paint binders by FTIR spectroscopy. *Studies in conservation*, *35*(1), 33-51.

Melessanaki, K., Stringari, C., Fotakis, C., & Anglos, D. (2006). Laser cleaning and spectroscopy: a synergistic approach in the conservation of a modern painting. *Laser Chemistry*, *42709*.

Merimée, J. F. L.(1830). *De la peinture à l'huile*. Paris: Mme. Huzard.

Merrifield M.P. (1849). *Original Treatises on the arts of Painting,* London.

Michalski, S. (1990). A physical model of the cleaning of oil paint. *Cleaning, retouching and coatings: Technology and practice for easel paintings and polychrome sculpture. London: International Institute for Conservation of Historic and Artistic Works*, 85-92.

Micheli, R. A., & Applewhite, T. H. (1962). Measurements on Isolated Double Bond Systems: Ultraviolet Absorption Spectra of Steroids and Triterpenoids1.*The Journal of Organic Chemistry*, *27*(2), 345-353.

Mills, J. S., & White, R. (1999). *The Organic Chemistry of Museum Objects*. Routledge.

Mills, J. S., & Werner, A. E. A. (1955). The chemistry of dammar resin. *Journal of the Chemical Society (Resumed)*, 3132-3140.

Mills, J. S., & White, R. (1977). Natural resins of art and archaeology their sources, chemistry, and identification. *Studies in Conservation*, *22*(1), 12-31.

Moron M. A. G. , et al., n.d. Laser cleaning to remove overpaint from paintings on canvas and wood. In: *LACONA IX.* s.l.:ed By D. Saunders, M. Strlic, C. Korenberg, N. Luxford, K. Birkholzer (Archetype Publications, 2013).

Newman, R. (1979). Some applications of infrared spectroscopy in the examination of painting materials. *Journal of the American Institute for Conservation*, *19*(1), 42-62.

Nevin, A., Comelli, D., Osticioli, I., Toniolo, L., Valentini, G., &Cubeddu, R. (2009). Assessment of the ageing of triterpenoid paint varnishes using fluorescence, Raman and FTIR spectroscopy. *Analytical and bioanalytical chemistry*, 395(7), 2139-2149.

Nevin, A., Spoto, G., & Anglos, D. (2012). Laser spectroscopies for elemental and molecular analysis in art and archaeology. *Applied Physics A*, *106*(2), 339-361.

Niemz, M. H. (2007). *Laser-tissue interactions: fundamentals and applications*. Springer.

Nuopponen, M., Willför, S., Jääskeläinen, A. S., Sundberg, A., & Vuorinen, T. (2004). A UV resonance Raman (UVRR) spectroscopic study on the extractable compounds of Scots pine (< i> Pinus sylvestris</i>) wood: Part I: Lipophilic compounds. *Spectrochimica Acta Part A: Molecular and Biomolecular Spectroscopy*, *60*(13), 2953-2961.

Osmond, G., Boon, J. J., Puskar, L., & Drennan, J. (2012). Metal Stearate Distributions in Modern Artists' Oil Paints: Surface and Cross-Sectional Investigation of Reference Paint Films Using Conventional and Synchrotron Infrared Microspectroscopy. *Applied spectroscopy*, *66*(10), 1136-1144.

Osmond, G. (2014). Zinc white and the influence of paint composition for stability in oil based media. In *Issues in Contemporary Oil Paint* (pp. 263-281). Springer International Publishing.

Oujja, M., García, A., Romero, C., de Aldana, J. R. V., Moreno, P., & Castillejo, M. (2011). UV laser removal of varnish on tempera paints with nanosecond and femtosecond pulses. *Physical Chemistry Chemical Physics*,*13*(10), 4625-4631.

Oujja, M., Pouli, P., Domingo, C., Fotakis, C., & Castillejo, M. (2010). Analytical spectroscopic investigation of wavelength and pulse duration effects on laser-induced changes of egg-yolk-based tempera paints. *Applied spectroscopy*, *64*(5), 528-536.

Oujja, M., Sanz, M., Rebollar, E., Marco, J. F., Domingo, C., Pouli, P., ... & Castillejo, M. (2013). Wavelength and pulse duration effects on laser induced changes on raw pigments used in paintings. *Spectrochimica Acta Part A: Molecular and Biomolecular Spectroscopy*, *102*, 7-14.

Phenix, A. (2002b). The Swelling of Artists' Paints in Organic Solvents. Part 1, a Simple Method for Measuring the In-Plane Swelling of Unsupported Paint Films. *Journal of the American Institute for Conservation*, 43-60.

Phenix, A. (2002a). The swelling of artists' paints in organic solvents. Part 2, Comparative swelling powers of selected organic solvents and solvent mixtures. *Journal of the American Institute for Conservation*, 61-90.

Platt, J. R. (1953). Classification and assignments of ultraviolet spectra of conjugated organic molecules. *JOSA*, *43*(4), 252-256.

Poli, T., Piccirillo, A., Zoccali, A., Conti, C., Nervo, M., & Chiantore, O. (2014). The role of zinc white pigment on the degradation of shellac resin in artworks.*Polymer Degradation and Stability*, *102*, 138-144.

Pouli, P., Emmony, D. C., Madden, C. E., & Sutherland, I. (2001). Analysis of the laser-induced reduction mechanisms of medieval pigments. *Applied surface science*, *173*(3), 252-261.

Pouli, P., Emmony, D. C., Madden, C. E., & Sutherland, I. (2003). Studies towards a thorough understanding of the laser-induced discoloration mechanisms of medieval pigments. *Journal of Cultural Heritage*, *4*, 271-275.

Pouli, P., & Emmony, D. C. (2000). The effect of Nd: YAG laser radiation on medieval pigments. *Journal of Cultural Heritage*, *1*, S181-S188.

Pouli, P., Paun, I. A., Bounos, G., Georgiou, S., & Fotakis, C. (2008). The potential of UV femtosecond laser ablation for varnish removal in the restoration of painted works of art. *Applied Surface Science*, *254*(21), 6875-6879.

Pouli, P., Selimis, A., Georgiou, S., & Fotakis, C. (2010). Recent studies of laser science in paintings conservation and research. *Accounts of chemical research*, *43*(6), 771-781.

Prati, S., Sciutto, G., Mazzeo, R., Torri, C., & Fabbri, D. (2011). Application of ATR-far-infrared spectroscopy to the analysis of natural resins. *Analytical and bioanalytical chemistry*, *399*(9), 3081-3091.

Rasti, F., & Scott, G. (1980). The effects of some common pigments on the photo-oxidation of linseed oil-based paint media. *Studies in conservation*, *25*(4), 145-156.

Rebollar, E., Bounos, G., Oujja, M., Georgiou, S., & Castillejo, M. (2006). Effect of molecular weight on the morphological modifications induced by UV laser ablation of doped polymers. *The Journal of Physical Chemistry B*, *110*(33), 16452-16458.

Reifsnyder, J. M. (1996). A note on a traditional technique of varnish application for paintings on panel. *Studies in conservation*, *41*(2), 120-122.

Rode, A. V., Freeman, D., Baldwin, K. G. H., Wain, A., Uteza, O., & Delaporte, P. (2008). Scanning the laser beam for ultrafast pulse laser cleaning of paint. *Applied Physics A*, *93*(1), 135-139.

Robinet, L., & Corbeil-a2, M. C. (2003). The characterization of metal soaps.*Studies in conservation*, *48*(1), 23-40.

Rowe, J. W. (1989). *Natural products of woody plants. I and II: Chemicals extraneous to the lignocellulosic cell wall*. Springer-Verlag.

Ruhemann, H. (1958). Criteria for distinguishing additions from original paint.*Studies in Conservation*, *3*(4), 145-161.

Salimbeni, R., Mazzinghi, P., Pini, R., Siano, S., Vannini, M., Matteini, M., & Aldrovandi, A. (1998, November). Laser restoration of paintings: issues and perspectives. In *Proceedings of the Congress on Science and Technology for the safeguard of Cultural Heritage in the Mediterranean Basin (Catania, Italy, 1995) A. Guarino et al.(Eds.), CNR, Roma*.

Sansonetti, A., & Realini, M. (2000). Nd: YAG laser effects on inorganic pigments. *Journal of Cultural Heritage*, *1*, S189-S198.

Sarkar, P. C., & Shrivastava, A. K. (2000). FT-IR spectroscopic studies on degradation of lac resin–part I: thermal degradation. *Pigment & resin technology*, *29*(1), 23-28.

Schneider, P., Hosseiny, S. S., Szczotka, M., Jordan, V., & Schlitter, K. (2009). Rapid solubility determination of the triterpenes oleanolic acid and ursolic acid by UV-spectroscopy in different solvents. *Phytochemistry Letters*,*2*(2), 85-87.

Schuller, W. H., Moore, R. N., & Lawrence, R. V. (1960). Air Oxidation of Resin Acids. II. The Structure of Palustric Acid and its Photosensitized Oxidation2.*Journal of the American Chemical Society*, *82*(7), 1734-1738.

Scott, A. I. (1964). Interpretation of the ultraviolet spectra of natural products.

Selimis, A., Vounisiou, P., Tserevelakis, G. J., Melessanaki, K., Pouli, P., Filippidis, G., ... & Fotakis, C. (2009, July). In-depth assessment of modifications induced during the laser cleaning of modern paintings. In *SPIE*

Europe Optical Metrology (pp. 73910U-73910U). International Society for Optics and Photonics.

Scalarone, D., Lazzari, M., & Chiantore, O. (2002). Ageing behaviour and pyrolytic characterisation of diterpenic resins used as art materials: colophony and Venice turpentine. *Journal of analytical and applied pyrolysis*, *64*(2), 345-361.

Scalarone, D., Lazzari, M., & Chiantore, O. (2003). Ageing behaviour and analytical pyrolysis characterisation of diterpenic resins used as art materials: Manila copal and sandarac. *Journal of analytical and applied pyrolysis*, *68*, 115-136.

Schaeffer, T. T. (2001). Effects of light on materials in collections: data on photoflash and related sources. Getty Publications.

Schnell, A., Goretzki, L., & Kaps, C. (2005). IR-laser effects on pigments and paint layers. In *Lasers in the Conservation of Artworks V* (pp. 291-296). Springer Berlin Heidelberg.

Sharma, S. K., Shukla, S. K., & Vaid, D. N. (1983). Shellac-structure, characteristics & modification. *Defence Sci. J*, *33*(3), 261-271.

Shearer, G. L. (1989). *An evaluation of Fourier transform infrared spectroscopy for the characterization of organic compounds in art and archaeology* (Doctoral dissertation, University of London).

Schuller, W. H., Moore, R. N., Hawkins, J. E., & Lawrence, R. V. (1962). The Ultraviolet Irradiation of the Cyclohexa-1, 3-diene, Levopimaric Acid2. *The Journal of Organic Chemistry*, *27*(4), 1178-1182.

Siano, S., & Salimbeni, R. (2001). The Gate of Paradise: physical optimization of the laser cleaning approach. *Studies in conservation*, *46*(4), pp. 269-281.

Siano, S., Pini, R., & Salimbeni, R. (1999). Variable energy blast modeling of the stress generation associated with laser ablation. *Applied physics letters*,*74*(9), 1233-1235.

Siano, S., Salimbeni, R., Pini, R., Giusti, A., & Matteini, M. 2003. Laser cleaning methodology for the preservation of the< i> Porta del Paradiso</i> by Lorenzo Ghiberti. *Journal of Cultural Heritage*, *4*, pp. 140-146.

Siano, S., Agresti, J., Cacciari, I., Ciofini, D., Mascalchi, M., Osticioli, I., & Mencaglia, A. A. (2012). Laser cleaning in conservation of stone, metal, and

painted artifacts: state of the art and new insights on the use of the Nd: YAG lasers. *Applied Physics A*, *106*(2), 419-446.

Siano S., Multiple temporal regime laser for art conservation [accessed 18 June 2013]. Available at: < http://spie.org/x94822.xml>.

Singh, A. N., Upadhye, A. B., Wadia, M. S., Mhaskar, V. V., & Dev, S. (1969). Chemistry of lac resin—II lac acids (Part 2): Laccijalaric acid. *Tetrahedron*,*25*(17), 3855-3867.

Srinivasan, R., Braren, B., Dreyfus, R. W., Hadel, L., & Seeger, D. E. (1986). Mechanism of the ultraviolet laser ablation of polymethyl methacrylate at 193 and 248 nm: laser-induced fluorescence analysis, chemical analysis, and doping studies. *JOSA B*, *3*(5), 785-791.

Srinivasan, R., (1986). Ablation of polymers and biological tissue by ultraviolet lasers. Science, 234 (4776), pp. 559-565.

Srinivasan, R., Braren, B., & Casey, K. G. (1990). Nature of ‘‘incubation pulses’’in the ultraviolet laser ablation of polymethyl methacrylate. *Journal of applied physics*, *68*(4), 1842-1847.

Stavroudis, C., Doherty, T., & Wolbers, R. (2005). A New Approach to Cleaning I: Using Mixtures of Concentrated Stock Solutions and a Database to Arrive at an Optimal Aqueous Cleaning System. *WAAC newsletter*, *27*(2), 17-28.

Stolow, N. (1956). Some investigations of the action of solvents on drying oil films., Ph.D.. thesis, University of London.

Stringari, C., McGlinchey, C. W., Melessanaki, K., Postma, S., & D'Augustine, C. (2007). Laser Cleaning of a Study Painting by Ad Reinhardt and the Analysis/Assessment of the Surface after Treatment. In *Modern Paints Uncovered: Proceedings from the Modern Paints Uncovered Symposium* (p. 208). Getty Publications.

Striova, J., Camaiti, M., Castellucci, E. M., & Sansonetti, A. (2011). Chemical, morphological and chromatic behavior of mural paintings under Er: YAG laser irradiation. *Applied Physics A*, *104*(2), 649-660.

Stulik, D., & Dorge, V. (Eds.). (2004). *Solvent gels for the cleaning of works of art: the residue question*. Getty Publications.

Sutherland, K. (2010). Bleached shellac picture varnishes: characterization and case studies. *Journal of the Institute of Conservation*, *33*(2), 129-145.

Sutherland, K. R. (2001). Solvent extractable components of oil paint films.

Sutherland, K. (2003). Solvent-extractable components of linseed oil paint films. *Studies in conservation*, *48*(2), 111-135.

Teule, R., Scholten, H., van den Brink, O. F., Heeren, R., Zafiropulos, V., Hesterman, R., Castillejo, M., Martín M., Ullenius, U., Larsson, I., Guerra-Librero, F., Silva, A., Gouveia, H., Albuquerque, M. B. (2003). Controlled UV laser cleaning of painted artworks: a systematic effect study on egg tempera paint samples. *Journal of Cultural Heritage*, *4*, pp. 209-215.

Theodorakopoulos C. (2005), *The Excimer Laser Ablation of Picture Varnishes*: *An evaluation with reference to light-induced deterioration*, Ph.D Thesis, Royal College of Art, RCA/V&A Conservation, London.

Theodorakopoulos, C., Boon, J. J., & Zafiropulos, V. (2009a). Direct temperature mass spectrometric study on the depth-dependent compositional gradients of aged triterpenoid varnishes. *International Journal of Mass Spectrometry*, *284*(1), 98-107.

Theodorakopoulos, C., Zafiropulos, V., Boon, J. J., & Boyatzis, S. C. (2007). Spectroscopic investigations on the depth-dependent degradation gradients of aged triterpenoid varnishes. *Applied spectroscopy*, *61*(10), 1045-1051.

Theodorakopoulos, C., & Zafiropulos, V. (2009b). Depth-profile investigations of triterpenoid varnishes by KrF excimer laser ablation and laser-induced breakdown spectroscopy. *Applied Surface Science*, *255*(20), 8520-8526.

Theophilus, (1961). *De Diversis Artibus*, edCR Dodwell, Oxford.

Upadhye, A. B., Wadia, M. S., Mhaskar, V. V., & Dev, S. (1970). Chemistry of lac resin—IV: Pure lac resin—1: Isolation and quantitative determination of constituent acids. *Tetrahedron*, *26*(17), 4177-4187.

Van den Berg, J. D. J. 2002. *Analytical chemical studies on traditional linseed oil paints*. PhD thesis, University of Amsterdam.

Van Den Berg, J. D., Vermist, N. D., Carlyle, L., Holčapek, M., & Boon, J. J. (2004). Effects of traditional processing methods of linseed oil on the composition of its triacylglycerols. *Journal of separation science*, *27*(3), 181-199.

Van den Berg, K. J. (2012). *Analysis of Diterpenoid Resins and Polymers in Paint Media and Varnishes: With an Atlas of Mass Spectra*. FOM Institute AMOLF.

Van der Doelen, G. A. (1999). Molecular studies of fresh and aged triterpenoid varnishes.

Van der Doelen, G. A., & Boon, J. J. (2000). Artificial ageing of varnish triterpenoids in solution. *Journal of Photochemistry and Photobiology A: Chemistry*, *134*(1), 45-57.

Van Der Weerd, J. (2002). Microspectroscopic analysis of traditional oil paint.

Van der Weerd, J., van Loon, A., & Boon, J. J. (2005). FTIR studies of the effects of pigments on the aging of oil. *Studies in conservation*, *50*(1), 3-22.

Vounisiou, P., Selimis, A., Tserevelakis, G. J., Melessanaki, K., Pouli, P., Filippidis, G., ... & Fotakis, C. (2010). The use of model probes for assessing in depth modifications induced during laser cleaning of modern paintings. *Applied Physics A*, *100*(3), 647-652.

Vandenabeele, P., Wehling, B., Moens, L., Edwards, H., De Reu, M., & Van Hooydonk, G. (2000). Analysis with micro-Raman spectroscopy of natural organic binding media and varnishes used in art. *Analytica Chimica Acta*,*407*(1), 261-274.

Vandenabeele, P., & Moens, L. (2003). Micro-Raman spectroscopy of natural and synthetic indigo samples. Analyst, 128(2), 187-193.

Wadia, M. S., Mhaskar, V. V., & Dev, S. (1963). On the constitution of Jalaric acid. Tetrahedron Letters, 4(8), 513-517.

Wadia, M. S., Khurana, R. G., Mhaskar, V. V., & Dev, S. (1969). Chemistry of lac resin—I: Lac acids (part 1): Butolic, jalaric and laksholic acids. Tetrahedron, 25(17), 3841-3853.

Wolbarsht, M. & de Cruz A. (1990), Method for cleaning artwork. *US Patent, 5,951,778*.

Yu, M. M., Schulze, H. G., Jetter, R., Blades, M. W., & Turner, R. F. (2007). Raman microspectroscopic analysis of triterpenoids found in plant cuticles.*Applied spectroscopy*, *61*(1), 32-37.

Zafiropulos, V., Balas, C., Manousaki, A., Marakis, Y., Maravelaki-Kalaitzaki, P., Melesanaki, K., ... & Dogariu, A. (2003). Yellowing effect and discoloration of pigments: experimental and theoretical studies. *Journal of Cultural Heritage*,*4*, 249-256.

Zafiropulos, V., Galyfianaki, A., Boyatzis, S., Fostiridou, A., & Ioakimoglou, E. (2000). UV-laser ablation of polymerized resin layers and possible oxidation processes in oil-based painting media. In *Optics and Lasers in Biomedicine and Culture* (pp. 115-122). Springer Berlin Heidelberg.

Zafiropulos, V. (2002). *Laser ablation in cleaning of artworks* (p. 343). World Scientific: Singapore.

Zergioti, I., Petrakis, A., Zafiropulos, V., Fotakis, C., Fostiridou, A., & Doulgeridis, M. (1997). Laser applications in painting conservation. In *Lacona I: lasers in the conservation of artworks, workshop, 4-6 October 1995, Heraklion, Crete, Greece* (pp. 57-60). Mayer & Comp..

Zumbühl, S., Knochenmuss, R., Wülfert, S., Dubois, F., Dale, M. J., & Zenobi, R. (1998). A graphite-assisted laser desorption/ionization study of light-induced aging in triterpene dammar and mastic varnishes. Analytical Chemistry, 70(4), 707-715.

Acknowledgements

I'd like to acknowledge first the University of Florence and the "Nello Carrara" Institute of Applied Physics (IFAC-CNR).

Thanks to my supervisor Dr. Salvatore Siano for his guidance, for sharing his experience and for the support along this three years of PhD. Clearly, special thanks to my colleagues at IFAC for helping and supporting me in many occasions, both from the technical and human standpoint.

I would like to thank Dr. Mara Camaiti and Dr. Jana Striova for helping me in the samples preparation and for providing the instrumentation and the technical support.

The research on modern paintings has been possible thanks to the collaboration with Alessandro Pavia (Pavia Restauro s.r.l, Roma), which is kindly acknowledged.

A special thanks to Dr. Marta Castillejo, to Dr. Mohamed Oujja and all the members of her group for the warm welcome during my stay at the Institute of Physical Chemistry "Rocasolano" (IQFR-CSIC, Madrid). Working in your team has been very inspiring and has been a very positive learning experience for me.

Many thanks to Dr. María Vega Cañamares (IEM-CSIC) for the Raman measurements and for supporting me with useful discussions.